Geneeskundige Stichting Koningin Elisabeth
Fondation Médicale Reine Elisabeth
Königin-Elisabeth-Stiftung für Medizin
Queen Elisabeth Medical Foundation

Verslag – Rapport – Bericht – Report

2018

G.S.K.E. – F.M.R.E. – K.E.S.M. – Q.E.M.F.

www.fmre-gske.be
www.fmre-gske.eu
www.fmre-gske.com

Geneeskundige Stichting Koningin Elisabeth
2018
Inleiding verslag activiteiten van de GSKE – FMRE

Het wetenschappelijk onderzoek in het domein van de neurowetenschappen wordt door de stichting gesteund en sinds 2017 genieten 16 onderzoeksploegen van deze financiële steun.
Verschillende van deze onderzoeksploegen zijn naar waarde geschat tijdens de prijsuitreiking van de stichting op 26 april 2018. Deze academische zitting vond plaats in het bijzijn van Z.K.H. Prins Lorenz en verschillende personaliteiten van het land.
De zitting werd geopend door de Voorzitter van de Raad van Bestuur, de heer Hein Deprez en de voorstelling van de lauréaten van de prijzen gebeurde met het tonen van video's over hun onderzoek.

Dit waren de laureaten:
De onderzoeksploeg van Professor An Goris (KU Leuven) ontving de prijs Burggravin Valine de Spoelberch voor haar onderzoeksproject: "Unraveling the BAFF pathway towards targeted treatment of multiple sclerosis".

De onderzoeksploeg van Professor Peter Vangheluwe (KU Leuven) ontving de Ernest Solvay prijs 2018 voor zijn onderzoeksproject ''Neuroprotection by lysosomal transport mechanisms in Parkinson's disease"

De onderzoeksploeg van Professor Benoit Vanhollebeke (ULB) ontving de Janine en Jacques Delruelle prijs voor zijn onderzoeksproject "Organ-wide analysis of brain neurovascular communication in real-time and at single-cell resolution"

De zitting werd verdergezet met een voordracht over "De Koningin en de Farao"door de heer Jean-Michel Bruffaerts, Directeur van het project Jean Capart en wetenschappelijk medewerker van de Koninklijke Musea voor Kunst en Geschiedenis in Brussel.

Deze uiteenzetting onderstreept nogmaals de rol van Koningin Elisabeth en van België in de Egyptologische ontwikkeling.

Aan het einde van de 19de eeuw, tijdens een cruise op de Middellandse Zee, met haar tante de Keizerin van Oostenrijk ("Sissi"), zag de jonge hertogin-van Beieren, Egypte voor de eerste keer. Nadat Zij Koningin der Belgen werd, keerde ze drie keer terug, met of zonder haar man Koning Albert: in 1911, 1923 en 1930.

Koningin Elisabeth werd gedreven door vele passies. Sommige zijn beter gekend dan andere: zoals de "muzikale Koningin", of "Koningin verpleegster", maar er zijn weinigen die hebben horen spreken over de "Egyptologische Koningin".
Tijdens deze reizen was er één die de geschiedenis van Egypte grondig heeft veranderd. Het is de reis van 1923, waarin Elisabeth, vergezeld door haar zoon Leopold (de toekomstige Koning Leopold III) en Jean Capart (de oprichter van de Belgische Egyptologie), het voorrecht had om de onlangs ontdekte begrafeniskamer van farao Tutankhamon in te huldigen.

Het is in het globale enthousiasme van dit evenement dat een Egyptologische Stichting Koningin Elisabeth werd gecreëerd binnen de Koninklijke Musea in het Jubelpark met als doel de Egyptologie in België te bevorderen.

Onder de leiding van Jean Capart, slaagde Ze erin, tussen de twee wereldoorlogen, om van Brussel de wereldstad te maken van de Egyptologie en de Papyrologie.
De zitting werd afgesloten met een receptie waarop de onderzoekers, de mecenassen, de toeschouwers en de aanwezige autoriteiten elkaar konden ontmoeten en van gedachten wisselen.

Wij danken zeer hartelijke Z.K.H. Prins Lorenz voor Zijn aanwezigheid tijdens de wetenschappelijk dag van de Stichting en H.K.H. Prinses Astrid voor Haar niet aflatende steun aan de werkzaamheden van de Stichting. Wij danken alle leden van de Raad van Bestuur en van het wetenschappelijke comite voor het werk dat zij verrichten ten voordele van de neurowetenschappelijke onderzoekers in ons land die dankzij de mecenassen kunnen doorgaan met de ontwikkeling van de neurowetenschappen.

Prof. dr. Jean-Marie Maloteaux,
wetenschappelijk directeur
Brussel, 30 december 2018

Fondation Médicale Reine Elisabeth
2018
Introduction rapport d'activités de la FMRE – GSKE

La recherche scientifique en Neurosciences est soutenue par la Fondation et depuis 2017, seize équipes de recherche bénéficient d'un soutien financier. Plusieurs de ces équipes de recherche ont été mises en valeur au cours de la séance de remise de prix de la Fondation le 26 avril 2018. Cette séance académique s'est déroulée en présence de S.A.R. le Prince Lorenz et de nombreuses personnalités du pays.
La séance académique a été ouverte par le Président du Conseil d'Administration Monsieur Hein Deprez et la présentation des lauréats des prix scientifiques s'est faite par la diffusion de vidéos consacrées à leurs travaux originaux.
Les lauréats cette année furent:
L'équipe du Professeur An Goris (KU Leuven) a reçu le Prix Vicomtesse Valine de Spoelberch pour le travail intitulé "Unraveling the BAFF pathway towards targeted treatment of multiple sclerosis.

L'équipe du Professeur Peter Vangheluwe (KU Leuven) a reçu le Prix Ernest Solvay 2018 pour son travail "Neuroprotection by lysosomal transport mechanisms in Parkinson's disease".

L'équipe du Professeur Benoit Vanhollebeke (ULB) a reçu le Prix Janine et Jacques Delruelle pour son travail "Organ-wide analysis of brain neurovascular communication in real-time and at single-cell resolution".

La séance s'est poursuivie par un exposé intitulé « La Reine et le Pharaon », présenté par Monsieur Jean-Michel Bruffaerts, Directeur du projet Jean Capart et Collaborateur scientifique des Musées d'art Royaux et d'histoire à Bruxelles.
Cet exposé a souligné le rôle de la Reine Elisabeth et de la Belgique dans le développement de l'égyptologie

La Reine Elisabeth était animée par de multiples passions. Certaines sont mieux connues que d'autres : si chacun a entendu parler de la Reine "musicienne" ou de la Reine "infirmière", rares sont ceux qui ont entendu parler de la Reine "égyptologue".

C'est à la fin du 19e s., au cours d'une croisière en Méditerranée avec sa tante l'impératrice Elisabeth d'Autriche ("Sissi"), que la jeune duchesse en Bavière vit l'Egypte pour la première fois. Après être devenue reine des Belges, elle y retourna à trois reprises, avec ou sans son époux le roi Albert : en 1911, en 1923 et en 1930.

Parmi ces voyages, il en est un qui a profondément marqué l'histoire de l'égyptologie. Il s'agit du voyage de 1923 au cours duquel Elisabeth, accompagnée de son fils Léopold (le futur Roi Léopold III) et de Jean Capart (le fondateur de l'égyptologie belge), eût le privilège d'inaugurer la Chambre funéraire du pharaon Toutankhamon récemment découverte.

C'est dans l'enthousiasme de cet événement au retentissement planétaire qu'une Fondation Egyptologique Reine Elisabeth fut créée au sein des Musées Royaux du Cinquantenaire en vue de promouvoir l'égyptologie en Belgique. Dirigée par Capart, elle allait réussir l'exploit de faire de Bruxelles, durant l'Entre-deux-guerres, la capitale mondiale de l'égyptologie et de la papyrologie.

La séance s'est terminée par une réception qui a permis aux chercheurs de discuter et de rencontrer les mécènes, les membres du public et les autorités présentes.
Nous remercions vivement S.A.R. le Prince Lorenz pour sa présence au cours de la journée scientifique de la Fondation et S.A.R. la Princesse Astrid pour son soutien constant aux travaux de celle-ci. Nous remercions tous les membres du Conseil d'Administration et du Comité scientifique pour le travail qu'ils accomplissent au bénéfice des chercheurs en neurosciences de notre pays qui grâce aux mécènes peuvent poursuivre le développement des Neurosciences.

Prof. dr. Jean-Marie Maloteaux,
directeur scientifique
Bruxelles, 30 décembre 2018

Universiteiten met onderzoeksprogramma's die gesteund worden door de G.S.K.E.

Universités ayant des programmes de recherche subventionnés par la F.M.R.E.

Universities having research programs supported by the Q.E.M.F.

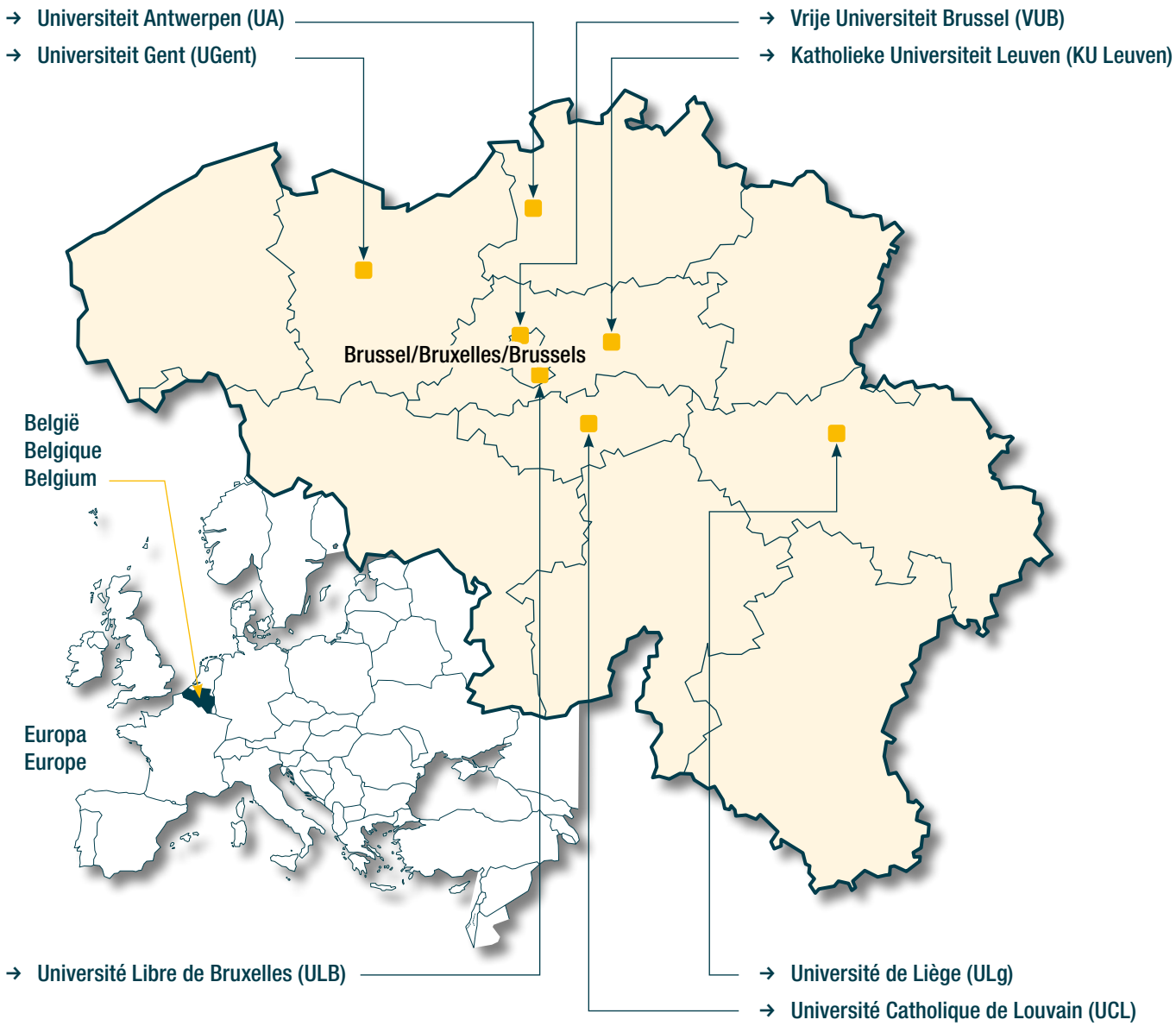

Onderzoeksprogramma's gefinancierd door de G.S.K.E. - Programma 2017-2019

Programmes de recherche subventionnés par la F.M.R.E. - Programme 2017-2019

Q.E.M.F. funded research projects - Program 2017-2019

KU Leuven

- **Prof. dr. Baekelandt Veerle, PhD**
  The role of alpha-synuclein aggregation, spreading and neuroinflammation in Parkinson's disease and related disorders.
- **Prof. dr. Ir De Meyer Simon**
  Neutrophil extracellular traps: novel targets for neuroprotection in stroke.
- **Prof. dr. De Strooper Bart, MD. PhD**
  The study of the initial cellular phase of Alzheimer's disease.
- **Prof. Goris An, PhD**
  Unraveling the BAFF pathway towards targeted treatment of multiple sclerosis.
- **Prof. dr. Vandenberghe Wim, MD. PhD**
  LRRK2, Rab10 and mitochondrial quality control in Parkinsons's disease.
- **Prof. dr. Vangheluwe Peter, PhD**
  Neuroprotection by lysosomal transport mechanisms in Parkinson's disease.
- **Prof. dr. Verfaillie Catherine**
  Unraveling the role of TREM2 mutations in Alzheimer's disease using human Pluripotent Stem Cells.
- **Prof. Voets Thomas**
  Unraveling the role of TRMP3 in neuropathic and inflammatory pain.

UA

- **Prof. dr. Timmerman Vincent, PhD**
  Unravelling the novel molecular pathways contributing to distal hereditary motor neuropathy caused by mutant HSPB8 with the aim to identify potential therapeutic targets.

UCL

- **Prof. Fadel Tissir, PhD**
  Development and malformations of the cerebral cortex: role of the diaphanous 3 gene.

UGent

- **Prof. dr. Leybaert Luc, MD. PhD**
  Exploring the role of astroglial Cx43 hemichannels as therapeutic targets in stroke.
- **Prof. dr. Geert van Loo, PhD**
  Microglia, inflammasomes and multiple sclerosis.
- **Prof. dr. Vonck Kristl**
  The role of locus coeruleus noradrenergic neurons in the mechanism of vagus nerve stimulation and the effect of selective activation of these neurons in epilepsy.

ULB

- **Prof. Vanhollebeke Benoit, PhD**
  Organ-wide analysis of brain neurovascular communication in real-time and at single-cell resolution.

ULg

- **Dr. Nguyen Laurent, PhD**
  Deciphering the role of protein ubiquitination in human cortical malformation and hearing impairment.

VUB

- **Prof. dr. De Bundel Dimitri, PhD**
  Chemogenetic interrrogation of neuromedin U involvement in stress-induced psychopathology.

Progress reports of the university research groups, supported by the Queen Elisabeth Medical Fondation in collaboration with the following professors and doctors (2018)

Geneeskundige Stichting Koningin Elisabeth
Fondation Médicale Reine Elisabeth
Königin-Elisabeth-Stiftung für Medizin
Queen Elisabeth Medical Foundation

Progress report of the research group of

Prof. dr. Baekelandt Veerle, PhD

Katholieke Universiteit Leuven (KU Leuven)

Principal investigator

Prof. dr. Baekelandt Veerle, PhD
Laboratory for Neurobiology and Gene Therapy
Division of Molecular Medicine K.U.Leuven –
Faculty of Medicine Kapucijnenvoer 33 VCTB+5
B-3000 Leuven
Belgium
Tel.: +32 16 37 40 61
Fax: +32 16 33 63 36
E-mail: Veerle.Baekelandt@kuleuven.be

The role of α-synuclein aggregation, spreading and neuroinflammation in Parkinson's disease and related disorders

1. Introduction

Misfolded protein aggregates are a common feature of several neurodegenerative diseases, although the major protein component and the affected brain regions differ for each neurodegenerative disorder, e.g. α-synuclein (αSYN) in Parkinson's disease (PD), amyloid-β (Aβ)/Tau in Alzheimer's disease (AD) and huntingtin in Huntington's disease. Familial forms of neurodegenerative disorders are often linked to mutations that change the aggregation propensity of the disease-related protein, suggesting that protein misfolding and aggregation are likely to play a decisive role in the pathogenesis of neurodegenerative diseases. A distinctive pattern of pathological changes throughout the brain has been described for all the major neurodegenerative diseases[1,2]. The recent discovery of the transmissible nature of amyloidogenic proteins puts forward a hypothesis of a pathogenic trigger that spreads throughout the nervous system, underlying the progression of the disease[3]. Furthermore, evidence is emerging that these protein aggregates can adopt distinct conformations or 'strains' with remarkable differences in their structural and phenotypic traits, both in AD and PD[4-7]. Now, often referred to as prion-like diseases, the transmissibility and seeding mechanisms of these amyloidogenic proteins are the subject of intense research.

Synucleinopathies are determined by the formation of αSYN-rich deposits but segregate in distinct pathological phenotypes and diagnostic criteria including PD, Dementia with Lewy bodies (DLB) and Multiple System Atrophy (MSA). However, why αSYN inclusions are found in diseases that present with different phenotypic traits remains unresolved.
PD is the most common neurodegenerative movement disorder affecting approximately 10 million people worldwide. The neuropathological hallmarks of PD are the deposition of misfolded protein aggregates, predominantly composed of αSYN, in distinct brain regions and the progressive degeneration of dopaminergic neurons in the substantia nigra pars compacta (SNpc), subsequently leading to striatal dopamine depletion, which is responsible for the classical motor symptoms.

Nevertheless, several questions remain unanswered regarding the cause of neuronal cell death and the role of misfolded protein aggregates in PD. It has been postulated that neuroinflammatory processes might play a crucial role in the pathogenesis of PD and other neurodegenerative disorders[8,9]. Numerous post-mortem, brain imaging, epidemiological and animal studies have documented the involvement of the innate and adaptive immunity in neurodegeneration[10-14]. Whether these inflammatory processes are directly involved in the etiology of PD or represent secondary consequences of nigrostriatal pathway injury is the subject of intensive research. Immune alterations in response to extracellular αSYN may play a critical role in modulating Parkinson's disease progression.

2. Specific aims

We hypothesize that distinct phenotypes in synucleinopathies might correlate to heterogeneity in αSYN strains in patients. We also postulate that neuroinflammatory processes are closely involved in αSYN transmission and neurotoxicity. In line with these hypotheses, we aim to further study - in a detailed and quantitative way - how different αSYN assemblies are linked to αSYN transmission, neurodegeneration and neuroinflammation in rodent models of PD. Importantly, we will translate our findings to human disease and therapy by investigating the properties of αSYN-rich fractions from the brain of patients

with different synucleinopathies. A better understanding of the role of intercellular transmission and neuroinflammation in αSYN-linked neurodegeneration will contribute to the early diagnosis, prevention and the development of novel therapeutic strategies and compounds for synucleinopathies and other ageing-related disorders.

Specific objectives:
- Characterization of seeding and spreading properties of patient-derived αSYN assemblies in rodent models
- Elucidation of the role of the innate immune system in αSYN spreading and neurotoxicity in rodent models

3. Results

WP1. Characterization of seeding and spreading properties of patient-derived αSYN assemblies

In WP1 we aim to bridge the gap between preclinical studies using recombinant protein and the human pathology. To this end, we tested patient-derived *in vitro* amplified αSYN assemblies in the rodent brain and compared those to recombinant αSYN assemblies for disease-inducing properties in terms of αSYN spreading and pathology.

1.1. Isolation and characterization of patient-derived αSYN assemblies

Brain samples of patients with PD, MSA and DLB obtained from the UK Brain Bank via Prof. S. Gentleman (Imperial College London, UK; n=6/group) have been extensively characterized from a clinicopathological point of view. These samples were transferred to the group of our collaborator Prof. R. Melki (CNRS, France) who has isolated, purified and characterized the different ***αSYN*** assemblies present *in vitro*. He also implemented a Protein Misfolding Cyclic Amplification (PMCA) assay for Lewy bodies containing tissues to amplify the αSYN assemblies *in vitro*.

1.2. *In vivo* characterization of patient-derived αSYN strains

Patient-derived homogenates as well as PMCA-amplified ***αSYN*** assemblies have been injected into the substantia nigra (SN) of wild-type rats with or without rAAV2/7-based overexpression of αSYN. These injected animals were subjected to the cylinder test on a monthly basis and sacrificed at five months post injection based on their behavioral performance. Additionally, the effect of the different αSYN species on dopaminergic neurodegeneration in wild-type rat brains was assessed by stereological quantification of tyrosine hydroxylase (TH) positive cell bodies and nerve terminals.
In wild-type rats injected with the different patient-derived homogenates including MSA, PD, DLB and age-matched control patients we did not observe clear differences in the use of the left forepaw up to five months after stereotactic injection (**Fig. 1A**). However, we noticed a remarkable decrease in the number of TH-positive cells in the injected SN after injection of DLB- and MSA-derived homogenates (respectively 48.5% and 38.6% compared to the non-injected side). A less pronounced decrease in the number of TH positive nigral neurons was observed upon exposure to PD and age-matched control patients (30% and 28% compared to the non-injected side; **Fig. 1A**). The MSA and DLB group presented significantly more cell loss than the PD group. In the rats where homogenates were combined with rAAV2/7-based overexpression of αSYN, the MSA-derived homogenates led to a significant decrease in the use of the left forepaw compared to control-derived homogenates (**Fig. 1B**). We also found a trend towards a decreased use of the left forepaw after injection of PD- and DLB-derived homogenates in the PD rat model. In line with these findings, we observed significant neuronal cell loss after exposure to MSA- and PD-derived homogenates combined with αSYN overexpression (respectively 74% and 63.5% in comparison to the non-injected side); while the decrease in the number of TH-positive nigral

neurons after injection of DLB homogenates was less pronounced (40.5% in comparison to the non-injected side; **Fig. 1B**). The MSA injected animals were significantly different from the DLB injected animals.

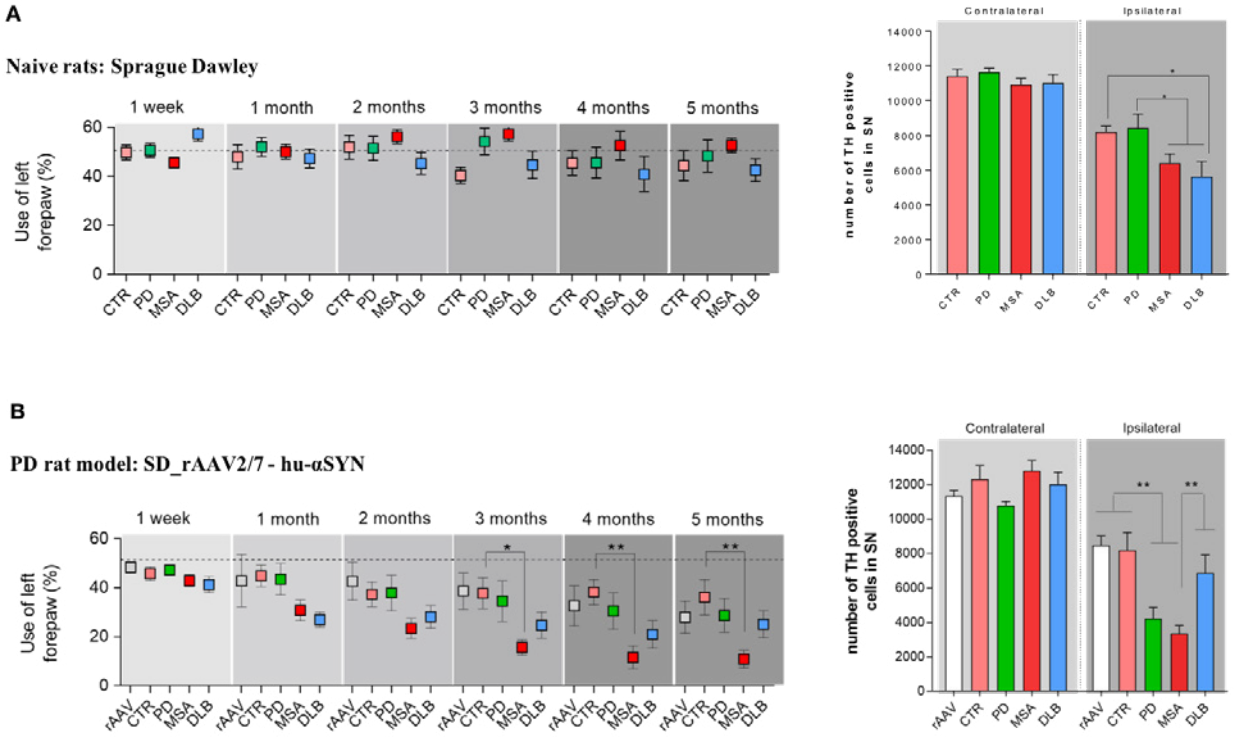

Figure 1 – Patient-derived homogenates with or without rAAV2/7-mediated αSYN overexpression lead to differences in terms of motor deficits and neuropathology *in vivo*. A. Cylinder test at different time points after injection of the different patient-derived homogenates (MSA, PD, DLB and age-matched control). IHC staining for TH in the rat SN five months after stereotactic injection of the patient-derived homogenates. B. Cylinder test at different time points after injection of patient-derived homogenates (MSA, PD, DLB and control) in combination with rAAV2/7-mediated overexpression of αSYN**.** IHC staining for TH in the rat SN five months after stereotactic injection of patient-derived homogenates in association with rAAV2/7-based αSYN overexpression. Mean ± SEM are shown (n=12). * $p < 0.05$, ** $p < 0.01$ (Unpublished results).

In wild-type rats injected with PMCA-amplified αSYN assemblies including MSA, PD and DLB we observed a small decrease in motor behavior (**Fig. 2A**). The number of TH-positive cells in the SN was decreased by 20% compared to the non-injected side in all the conditions. However no difference in neuronal cell loss was found between the different conditions (**Fig. 2A**).When combining the PMCA-amplified αSYN assemblies with rAAV2/7-mediated overexpression of αSYN we observed a decreased use of the left forepaw over time after injection of PMCA- amplified MSA, PD and control assemblies. Strikingly, no changes in the use of the left forepaw were found in the DLB condition in association with rAAV2/7-mediated αSYN overexpression (**Fig. 2B**). A significant decrease in the number of TH positive nigral neurons was shown upon exposure to PMCA-amplified MSA and PD assemblies (60% and 53% compared to the non-injected side), whereas the condition with DLB in association with αSYN overexpression only presented mild cell loss (25.5 % compared to the non-injected side; **Fig. 2B**). The MSA and PD injected animals were significantly different form the DLB injected animals.

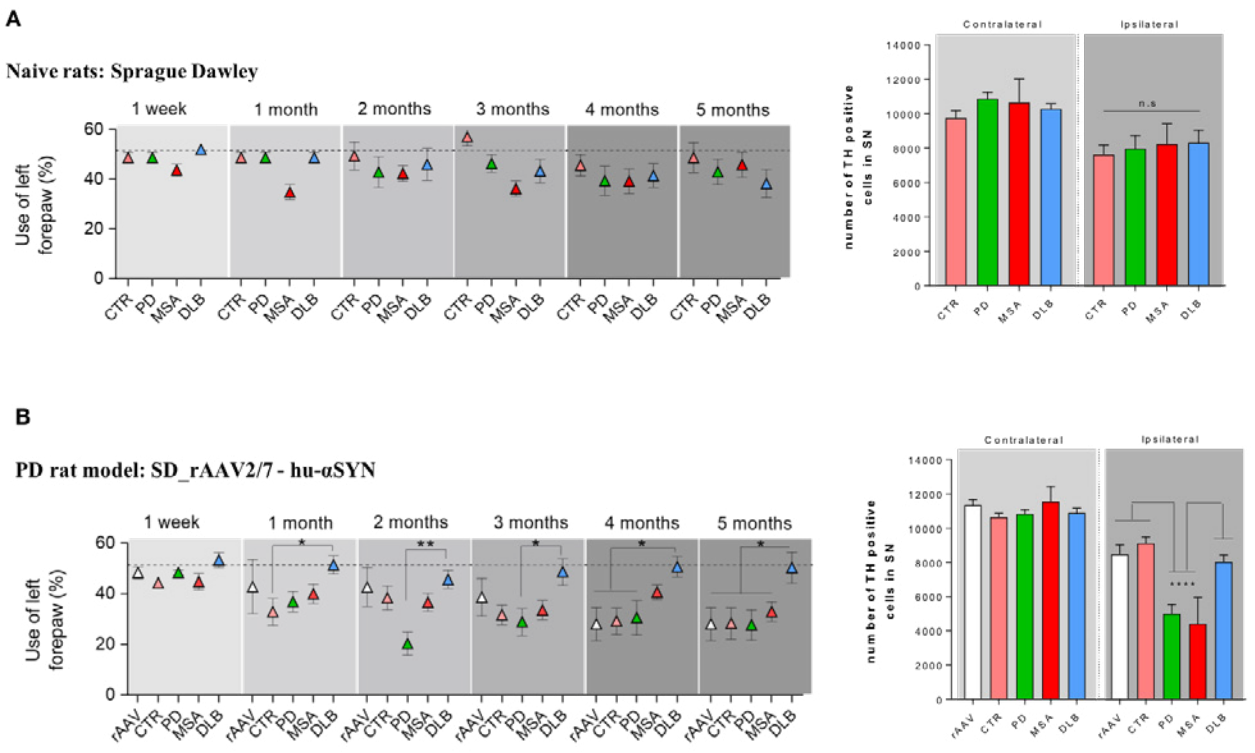

Figure 2 – PMCA-amplified *αSYN* assemblies with or without rAAV2/7-mediated αSYN overexpression lead to differences in terms of motor deficits and neuropathology *in vivo*. A. Cylinder test at different time points after injection of the different PMCA-amplified ***αSYN*** assemblies (MSA, PD, DLB and age-matched controls). IHC staining for TH in the rat SN five months after stereotactic injection of the PMCA-amplified ***αSYN*** assemblies. B. Cylinder test at different time points after injection of the different PMCA-amplified ***αSYN*** assemblies (MSA, PD, DLB and control) in combination with rAAV2/7-mediated overexpression of αSYN**.** IHC staining for TH in the rat SN five months after stereotactic injection of the PMCA-amplified ***αSYN*** assemblies in association with rAAV2/7-based αSYN overexpression. Mean ± SEM are shown (n=12). * $p < 0.05$, ** $p < 0.01$ (Unpublished results).

In addition, immunohistochemical analysis for phosphorylated αSYN (which is a pathology-related form of the protein) was performed in the rat SN. We found that the number of phosphorylated αSYN (PSYN) positive cells in the rat SN was significantly increased in the rats overexpressing αSYN which were injected with MSA-derived homogenates in comparison to PD, DLB- and control-derived homogenates (**Fig. 3A**). We are planning to perform double stainings combining TH and PSYN in order to check whether we can find a correlation between neuronal cell loss in the SN and the presence of αSYN-related pathology in these neurons.

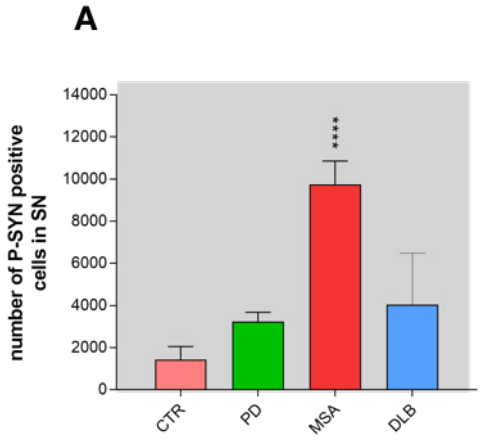

Figure 3 – Patient-derived homogenates in association with rAAV2/7-mediated αSYN overexpression lead to differences in terms of αSYN-related pathology *in vivo*. A. Quantification of the number of PSYN positive cells in the rat SN five months after injection of patient-derived homogenates (MSA, PD, DLB and control). Mean ± SEM are shown (n=12). * $p < 0.05$, ** $p < 0.01$, *** $p < 0.001$ (Unpublished results).

We are currently characterizing αSYN pathology and spreading in different brain regions including the striatum, the hippocampus and the cortex. Furthermore, we are characterizing the inflammatory profile based on stainings for Iba1 (microglia), MHCII (antigen presentation), CD4 (T helper cells) and CD8 (cytotoxic T cells). We plan to finish the immunohistochemical analysis by March 2018.
BAC transgenic rats expressing human full-length wild-type αSYN have also been injected as mentioned in the previous report. We are currently analyzing the brains from these rats, which were sacrificed eight months post injection, performing immunohistochemical analysis for the different markers used for the wild-type model.

WP2. Elucidation of the role of the innate immune system in αSYN spreading and neurotoxicity

Evidence is emerging that αSYN can adopt distinct conformations, also referred to as 'strains', which are characterized by remarkable differences in structural and phenotypic features[4,5]. Therefore, presentation of different αSYN assemblies (monomers, oligomers or fibrils) to the innate immune system and the subsequent immune response might be a driving force in the disease, although the exact αSYN strains which might trigger this inflammatory response have not yet been identified[3].

2.1. Characterization of the microglial response to different αSYN assemblies

In this part of the WP, we have studied the phenotype of BV2 cells (immortalized murine microglial cell line) and primary microglia in response to exogenous administration of recombinant αSYN assemblies including oligomers and two different fibrillar αSYN strains, called fibrils and ribbons. Fibrils and ribbons display distinct structural properties and present different toxicity and propagation propensity in cell culture[4]. We have shown that both αSYN fibrils and ribbons induce the classical pro-inflammatory microglial phenotype and suppress the alternative repair state in BV2 cells, as characterized by the expression of anti-inflammatory markers. In line with the results obtained in BV2 cells, primary microglia showed a pronounced pro-inflammatory response towards the fibrillar forms of αSYN.

As shown in our previous report, different αSYN assemblies are taken up by primary microglia based on qualitative analysis of confocal images. We now performed more thorough analysis on the uptake and degradation of αSYN assemblies over time (from 2 hours up to 24 hours post treatment). We thereby demonstrated that ***αSYN fibrils and ribbons*** appear to be internalized more efficiently and degraded more slowly by microglial cells than monomeric and oligomeric ***αSYN based*** on immunocytochemistry staining. Uptake of labeled (Alexa 488) αSYN assemblies by $CD11b^{+}$ $CD45^{+}$ primary microglia was further assessed by flow cytometric analysis. The percentage of αSYN positive microglial cells was substantially increased upon exposure to fibrils and ribbons when compared to αSYN monomers and oligomers (**Fig. 4**).

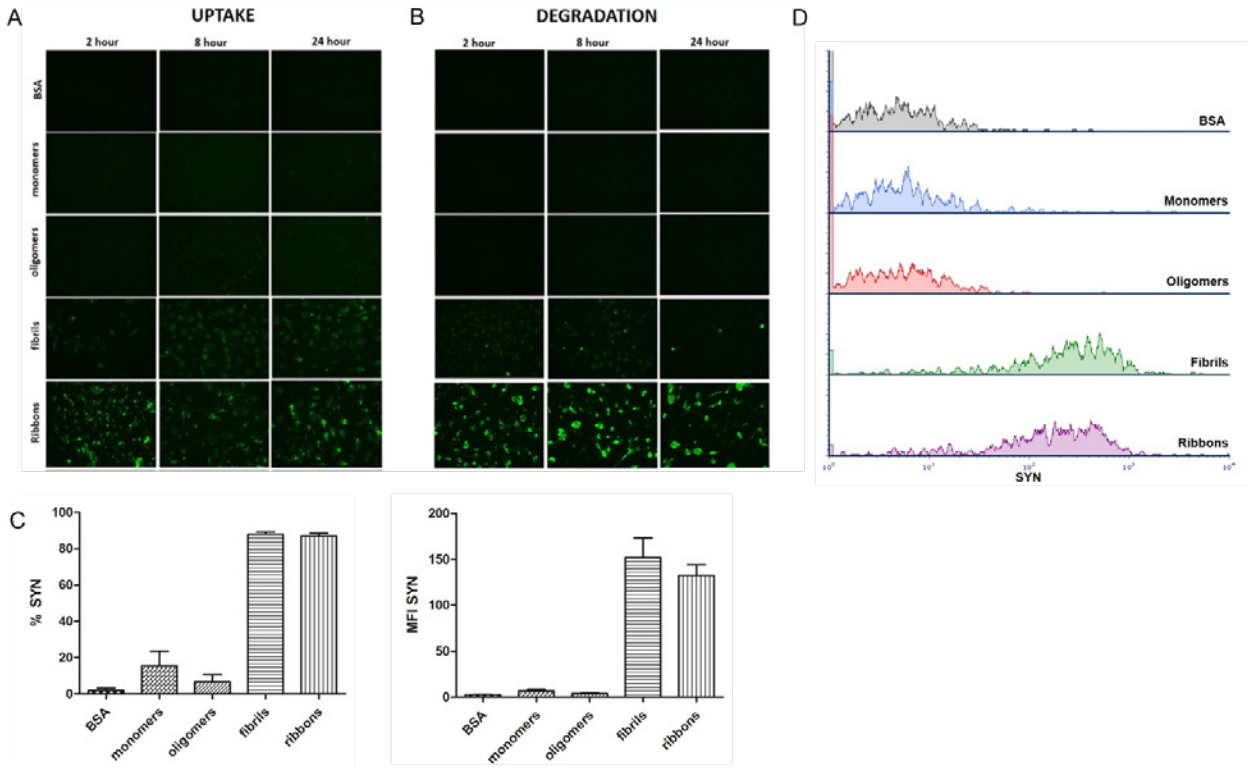

Figure 4 – Detailed uptake and degradation by murine primary microglia.
A-B. Immunocytochemistry staining for αSYN (green) of primary microglia treated with different αSYN strains up to 24 hours. C-D. Representative histograms depicting αSYN uptake by CD11b+ CD45+ microglial cells assessed by flow cytometry. BSA was used as a negative control (Van der Perren *et al.*, unpublished results).

In order to study the microglial immune response to different αSYN assemblies in vivo, we have stereotactically injected αSYN monomers, oligomers and the two fibrillar αSYN strains into the SN of adult mice. Two days post injection, we sacrificed the animals and performed immunohistochemical analysis using the CD11b antibody in order to visualize the microglial cells. As a result, we found that the fibrillar αSYN assemblies are more prone to induce microglial activation in vivo compared to oligomeric and monomeric species.

A second cohort of animals stereotactically injected with the different αSYN assemblies into the SN, was subjected to the cylinder test after 2 weeks and 6 months post stereotactic injection. However, we did not observe clear changes in the use of the left forepaw within the different experimental groups over time (**Fig. 5**).

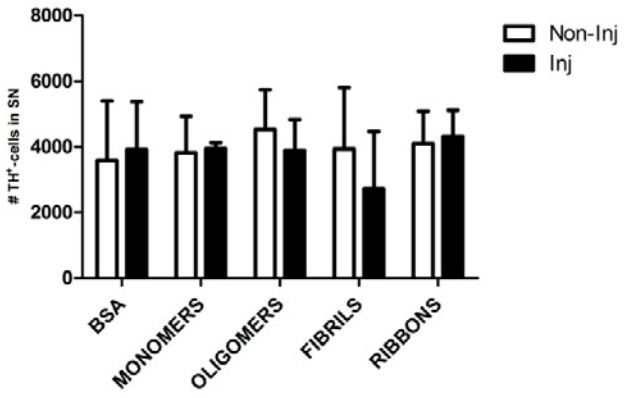

Figure 5 – Cylinder test after stereotactic injection of different αSYN assemblies in the mouse SN. Animals were subjected to the cylinder test 2 weeks and 6 months post stereotactic injection in order to quantify the spontaneous use of the forelimbs. BSA was included as a negative control (Gelders G *et al.*, unpublished results).

These animals were sacrificed six months post injection and the level of neurodegeneration was assessed over time (**Fig. 6**). We observed a decrease in the number of TH positive cells after injection of αSYN fibrils compared to the other conditions. No changes in neuronal cell loss were found in the injected side of the brain upon administration of αSYN monomers, oligomers and ribbons. These results suggest that the αSYN fibrils are more prone to induce neuronal cell death *in vivo* compared to the other αSYN assemblies. Immunohistochemical analysis for phosphorylated αSYN, as well as Iba1, Arg, CD68, and YM1 in order to study possible alterations in the microglial immune response over time, is currently ongoing.

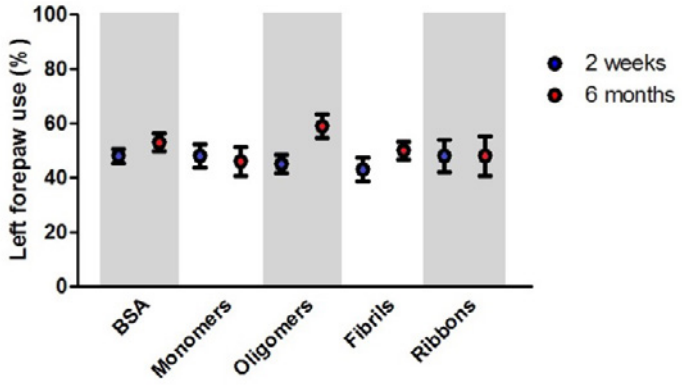

Figure 6 – Assessment of the level of neurodegeneration upon stereotactic injection of different αSYN assemblies in the mouse SN. Stereological quantification of the number of TH immunoreactive nigral neurons, six months after injection of recombinant αSYN strains. BSA was injected as a negative control (Gelders G *et al.*, unpublished results).

2.2. Analyze the involvement of inflammatory cells in SYN spreading

The discovery of misfolded αSYN protein aggregates with different structural characteristics, that could account for the distinct pathological traits within synucleinopathies and which amplify in a "prion-like" fashion[15-18], has led us to consider that pathogenic αSYN might be hijacking the activation and mobilisation mechanism of the peripheral immune system to reach and disseminate within the CNS. Therefore, we assessed the impact of peripheral inflammation on αSYN spreading in order to understand the participation of the immune system in αSYN pathology.

The results presented here show that intraperitoneal LPS injection combined with intravenous administration of two different recombinant αSYN pathogenic strains (fibrils or ribbons) in wild-type mice, induces an increase in brain resident microglia and promotes the recruitment of leukocytes towards the brain (**Figure 7A**) and the spinal cord (**Figure 7C**). When further characterising the phenotypic traits of the peripheral cells trafficking to the CNS, we identified neutrophils and professional antigen presenting cells among innate myeloid leukocytes (data not shown), as well as a distinct migration of $CD4^+$ and $CD8^+$ T cell subsets after administration of αSYN strains, which was most prominent in the brain for ribbons compared to fibrils **(Figure 7B, D)**. Moreover, LPS-primed inflammatory monocytes proved to be the major source of CNS-associated phagocytes after systemic challenge with αSYN strains. In the brain, fibrils induced a stronger response compared to ribbons, while the effect in the spinal cord was similar for both αSYN strains **(Figure 7A, C)**. Interestingly, we noticed that LPS priming favoured αSYN spreading towards the brain and spinal cord, as observed by an upregulation of $αSYN^+$-expressing microglia and inflammatory monocytes (**Figure 7E, F**).

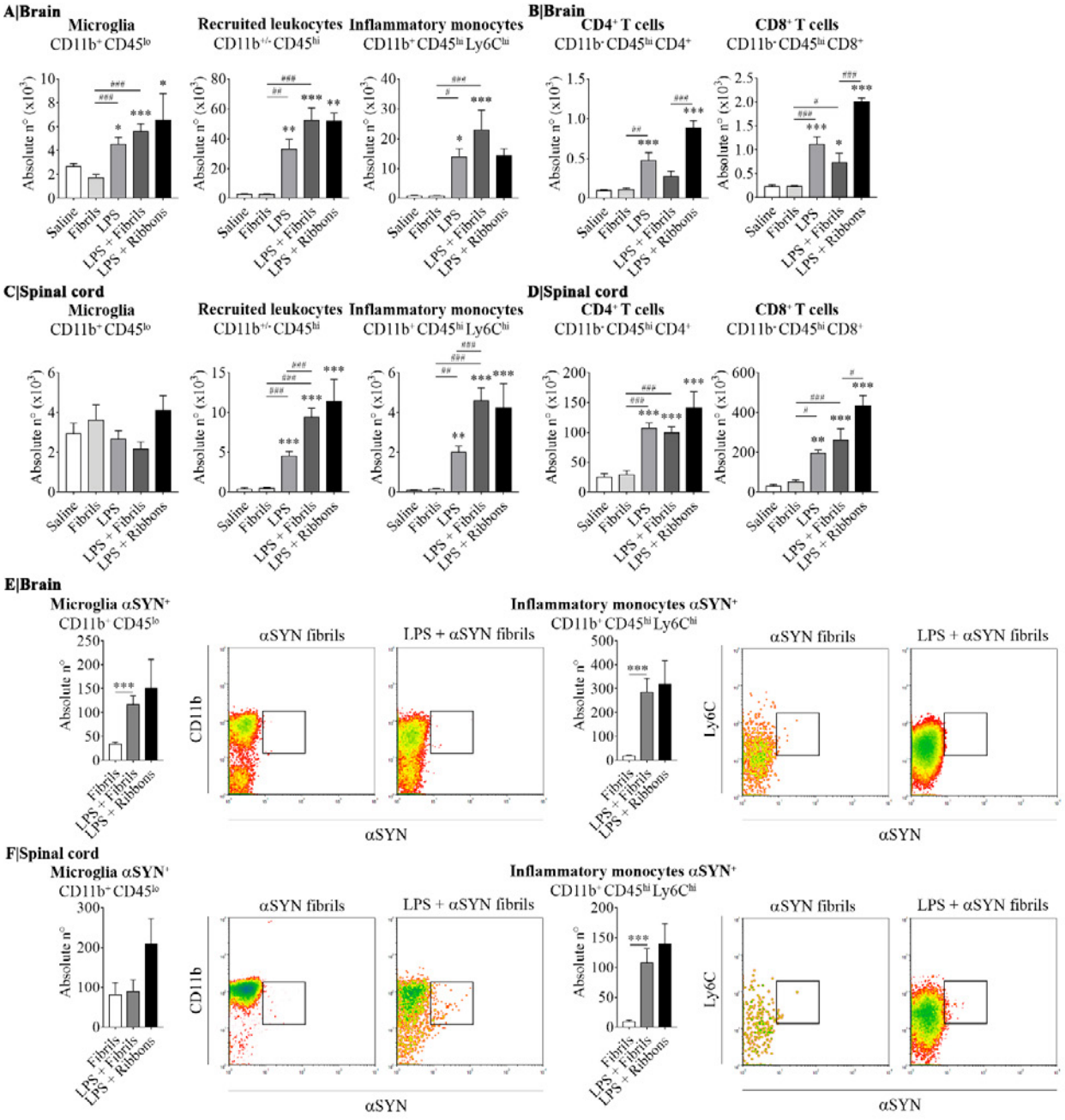

Figure 7 – Flow cytometric analysis of inflammatory cells in the brain and spinal cord after peripheral administration of aSYN assemblies combined with interaperitoneal LPS. Twelve hours after the last injection, mice were euthanised and immune cells were isolated from either whole brain **(A, B)** or spinal cord **(C, D)** and stained for subsequent flow cytometric analysis. Absolute numbers of CD11b^{+} CD45^{lo} microglial cells, CD11b$^{+/-}$ CD45^{hi} recruited cells, CD11b^{+} CD45^{hi} Ly6C^{hi} inflammatory monocytes, CD11b^{-} CD45^{hi} CD4^{+} and CD11b^{-} CD45^{hi} CD8^{+} lymphocytes were assessed by flow cytometry. Absolute numbers of αSYN-internalized CD11b^{+} CD45^{lo} microglial cells or CD11b^{+} CD45^{hi} Ly6C^{hi} inflammatory monocytes purified from brain **(E)** or spinal cord **(F)**, were assessed by flow cytometry. Results are representative of two independent experiments combined (n= 3-4 animals per group). Representative CD11b vs. αSYN and Ly6C vs. αSYN density-plots illustrate the gating analysis strategy employed for microglial cells and inflammatory monocytes, when gated in CD45^{lo} or CD45^{hi} cells respectively. Data are expressed as mean ± s.e.m. Means between groups were compared with one-way analysis of variance followed by a Tukey's *post hoc* test. Statistical significance levels were set as follows: $^{*/\#}$ if $p < 0.05$, $^{**/\#\#}$ if $p < 0.01$, and $^{***/\#\#\#}$ if $p < 0.001$. The asterisks indicate the comparison against the saline-treated group. (Peralta Ramos et al. Frontiers in Immunology January 2019).

2.3. Manipulation of the microglial response

To better understand the role of the innate immune system in αSYN spreading and neurotoxicity, we will experimentally deplete the microglia using a CSF1R inhibitor (PLX3397) in the CX3CR1^{GFP}/CCR2^{RFP} transgenic mice. To investigate the effect of microglial depletion on αSYN induced neuronal cell death, CX3CR1^{GFP}/CCR2^{RFP} transgenic mice will be stereotactically injected with rAAV αSYN vector into the SN. In this experimental set-up, we will analyze the impact of microglial cell depletion on neurodegeneration

as well as motor behavior, six weeks post injection. In a second approach, we will assess the involvement of the innate immune system in αSYN spreading. Therefore, recombinant αSYN assemblies (fibrils or ribbons), will be administered to CX3CR1^{GFP}/CCR2^{RFP} transgenic mice through different routes: directly into the brain or peripherally into the blood stream. Subsequent pathology will be assessed using immunohistochemical analysis to examine αSYN aggregation and spreading. Moreover, we will study the effect of microglia depletion on other cell types present in the central nervous system (neurons and astrocytes) and in the periphery (macrophages) via immunocytochemistry and flow cytometry. Finally, we will investigate whether the absence of microglia alters the adaptive immune response by analyzing and quantifying T cell infiltration in the brain by immunohistochemistry and flow cytometry. We plan to start a pilot study later this year to check the microglia depletion in naïve animals after 7 days and six weeks.

4. Scientific communication

We have presented our intermediate results at international conferences and meetings. We are currently writing down our results and plan to publish in highly-ranked peer-reviewed scientific journals.

4.1. Publications

- Gelders G, Baekelandt V and Van der Perren A, (2018) **Linking Neuroinflammation and Neurodegeneration in Parkinson's disease,** Journal of Immunology Research, Special Issue: "Immune and Inflammatory-Mediated Disorders: From Bench to Bedside", 2018:4784268.
- Peelaerts W., Bousset L. , Baekelandt V. and Melki R. (2018) **α-Synuclein Strains and Seeding in Parkinson's Disease, Incidental Lewy Body Disease, Dementia with Lewy Bodies and Multiple System Atrophy: Similarities and Differences.** *Cell and Tissue Research* (Special Issue Parkinson´s disease Molecules, cells, and circuitries), 373(1):195-212
- Veys L, Vandenabeele M, Ortuño-Lizarán I, Baekelandt V, Cuenca N, Moons L, De Groef L (2019) **Retinal alpha-synuclein deposits in Parkinson's disease patients and animal models.** *Acta Neuropathologica,* in press
- Peralta Ramos J, Iribarren P, Bousset L, Melki R, Baekelandt V, Van der Perren A. (2019) **Peripheral inflammation regulates CNS immune surveillance through the recruitment of inflammatory monocytes upon systemic α-synuclein administration.** Frontiers in Immunology, January 2019, *in press*.

4.2. List of conferences and meetings

- Van der Perren A, Gelders G, Macchi F, Peelaerts W, Bousset L, Van den Haute C, Melki R and Baekelandt V. Differential response of microglia to distinct alpha-synuclein assemblies.
  Alzheimer Disease & Parkinson's Disease (ADPD) meeting, Vienna, Austria, March 29 - April 2 2017. Poster presentation
- Van der Perren A, Gelders G, Macchi F, Peelaerts W, Bousset L, Van den Haute C, Melki R and Baekelandt V. Differential response of microglia to distinct alpha-synuclein assemblies.
  Venusberg Meeting on Neuroinflammation, Bonn, Germany, May 11-15 2017. Poster presentation
- Van der Perren A, Gelders G, Macchi F, Peelaerts W, Bousset L, Van den Haute C, Melki R and Baekelandt V. Differential response of microglia to distinct alpha-synuclein assemblies.
  12th National Congress of the Belgian Society for Neuroscience, Ghent, Belgium, May 22 2017. Poster presentation
- Van der Perren A, Gelders G, Macchi F, Peelaerts W, Bousset L, Van den Haute C, Melki R and Baekelandt V. Differential response of microglia to distinct alpha-synuclein assemblies.
  20 years of alpha-synuclein in Parkinson's disease and other related synucleinopathies. "From the bedside to the bench and back to the patient". Athens, Greece, September 7-10 2017. Poster presentation
- Baekelandt V. Systemic transmission of alpha-synuclein strains. Invited speaker at «20 years of alpha-synuclein in Parkinson's Disease and related synucleinopathies: from the bedside to the bench and back to the patient», Athens, Greece, 7-10 Sept 2017
- Baekelandt V. Modeling alpha-synuclein aggregation, propagation and neurotoxicity in rodent brain. Invited speaker at the **Research Summer School within the EU-Project BrainMatTrain**, Galway, Ireland, 9-10 Oct 2017
- Van der Perren A, Gelders G, Macchi F, Peelaerts W, Bousset L, Van den Haute C, Melki R and Baekelandt V. Differential response of microglia to distinct alpha-synuclein assemblies.
  Neuroscience meeting (SFN), Washington DC, US, November 9-15 2017. Selected for dynamic poster presentation
- Baekelandt V. Modeling alpha-synuclein aggregation, propagation and neurotoxicity in rodent brain. Invited speaker at the **NECTAR meeting**, Dublin, Ireland, 6-8 Dec 2017

– Van der Perren A, Gelders G, Macchi F, Peelaerts W, Bousset L, Van den Haute C, Melki R and Baekelandt V. Differential response of microglia to distinct alpha-synuclein assemblies.
Keystone Meeting, Keystone, US, June 17-21 2018. Poster presentation
– Gelders G, **CAJAL Advanced Neuroscience Training Programme: Neuroinflammation and How to Study It**, Bordeaux, France, June 25 – July 7 2018. Summer School
– Van der Perren A, Gelders G, Fenyi A, Bousset L, Brito F, Peelaerts W, Gentleman S, Melki R, Baekelandt V. In vivo characterization of distinct patient-derived alpha-synuclein strains.
Cold Spring Harbor, New York, US, November 28 – December 1 2018. Poster presentation
– Van der Perren A, Gelders G, Fenyi A, Bousset L, Brito F, Peelaerts W, Gentleman S, Melki R, Baekelandt V. In vivo characterization of distinct patient-derived alpha-synuclein strains.
AD/PD 2019, Lisbon, Portugal, March 26-31 2019. Selected for oral presentation
– Baekelandt V. Invited speaker at the **Synuclein meeting 2019**, 1-4 Sept 2019, Porto, Portugal

5. References

1. Braak, H. & Braak, E. Neuropathological stageing of Alzheimer-related changes. *Acta Neuropathol* **82**, 239-259 (1991).
2. Braak, H. *et al.* Staging of brain pathology related to sporadic Parkinson's disease. *Neurobiol Aging* **24**, 197-211 (2003).
3. Hansen, C. *et al.* α-Synuclein propagates from mouse brain to grafted dopaminergic neurons and seeds aggregation in cultured human cells. *J Clin Invest* **121**, 715-725, doi:10.1172/JCI43366 (2011).
4. Bousset, L. *et al.* Structural and functional characterization of two alpha-synuclein strains. *Nat Commun* **4**, 2575, doi:10.1038/ncomms3575 (2013).
5. Peelaerts, W. *et al.* α-Synuclein strains cause distinct synucleinopathies after local and systemic administration. *Nature* **522**, 340-344, doi:10.1038/nature14547 (2015).
6. Guo, J. L. *et al.* Distinct α-synuclein strains differentially promote tau inclusions in neurons. *Cell* **154**, 103-117, doi:10.1016/j.cell.2013.05.057 (2013).
7. Stöhr, J. *et al.* Distinct synthetic Aβ prion strains producing different amyloid deposits in bigenic mice. *Proc Natl Acad Sci U S A* **111**, 10329-10334, doi:10.1073/pnas.1408968111 (2014).
8. Hirsch, E. C. & Hunot, S. Neuroinflammation in Parkinson's disease: a target for neuroprotection? *Lancet Neurol* **8**, 382-397, doi:10.1016/S1474-4422(09)70062-6 (2009).
9. Gelders, G., Baekelandt, V. & Van der Perren, A. Linking Neuroinflammation and Neurodegeneration in Parkinson's Disease. *J Immunol Res* **2018**, 4784268, doi:10.1155/2018/4784268 (2018).
10. Heneka, M. T. *et al.* NLRP3 is activated in Alzheimer's disease and contributes to pathology in APP/PS1 mice. *Nature* **493**, 674-678, doi:10.1038/nature11729 (2013).
11. McGeer, P. L., Itagaki, S., Boyes, B. E. & McGeer, E. G. Reactive microglia are positive for HLA-DR in the substantia nigra of Parkinson's and Alzheimer's disease brains. *Neurology* **38**, 1285-1291 (1988).
12. Holmans, P. *et al.* A pathway-based analysis provides additional support for an immune-related genetic susceptibility to Parkinson's disease. *Hum Mol Genet* **22**, 1039-1049, doi:10.1093/hmg/dds492 (2013).
13. Tansey, M. G. & Goldberg, M. S. Neuroinflammation in Parkinson's disease: its role in neuronal death and implications for therapeutic intervention. *Neurobiol Dis* **37**, 510-518, doi:10.1016/j.nbd.2009.11.004 (2010).
14. Gerhard, A. *et al.* In vivo imaging of microglial activation with [11C](R)-PK11195 PET in idiopathic Parkinson's disease. *Neurobiol Dis* **21**, 404-412, doi:10.1016/j.nbd.2005.08.002 (2006).
15. Li, J. Y. *et al.* Lewy bodies in grafted neurons in subjects with Parkinson's disease suggest host-to-graft disease propagation. *Nature medicine* **14**, 501-503, doi:10.1038/nm1746 (2008).
16. Kordower, J. H., Chu, Y., Hauser, R. A., Freeman, T. B. & Olanow, C. W. Lewy body-like pathology in long-term embryonic nigral transplants in Parkinson's disease. *Nature medicine* **14**, 504-506, doi:10.1038/nm1747 (2008).
17. Olanow, C. W. & Prusiner, S. B. Is Parkinson's disease a prion disorder? *Proc Natl Acad Sci U S A* **106**, 12571-12572, doi:10.1073/pnas.0906759106 (2009).
18. Peelaerts, W. *et al.* alpha-Synuclein strains cause distinct synucleinopathies after local and systemic administration. *Nature* **522**, 340-344, doi:10.1038/nature14547 (2015).

Geneeskundige Stichting Koningin Elisabeth
Fondation Médicale Reine Elisabeth
Königin-Elisabeth-Stiftung für Medizin
Queen Elisabeth Medical Foundation

Progress report of the research group of

Prof. dr. De Bundel Dimitri, PhD

Vrije Universiteit Brussel (VUB)

Principal investigator

Prof. dr. Dimitri De Bundel

Co-investigators

Prof. dr. Ilse Smolders
Prof. dr. Ann Van Eeckhaut

Research Group Experimental Pharmacology, Center for Neurosciences
Department of Pharmaceutical and Pharmacological Sciences
Vrije Universiteit Brussel
Laarbeeklaan 103
1090 Brussels

Neuromedin U involvement in stress-induced psychopathology

1. Stress and the hypothalamus-pituitary-adrenal axis

The brain is the central organ for adaptation to psychobiological stressors because it determines what is threatening, stores relevant memories, and regulates physiological and behavioural responses (1). These allostatic responses enable an organism to actively adapt to its changing environment and achieve stability. Activation of the hypothalamus-pituitary-adrenal-axis (HPA axis) is a key physiological allostatic process characterized by release of corticotropin-releasing hormone (CRH) from the hypothalamic paraventricular nucleus (PVH), adrenocorticotropic hormone (ACTH) from the pituitary and glucocorticoids such as cortisol and corticosterone (CORT) from the adrenal cortex (1). Release of glucocorticoids initiates a series of cardiovascular, metabolic and behavioural coping mechanisms. However, when allostatic load exceeds the physiological regulatory capacity, due to the unpredictable or uncontrollable nature of stressors, HPA axis activity can become maladaptive, leading to inappropriate physiological and behavioural responses that may impede coping and recovery (1, 2). Not surprisingly, stress has been identified as a major risk factor for the development of cardiovascular, metabolic and mental disorders (3-5). More specifically, excessive HPA axis activation following stress exposure is associated with alterations in neuronal activity, changes in spine morphology, dendritic remodelling, suppression of dentate gyrus neurogenesis, and inappropriate behavioural responses that are proposed to be core features in the aetiology of psychiatric disorders such as post-traumatic stress disorder and major depression (6). Neuropeptides are typically released by discrete neuronal populations and may enable diversified physiological and behavioural responses to a wide range of stressors through their specific projections in the brain.

Position	**1**	**2**	**3**	**4**	**5**	**6**	**7**	**8**	**9**	**10**	**11**	**12**	**13**	**14**	**15**	**16**	**17**	**18**	**19**	**20**	**21**	**22**	**23**	**24**	**25**
Human NMU-25	Phe	Arg	Val	Asp	Glu	Glu	Phe	Gln	Ser	Pro	Phe	Ala	Ser	Gln	Ser	Arg	Gly	Tyr	**Phe**	**Leu**	**Phe**	**Arg**	**Pro**	**Arg**	**Asn**	NH_2
Rat NMU-23	Tyr	Lys	Val	Asn	Glu	*	–	Tyr	Gln	Gly	Pro	*	–	Val	Ala	Pro	Ser	Gly	Gly	Phe	**Phe**	**Leu**	**Phe**	**Arg**	**Pro**	**Arg**	**Asn**	NH_2
Mouse NMU-23	Phe	Lys	Ala	*	–	Glu	*	–	Tyr	Gln	Ser	Pro	Ser	Val	Gly	Gln	Ser	Lys	Gly	Tyr	**Phe**	**Leu**	**Phe**	**Arg**	**Pro**	**Arg**	**Asn**	NH_2

Figure 1. *The structure of NMU in distinct species. The highly conserved C-terminus is shown in bold. Structural homology between human, rat and mouse sequences is emphasized by elongation with gaps represented by an asterix (*). Adapted from (7)*

2. Neuromedin U and the stress response

Neuromedin U (NMU) is a neuropeptide coded by the Nmu gene showing a remarkable amino acid sequence homology across mammals (7), suggesting a strong evolutionary pressure to maintaining its structure and function (Figure 1). The C-terminal amidated heptapeptide is entirely conserved in mammals and the C-terminal amidated octapeptide NMU-8 exerts the same biological effects as its longer endogenous isoforms, NMU-25 in humans or NMU-23 in rodents (7). NMU-like immunoreactivity has been detected in neurons of the brain, spinal cord and mesenteric plexus (7). NMU activates two G-protein coupled receptors: NMUR1 receptors that are mainly expressed in the periphery and NMUR2 receptors that mainly expressed in the brain and spinal cord (8, 9). NMU was previously demonstrated to modulate food intake and stress responsiveness through activation of hypothalamic NMUR2 receptors (8, 10-13). Nevertheless, precise anatomical knowledge remains lacking and in-depth insight in the role of NMU systems in the brain remains hampered by the lack of specific and sensitive research tools. For this reason, we developed a knock-in mouse model expressing Cre recombinase under the Nmu promotor to enable a highly specific expression of proteins for anatomical and physiological characterization of NMU-producing cells based on tools exploiting Cre-lox recombination.

3.1. Behavioural effects of central administration of NMU-8

We investigated the effects of central administration of NMU-8 on stress-related behaviour in the home cage and in the forced swim test. We observed an increase in grooming behaviour following intracerebroventricular (i.c.v.) administration of NMU-8 but no significant effects on digging activity or overall locomotor activity (Figure 2 A-C). NMU-induced grooming behaviour was previously observed in rats and was attributed to activation of the HPA axis (13). We next investigated whether central NMU-8 administration increased stress vulnerability in the forced swim test. We found that i.c.v. administration of NMU-8 increased immobility without significant effect on swimming or climbing in the forced swim test in naïve mice (Figure 2 D-F). Our findings contrasted with a previous study in which i.c.v. administration of NMU-23 was found to decrease immobility while increasing climbing and swimming time in a modified version of the forced swim test (14). Here, mice were exposed to an additional forced swim session one day before the forced swim test (14). However, using these experimental conditions, we found that NMU-8 increased immobility, while not significantly affecting swimming or climbing in mice that were pre-exposed to forced swim stress one day prior to the forced swim test (Figure 2 G-H). Taken together, our results demonstrate that central administration of NMU-8 increases stress-related behaviour in the home cage and stress-related behaviour in the forced swim test in mice. We hypothesize that blocking NMU function in the brain may be beneficial in stress-related mental disorders such as depression. In subsequent experiments we explored the mechanism through which NMU-8 may exert its central effects.

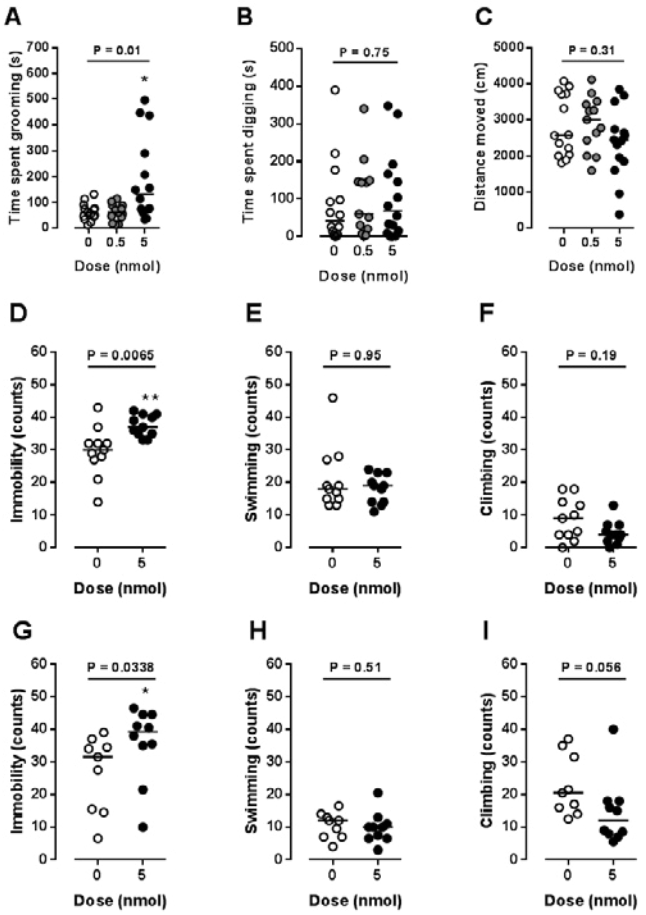

Figure 2. *Effects of i.c.v. administration of NMU-8 on stress-related behaviour in C57BL6/J mice. Intracerebroventricular (i.c.v.) administration of vehicle or NMU-8 was carried out at the onset of a 20 min observation period and the total time spent grooming, digging and the total distance moved were scored by an observer blinded to treatment while mice remained in the home cage (A-C). In a separate series of experiments, we investigated the effect of i.c.v. administration of NMU-8 on immobility, swimming and climbing behaviour in a 5 min forced swim test in naïve mice (D-F) or in mice exposed to a 15 min forced swim session one day before the 5 min forced swim test session (G-I). NMU-8 was administered 20 min before the forced swim test. Data are presented as a dot blot for individual values with designation of the median and N=10-11 per group. * P<0.05 versus vehicle controls analysed by a Mann-Whitney test.*

3.2. Neuroanatomical activity mapping following central administration of NMU-8

We used an immunohistochemical approach to map neuronal activation following i.c.v. administration of NMU-8 using c-Fos immunoreactivity as a marker for neuronal activation. We found that NMU-8 affected c-Fos expression in the paraventricular hypothalamus (PVH, Figure 3, top panels) and in the arcuate nucleus (ARC, Figure 3, bottom panels). Indeed, NMU-8 significantly and consistently increased c-Fos expression in the PVH and ARC of mice that remained in the home cage (Figure 3 A,D).

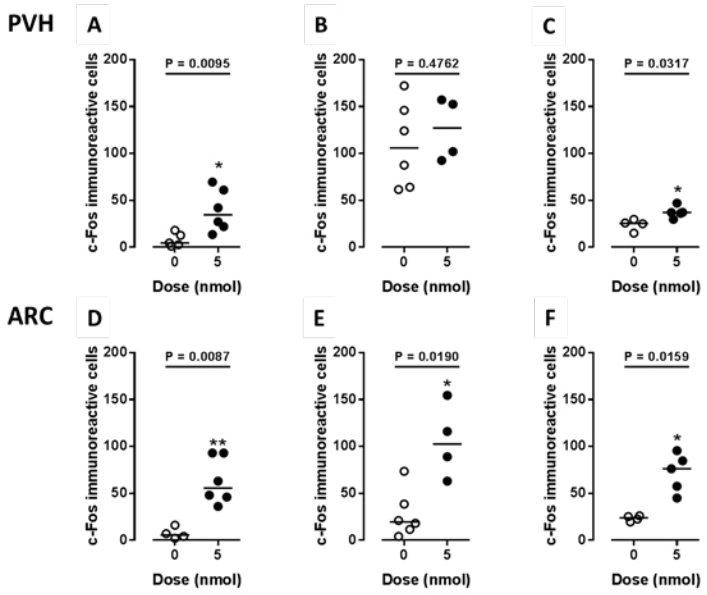

Figure 3. *Effects of central administration of NMU-8 on expression of the immediately early gene c-Fos in the paraventricular hypothalamus (PVH), and in the arcuate nucleus (ARC) of C57BL6/J mice. Quantification by an observer blinded to treatment shows that intracerebroventricular (i.c.v.) administration of NMU-8 (5 nmol) differentially affected the amount of c-Fos immunoreactive cells in both the ARC and PVH of mice that remained in their home cage (A,D), mice subjected to a single forced swim test (B,E) or mice subjected to 15 min forced swim session one day before the forced swim test (C,F). NMU-8 was administered 20 min before the forced swim test. Mice were sacrificed 90 min after administration of NMU-8. Data are represented as a dot plot for individual values with designation of the median value and N=4-6 per group. * P<0.05 and **P<0.01 versus vehicle (0 nmol) analysed by Mann-Whitney test.*

We next investigated whether NMU-8 administration further affected c-Fos expression when mice were subjected to a stressful experience. Following a single forced swim test, baseline c-Fos expression was high in the PVH but not in the ARC. Consequently, NMU-8 did not significantly increase c-Fos levels in the PVH but it increased c-Fos levels in the ARC (Figure 3 B,E). However, in mice that were pre-exposed to forced swim stress one day prior to the forced swim test, baseline c-Fos expression was low in both the PVH and the ARC. NMU-8 significantly increased c-Fos expression in both the PVH and the ARC (Figure 3 C,F). However, it should be noted that the increase in c-Fos expression in mice previously exposed to stress was less pronounced compared to mice that remained in the homecage. We conclude that i.c.v. administration of NMU-8 increases neuronal activity in the HPA axis under baseline conditions and up to an upper limit under stressful conditions. These data confirm our behavioural observations.

3.3. Plasma corticosterone levels following central administration of NMU-8

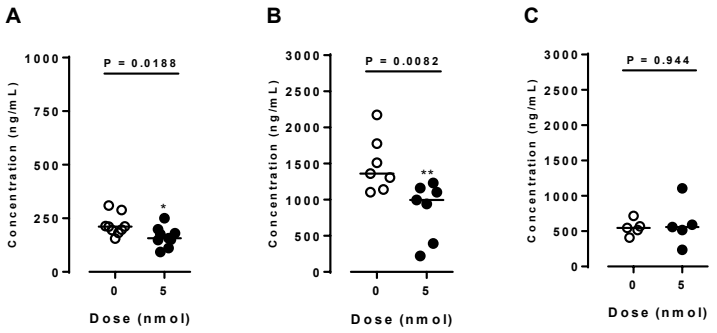

Figure 4. *Effects of central administration of NMU-8 on the plasma concentration of corticosterone. Plasma corticosterone was measured 10 min after i.c.v. administration of NMU-8 in mice remaining in the home cage (A), 10 min after a 5 min forced swim test in naïve mice (B) or 10 min after a 5 min forced swim test in mice that were subjected to a 15 min forced swim session one day earlier (C). Data are represented as a dot plot for individual values with designation of the median value and N=5-7 per group. * P<0.05 and **P<0.01 versus vehicle (0 nmol) analysed by Mann-Whitney test.*

We used an enzyme-linked immunosorbent assay (ELISA) to monitor plasma corticosterone levels following i.c.v. administration of NMU-8. Surprisingly, we observed a small but significant decrease in plasma corticosterone after i.c.v. administration of NMU-8 in mice that remained in the home cage (Figure 4 A). Similarly, NMU-8 significantly decreased the high plasma corticosterone concentration observed after a 5 min forced swim test (Figure 4 B). However, we no longer observed a significant decrease in the plasma corticosterone concentration when mice were pre-exposed to a forced swim session prior to the forced swim test (Figure 4 C). Presently, it remains unclear how i.c.v. administration of NMU-8 may decrease plasma corticosterone levels. We propose that central administration of

NMU-8 elicits a negative feedback signal towards peripheral corticosterone production while increasing stress-related signalling in the brain and the resulting behaviours. In line with this notion, NMU-8 no longer induced a decrease in the plasma corticosterone concentration when mice were previously exposed to a forced swim session and a negative feedback signal is expected to be set already.

3.4. Neuroanatomical characterization of NMU-expressing cells in the central nervous system

We generated a B6.NmuCre-IRES-Nmu knock-in mouse model constitutively expressing a Cre recombinase in NMU-producing cells in collaboration with Dr. Peter Boyd (GeneOway, France). This was achieved by insertion of Cre-IRES-Nmu cDNA in frame with the ATG coding sequence of the *Nmu* gene on chromosome 5qC3.3. We obtained offspring of crossings between heterozygous B6.NmuCre-IRES-Nmu mice and homozygous B6.*ROSA26RCL-ZsGreen1* reporter mice that harbour a targeted mutation of the ROSA26 gene locus with a loxP-flanked STOP cassette preventing transcription of a CAG promotor-driven enhanced green fluorescent protein (ZsGreen1). In these *Nmu:ZsGreen1* mice, we observed ZsGreen1 marked neurons throughout the neocortex and in a selected set of subcortical structures such as the ventromedial hypothalamus (VMH) (Figure 5 A,B). ZsGreen1 expression appeared stable and consistent in both male and female *Nmu:ZsGreen1 mice*. We are presently finalizing the design of a fluorescent probe to carry out fluorescence in situ hybridization (FISH) to cross-validate Cre expression in our NmuCre-IRE-Nmu knock-in model in collaboration with Dr. Eve Seuntjens (Dept…, KULeuven). We have carried out preliminary experiments to carry out a complete mapping of cells expressing ZsGreen1 under the NMU promotor in both male and female *Nmu:ZsGreen1* mice. Interestingly, NMU neurons appear to constitute a distinct population of hypothalamic cells (Figure 5 C-D). We observed no overlap with POMC expressing cells or NPY expressing cells and a limited overlap with ER1a expressing cells. We are presently carrying out additional experiments to further characterize NMU cells.

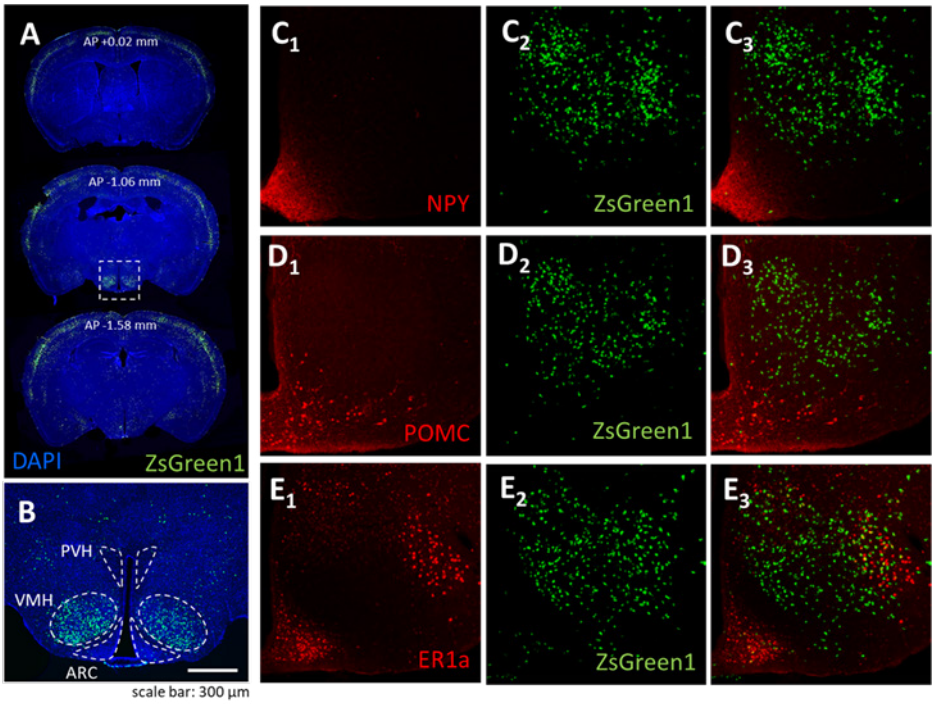

Figure 5. *Characterization of ZSGreen1 expression in Nmu:Zsgreen. Overview of ZsGreen1 expression mice using 4',6-diamidino-2-phenylindole (DAPI) to mark cellular nuclei on coronal mouse brain sections (A) and expression in the mouse hypothalamus (B). Labelling of Nmu:ZsGreen1 mouse brain sections with antibodies against neuropeptide Y (NPY), proopiomelanocortin (POMC) and estrogen receptor 1a (ER1a). PVH: paraventricular hypothalamus, VMH: ventromedial hypothalamus, ARC: arcuate nucleus.*

3.5. Chemogenetic modulation of hypothalamic NMU neurons.

Ultimately, we aim to investigate the behavioural effects of direct manipulation of NMU expressing cells in the mouse hypothalamus using chemogenetic intervention. We obtained the commercially available adeno-associated viral (AAV) control vector AAV8-DIO-mCherry and DREADD (Designer Receptor Exclusively Activated by Designer Drugs) vectors AAV8-DIO-hM3Dq-mCherry or AAV8-DIO-hM4Di-mCherry. These vectors use a Cre-dependent expression system based on a double-inverted open (DIO) reading frame sequence, to drive expression of a red fluorescent protein (mCherry) and engineered human muscarinic receptors, hM4Di (Gi-coupled) or hM3Dq (Gq-coupled) DREADDs specifically by Cre-containing neurons, in our case NMU neurons (Figure 6 A).. We carried out initial experiments demonstrating that mCherry is expressed in *ZsGreen1* expressing neurons of Nmu:ZsGreen1 mice following local infusion of the AAV8-DIO-mCherry control virus into the hypothalamus (Figure 6 B-D). We will now target the hypothalamus of NMU:Cre mice using our active DREADD AAV constructs to carry out behavioural experiments. Initially, we will carry out chronic experiments to understand how NMU affects global activity and food intake. Hereto, mice will be monitored in their home cage by using telemetric running wheels and daily body weight recordings. For time reasons we will not carry out the social defeat model but will elaborate our earlier findings on stress-related behaviour by investigating the effects of activation and inactivation of hypothalamic NMU neurons in the forced swim test

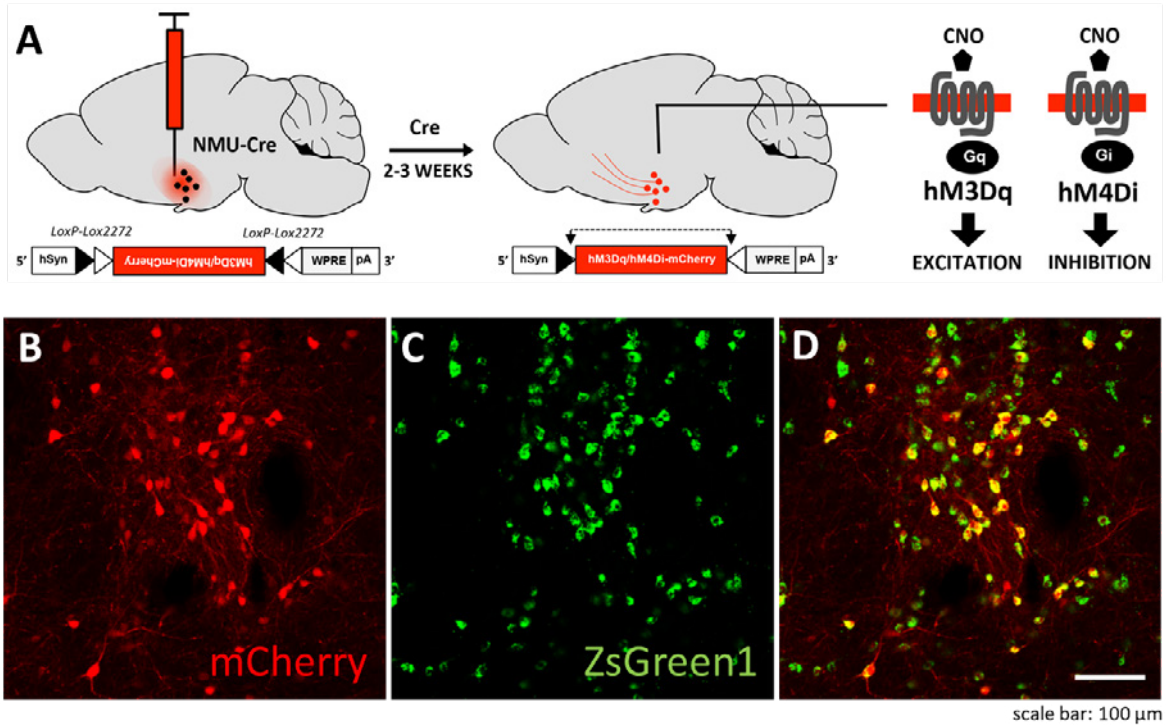

Figure 6. *Chemogenetic strategy to drive the expression of excitatory (hM3Dq) DREADDs or inhibitory (hM4Di) DREADDs specifically in hypothalamic NMU neurons. Expression is based on local infusion of an AAV8 viral vector and recombination of the DIO sequences (LoxP-Lox2272) by Cre expressed in NMU neurons leading to expression of a red fluorescent protein (mCherry) and the DREADD of choice. Systemic injection of clozapine-N-oxide (CNO) specifically activates the DREADDs and excites or inhibits the neurons in which they are expressed (A). Representative images showing mCherry labelled cells (A), ZsGreen1 labelled cells (B) and co-expression of mCherry and ZsGreen1 following administration of an AAV8-DIO-mCherry control virus in the ventral hypothalamus of Nmu:ZsGreen1 mice.*

3.6. Optimization of nanoUHPLC-MS/MS parameters for NMU quantification

We also aim to investigate NMU release in targeted brain areas following direct manipulation of NMU-containing neurons. We will adopt an optogenetic approach using Cre-dependent expression of channel rhodopsin (ChR2), a yellow light-sensitive cation channel, in B6.NmuCre-IRES-Nmu mice. ChR2 expression will permit stimulating NMU-containing cells at a specific frequency (1-20 Hz) using an implanted optical fibre connected to an appropriate light-source. NMU release will be determined by intracerebral microdialysis and miniaturized UHPLC-MS/MS. Recently, we have acquired a NanoAcquity NanoUPLChip (IonKey) system coupled to the most recent and most sensitive triple quadrupole mass

spectrometer (Xevo TQ-QS; both Waters) through funding from the Hercules Foundation, opening new opportunities to obtain unpreceded sensitivity in very small sample volumes (≤ 20 µL). We are developing a microchip-electrospray ionization (ESI)-tandem mass spectrometry (MS/MS) method with detection limits in the low picomolar range (attomole on column) for the quantification of NMU in volume-restricted samples, namely mouse brain microdialysates. The development of this method for the quantification of endogenous, sub-picomolar levels of neuropeptide in small sample volumes remains very demanding. Optimization of all chromatographic, ionization and MS/MS parameters is crucial to obtain the highest sensitivity possible.

One of the causes of lower sensitivity is that the peptide ion current is divided amongst multiple charge states that are commonly observed in ESI. The acquisition of multiple charge states splits the available ion current for the peptide into parts which is severely detrimental for quantitative and sensitive analyses. Moreover, sensitivity is negatively affected by a more pronounced increased background noise level when monitoring multiple transitions at the time. Supercharging agents allow modifying the maximal charge state and the corresponding distribution of charges, thereby potentially increasing the number of ions reaching the detector in selected reaction monitoring mode. The tetravalent charged precursor of NMU was selected as charge state of interest based on its abundancy and the production of stable fragment ions, suitable for quantification. We examined the effect of different superchargers and their simultaneous presence on the ionization of NMU and defined optimal conditions for the signal-to-noise ratio for a given concentration (Figure 7). The results of this study are under revision for publication in Talanta (15)

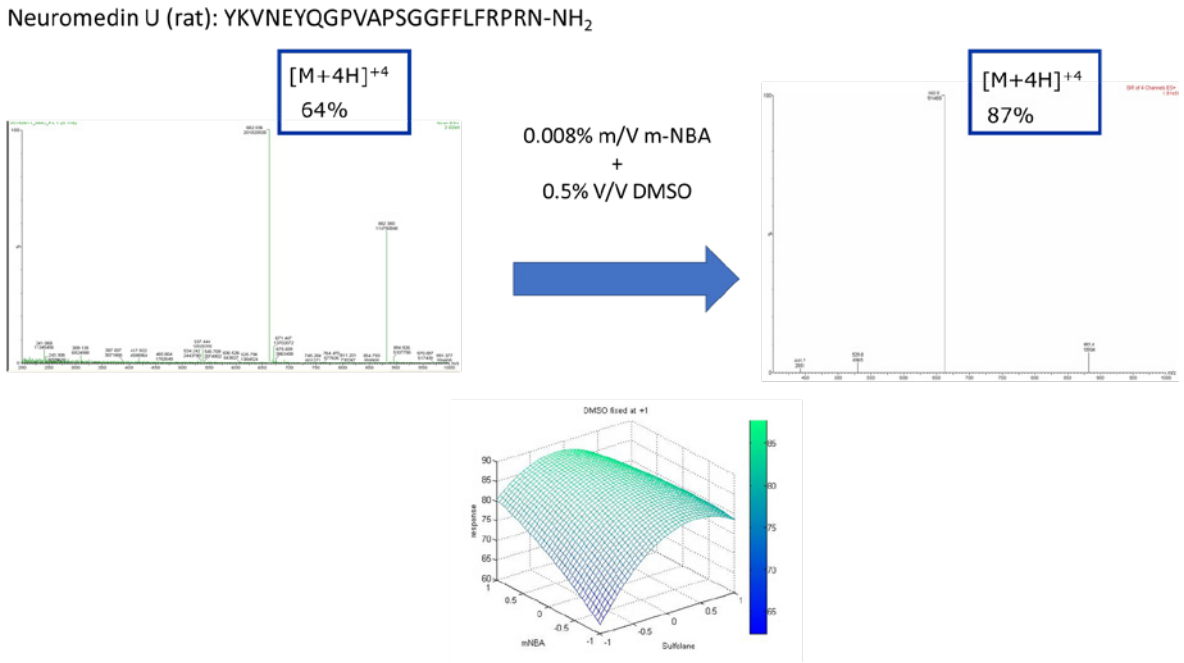

Figure 7. *Optimization of the supercharger composition to improve the signal-to-noise ratio for a given concentration of NMU.*

3.7. In search for potent NMUR2 antagonists

As stated above our current hypothesis suggests that central NMUR2 antagonists could reduce or normalize the functioning of the hypothalamus-pituitary-adrenal axis at the level of the paraventricular nucleus. An elaborate structure-activity relationship study was performed around the NMU-8 sequence aiming for the development of potent, proteolytically stable and NMUR-subtype selective ligands, leading ultimately into the synthesis of NMUR2 antagonists A broad range of NMU-8 analogs have been developed, but unfortunately all displayed agonist properties (16, 17). One of the most promising potent and proteolytic stable NMU agonists has been tested for its anorexigenic properties, a function ascribed to NMUR agonists, in a food intake study and was found to significantly reduce food consumption. Our search for a pharmacological ligand antagonizing NMUR2 is still ongoing.

4. References

1. McEwen BS, et al. (2015) Mechanisms of stress in the brain. Nature neuroscience 18(10):1353-1363.
2. Koolhaas JM, et al. (2011) Stress revisited: a critical evaluation of the stress concept. Neuroscience and biobehavioral reviews 35(5):1291-1301.
3. Steptoe A (2016) Diabetes: Stress resilience and risk of type 2 diabetes mellitus. Nature reviews. Endocrinology 12(4):189-190.
4. Steptoe A & Kivimaki M (2012) Stress and cardiovascular disease. Nature reviews. Cardiology 9(6):360-370.
5. Pittenger C & Duman RS (2008) Stress, depression, and neuroplasticity: a convergence of mechanisms. Neuropsychopharmacology : official publication of the American College of Neuropsychopharmacology 33(1):88-109.
6. McEwen BS, Nasca C, & Gray JD (2016) Stress Effects on Neuronal Structure: Hippocampus, Amygdala, and Prefrontal Cortex. Neuropsychopharmacology : official publication of the American College of Neuropsychopharmacology 41(1):3-23.
7. Brighton PJ, Szekeres PG, & Willars GB (2004) Neuromedin U and its receptors: structure, function, and physiological roles. Pharmacological reviews 56(2):231-248.
8. Howard AD, et al. (2000) Identification of receptors for neuromedin U and its role in feeding. Nature 406(6791):70-74.
9. Gartlon J, et al. (2004) Localisation of NMU1R and NMU2R in human and rat central nervous system and effects of neuromedin-U following central administration in rats. Psychopharmacology 177(1-2):1-14.
10. Zeng H, et al. (2006) Neuromedin U receptor 2-deficient mice display differential responses in sensory perception, stress, and feeding. Molecular and cellular biology 26(24):9352-9363.
11. Peier A, et al. (2009) The antiobesity effects of centrally administered neuromedin U and neuromedin S are mediated predominantly by the neuromedin U receptor 2 (NMUR2). Endocrinology 150(7):3101-3109.
12. Graham ES, et al. (2003) Neuromedin U and Neuromedin U receptor-2 expression in the mouse and rat hypothalamus: effects of nutritional status. Journal of neurochemistry 87(5):1165-1173.
13. Hanada R, et al. (2001) A role for neuromedin U in stress response. Biochemical and biophysical research communications 289(1):225-228.
14. Tanaka & Telgedy (2014). Neurotransmissions of antidepressant-like effects of neuromedin U-23 in mice. Behav Brain Res. 259(1):196-9.
15. Van Wanseele et al. Assessing mixtures of supercharging agents to increase the abundancy of a specific charge state of Neuromedin U. Talanta. Under revision
16. De Prins A et al. (2018). Synthesis and in Vitro Evaluation of Stabilized and Selective Neuromedin U-1 Receptor Agonists. ACS Med Chem Lett. 9(5):496-501.
17. De Prins A et al. (2018). Development of potent and proteolytically stable human neuromedin U receptor agonists. Eur J Med Chem. 144:887-897.

5. Publications acknowledging support from G.S.K.E.

Research papers

- Bongaerts J, De Bundel D, Mangelings D, Smolders I, Vander Heyden Y, Van Eeckhaut A. Sensitive targeted methods for brain metabolomics studies in microdialysis samples. J Pharm Biomed Anal. 2018 Nov 30;161:192-205. doi: 10.1016/j.jpba.2018.08.043. Epub 2018 Aug.23. Review.
- De Prins A, Martin C, Van Wanseele Y, Tömböly C, Tourwé D, Caveliers V, Holst B, Van Eeckhaut A, Rosenkilde MM, Smolders I, Ballet S. Synthesis and in Vitro Evaluation of Stabilized and Selective Neuromedin U-1 Receptor Agonists. ACS Med Chem Lett. 2018 Apr 23;9(5):496-501. doi: 10.1021/acsmedchemlett.8b00105. eCollection 2018 May 10.
- De Prins A, Martin C, Van Wanseele Y, Skov LJ, Tömböly C, Tourwé D, Caveliers V, Van Eeckhaut A, Holst B, Rosenkilde MM, Smolders I, Ballet S. Development of potent and proteolytically stable human neuromedin U receptor agonists. Eur J Med Chem. 2018 Jan 20;144:887-897. doi: 10.1016/j.ejmech.2017.12.035. Epub 2017 Dec 14.
- Y. Van Wanseele, J. Viaene, L. Van den Borre, K. Dewachter, Y. Vander Heyden, I. Smolders, A. Van Eeckhaut, LC-method development for the quantification of neuromedin-like peptides. Emphasis on column choice and mobile phase composition. J Pharm Biomed Anal 137, 104-112 (2017); published online EpubApr 15 (10.1016/j.jpba.2017.01.014).
- Y. Van Wanseele, K. Maes, K. Lanckmans, J. Van Schoors, I. Smolders, A. Van Eeckhaut, Surface and Solvent Dependent Adsorption of Three Neuromedin-Like Peptides in Glass and Plastic Syringes. Chromatographia, (2017); published online EpubOctober 12 (10.1007/s10337-017-3397-9).

Doctoral theses

- Development and biological evaluation of neuromedin U analogs as tools for functional elucidation: focus on stress-related disorders. An De Prins, VUB PRESS 2019.
- Miniaturized UHPLC-MS/MS for the in vivo quantification of neuropeptides in microdialysis samples. Yannick Van Wanseele, VUB PRESS 2019.

Geneeskundige Stichting Koningin Elisabeth
Fondation Médicale Reine Elisabeth
Königin-Elisabeth-Stiftung für Medizin
Queen Elisabeth Medical Foundation

Progress report of the research group of

Prof. dr. Ir. De Meyer Simon

Katholieke Universiteit Leuven (KU Leuven)

Principal investigator

Prof. dr. ir. Simon De Meyer
Laboratory for Thrombosis Research
IRF Life Sciences Department of Cardiovascular Sciences
KU Leuven Kulak
E. Sabbelaan 53
8500 Kortrijk
Belgium
Tel.: +32 56 24 62 32
Fax: +32 56 24 69 97
E-mail: simon.demeyer@kuleuven-kortrijk.be
www.kuleuven-kulak.be/irf/thrombosis

Table of contents

Neutrophil extracellular traps: Novel targets for neuroprotection in stroke

1. Summary of the project

Ischemic stroke is one of the leading causes of death and sustained disability worldwide. Blockade of blood flow to the brain by an occlusive thrombus leads to irreversible damage of the associated brain tissue. The **enormous clinical, economic and social burden** of ischemic stroke is in strong contrast with the **limited treatment** options that are currently available. Despite the huge clinical need, only one pharmacological intervention is currently approved: early thrombolysis using the fibrinolytic agent tissue plasminogen activator (t-PA). However, t-PA can only be administered in the limited time window of 4.5 hours post-stroke onset due to the unacceptable risk of cerebral bleeding when treatment is delayed. As a consequence, t-PA treatment is available to less than 10% of patients.[1] Most remarkably, t-PA results in recanalization only in less than half of the patients that receive it and factors that contribute to this so-called **'t-PA resistance'** are not well understood.[2] Furthermore, although timely recanalization of the occluded cerebral artery is fundamental to salvage threatened ischemic brain tissue, reperfusion of the ischemic territory itself can also seriously exacerbate tissue damage by **reperfusion injury**. This problem does not only occur after successful thrombolysis but also often complicates stroke outcome after successful mechanical thrombectomy. Even though reperfusion injury significantly accelerates neurodegeneration, the underlying cellular and molecular interactions are still poorly understood.

It has become clear that both thrombotic and inflammatory pathways are involved in ischemic brain damage, known as "thrombo-inflammation".[3] Without a doubt, neutrophils and especially **neutrophil extracellular traps (NETs)** have recently led to a paradigm shift in various fields. NETs have been discovered by Brinkmann et al. as a novel mechanism by which neutrophils contribute to the innate immune response.[4] Indeed, as a result of a unique form of cell death, dubbed "NETosis", neutrophils **release their chromatin** that is lined with granular components, creating fibrous nets with antimicrobial properties that prevent microorganisms from spreading (Figure 1). Although much of the cell biological mechanisms of NETosis are still being characterized, one essential step is histone citrullination by peptidylarginine deiminase 4 (PAD4).

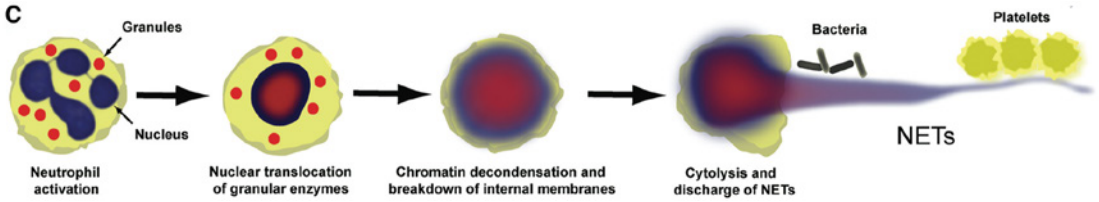

Figure 1: Scheme of NET formation (NETosis) [5] Enzymes such as PAD4 from granules (red) translocate to the nucleus (blue) and facilitate chromatin decondensation. Internal membranes break down and cytolysis releases NETs

PAD4 enters the nucleus to modify histones via hypercitrullination of specific arginine residues on histones H3 and H4. This results in a loss of positive charge from the transformed arginine residues allowing chromatin decondensation (figure 1). Apart from their role in immunity, it has become clear that NETs are also strongly implicated in various thrombotic and thrombo-inflammatory pathologies.[6]

To date, nothing is known yet about the potential effect of NETs in stroke-associated brain damage. Yet, our hypothesis is that, on the one hand, NETs could contribute to cerebral thrombus stabilization preventing fast restoration of cerebral blood flow and, on the other hand, that NETs could further aggragavate brain damage by promoting thrombo-inflammatory reperfusion injury after restoration of

blood vessel patency. The general objective of this research project was to identify NETs as potential new players in the pathophysiology of ischemic stroke in order to develop novel neuorprotective strategies in stroke management.

2. Progress and next steps

In order to successfully complete this project, four delineated work packages (WP) were defined:
- WP1: Nets in thrombi obtained from stroke patients
- WP2: Prothrombolytic capacity of DNAse-1
- WP3: NETs in a mouse model of tMCAO
- WP4: NETs markers in plasma of stroke patients

In this section, the 2-year progress for each work package is detailed, as well as the planned next steps for the last year.

WP 1: NETs in thrombi obtained from stroke patients

The goal of this work package was to assess the presence of NETs in thrombi retrieved from ischemic stroke patients. Recent studies demonstrate that NETs can form a scaffold for platelets and pro-thrombotic plasma proteins and consequently participate in both arterial and venous thrombus formation.[7-10] It is surprising how little is known about the exact composition of thrombi that cause ischemic stroke. Yet, such information is crucial for designing efficient and safe thrombolytic strategies.
To investigate the presence of NETs in thrombi from ischemic stroke patients, we take advantage of the unique opportunity offered by the emergence of cerebral thrombectomy in the clinic. In collaboration of AZ Groeninge hospital in Kortrijk (Prof. Tommy Andersson and Dr. Olivier Francois), more than 250 thrombi retrieved from stroke patients have been collected.
In this work package we already completed and published a first important study.[11] A first set of 68 thrombi retrieved from ischemic stroke patients undergoing endovascular treatment were characterized by immunostaining using neutrophil markers (CD66b and neutrophil elastase) and NETs markers (citrullinated histones H3 (H3Cit) and extracellular DNA).

Observation 1: Neutrophils are abundant in ischemic stroke thrombi

Classically, blood clots are thought to be formed mainly by platelets, fibrin and trapped red blood cells. Upon examination of the stroke thrombi, however, H&E stainings revealed a large number of leukocytes, visible as nucleated cells in all thrombus specimens (Fig. 2A, 2B and 2E). To specifically assess the presence of neutrophils, we stained thrombi samples for the granulocyte marker CD66b (Fig. 2A, 2C and 2F) and for neutrophil elastase (NE, Fig. 2A, 2D and 2G). Neutrophils were abundant in all 68 thrombi, with varying amounts (Fig. 2J and 2K). No differences in neutrophil counts were observed between thrombi with different etiology (Fig. 2J). Interestingly, older thrombi (> 1 day) contained significantly higher amounts of neutrophils (8726 ± 4493 per mm^2) compared to fresh thrombi (< 1 day) (5292 ± 2551 per mm^2, $p < 0.001$, Fig. 2K). In conclusion, these results clearly show a high cellular load of ischemic stroke thrombi with a specific abundance of neutrophils.

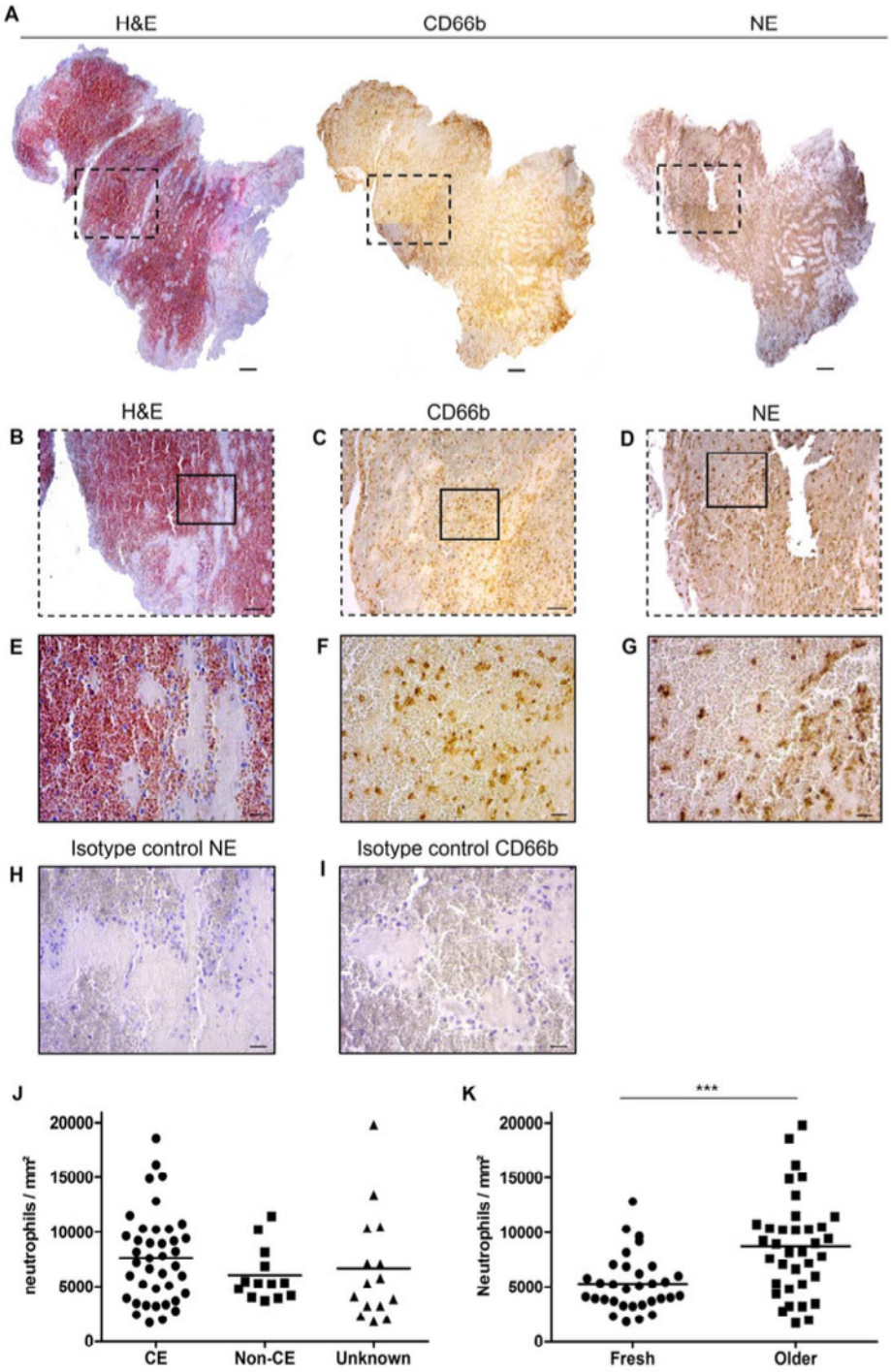

Figure 2: Neutrophils are abundant in ischemic stroke thrombi. To visualize the presence of neutrophils, sections of thrombi retrieved from ischemic stroke patients were stained with H&E and with antibodies against CD66b and neutrophil elastase (NE). Panel (A) shows representative composite images of one thrombus stained for H&E (left), CD66b (middle) and NE (right) (scale bar: 100 µm.). Magnifications show the presence of leukocytes on H&E staining (B) and in particular neutrophils via either CD66b (C) or NE (D) staining. Scale bar: 50 µm. Larger magnifications of these areas are shown for H&E (E), CD66b (F) and NE (G). Scale bar: 10 µm. Isotype control staining is shown for NE (H) and CD66b (I). Scale bar: 10 µm. Neutrophil numbers in thrombi were quantified and are presented according to stroke etiology (J) (CE: cardioembolic, non-CE: non-cardioembolic) and thrombus age (K) (fresh: < 1 day, older: > 1 day). *** $p < 0.001$. Published in Annals of Neurology.[11]

Observation 2: NETs are present in ischemic stroke thrombi

Careful analysis of H&E staining sometimes revealed prominent extracellular nucleic acid rich areas that were located in neutrophil-rich zones (Fig. 3A). We hypothesized that these structures could be NETs. To confirm this hypothesis, thrombus sections were also stained for citrullinated H3 histones (H3Cit), a defining marker of NETs. These stainings revealed that the areas containing extracellular nucleic acids

visible by H&E indeed are rich in citrullinated histones (Fig. 3B). These extensive networks typically also stained positive for NE, further demonstrating their neutrophil origin (Fig. 3C).

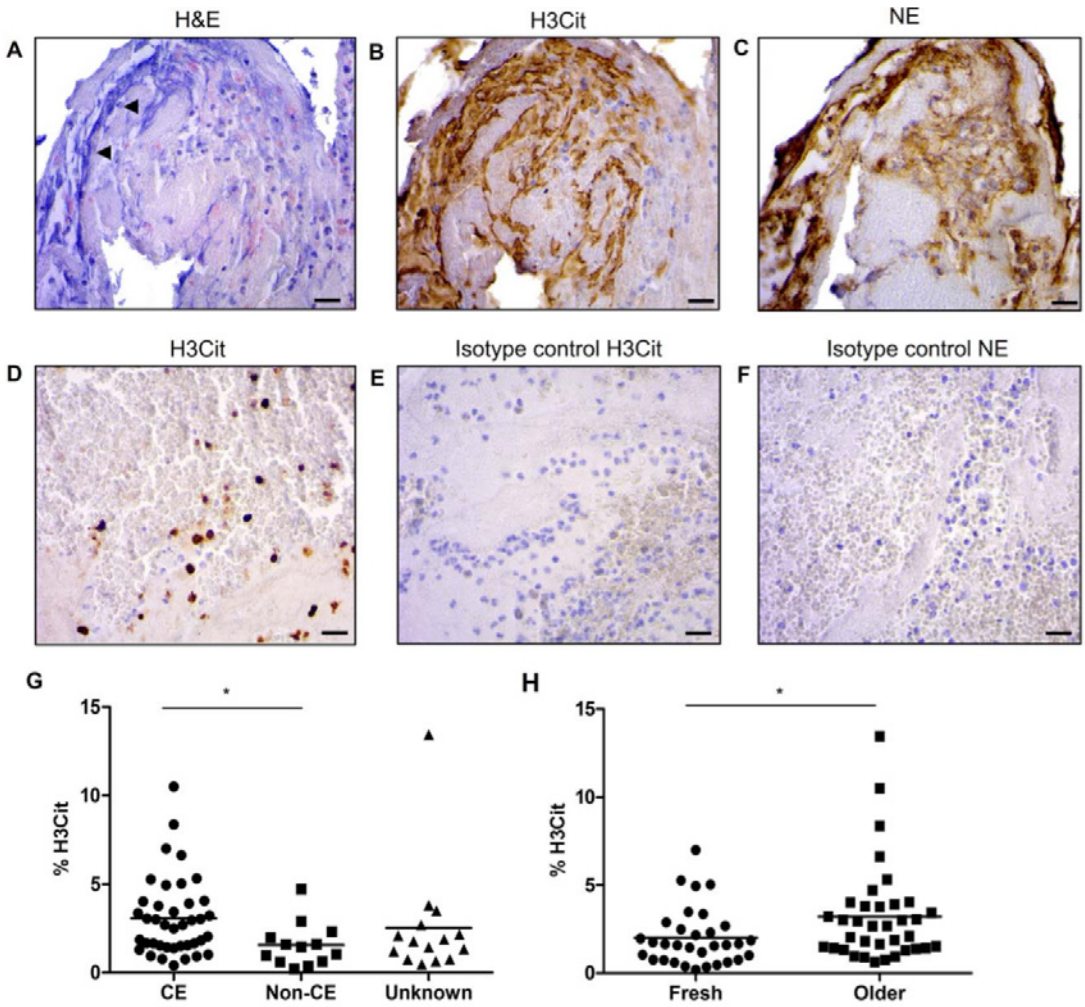

Figure 3: Citrullinated histones reveal the presence of NETs in ischemic stroke thrombi. The presence of citrullinated histones was analyzed via immunohistochemistry using an antibody against H3Cit. Extracellular zones of nuclear material were often observed on H&E stainings (A, arrow heads). These chromatin strands corresponded with areas staining positive for H3Cit (B, brown staining) and NE (C, brown staining). In other places, no extracellular structures were visible and H3Cit-positive signal was observed only intracellularly, indicative of early NETosis processes (D). No H3Cit nor NE signal was present on isotype control stainings (E and F). Scale bars: 10 µm. H3Cit-positive signal was present in all thrombi and quantification of H3Cit staining per thrombus is shown according to stroke etiology (G) (CE: cardioembolic, non-CE: non-cardioembolic) or thrombus age (H) (fresh: < 1 day, older: > 1 day). * $p < 0.05$. Published in Annals of Neurology.[11]

H3Cit-positive signal was found in all thrombi, indicating that NETs are a common component of ischemic stroke thrombi. Besides the presence of neutrophils that had already formed extracellular fibrous NET structures (as e.g. shown in Fig. 3B), thrombi typically also contained neutrophils in the initiation phase of NETosis. These neutrophils show H3Cit-positive chromatin that was still inside cells that had not bursted yet, hence the term intracellular (Fig. 3D). H3Cit quantification showed a broad range of NET amounts among different thrombi (Fig 3G and 3H). Of note, thrombi of cardioembolic origin contained nearly double the amount of NETs compared to non-cardioembolic thrombi ($p<0.05$, Fig. 3G). Furthermore, older thrombi showed significantly higher amounts of H3Cit compared to fresh thrombi (Fig. 3H).

Observation 3: fluorescent stainings confirm the presence of NETs in ischemic stroke thrombi and further illustrate the presence of various stages of NETosis

To further confirm the presence of NETs and origin of citrullinated histones, immunofluorescent stainings were performed combining H3Cit with the granulocyte marker CD66b and a DNA dye (DAPI).

Fluorescent co-staining of H3Cit together with CD66b and extracellular DNA further corroborate the abundance of decondensed DNA networks containing citrullinated histones that originate from CD66b positive cells (Fig. 4). In line with the immunohistochemical stainings, fluorescent staining also showed neutrophils in the initial stages of NETosis (Fig. 4A), with sometimes even only one nuclear lobe containing H3Cit positive chromatin (middle row of Fig. 4A) and neutrophils that had already fully ejected their decondensated chromatin into the extracellular space (Fig. 4B). Neutrophil origin of extracellular DNA was also confirmed by immunofluorescent co-staining with neutrophil elastase (not shown, see publication). In conclusion, these results clearly show the abundant presence of NETs in ischemic stroke thrombi.

Observation 4: RBC-rich and platelet-rich areas form distinct structural components of stroke thrombi

Given our findings on the the abundant presence of leukocytes in stroke thrombi we aimed to further characterize the specific cellular or molecular distribution of these leukocytes and extracellular DNA in stroke thrombi. We analyzed 177 thrombi from patients with ischemic stroke who were treated by thrombectomy. All thrombi were stained with Haemtoxylin and Eosoin (H&E) and Martius Scarlet Blue (MSB) to visualize their general organization (Figure 5). H&E allows identification of fibrin/platelet aggregates (pink), RBCs (red) and nucleated cells (dark blue), whereas MSB staining selectively demonstrates the presence of fibrin (dark pink/red), RBCs (yellow) and collagen (blue). These studies revelad that stroke thrombi typically contain two distinct types of thrombus material: (i) RBC-rich/fibrin-poor material that appears red on H&E stainings and yellow on MSB stainings and (ii) RBC-poor/fibrin-rich areas that appear as light pink areas on H&E staining and pink to red areas on MSB stainings. Interestingly, blood platelets are only present in the RBC-poor/fibrin-rich areas and not in the RBC-rich areas, as shown via platelet-specific immunostaining (Figure 5). Based on these clear and distinct differences, RBC-rich/fibrin-poor areas will be referred to as RBC-rich (R), whereas the term platelet-rich (P) will be used to indicate the RBC-poor/fibrin-rich/platelet-rich areas.

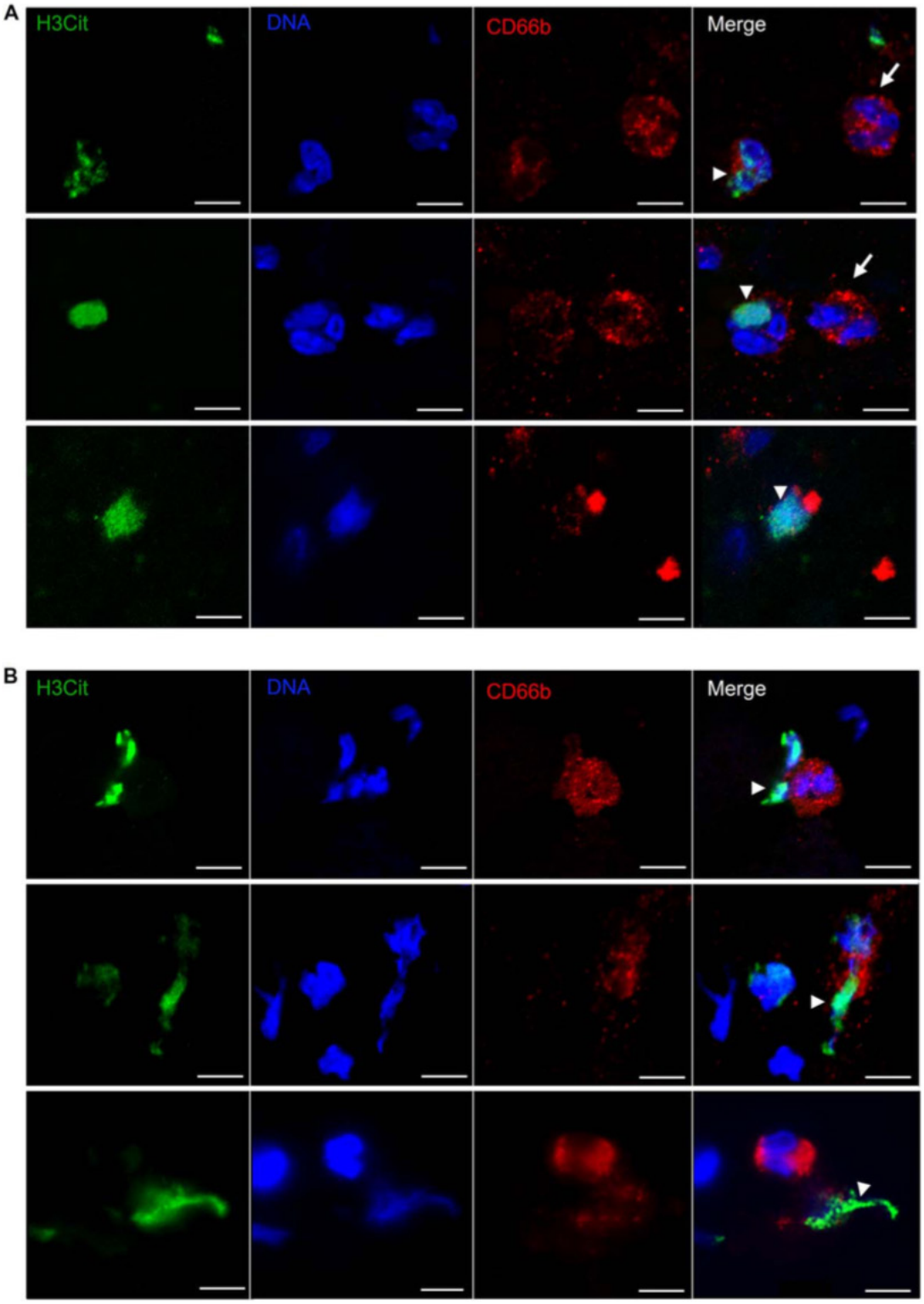

Figure 4: Immunofluorescent identification of NETs in stroke thrombi. NETs were visualized in human ischemic stroke thrombi by co-staining of the granulocyte marker CD66b (red) with H3Cit (green) and DNA (DAPI, blue). (A) Three representative images of neutrophils at the initial stage of NET formation. H3Cit positive signal is only detected inside the cell (arrowhead). Neutrophils without citrullinated histones are also shown (arrows). (B) Three representative images of neutrophils that underwent complete NETosis. Neutrophils released their decondensated chromatin in the extracellular space. Arrowheads indicate extracellular co-staining of DNA with H3Cit. Scale bar: 5 µm. Published in Annals of Neurology.[11]

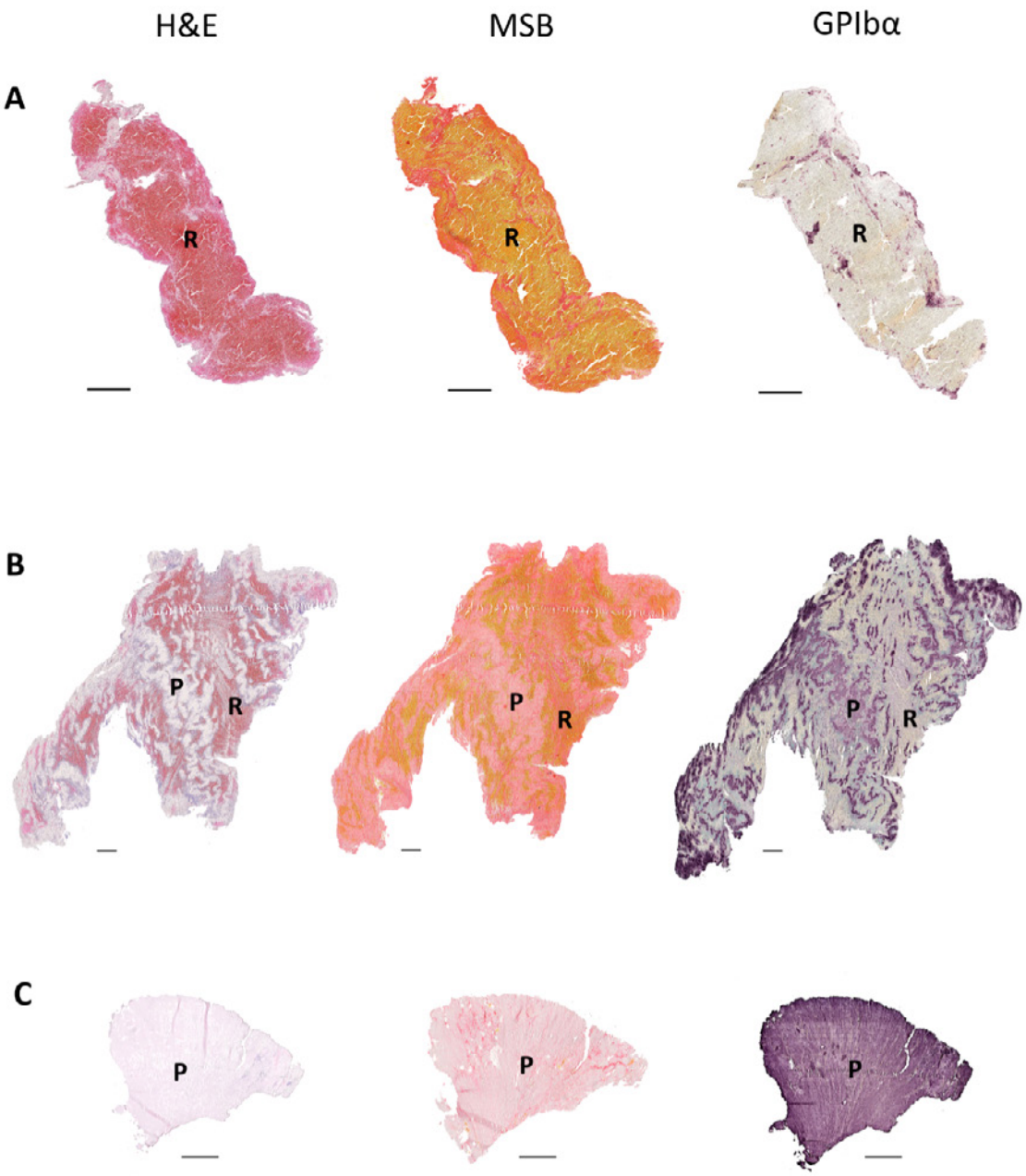

Figure 5: Stroke thrombi typically consist of RBC-rich areas and platelet-rich areas. Consecutive thrombus sections were stained with H&E, MSB and an anti-GPIbα antibody. Classical H&E staining (left) was used to visualize overall thrombus composition and organization. On H&E staining, RBC-rich areas appear red on H&E stainings whereas RBC-poor areas appear light pink. On MSB staining (middle), red areas show the presence of fibrin, whereas red blood cells (RBC) appear yellow. Platelets (purple) were immunohistochemically stained using an anti-GPIbα antibody (right). Overall, stroke thrombi consist of two distinct areas: RBC-rich areas, indicated by R, and platelet-rich areas, indicated by P. Examples of representative thrombi are shown, which are RBC-rich/platelet-poor (A), mixed (B) and RBC-poor/platelet-rich (C). Scale = 500 µm

Observation 5: Leukocytes and DNA are mainly present on the interface between RBC-rich en platelet-rich areas

Remarkably, we observed that leukocytes are primarily found on the interface between red blood cell-rich and platelets-rich areas (Figure 6). Besides their specific presence on these boundary zones, leukocytes are also abundantly present within the platelet-rich zones. In contrast, leukocytes are not common in RBC-rich areas, where, if present, they are homogenously distributed throughout the RBCs (Figure 6).

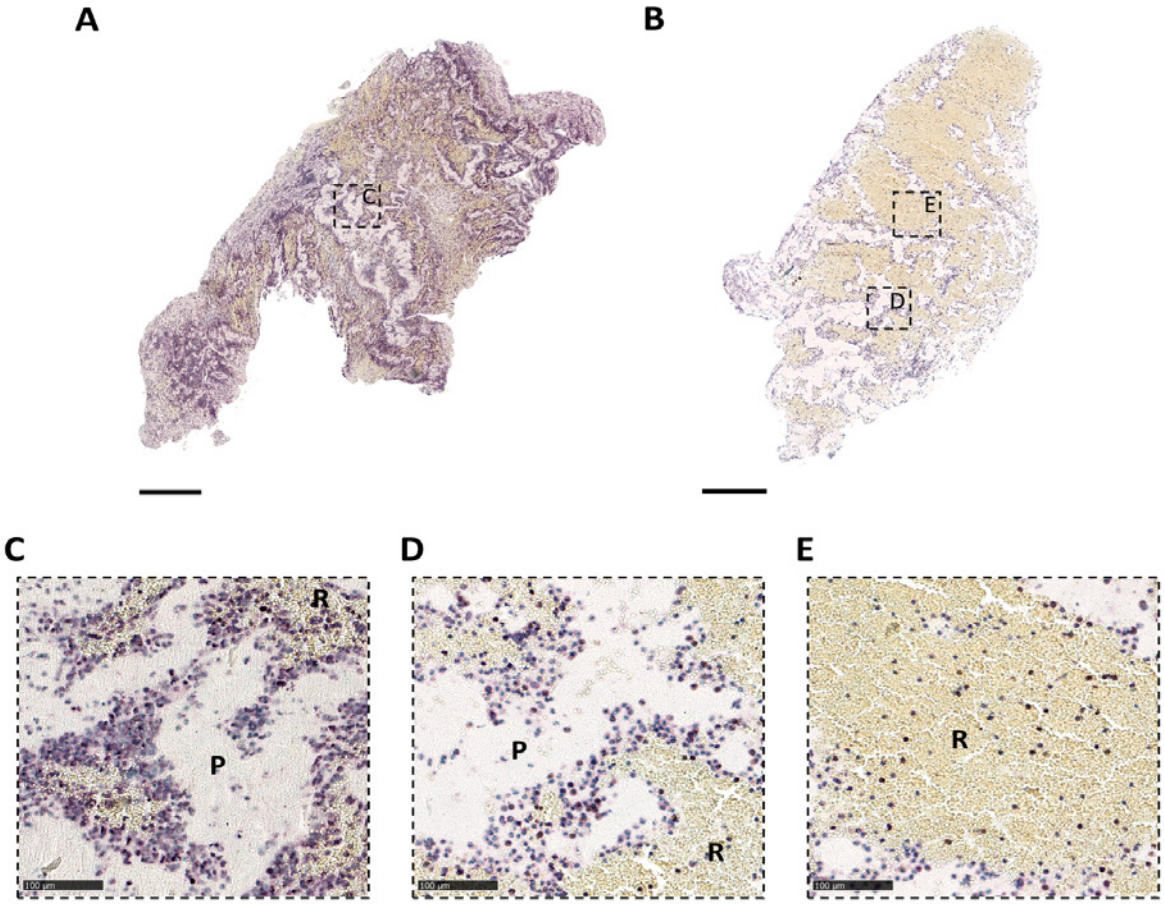

Figure 6: Leukocytes accumulate in platelet-rich areas and on the interface between platelet-rich and RBC-rich areas. Stroke thrombi were immunohistochemically analyzed for leukocytes (purple). (A-B) Two representative images of a stroke thrombi stained for leukocytes (purple). (C-E) Magnifications show that leukocytes tend to accumulate in platelet-rich areas (C) or on the boundary areas between platelet-rich and RBC-rich areas (D), whereas leukocytes are homogenously spread within RBC-rich areas (E). Scale bar = 500 µm for A and B and 100 µm in panels C-E. P = platelet-rich area, R = red blood cell-rich area.

To further examine the presence and internal organization of DNA networks in stroke thrombi, we optimized and performed a highly sensitive Feulgen's DNA staining on a subset of 100 stroke thrombi. Strikingly, large extracellular DNA networks were seen throughout the majority of thrombi. Again abundant amounts of extracellular DNA, were particularly observed in the platelet-rich areas and in the boundary areas between platelet-rich and RBC-rich regions (Figure 7). No extracellular DNA was found within the RBC-rich regions. In conclusion, leukocytes and networks of extracellular DNA were found specifically on the interface of the platelet-rich and RBC-rich regions and in the platelet-rich regions.

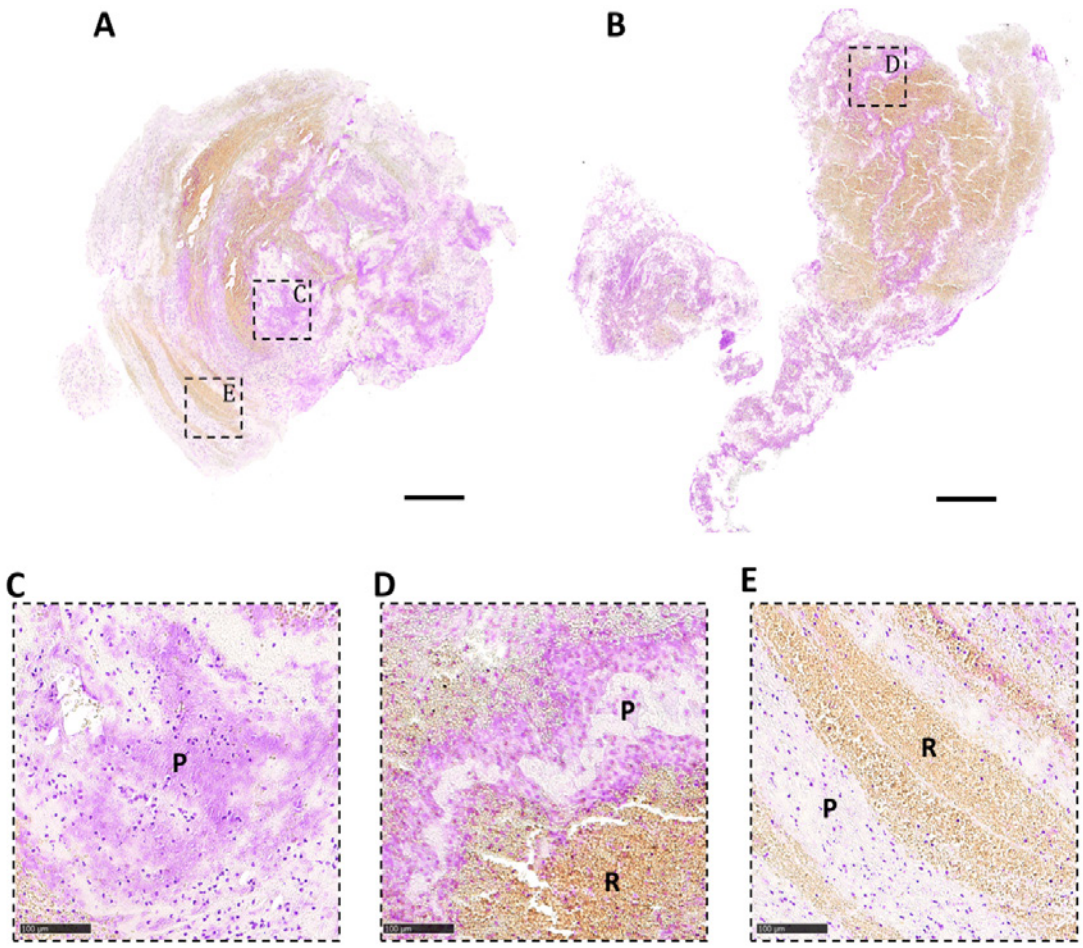

Figure 7: Extracellular DNA accumulates in platelet-rich areas and on the interface between platelet-rich and RBC-rich areas. Stroke thrombi were stained using a Feulgen's reaction to visualize intra/extracellular DNA (pink). (A-B) Two representative images of stroke thrombi stained for DNA (pink). (C-E) Magnifications show that extracellular DNA tends to accumulate within platelet-rich areas (C) or on the boundary areas between platelet-rich and RBC-rich areas (D). No extracellular DNA is observed in RBC-rich areas (E). Scale bar = 500 µm for A and B and 100 µm in panels C-E. P = platelet-rich area, R = red blood cell-rich area.

Future research related to WP1

Within the framework of WP1, we have shown that neutrophils are an important constituent of thrombo-embolic occlusions in ischemic stroke. We demonstrated for the first time the presence of NETs in ischemic stroke thrombi and found that their presence is correlated with cardioembolic etiology as well as with thrombus organization. In addition,extracellular DNA networks form a distint structural component of thrombi and are specifically localized around and in platelet-rich areas. With this work, the intial goals of WP1 have been largely completed. Future research will focus on expanding this studies to a larger set of samples. In the meantime, we have more than 250 thrombi via our collaboration with the AZ Groeninge hospital. In the meantime we have expanded our network and also recieve ischemic stroke thrombi from the CHRU in Lille (France) and plan to receive thrombi from other hosptials in Belgium and abroad. Large numbers are needed (we aim van >500 thrombi) as we plan to match NETs presence with more clinical patient data (MRI, CT, thrombus origin, stroke etiology, patient recovery, thrombectomy success rates...).

WP 2: Pothrombolytic capacity of DNase-1

Since use of t-PA leads to the dissolution of occluding thrombi in some cases, but not in others, we believe that factors other than fibrin are involved in thrombus stability. Such newly identified factors can become promising targets for thrombolytic therapy. We recently showed that von Willebrand confers tPA-resistance to cerebral thrombi and that the von Willebrand factor-cleaving protease ADAMTS13 has a prothrombolytic activity that may become useful in stroke.[12] Similarly, we hypothesize that extracellular

DNA traps are likely candidates as stabilizers of thrombi. Strikingly, the co-distribution of fibrin and extracellular DNA traps is apparent in arterial thrombi and a fascinating study showed that these DNA traps change the structure of fibrin, rendering it resistant to mechanical and enzymatic destruction.[13] The goal of this work pacakge therefore is to test the capacity of DNase-1 to support acute thrombolytic activity by disassembling extracellular DNA traps in stroke thrombi.

Observation: DNase 1 promotes ex vivo lysis of ischemic stroke thrombi

Given our observations that NETs can form extensive DNA networks in stroke thrombi, we reasoned that pharmacological breakdown of NETs could enhance thrombus dissolution. To test this, two equal parts of fresh patient thrombi (n=8) were submitted to ex vivo lysis by t-PA (1 µg/ml) or by a combination of t-PA (1 µg/ml) and DNase 1 (100 IE/ml) for 120 min at 37°C. Thrombus lysis was calculated in function of time as percentage of thrombus weight compared to the original weight (Figure 8). Standard t-PA alone induced gradual, partial lysis of the thrombi (residual weight at 120 min was 62.84 % ± 20.59 % of original thrombus weight). Strikingly, addition of DNase 1 to t-PA significantly accelerated ex vivo lysis compared to t-PA alone, reducing the thrombus weight at 120 min to 40.65 % ± 27.25 % ($p < 0.01$). These findings show that DNase 1 can promote ex vivo stroke thrombus dissolution and provide proof-of-concept to target NETs as a novel prothrombolytic strategy.

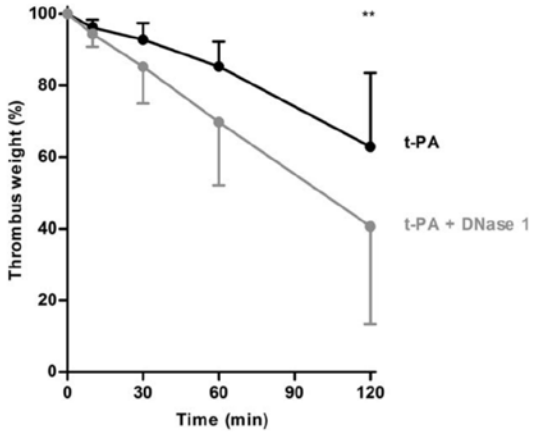

Figure 8: DNase 1 promotes ex vivo lysis of ischemic stroke thrombi. For ex vivo lysis of thrombi (n=8) retrieved from ischemic stroke patients, 2 equal parts were used. The thrombus parts were incubated for 120 min at 37°C in the presence of either t-PA alone (black) or t-PA plus DNase 1 (grey). Thrombus weight % of original weight) was measured at time points 0, 10, 30, 60 and 120 minutes. Data are represented as mean with SD (** $p < 0.01$). Published in Annals of Neurology.11

Next steps for WP2

Our first results show already the potential of DNase-1 to promote thrombus dissolution on human material retrieved from stroke patient via endovascular procedures. In a next step we want to extend these findings in an established and pathophysiologically relevant mouse stroke model in which an occlusive thrombus is formed at the origin of the middle cerebral artery (MCA) after local administration of thrombin or FeCl3. Using this model, we recently showed a novel thrombolytic activity of ADAMTS13 in stroke.[12] Important for clinical translation, we will also investigate the additional benefit of combining DNase-1 together with t-PA (or even ADAMTS13).[12] This model is currently being set up for DNase-1 experiments. Current studies examine the formation of the development of thrombi that are rich in NETs and/or DNA in the MCA of mice.

WP 3: NETs-formation in a mouse model of transient middle cerebral artery occlusion

In this WP, the goal is to assess the involvement of NETs in progressive ischemic brain damage during ischemia and reperfusion in mice. Pathogenic mechanisms underlying this reperfusion injury are not completely understood but involve a complex interplay of thrombo-inflammatory processes.[3] We recently showed that NET formation worsened outcome in mouse models of myocardial ischemia/reperfusion.[14]

The role of NETs in (mouse models of) cerebral ischemia/reperfusion brain damage has never been investigated. To clarify the potential involvement of NETs in we will use an established model of cerebral ischemia/reperfusion injury[15], which in the past year has been learned and acquired the researcher on this GSKE WP. In the past year, we also developed a new mouse strain that will be of great value for this WP. Indeed, we have been intercrossing specific mouse strains to obtain neutrophil-specific PAD4 knock-out mice. The crossing of these mice has been completed and we are now breeding the first offspring that can be used for experiments.

Next steps for WP3

At different time points after induction of ischemia (up to 48 hours), mice will be sacrificed and brain histology for NETs will be performed. In addition 3D imaging via confocal microscopy will also be used to visualize cerebral NETosis. In 2019, a novel method will be added via light sheet microscopy on the brain of mice.

WP 4: NETs markers in plasma of stroke patients

In this WP, the goal was to investigate the presence of established circulating biomarkers of NETs (cell-free DNA, nucleosomes, DNA-MPO complexes) in stroke patients. Such NETs -markers were recenlty shown to be increased in a variety of pathological conditions, such as sepsis, small vessel vasculitis, venous thrombosis and coronary atherosclerosis[6,16] but almost nothing is known yet about circulating NETs markers in stroke patients. We therefore planned to assess plasma of different groups of stroke patients (and healthy controls) and determine levels of NETs biomarkers. In the mean time, cell-free DNA and nucleosome levels have been measured.

Observation 1: Cell-free DNA is elevated in stroke patients

We already obtained a large cohort of stroke patients (and healthy volunteers) through our collaboration with Prof. C. Kleinschnitz (Würzbrug, now Essen in Germany).[17] As a first maker, we already tested our cohort for cell-free DNA as an indication of NETs in stroke. In total, 104 patients with stroke (AIS or TIA) and 85 healthy volunteers (HV) were included in the study. Trisodium citrate anticoagulated blood was collected on day 0, 1, and 3 in patients with stroke, and once in HV between 08.00 and 12.00 hours from an antecubital vein using a 21-gauge butterfly needle. Cell-free DNA in plasma was analyzed using PicoGreen and quantified via a DNA standard curve. Interestingly, patients with ischemic stroke presented with significantly higher levels of circulating DNA (compared to healthy volunteers) and this was true for day 0, 1 and 3 of stroke (Figure 9).

Observation 2: Nucleosome levels are elevated in stroke patients

In the mean time we have also completed the nucleosome measurement (Figure 10). Similar to cell-free DNA, we see that stroke patients have significant increase in circulating nucleosome levels compared to healthy volunteers. These results are line with our previous data showing that plasma nucleosome levels are elevated in mice after stroke, which could potentially be derived from NETs that are formed in the ischemic area.[18] Thus, we show that stroke patients have increased numbers of NETs markers in their circulation.

Next steps for WP4

Along the same lines of our results on DNA and nucleosomes, we plan to also measure other established markers of NETs, soluble H3cit and DNA-MPO complexes. Assays to measure these parameters have in the mean time been set up in the lab and measurements of the samples are planned. Since all clinical data of our patient cohort is available, we will be able to correlate levels of circulating NETs markers with clinical parameters such as treatment success, morbidity, disability and mortality.

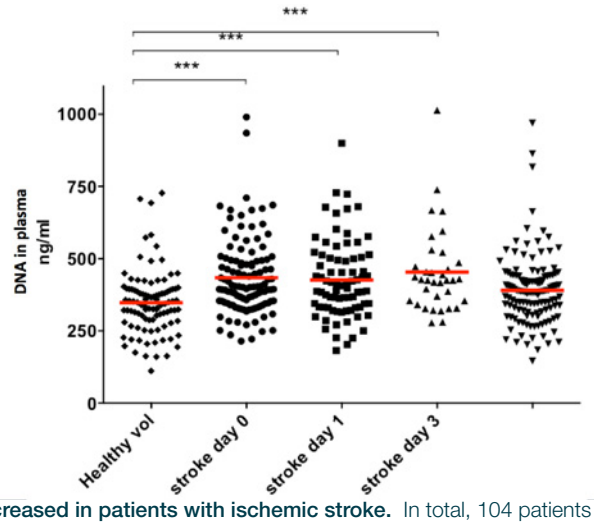

Figure 9: Plasma DNA levels are increased in patients with ischemic stroke. In total, 104 patients with stroke and 85 healthy volunteers were included in the study. Trisodium citrate anticoagulated blood was collected on day 0, 1, and 3 in patients with stroke, and once in HV Cell-free DNA in plasma was analyzed using PicoGreen and quantified via a DNA standard curve. Unpublished results.

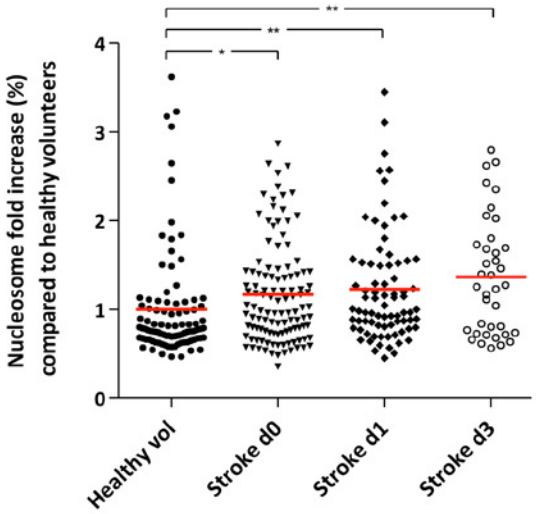

Figure 10: Nucleosome levels are increased in patients with ischemic stroke. In total, 104 patients with stroke and 85 healthy volunteers were included in the study. Trisodium citrate anticoagulated blood was collected on day 0, 1, and 3 in patients with stroke, and once in HV nucleosome levels in plasma was analyzed using a commerical nucleosome detection kit. Unpublished results.

3. Novel opportunities and impact of 2-year progress

As shown by the progress in the first 2 years of this GSKE project, some important findings have been achieved. We demonstrated for the first time the presence of NETs in ischemic stroke thrombi and found that their presence is correlated with cardioembolic etiology as well as with thrombus organization. Targeting NETs with DNase-1 successfully improved ex vivo thrombolysis, calling for further investigation of DNase-1-based strategies to improve thrombus dissolution and prevent excessive neurodegeneration in acute ischemic stroke. We found that extracellular DNA-structures are a common structural feature of ischemic stroke thrombi that specifically localize in and around platelet-rich areas. In addition, we found that NET's markers are elevated in stroke patients, suggesting a direct clinical link between NETs and stroke pathology.

Given the serious limitations in current stroke therapy, the clinical implications of our findings could be of high relevance for acute ischemic stroke management. Our detailed histological analysis reveals

different structural features in ischemic stroke thrombi that could be highly relevant for developing efficient pharmacological thrombolysis strategies. Serving as a thrombotic scaffold, NETs and extracellular DNA most likely contributes to overall thrombus stability and might confer resistance to fibrinolytic therapy thereby exacerbating ischemic stroke neurodegeneration. The presence of fibrin and DNA could explain why the current 'one size fits all' therapy aiming only at fibrinolysis via t-PA is not always sufficient in patients.

DNase-1 already is a safe, low-cost, FDA-approved drug routinely used for cystic fibrosis to clear extracellular DNA in the lungs. Combination of DNase-1 with t-PA could potentially allow decreasing the dose of t-PA utilized, limiting its side effects and potentially increasing its therapeutic time window. Even a small prolongation of the therapeutic window for safe thrombolytic therapy would already help hundreds of thousands of patients each year. This would allow a drastic reduction of the current burden caused by the negative side-effects of t-PA. Additional studies are needed to further assess this hypothesis and are planned in the future.

Importantly, use of DNAse-1 could become a therapeutic strategy that kills two birds with one stone. We previously demonstrated that DNase-1 also had a protective effect in a mouse model of cerebral ischemia/reperfusion injury.18 Hence, besides its potential prothrombolytic activity that could promote fast restoration of blood vessel patency, DNase-1 could additionally reduce subsequent reperfusion injury and thus improve neurological outcome in ischemic stroke.

Apart from the direct potential therapeutic opportunities, the progress described in this progress report also led to multiple new networks and collaborations that will be valuable for the future research on this topic (see further).

4. Output

The results that were obtained with support of the GSKE already led to significant output, visibility and novel collaborations. In the following section an overview of the most important output achievements is given.

Papers with GSKE acknowledgement:

- Laridan E., Denorme F., Desender L., François O., Deckmyn H., Vanhoorelbeke K., De Meyer S. (2017). Neutrophil extracellular traps in ischemic stroke thrombi. *Annals of Neurology, 82* (2): 223-232. (Impact factor: 10.24).
- Brouwer PA., Brinjikji W., De Meyer SF. (2018). Clot Pathophysiology Why Is It Clinically Important?. *Neuroimaging clinics of North America, 28* (4), 611-623. (Impact factor: 1.28).
- Laridan E., Martinod K., De Meyer SF. (2019) Neutrophil extracellular traps in thrombosis. *Seminars in Thrombosis and Haemotasis*. doi: 10.1055/s-0038-1677040. [Epub ahead of print] (Impact factor: 3.3)
- Staessens S., Denorme F., François O., Desender L., Dewaele T., Vanacker P., Deckmyn H., Vanhoorelbeke K., Andersson T., De Meyer S.F. Dense fibrin, von Willebrand factor and extracellular DNA are specific structural hallmarks of platelet-rich regions of ischemic stroke thrombi (submitted in *Acta Neuropathologica* -IF: 15.9)
- Denorme F., Martinod K., Vandenbulcke A., Denis C.V., Lenting P.J., Deckmyn H., Vanhoorelbeke K. and De Meyer S.F. VWF A1 domain mediates thrombo-inflammation through recruitment of monocytes, neutrophils and T-cells in murine stroke. (submitted in Blood - IF 15.3)
- Staessens S. et al., Fitzgerald S., Denorme F., Clarençon F., Hacke W., Szikora I.,, Gounis M., Liebeskind D., Brinjikji W., Doyle K., De Meyer S.F. Histological stroke clot analysis after thrombectomy: technical aspects and recommendations (in preparation for submission in *Translational Stroke Research*, IF: 8,2)

Awards:

The work supported by the GSKE grant has already led to several awards, including:

- *2017 Eberhard F. Mammen Young Investigator Award (to my PhD student Elodie Laridan).*
  The Eberhard F. Mammen Young Investigoar Awards (up to a total of six in any year) are given for the "Best presentation or meeting abstract by a young investigator — as presented or delivered to an international or large regional meeting on a topic related to the fields of thrombosis and hemostasis and whose subject matter is determined to be in the spirit of Dr. Mammen." (Dr Mammen was the Founding Editor of **'Seminars in Thrombosis & Hemostasis'** (STH)). *ISTH Young Investigator Award (to my PhD student Elodie Laridan).*
- *ISTH Young Investigator Award (to my PhD student Elodie Laridan).*
  The Young Investigator Awards of the International Society of Thrombosis and Hemostasis are given to the highest scored abstracts of the bi-annual international meeting of the ISTH. Elodie Laridan received this awards for her presentation "Neutrophil extracellular traps in thrombi retrieved from ischemic stroke patients" during the 2017 ISTH meeting in Berlin.
- *2018 Paul Capel Prize of the BSTH (to my PhD student Senna Staessens).*
  The Paul Capel Prize of the Belgian Society of Thrombosis and Hemostasis is given to the best presentation of the annual international meeting of the BSTH. Senna Staessens received this prize for her presentation " Dense fibrin, von Willebrand factor and extracellular DNA are specific structural hallmarks of platelet-rich regions of ischemic stroke thrombi " during the 2018 BSTH.
- *2018 Prize for best clinical contribution at research day of the Department of Cardiovascluar Sciences, KU Leuven (to my PhD student Senna Staessens).*
- *Prize Baron Marc Verstraete for the study of hemato-angiology (Royal Academy for Medicine of Belgium),*
  This five-annual Prize was awared to Simon F De Meyer (Brussels, Belgium 2017)

Invited lectures:

The scientific results from this grant have been well received in the international community as is reflected by the many invitations I received to present this work at international conferences. These invitations include:

- 2nd Thrombosis Meeting, February 2017 Freiburg, Germany (invited speaker)
- Haematology Lectures Program, Erasmus Medical Center, May 2017, Rotterdam, The Netherlands (invited speaker)
- International Society on Thrombosis and Hemostasis Congress, July 2017, Berlin, Germany (invited speaker)
- The 9th Bari International Conference, September 2017, Bari, Italy (invited speaker)
- GFHT meeting, October 2017, Caen, France (invited speaker - Plenary Lecture)
- 14th Congress of the World Federation of Interventional and Therapeutic Neuroradiology, October 2017, Budapest, Hungary (invited speaker - Plenary Lecture)
- 3rd Neuravi Clot summit, December 2017, Amsterdam, The Netherlands (invited speaker)
- ECMINT 1.3 European Course on Minimally Invasive Neurological Therapy, December 2017, Oxford, UK (invited speaker)
- 2017 meeting of the Belgian Society of Interventional and Therapeutic Neuroradiology, December 2017, Brussels, Belgium (invited speaker)
- 4th European Stroke Organisation Conference, May 2018, Gôteborg, Sweden (invited speaker)
- International Society on Thrombosis and Hemostasis SSC meeting, July 2018, Dublin, Ireland (invited speaker)
- 4th EUPLAN platelet conference, September 2018, Bruges, Belgium (co-organizer)
- 11th World Stroke Congress, October 2018, Montreal, Canada (invited speaker, co-convener)
- Annual Meeting of the Irish Haematology Society, October 2018, Cork, Ireland (invited speaker - Plenary Lecture)
- 14th International Symposium on Thrombolysis, Thrombectomy and Acute Stroke Therapy, October 2018, Houston, Texas (invited speaker)
- European Stroke Course on Minimally Invasive Neuroradiological Therapy, November 2018, Prague, Czech Republic (invited speaker)
- 5th International Symposium on Collaterals in the Brain, December 2018, Los Angeles, USA (invited speaker)
- Clot Summit, December 2018, Los Angeles, USA (invited speaker)
- 3rd Conference of the European Society for Microcirculation / European Vascular Biology Organization, April 2019, Maastricht, The Netherlands (invited speaker)
- International Society on Thrombosis and Hemostasis Congress, July 2019, Melbourne, Australia (invited speaker)

New collaborations and networks:

The progress made in the GSKE project opened new research avenues (as described above) and, in particular, also led to novel research collaborations. The most important include:

- Participation in the EU HORIZON2020 INSIST consortium (In Silico Clinical Trials for Acute Ischemic Stroke) (http://www.insist-h2020.eu). Start in 2018.
- New research contacts with technology companies Neuravi (Galway, Ireland), Sensome (Paris, France) and Matisse Pharmaceuticals (Geleen, The Netherlands)
- New research collaborations with academic partners and hospitals (AZ Sint Jan in Bruges, UZ Antwerp, UZ Gasthuisberg Leuven in Belgium and CHRU in Lille, France, NUI in Galway Ireland)

5. References

1. Hacke W, Kaste M, Bluhmki E, et al. Thrombolysis with alteplase 3 to 4.5 hours after acute ischemic stroke. *N. Engl. J. Med.* 2008;359(13):1317–1329.
2. Rha J-H, Saver JL. The impact of recanalization on ischemic stroke outcome: a meta-analysis. *Stroke.* 2007;38(3):967–973.
3. De Meyer SF, Denorme F, Langhauser F, et al. Thromboinflammation in Stroke Brain Damage. *Stroke.* 2016;47(4):1165–1172.
4. Brinkmann V, Reichard U, Goosmann C, et al. Neutrophil extracellular traps kill bacteria. *Science.* 2004;303(5663):1532–1535.
5. Fuchs TA, Brill A, Wagner DD. Neutrophil extracellular trap (NET) impact on deep vein thrombosis. *Arteriosclerosis, Thrombosis, and Vascular Biology.* 2012;32(8):1777–1783.
6. Martinod K, Wagner DD. Thrombosis: tangled up in NETs. *Blood.* 2014;123(18):2768–2776.
7. Fuchs TA, Brill A, Duerschmied D, et al. Extracellular DNA traps promote thrombosis. *Proc. Natl. Acad. Sci. U.S.A.* 2010;107(36):15880–15885.
8. Brill A, Fuchs TA, Savchenko AS, et al. Neutrophil extracellular traps promote deep vein thrombosis in mice. *J Thromb Haemost.* 2012;10(1):136–144.
9. Oklu R, Albadawi H, Watkins MT, et al. Detection of extracellular genomic DNA scaffold in human thrombus: implications for the use of deoxyribonuclease enzymes in thrombolysis. *J Vasc Interv Radiol.* 2012;23(5):712–718.
10. Brühl von M-L, Stark K, Steinhart A, et al. Monocytes, neutrophils, and platelets cooperate to initiate and propagate venous thrombosis in mice in vivo. *Journal of Experimental Medicine.* 2012;209(4):819–835.
11. Laridan E, Denorme F, Desender L, et al. Neutrophil extracellular traps in ischemic stroke thrombi. *Ann Neurol.* 2017;313:1451–10.
12. Denorme F, Langhauser F, Desender L, et al. ADAMTS13-mediated thrombolysis of t-PA–resistant occlusions in ischemic stroke in mice. *Blood.* 2016;127(19):2337–2345.
13. Longstaff C, Varjú I, Sótonyi P, et al. Mechanical stability and fibrinolytic resistance of clots containing fibrin, DNA, and histones. *J. Biol. Chem.* 2013;288(10):6946–6956.
14. Savchenko AS, Borissoff JI, Martinod K, et al. VWF-mediated leukocyte recruitment with chromatin decondensation by PAD4 increases myocardial ischemia/reperfusion injury in mice. *Blood.* 2014;123(1):141–148.
15. Verhenne S, Denorme F, Libbrecht S, et al. Platelet-derived VWF is not essential for normal thrombosis and hemostasis but fosters ischemic stroke injury in mice. *Blood.* 2015;126(14):1715–1722.
16. Fuchs TA, Hovinga JAK, Schatzberg D, Wagner DD, Lämmle B. Circulating DNA and myeloperoxidase indicate disease activity in patients with thrombotic microangiopathies. *Blood.* 2012;120(6):1157–1164.
17. Kraft P, Drechsler C, Gunreben I, et al. Von Willebrand Factor Regulation in Patients with Acute and Chronic Cerebrovascular Disease: A Pilot, Case–Control Study. *PLoS ONE.* 2014;9(6):e99851.
18. De Meyer SF, Suidan GL, Fuchs TA, Monestier M, Wagner DD. Extracellular chromatin is an important mediator of ischemic stroke in mice. *Arteriosclerosis, Thrombosis, and Vascular Biology.* 2012;32(8):1884–1891.

Geneeskundige Stichting Koningin Elisabeth
Fondation Médicale Reine Elisabeth
Königin-Elisabeth-Stiftung für Medizin
Queen Elisabeth Medical Foundation

Progress report of the research group of

Prof. dr. De Strooper Bart, MD. PhD

Katholieke Universiteit Leuven (KU Leuven)

Principal investigator

Prof. dr. De Strooper Bart, MD. PhD
VIB Center for Brain and Disease Research
Herestraat 49
3000 Leuven
Belgium
Tel.: +32 495 77 10 44
E-mail: Bart.Destrooper@vib.be

Hilde Govaert
Administrative Director
hilde.govaert@kuleuven.vib.be

Wei-Ting Chen
Postdoctoral Researcher
weiting.chen@kuleuven.vib.be

Mark Fiers
VIB Expert Technologist
mark.fiers@kuleuven.vib.be

Katleen Craessaerts
Staff employee
katleen.craessaerts@kuleuven.vib.be

Ashley Lu
PhD student
ashley.lu@kuleuven.vib.be

Carlo Sala Frigerio
Staff scientist
carlo.salafrigerio@kuleuven.vib.be

Benjamin Pavie
Imaging Analysis Expert
benjamin.pavie@kuleuven.vib.be

The study of the initial cellular phase of Alzheimer's Disease

1. Overall summary of the report

As reported in the first year we have redirected our single cell sequencing research efforts to analyze microglia. Microglia are involved in Alzheimer's disease (AD) by adopting activated phenotypes. We investigated how ageing in the absence or presence of β-amyloid (Aβ) deposition in different brain areas affect their response and whether sex and AD risk genes are involved. We analyzed the gene expression profiles of more than 10,000 individual microglia cells isolated from cortex and hippocampus of male and female *App*$^{NL\text{-}G\text{-}F}$ at 4 different stages of Aβ deposition and in age-matched control mice. We demonstrate that microglia adopt two major activated states during normal aging and after exposure to amyloid plaques. One of the responses (activated response microglia, ARM) is enhanced in particular by amyloid plaques and is strongly enriched with AD risk genes. The ARM response is not homogeneous, as subgroups of microglia overexpressing MHC type II and tissue repair genes (*Dkk2*, *Gpnmb*, *Spp1*) are induced upon prolonged Aβ exposure. Microglia in female mice advance faster in the activation trajectories. Similar activated states were also found in a second AD model and in human brain. We demonstrate that abolishing the expression of *Apoe*, the major genetic risk factor for AD, impairs the establishment of ARMs, while the second microglia response type, enriched for interferon response genes, remains unaffected. Our data indicate that ARMs are the converging point of multiple AD risk factors. A manuscript mentioning the support of the Queen Elisabeth foundation is submitted.

We have also made significant progress with a novel approach to tackle the cellular complexity of aged brain via spatial transcriptomics. Spatial information is critical for neuroscience and this cannot be achieved by classical single-cell sequencing approaches as one need to dissociate cells. Spatial Transcriptomics (ST) provides great spatial resolution within the tissue blocks without cell dissociation. We collected last year global transcriptomic profiles at 4 different time-points to cover expressomes over disease progression. This enormous database has enabled us for the first time to understand the co-expression molecular network that is associated with the amyloid plaques (discussed in detail below). In the second year of this grant we have made major technical progress and developed a series of novel bioinformatics approaches on which we report briefly below. We expect that these efforts will bring us an additional manuscript in 2019 (we are actually busy writing this).

Finally we have published and submitted a series of manuscripts in which the help of the Elisabeth foundation has been fully acknowledged because some people or work was contributed to achieve those publications. The papers are mentioned at the end of this report. One paper covers work on a new model for neurodegeneration that reproduces many aspects of encephalomyelopathy similar to Leigh syndrome and which we published in PNAS. The second paper solves a problem that I have been working on for 25 years, i.e. the function of the amyloid precursor protein (APP). We found that it is an allosteric modulator of the GabaB1 receptor. This work has important implications for the biology of Alzheimer's disease and the modeling of the disease in overexpressing mouse models (part of the seizure phenotypes in these models might be induced by APP overexpression). This work was published in Science and received broad coverage. Finally we have papers submitted on transplanted human microglia in brain (submitted to nature neuroscience) and on the genetic risk of Alzheimer disease that is mainly medicated by microglia (submitted to Science translational medicine). The two latter papers report on profound analysis of genetic risk factors in microglia and how those influence our risk for AD. The papers are provocative and we need to wait and see whether the referees will like the work, but we reported these data at the Brain Prize Confernce in Kopenhagen last year and got very positive feedback from the audience.

Of note, I was awarded the Brain Prize 2018 together with three other colleagues for my work on Alzheimer's Disease and I received the honor of becoming "Commandeur in de Leopoldsorde".

1.1. Publications mentioning support from GSKE

- Rice HC, de Malmazet D, Schreurs A, Frere S, Van Molle I, Volkov AN, Creemers E, Vertkin I, Nys J, Ranaivoson FM, Comoletti D, Savas JN, Remaut H, Balschun D, Wierda KD, Slutsky I, Farrow K, De Strooper B, de Wit J. Secreted amyloid-β precursor protein functions as a GABA(B)R1a ligand to modulate synaptic transmission. **Science**. 2019 Jan 11;363(6423). (shared corresponding author)
- Spinazzi M, Radaelli E, Horré K, Arranz AM, Gounko NV, Agostinis P, Maia TM, Impens F, Morais VA, Lopez-Lluch G, Serneels L, Navas P, De Strooper B. PARL deficiency in mouse causes Complex III defects, coenzyme Q depletion, and Leigh-like syndrome. **Proc Natl Acad Sci U S A**. 2019 Jan 2;116(1):277-286.

1.2. Submitted

- Carlo Sala Frigerio, Leen Wolfs, Nicola Fattorelli, Nicola Thrupp, Iryna Voytyuk, Inga Schmidt, Renzo Mancuso, Wei-Ting Chen, Maya Woodbury, Gyan Srivastava, Thomas Möller, Eloise Hudry, Sudeshna Das, Takaomi Saido, Eric Karran, Bradley Hyman, V. Hugh Perry, Mark Fiers, Bart De Strooper. **The major risk factors for Alzheimer's disease: Age, Sex and Genes, modulate the microglia response to Aβ plaques**.
- Annerieke Sierksma, Ashley Lu,, Evgenia Salta, Renzo Mancuso, Jesus Zoco, David Blum, Luc Buée, Bart De Strooper, Mark Fiers, (shared corresponding author). **Novel Alzheimer risk genes determine the microglia response to amyloid-β but not to TAU pathology**.
- Renzo Mancuso, Johanna Van Den Daele, Nicola Fattorelli, Leen Wolfs, Sriram Balusu, Oliver Burton, Annerieke Sierksma, Yannick Fourne, Suresh Poovathingal, Amaia Arranz-Mendiguren, Carlo Sala Frigerio, Christel Claes, Lutgarde Serneels, Tom Theys, V. Hugh Perry, Catherine Verfaillie, Mark Fiers, Bart De Strooper. **Stem cell derived human microglia transplanted in mouse brain to study genetic risk of Alzheimer's Disease**

2. Details of scientific work

2.1. Single Cell sequencing

We analysed cortical and hippocampal microglia in female and male *C57Bl/6* wild type and in *App*$^{NL\text{-}G\text{-}F}$ mice, at four different time points: at the beginning of Aβ deposition (3 months old, m.o.), at the beginning of overt histologically detectable microgliosis (6 m.o.), when both processes are well underway (12 m.o.) and at a late stage (21 m.o.) (Figure 1A). All together, we analysed 32 different experimental conditions, taking into consideration the combinations of genotype, age, sex, and tissue (Figure 1A). Tissue and cell suspensions were kept < 4°C during all steps of microglia isolation, to minimize artefactual activation. We isolated single live microglia cells (Cd11b+/DAPI-) by FACS and prepared single cell full length mRNA sequencing libraries using a modified SmartSeq2 method (See Figure 1A). We sequenced a total of 12,024 single cells across the different experimental conditions. After quality control and removal of peripheral neutrophils we retained 10,801 microglia cells for further analysis.

Two clusters expressing high levels of known homeostatic microglia markers (*Tmem119*, *P2ry12*, *Cx3cr1*, Figure 1D) dominated the whole microglia population (homeostatic 1 microglia and homeostatic 2 microglia, H1M and H2M, Figure 1B). The other clusters were quite divergent from the homeostatic ones (Figure 1D). One cluster (ARM, activated response microglia, Figure 1B) increased strongly in the *App*$^{NL\text{-}G\text{-}F}$ mice. It is characterized by the expression of gene sets involved in inflammatory processes (*Cst7*, *Clec7a*, *Itgax*), in MHC class II presentation (*Cd74*, *H2-Ab1*, *H2-Aa*, *Ctsb*, *Ctsd)*, and possibly involved in tissue regeneration (*Spp1, Gpnmb, Dkk2*) (Figure 1D-E). A second cluster (TRM, transiting response microglia, Figure 1B) has an overall transcriptomic profile similar to that of cluster ARM but had lower expression levels of *Apoe* and other inflammatory genes, and particularly of MHC type II genes, while it did not express tissue regeneration genes (Figure 1D-E). A third cluster (IRM, interferon response microglia, Figure 1B) displayed high expression of several genes involved in innate immune response and interferon response type I pathways (e.g. *Ifit2*, *Ifit3*, *Ifitm3*, *Irf7*, *Oasl2*) which were otherwise not expressed in other clusters (Figure 1D-E). Finally, we identified a very small cluster of cells corresponding to 0.3-1.2% of the total microglia pool (CPM, cycling/proliferating microglia) (Figure 1B-C) which was

enriched in genes involved in DNA replication, chromatin rearrangement and cell cycle (e.g. *Top2a*, *Mcm2*, *Tubb5*, *Mki67*, *Cdk*1) (Figure 1D). Cluster CPM did not display any selective enrichment for specific phenotypic groups (Figure 1C), and may represent a small pool of cycling microglia.

We have analyzed this exceptional array of data. We find a remarkable flexibility of the microglia phenotype in brains of healthy and AD mice. The crucial role of microglia in AD is underlined by the convergence of the three major risk factors for AD (age, sex and genetics) into the multifunctional microglia response that we call here Activated Response Microglia, or ARM. ARM is present in young and older mice and is therefore a physiological state of microglia, but exposure to Aβ plaques strongly enhances this response. The crucial role of the ARM response for our understanding of sporadic AD is further underlined by the facts that it highly enriches for GWAS AD risk genes and that ablation of the major risk gene for AD, i.e. *Apoe*, aborts the ARM response dramatically. These data provide a potential synthesis between aspects of the amyloid hypothesis and the inflammatory hypothesis for AD.
Progressive Aβ deposition in $App^{NL\text{-}G\text{-}F}$ mice drives more than 50% of the total microglia pool into reactive states, and principally to the ARM state (Figure 1C). Thus, the response to Aβ deposition does not involve a novel disease-associated reactive state, but consists of a redistribution of a larger fraction of microglia to the physiological ARM pool. The ARM cluster overlaps with the DAM response described by Keren-Shaul et al., Cell, 2017, but we find it to be less homogeneous, and not only a response to disease or damage but also part of the normal physiology of the brain. We show that the response to Aβ deposition evolves stereotypically across brain areas (cortex and hippocampus) in animals of both sexes.
Microglia in female mice progressed faster over the ARM trajectory compared to microglia in male mice. Our observation that many AD GWAS associated genes appear to change their expression in the ARM microglia indicates an overlap between the pathogenesis of AD in humans and the microglial response to the accumulation of amyloid in the brain of the mouse models. Thus, these GWAS variants, when present in a patient, likely affect the way that microglia cope with the accumulation of amyloid over age. In that capacity they either exacerbate or act protectively with regard to the onset of the disease. Such view predicts that patients with a high load of amyloid but with a protective combined polygenic risk score, will respond in a beneficial way to amyloid and will not develop full blown AD.
ARM microglia induce *Apoe* expression up to 27 fold, compared to homeostatic microglia. In particular, in proximity to plaques, microglia express higher levels of *Apoe* than astrocytes (~2.3 fold higher median *Apoe* intensity per cell). We show also that *Apoe* is not merely a marker for this cell state, but is a key component of the ARM response, as its deletion severely reduces the number of microglia displaying an ARM signature. Given this spectacular influence of *Apoe* expression on the microglia phenotype, we speculate that a large part of the genetic risk associated with the *APOE4* genotype is likely executed via modification of the microglia function rather than other mechanisms. While we cannot exclude that the abnormal plaques that are generated in the absence of ApoE affect the microglia response, it seems more likely that ApoE directly modulates the response of the microglia to the plaques, and that ApoE is responsible for the induction of the ARM response to amyloid. Thus, the major genetic risk factor for AD, together with most of other identified risk genes in GWAS studies, modulates the neuroinflammatory response of the microglia to amyloid plaques.

2.2. Spatial Transcriptomics (ST)

The high quality of our database has been described in the previous report. In the second year of this grant, we analyzed the effect of amyloid plaques on local expression profiles of genes. We developed a bioinformatics method to quantify the amyloid burden based on the immunostaining via anti-$Aβ_{1\text{-}16}$ antibody, 6E10 (Figure 2B). The range of this plaque index varies between 0 and 13000 arbitrary units. Figure 2C shows the plaque index per region at the indicated age in APP NL-G-F mice. The result is consistent with the stereotypical propagation starting from the dorsal cortex, then propagating into ventral cortex, thalamus, and hippocampus (Figure 2A).

To understand the molecular alterations of cells in the vicinity of amyloid plaques, we performed linear regression to model the relationship between a response variable (gene expression profile) and an explanatory variable (plaque index). The goal is to explain variation of the expression profile of genes at different locations of APP NL-G-F that can be attributed to the variation in the amyloid burden. The result of linear regression analysis provides the log2 fold-change of each gene per plaque index for each single time-point (Figure 3A). Amyloid plaque positive spots were enriched with myelin-encoding genes (eg. *Plp1, Mobp, Mal, Cnp, Ermn, Mog, Mbp, Cldn11, Mag, Apod,* and *Tspan2* among the top 100 ranks, FDR < $1e^{-5}$) at 3-months of age, but switched to the enrichment of microglial genes (eg. *Cst7, Cd68, Ccl6, Tyrobp, Fcrls, Trem2, Lyz2, C1qb, C1qc, Hexa, Hexb, Ctss, Ctsb, Ctsd,* and *B2m* among top 20 ranks, FDR < $1e^{-15}$) and astroglial genes (eg. *Gfap* and *Apoe* among top 50 ranks, FDR <$1e^{-10}$) at 18-month of age. Notably, *Plp1, Mobp,* and *Mal* were initially up-regulated but eventually down-regulated around plaques (among the top 100 ranks, FDR < $1e^{-5}$, Figure 3A). Our results indicate the early response of oligodendrocytes to amyloid plaques and micro- and astrogliosis in the late stage of AD. Amyloid plaques mainly drive inflammation in the disease model at the late stage.

We took advantage of our database to investigate gene co-expression networks related to amyloid plaques burden. We performed Weighted Gene Co-expression Network Analysis (WGCNA) and grouped genes into modules in an unsupervised approach. WGCNA is useful to identify modules of biologically related genes that are co-expressed and co-regulated. We identified 12 networks, one of which was very highly up-regulated in the presence of amyloid plaques at 18-month of age. This network has 57 co-expression molecules and is enriched with microglial markers, astroglial markers, and components of innate immune response and proteolysis as defined by Gene Ontology. We call these 57 co-expressors Plaque-induced Inflammatory Genes (PIGs). Interestingly, among the 57 PIGs, 26 genes have been identified as markers of disease-associated microglia and 5 genes have been identified as markers of the LPS-induced inflammatory astroglia (Figure 4A). Notably, 12 genes have been identified as GWAS hits in Alzheimer's disease (Figure 4A, red genes). In addition, we identified 5 genes involved in the initiation of the classical complement system (*C1qa, C1qb, C1qc, C4a, C4b*), 6 genes involved in microglia activation and inflammation (*Apoe, Trem2, Tyrobp, Csf1r, Ly86, Mpeg1*), 20 genes involved in phagocytosis and proteolysis via lysosomal system (*Lyz2, Ctsz, Ctsd, Laptm5, Ctss, Hexb, Hexa, Grn, Ctsl, Gusb, Ctsa, Cd63, Npc2, Ctsh, Man2b1, Ctsb, Cd63-ps, Gns, Lgmn, Cst3*), 3 genes involved in oxidative stress (*Gpx4, Gpx4-ps, Prdx6*), 3 genes involved in MHC class I (*H2-D1, H2-K1, B2m*), and 3 genes involved in Fc receptor (*Fcrls, Fcgr3, Fcer1g*). Mostly, PIGs were up-regulated in AD versus WT from 6-month of age (Figure 4B), and up-regulated in the presence of amyloid plaques at18-months of age (Figure 4C).
It will be informative to understand how the different cell-types co-regulated via the 57 PIGs around amyloid plaques, contribute to the risk of disease in follow-up studies. We have developed an interactive online software package for visualizing and re-analysis all the data (AlzMap), which will be published as an open resource. We hope to deepen further the bioinformatics analysis of this project and provide validation using in situ hybridization in the third year of this project and provide a publication at the end of this year.

Figure 1

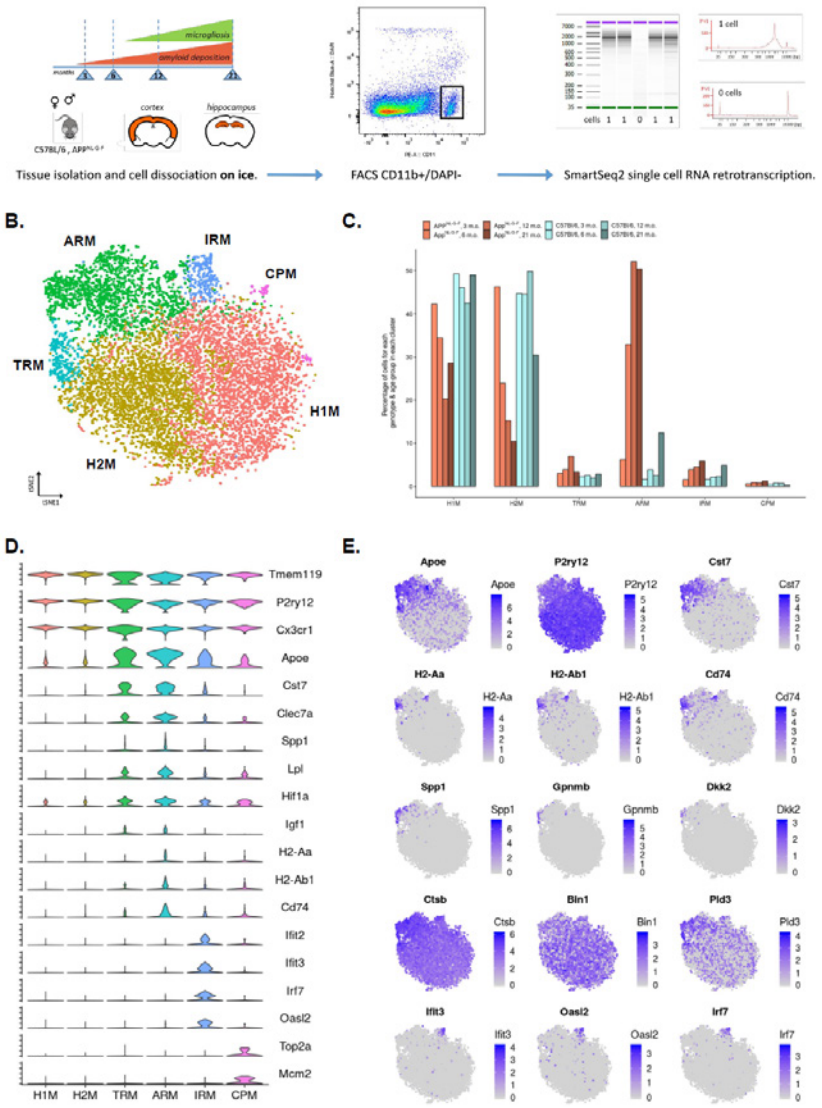

Figure 1. Microglia mount a heterogeneous response to β-amyloid, marked by *Apoe* overexpression. A. Dataset presentation. We used male and female *App*$^{NL\text{-}G\text{-}F}$ and wild type *C57BL/6* mice from four time points over the course of amyloid pathology and microgliosis as indicated. We dissected separately cortex and hippocampal tissues. The tissue from two animals for each experimental condition (age, sex, tissue, genotype) was pooled prior to microglia isolation. All procedures were performed on ice. Single live microglia cells were isolated by FACS (CD11b+, DAPI-) and single cell RNAseq libraries were prepared according to the SmartSeq2 and Nextera methods. **B.** t-SNE plot visualizing the 10,801 single microglia cells passing quality control, after removal of peripheral cells. Cells are coloured according to clusters identified with Seurat's kNN approach (H1M and H2M: homeostatic microglia, TRM: transiting response microglia, ARM: activated response microglia; IRM: interferon response microglia; CPM: cycling/proliferating microglia). **C.** Percentage of cells from each genotype-age group for each cluster identified. *App*$^{NL\text{-}G\text{-}F}$ are coloured in shades of red, while wild types are coloured in shades of blue. **D.** Violin plots of selected marker genes for each identified cluster. Y axes indicates normalized gene expression (ln scale). **E.** t-SNE plots as in B, coloured by the level of ln normalized expression of selected genes. Clusters TRM and ARM display increased expression of *Apoe* and inflammation markers (*Cst7*), and concurrently display a reduction of homeostatic markers (*P2ry12*). Two distinct regions of cluster ARM display increased expression of MHC type II genes (*H2-Aa*, *H2-Ab1*, *Cd74*), suggesting the existence of microglial subpopulations. Further, a small subset of cluster ARM displays an enrichment for tissue repair genes (*Spp1*, *Gpnmb*, *Dkk2*). Cluster ARM also displays differential expression of several AD-related genes (e.g. *Ctsb*, *Bin1*, *Pld3*) compared to clusters H1M and H2M. Cluster IRM is enriched for interferon genes (*Ifit3*, *Oasl2*, *Irf7*).

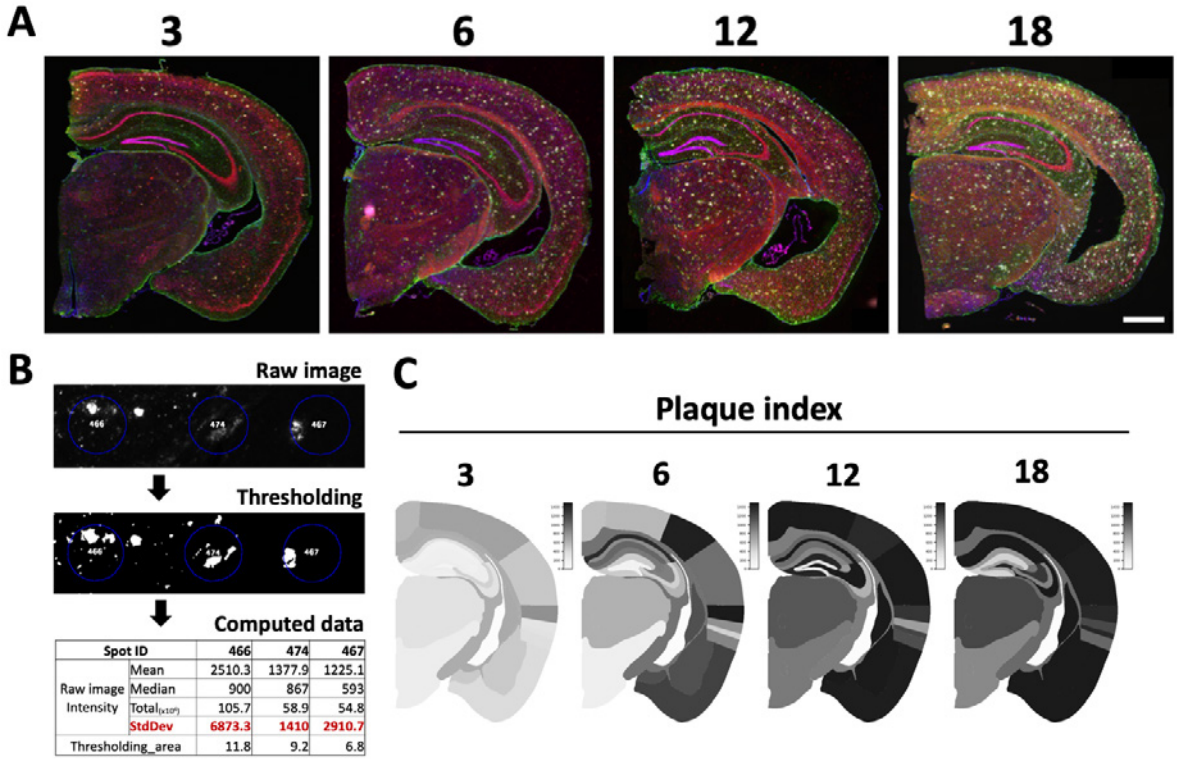

Spot ID		466	474	467
Raw image Intensity	Mean	2510.3	1377.9	1225.1
	Median	900	867	593
	Total$_{(x10^6)}$	105.7	58.9	54.8
	StdDev	6873.3	1410	2910.7
Thresholding_area		11.8	9.2	6.8

Figure 2. Computation of plaque index for each transcriptomic profile. (A) Immunostaining on coronal sections of APPNL-G-F KI mice at 3, 6, 12, and 18 months of age. Colors: DAPI (bule), anti-NeuN (red), anti-Gfap (green), anti-amyloid beta (6E10, white). Scale bar: 1 mm (coronal sections, upper panels) and 100 mm (zoom-ins, lower panels) (B) Computing 5 parameters for the indication of amyloid burden for each spot. (C) The resulted plaque index shown for the indicated brain region and age is similar to the result of immunostaining that amyloid propagated from cortex to hippocampus and thalamus.

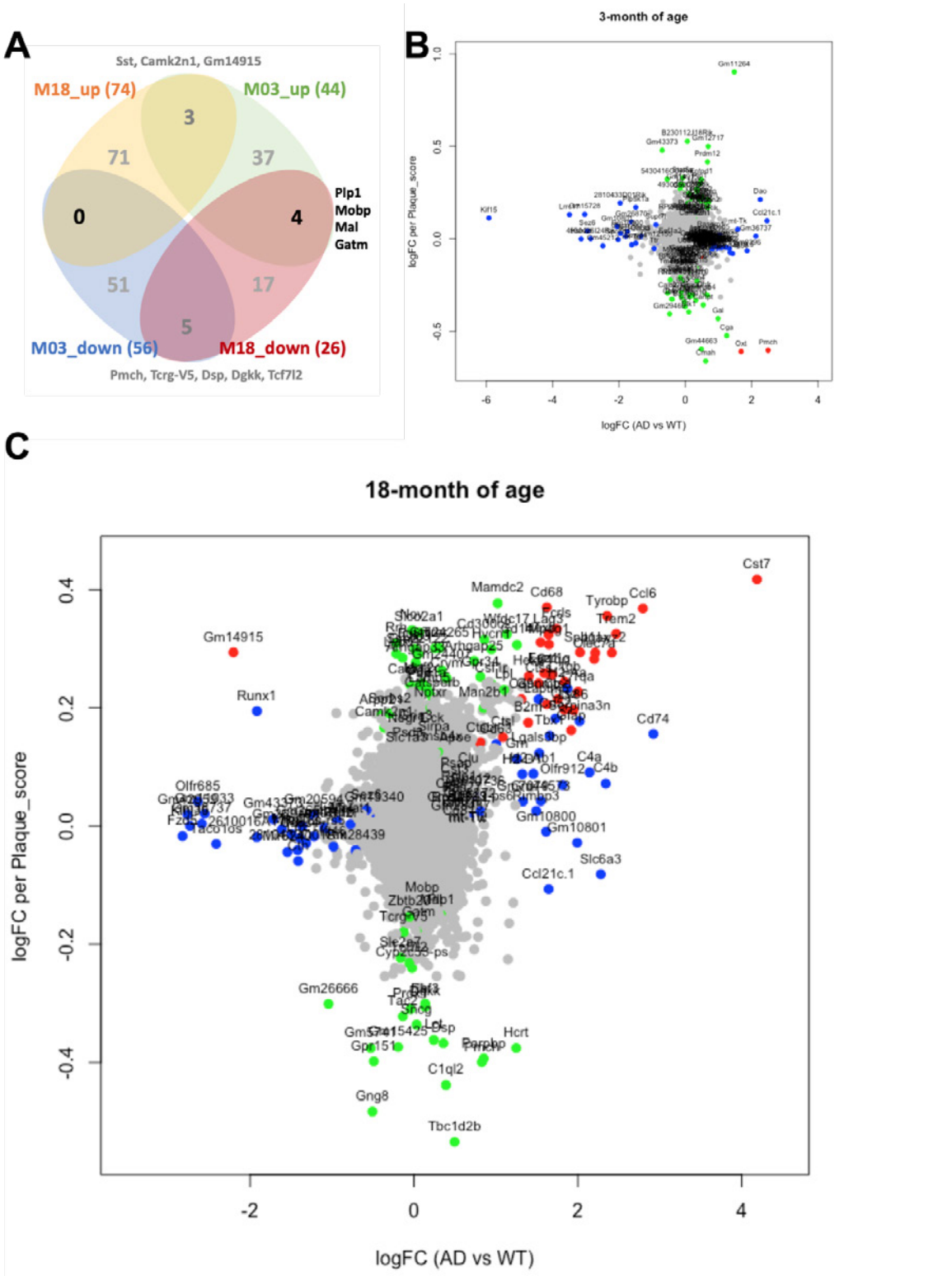

Figure 3. Link expression profiles to amyloid plaque. (A) Top 100 plaque-reactive genes ranked by FDR at 3-month or 18-month of age. (B, C) Molecular alteration around amyloid plaque (y-axis: log2 fold-changes per plaque index) and in APPNL-G-F (x-axis: log2 fold-changes of AD vs WT) at 3-month (B) and 18-month (C) of age. Green genes: top 100 plaque-reactive genes; blue genes: top 100 disease-reactive genes; red genes: the overlap of blue and green genes.

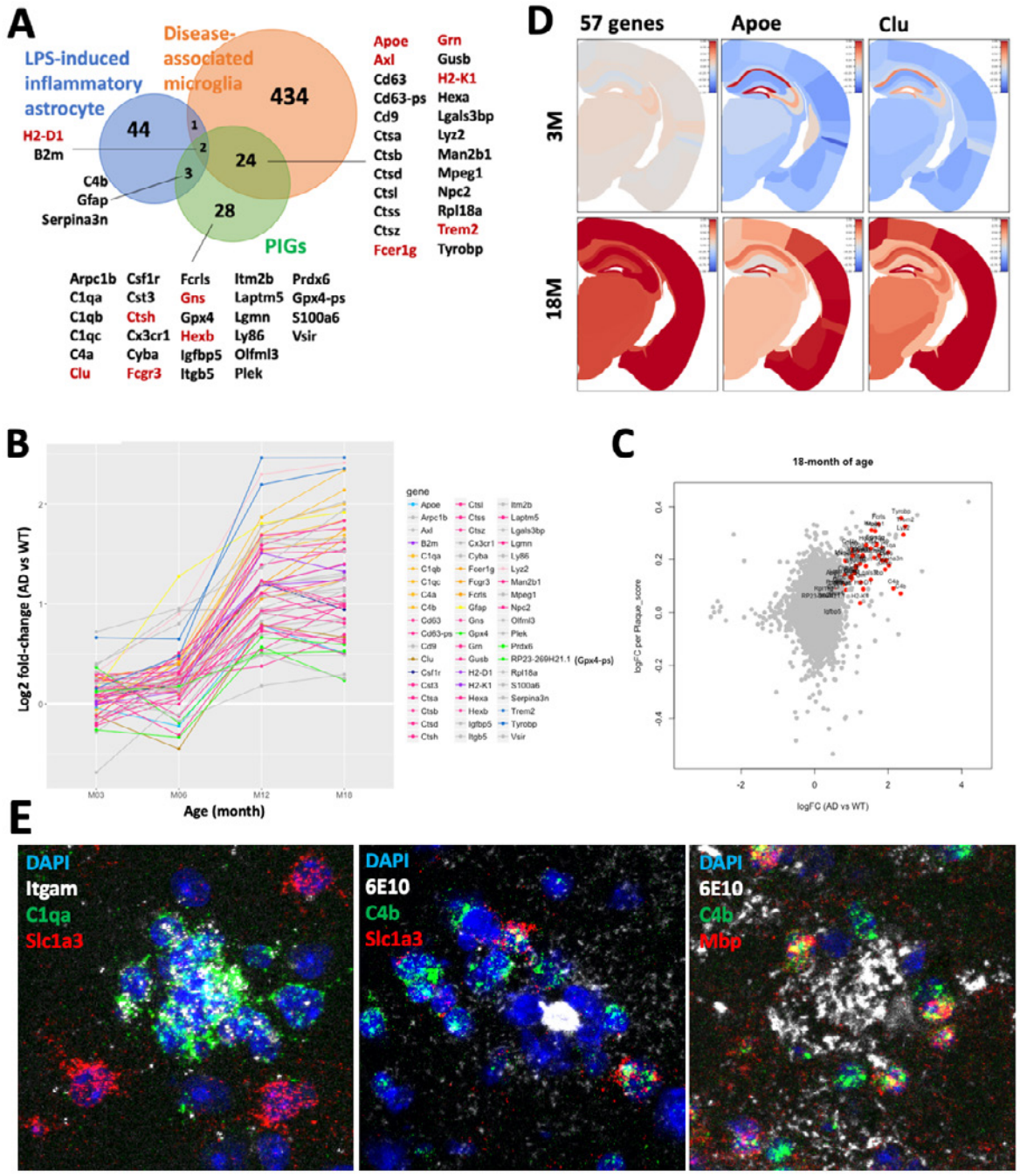

Figure 4. The co-regulated 57 Plaque-induced Inflammatory Genes (PIGs) around amyloid plaques. (A) PIGs are enriched with the marker genes for disease-associated microglia and the marker genes for LPS-induced inflammatory astrocyte. Red genes: GWAS hits. (B) Log fold-changes of gene expression of AD vs WT at the indicated age from whole brain regions. (C) The 57 PIGs (red genes) were up-regulated in the presence of amyloid plaques and in the APP NL-G-F model at 18-month of age. (D) Log fold-changes of gene expression of AD vs WT at the indicated age and brain region. (E) RNAscope of the indicated mRNA targets in the hippocampus of APP NL-G-F at 18-month of age.

Geneeskundige Stichting Koningin Elisabeth
Fondation Médicale Reine Elisabeth
Königin-Elisabeth-Stiftung für Medizin
Queen Elisabeth Medical Foundation

Progress report of the research group of

Prof. Goris An, PhD

Katholieke Universiteit Leuven (KU Leuven)

Principal investigator

Prof. Goris An, PhD
KU Leuven
Department of Neurosciences
Laboratory for Neuroimmunology
Tel.: +32 16 33 07 72
E-mail: an.goris@kuleuven.be

Table of contents

Unraveling the BAFF pathway towards targeted treatment of multiple sclerosis

1. Summary and current status of research program

Multiple sclerosis (MS) is one of the most common neurological disorders in young adults, affecting around 10,000 people in Belgium and 2.5 million worldwide. The disease can lead to important physical as well as cognitive disability at a time that is crucial in the personal and professional development of patients. MS is characterized by three hallmarks: inflammation, demyelination and neuronal loss[1]. The aetiology is unknown but the past few years have seen exciting progress in the field.
The International Multiple Sclerosis Genetics Consortium (IMSGC), of which I am the Belgian representative, has recently identified 200 common genetic susceptibility factors for MS (IMSGC, preprint available on http://dx.doi.org/10.1101/143933) as well as four less common genetic susceptibility factors[2]. These risk factors highlight the role not only of T cells, but increasingly also of B cells in the pathogenesis of MS. In a systems immunology approach comparing multiple immunomodulatory treatments, we have previously demonstrated a unique B cell pathway, including an increase in B cell activation factor (BAFF) and transitional B cells and a decrease in memory B cells, as shared across treatments[3]. This shared B-cell related mechanism has recently been extended to other novel treatments in the literature[4-6]. The combination of these data point to a key role for B cells not only in the pathogenesis but also in the treatment of MS[7,8]. This is also highlighted by the choice for B-cells as the topic of the next European Charcot Foundation conference in 2019. In the project supported by a Research Grant and the Prize Viscountess Valine de Spoelberch from GSKE, we set out to build on these data supporting the role of a specific B-cell pathway in the treatment of MS with two aims.

1. We unravel the role of the B cell pathway in detail, investigating the different contributions of known splice-forms, soluble and membrane-bound forms of BAFF and the different receptors and co-stimulatory molecules on transitional B cells. The role of B cells in the treatment of MS is emerging, but successful and failed B-cell related clinical trials indicate that a better understanding of the B cell pathway in treatment is required to develop targeted new treatments.

   This objective led to one published manuscript, and one manuscript in preparation.

   Maya Imbrechts, Karen De Samblancx, Karlien Fierens., Ellen Brisse, Jessica Vandenhaute, Tania Mitera, Claude Libert, Ide Smets, An Goris, Carine Wouters, Patrick Matthys IFN-γ stimulates CpG-induced IL-10 production in B cells via p38 and JNK signalling pathways. *European Journal of Immunology*, 2018, 48:1506-1521. IF: 4.248, 1 citation

   Ide Smets, Teresa Prezzemolo, Maya Imbrechts, Josselyn E. Garcia-Perez, Klara Mallants, James Dooley, Stephanie Humblet-Baron, Bénédicte Dubois, Patrick Matthys, Adrian Liston*@, An Goris*@, The role of the BAFF pathway in treatment-induced B cell changes in multiple sclerosis. manuscript in preparation

2. We correlate the B cell pathway with genetic and clinical factors in order to better understand how these contribute to patient-to-patient heterogeneity in pathogenesis and response to treatment. This outcome would provide a rationale for personalized medicine.

The correlation between genetic factors and the B cell pathway has led to two published research papers and an invited Editorial.

Ide Smets*, Barnaby Fiddes*, Josselyn E. Garcia-Perez*, Di He*, Klara Mallants, Wenjia Liao, James Dooley, George Wang, Stephanie Humblet-Baron, Bénédicte Dubois, Alastair Compston, Joanne Jones, Alasdair Coles, Adrian Liston, Maria Ban, An Goris@, Stephen Sawcer@. Multiple sclerosis risk variants alter expression of co-stimulatory genes in B cells. *Brain*, 2018, 141:786-796. IF 10.292, citations: 5

Vasiliki Lagou, Josselyn E. Garcia-Perez, Ide Smets, Lies Van Horebeek, Marijne Vandebergh, Liye Chen, Klara Mallants, Teresa Prezzemolo, Kelly Hilven, Stephanie Humblet-Baron, Matthieu Moisse, Philip Van Damme, Guy Boeckxstaens, Paul Bowness, Bénédicte Dubois, James Dooley, Adrian Liston*@, An Goris*@. Interrelationship between genetic control of human immune system variation and disease susceptibility. *Cell Reports*, 2018, 25, 798–810. IF 8.32

Liston A. and Goris A. The origins of diversity in human immunity (invited News and Views feature). *Nature Immunology*, 19:209-210. IF 21.809, 2 citations

2. Achievements

Achievement 1. Multiple sclerosis risk variants alter expression of co-stimulatory genes in B cells (Smets et al., *Brain,* 2018; awarded with the Research Prize 2018 of the Belgian Neurological Society to Ide Smets; part of the PhD obtained by Dr. Ide Smets on 25 Sept 2018)

1. Summary

The increasing evidence supporting a role for B cells in the pathogenesis of multiple sclerosis prompted us to investigate the influence of known susceptibility variants on the surface expression of co-stimulatory molecules in these cells. Using flow cytometry we measured surface expression of CD40 and CD86 in B cells from 68 patients and 162 healthy controls that were genotyped for the multiple sclerosis associated single nucleotide polymorphisms (SNPs) rs4810485, which maps within the CD40 gene, and rs9282641, which maps within the CD86 gene. We found that carrying the risk allele at rs4810485*T lowered the cell-surface expression of CD40 in all tested B cell subtypes (in total B cells $p \leq 5.10 \times 10^{-5}$ in patients and $\leq 4.09 \times 10^{-6}$ in controls), while carrying the risk allele rs9282641*G increased the expression of CD86, with this effect primarily seen in the naïve B cell subset ($p = 0.048$ in patients and 5.38×10^{-5} in controls). In concordance with these results analysis of RNA expression demonstrated that the risk allele rs4810485*T resulted in lower total CD40 expression ($p = 0.057$) but with an increased proportion of alternative splice-forms leading to decoy receptors ($p = 4.00 \times 10^{7}$). Finally, we also observed that the risk allele rs4810485*T was associated with decreased levels of interleukin-10 ($p = 0.020$), which is considered to have an immunoregulatory function downstream of CD40. Given the importance of these co-stimulatory molecules in determining the immune reaction that appears in response to antigen our data suggest that B cells might have an important antigen presentation and immunoregulatory role in the pathogenesis of multiple sclerosis.

2. Situation in the GSKE project

This study unraveled the mechanism of action of established MS susceptibility genes CD40 and CD86, which fall within the B-cell pathway that is the topic of this GSKE project. The study demonstrates that

the CD40 MS risk variant acts through a deficit in the protective role of immunoregulatory B cells. These immunoregulatory B cells are enriched amongst early (transitional) B cells, respond to the growth factor B cell activating factor (BAFF) and produce the immunoregulatory cytokine interleukin10.

3. Future perspectives and clinical implications

Blocking CD40 with monoclonal anti-CD40 antibodies has been proposed as a therapy for MS based on animal models and is currently considered by pharmaceutical companies. However, the results from our study suggest that decreasing or blocking CD40 is associated with increased risk for MS instead of protection. Whereas anti-CD40 may be beneficial for more antibody-driven autoimmune diseases such as lupus erythematosus, it calls for extreme caution in applying this treatment for MS. This is completely in line with the anti-BAFF therapies, which are successful in other autoimmune diseases but failed clinical trials in MS and even worsened instead of improved MS. Both anti-CD40 and anti-BAFF limit the important role of immunoregulatory B cells in MS.

Results also suggest that if limiting the role of immunoregulatory B cells worsens disease, enhancing the protective role of immunoregulatory B cells in MS may instead be beneficial. We have previously demonstrated that several currently used and efficacious MS treatments share this as a unique mechanism of action[3]. This shared B-cell related mechanism has recently been extended to other novel treatments in the literature[4-6]. Our results especially suggest that current, promising B cell depletion therapies may increase the efficacy/safety balance if they would deplete B cells more selectively, i.e. deplete likely pathogenic B cells such as memory B cells, but spare beneficial B cells such as the immunoregulatory B cells. Our research group is currently working towards a scientific basis for this aim.

Achievement 2. Interrelationship between genetic control of human immune system variation and disease susceptibility (Lagou et al., *Cell Reports*, 2018; invited News and View item Liston and Goris, *Nature Immunology*, 2018)

1. Summary

The immune system is highly diverse, but characterization of its genetic architecture has lagged behind the vast progress made by genome-wide association studies (GWASs) of emergent diseases. Our GWAS for 54 functionally relevant phenotypes of the adaptive immune system in 489 healthy individuals identifies eight genome-wide significant associations explaining 6%–20%of variance. Coding and splicing variants in *PTPRC* and *COMMD10* are involved in memory T cell differentiation. Genetic variation controlling disease-relevant T helper cell subsets includes *RICTOR* and *STON2* associated with Th2 and Th17, respectively, and the interferon-lambda locus controlling regulatory T cell proliferation. Early and memory B cell differentiation stages are associated with variation in *LARP1B* and *SP4*. Finally, the latrophilin family member *ADGRL2* correlates with baseline pro-inflammatory interleukin-6 levels. Suggestive associations reveal mechanisms of autoimmune disease associations, in particular related to pro-inflammatory cytokine production. Pinpointing these key human immune regulators offers attractive therapeutic perspectives.

2. Situation in the GSKE project

The recent advent of in-depth immune phenotyping across large sample sizes has enabled characterization of the extent and identification of the factors shaping variation in the human immune profile[9]. Longitudinal studies have reported high levels of inter-individual variation, with low longitudinal variation and a highly elastic structure, where transient antigen-induced changes are followed by a return to the individual's unique baseline[10,11]. Twin and family-based studies provide heritability estimates of 20-40% on average, but covering a wide range across individual traits[10,12,13]. Aging contributes up to 5% of variation[10-12,14], and environmental factors include obesity, cohabitation and chronic viral infections[11,12,14]. Identification of genetic factors controlling variation in the immune system is still in the initial discovery phase, with novel and strong associations emerging from pioneer studies[10,13,14]. We performed a GWAS of up to 10,246,977 autosomal variants in 489 healthy Caucasian individuals for 54 immune phenotypes

established as part of our previous study[11]. The 54 functionally relevant immune phenotypes for which genetic determinants were identified in this study include B cells and B cell subsets. We identified eight regions reaching genome-wide significance ($P < 5x\ 10^{-8}$) to at least one immune phenotype.
Amongst these genome-wide significant results, we identify genetic determinants controlling B cell immunophenotypes that are of relevance for the pathogenesis of MS. In particular, an intergenic variant on chromosome 7 was associated with memory B cell differentiation, a cell type we previously implicated in the immune profile of MS[3], and expression levels in B cells implicated the adjacent *SP4* gene, which is known to downregulate expression of the B cell differentiation factor *BCL2*[15,16]. A second association for a variant near *LARP1B* was observed for KREC excision circles. KREC is a marker for the early B cells which are enriched for the immunoregulatory B cells that form the topic of this GSKE project. LARP1B is still poorly characterized but highly resembles LARP1[17]. LARP1 acts downstream of mTORC1[18,19], which, in addition to its well known role in T cell metabolism and differentiation, controls early B cell development, survival, and metabolism in mice[20]. Our data now suggest an analogous function for the homolog LARP1B in early B cell development in humans. We demonstrated that treatments known to induce the formation of early B cells, such as interferon-beta[3], increase sjKREC excision circles and decrease *LARP1B* gene expression levels. We observed an inverse correlation with increased levels of LARP1B blocking early B cell differentiation. Our data provide the first evidence translating the key importance of these genes and pathways from animals to humans, and highlight that in humans these pathways are variable in vivo in a physiological range.

3. Future perspectives and clinical implications
We have previously demonstrated that KREC is increased upon treatment with current efficacious MS treatments[3]. We currently investigate whether KREC and/or the genetic determinant associated with KREC is associated with the efficacy of MS treatments and can be used as a biomarker for treatment response. Such biomarkers are much needed to ensure that each patient is treated as early as possible with the best possible treatment ("precision medicine") in the current context where the clinician is faced with the choice between a whole range of MS treatments, each with their own efficacy and safety profile. Further understanding of the role of how these novel genes and pathways control B cell numbers and B cell differentiation may additionally offer novel leads for rational treatment design in the context of targeting B cells as a promising therapeutic strategy for MS.

Achievement 3. The role of BAFF and BAFF receptors in the treatment of multiple sclerosis (Imbrechts et al., *European Journal of Immunology* 2018; part of the PhD obtained by Dr. Ide Smets on 25 Sept 2018; Smets et al., manuscript in preparation)

1. Summary
1. Mechanisms of IL-10 induction in B cells (Imbrechts et al. 2018)
IL-10 is an immunoregulatory cytokine produced by B cells and has been implicated in both the risk (see Achievement 1) and treatment of MS. The production of this potent immunosuppressive cytokine must be strictly regulated to ensure a balanced immune response. IFN-γ, a key cytokine in multiple immune processes and pathologies, is known as an inhibitor of IL-10 production by monocytes and macrophages, but also has some regulatory functions. In the present study, we explored the role of IFN-γ on Toll-like receptor (TLR)-induced IL-10 production in murine peritoneal and spleen cells and in human peripheral blood mononuclear cells. IFN-γ inhibited IL-10 production induced by TLR2, TLR3, TLR4 and TLR7/8 agonists, but stimulated IL-10 production when cells were triggered with CpG oligodeoxynucleotides, a specific TLR9 agonist. The stimulatory effect of IFN-γ on TLR9-induced IL-10 was restricted to B cells. In line with the increased IL-10, B cells stimulated with CpG and IFN-γ profoundly inhibited CD4 T cell proliferation. From our experiments with recombinant BAFF and neutralising BAFF- and TACI-antibodies, we conclude that BAFF does not promote IL-10 production by CpG-stimulated B cells but that a different mechanism unrelated to BAFF is at work. Further research into the mechanisms involved, revealed that the mitogen-activated protein kinases p38 and JNK are essential players in this stimulatory

effect, and that the phosphatase MKP1 – an inhibitor of p38 and JNK activity – is downregulated after combined stimulation with IFN-γ and CpG. Our data may represent a novel immunoregulatory role of IFN-γ in B cells after triggering of TLR9, by stimulating IL-10 production.

2. IL-10 and B cell related changes upon treatment in MS (ongoing work)

Interferon-beta (IFNB) and fingolimod are mechanistically distinct multiple sclerosis treatments but induce both B cell-activating factor (BAFF) and transitional B cells. To date we do not fully understand how BAFF, BAFF spliceforms and BAFF receptors behave under the influence of treatment and how a BAFF increase results in a regulatory immune phenotype. We collected a cross-sectional study population of 112 Caucasian patients (41 untreated, 42 IFNB, 29 fingolimod) diagnosed with multiple sclerosis. Using flow-cytometry, we determined B cell surface expression of BAFF-R, TACI and CD40 on the entire cohort. We used digital PCR to quantify the level of deltaBAFF, a full-length BAFF antagonizing spliceform. We followed up with an *in vitro* experiment in which BAFF-stimulated and unstimulated B cells of untreated and IFNB patients were brought into culture. These cells were subjected to a flow-cytometry panel focused at B cell subsets and intracellular IL-10 production. IFNB and fingolimod induced BAFF mRNA expression as well as soluble BAFF, which correlated with a surge in transitional B cells ($P = 5.70 \times 10\text{-}6$). However, there was no net change in the ratio of deltaBAFF relative to full-length BAFF ($P \geq 0.61$). Moreover, fingolimod and to a lesser extent IFNB treatment steeply reduced the expression levels of BAFF-R ($P \leq 1.77 \times 10\text{-}5$) on B cells while TACI expression remained unaltered. B cells from IFNB treated patients demonstrated an elevated intracellular IL-10 production, especially in naïve B cells ($P = 8.66 \times 10\text{-}3$). However, adding BAFF stimulation to B cells did not induce intracellular IL-10 production ($P > 0.05$). We conclude that IFNB and fingolimod have as only shared mechanism a shift towards transitional B cells, which appears associated with changes in the expression of BAFF and its receptors.

2. Situation in the GSKE project

In Achievement 1, we demonstrated that known MS genetic risk factors act through a shortage of the immunoregulatory cytokine IL-10. We previously identified a unique B cell related pathway shared across multiple MS treatments such as interferon-beta and fingolimod. This pathway consists of an increase in transitional B cells driven by elevated B cell activating factor (BAFF) levels and a decrease in memory B cells. The same treatments are known to induce IL-10 production in B cells but the mechanism of this IL-10 induction is unknown. We hypothesized that the BAFF alterations are responsible for increased IL-10 production but our experimental data not indicate that this is not the case. Hence, we are pursuing in two directions. First, we examine how BAFF contributes immunoregulatory effects in B cells that are independent of IL-10. Secondly, we examined BAFF-unrelated mechanisms of IL-10 induction in B cells in the published paper and in ongoing work.

3. Future perspectives and clinical implications

For the two directions being current pursued, we have selected two pathways for further investigation. The first one is a candidate pathway which involves other receptors on the B-cell surface than BAFF receptors and could explain how current efficacious treatments induce IL-10 production in immunoregulatory B-cells. The second pathway is a candidate pathway downstream of BAFF and BAFF receptors which could explain how BAFF exerts its regulatory B-cell function.

An improved understanding of how BAFF and regulatory B cells have a protective role in MS, but contribute to the pathogenesis of other autoimmune diseases where auto-antibody production is a hallmark, will provide novel leads for B cell related therapeutic strategies in MS. This would allow the development of more specific B cell therapies instead of the current promising but non-selective B cell therapies, which deplete all B cells with potential safety concerns.

3. Networking and collaborations

Achievement 1 was realized in collaboration with Prof. Stephen Sawcer of Cambridge University (UK). Importantly, concordant results and conclusions were reached in both the Belgian case and UK control study populations, independent of experimental design, providing replication and robustness of our results. Dr. Ide Smets obtained the Research Prize 2018 from the Belgian Neurological Society for her publication as output of achievement 1. Achievement 3 is being realized in collaboration with Prof. Patrick Matthys (KU Leuven), who identified regulatory circuits for controlling autoimmune and autoinflammatory diseases.

I recently became coordinator of the International Multiple Sclerosis Genetics Consortium (www.imsgc.org), and our research group is a member of the EU Horizon2020 Consortium MultipleMS (www.multiplems.eu).

Over the past year, members of my research group and I attended the European Conference on the Treatment and Research in Multiple Sclerosis (ECTRIMS) in Paris, France and the European Charcot Foundation Meeting in Baveno, Italy. Results from the achievements above were or will be presented at the following occasions:

- 24-October-2017: Research Community “Multiple Sclerosis” of the Research Foundation Flanders, Hasselt, Belgium
- 26-October-2017: European Conference on the Treatment and Research in Multiple Sclerosis (ECTRIMS), Paris (Travel Grant awarded to Dr. Ide Smets)
- 24-November-2017: Belgian Immunological Society, Leuven, Belgium
- 9-November-2017: Department of Human Genetics, KU Leuven, Belgium
- 6-December-2017: Neurology Department UZ Leuven, Belgium
- 15-May 2018: Yearly conference of EU Horizon2020 project “MultipleMS”
- 7-Feb 2019: Immunogenomics of Disease: Accelerating to Patient Benefit 2019, Cambridge, UK
- multiple times and locations in 2018: lecture on MS genetics for neurologists

4. Relevance and future perspectives

In summary, results obtained so far strongly indicate a role of B cells in the pathogenesis as well as the treatment of MS. Our genetic and immunological studies indicate, however, that not all B cell subsets contribute equally. Whereas the memory B cell subset is thought to exert a pathogenic role, the subset of immunoregulatory B cells appears protective in the disease process and contributes to the mechanism of action of current treatments. B cell depletion therapies, in which all B cells are wiped out, are the most promising novel treatment for MS that has entered the Belgian market. B cell depletion therapies highly reduce disease activity but their long-term safety, for example with respect to susceptibility to infections, remains to be evaluated. Our data indicate that a more selective or a more targeted B cell depletion, wiping out only pathogenic B cells but sparing beneficial B cells may increase the efficacy/safety balance of MS treatment. Whereas B cell depletion therapies are promising overall, there is a group of patients for whom the treatment is not effective but may even worsen disease. B-cell related biomarkers may indicate the subset of MS patients who are most likely to benefit from B cell therapies.

Our research group currently continues on these two lines: understanding the precise role of B cell subsets towards a more targeted therapy and identifying possible B-cell related biomarkers for precision medicine. Support from GSKE is instrumental in this B-cell research line within our research group, and any additional financial support would allow us to build maximally on the promising results obtained in the first two years. Please see the section “Future perspectives” for each of the manuscripts described

above on how we would specifically extend this research line in future. We expect to translate our research results to the much-anticipated and much-needed development of precision medicine in the clinical care for MS patients.

5. Financial report

As foreseen, GSKE project support has been assigned for 50% to staff and 50% to consumable costs dedicated to this project. The KU Leuven Financial Department will provide a detailed report. Staff cost in Year 1 was assigned to Ide Smets, first author of one of the GSKE-supported papers, who successfully obtained her PhD on 25 September 2018. Upon completion of her PhD, Dr. Ide Smets remains committed to this project as Neurology Resident at the University Hospitals Leuven. Staff cost in Year 2 was assigned to Klara Mallants for expert technical assistance on this project.

With the support of the **Prize Viscountess Valine de Spoelberch**, I was able to attract a new PhD student, Marijne Vandebergh, and thereby ensure continuity of this research line and maximally ensure that we can continue to build on the current results. As Marijne Vandebergh successfully obtained a personal PhD Fellowship of the Research Foundation Flanders (start date 01/10/2018), the budget foreseen for her reimbursement will now be re-allocated and will allow us in year 3 to use the latest, but still highly expensive, genetic technologies such as single-cell sequencing to enhance the current project to the current state-of-the-art.

6. Publications under GSKE support (Research Project and Prize Viscountess Valine de Spoelberch)

* indicates shared first/senior authors and @ indicates corresponding author

- Van Horebeek L.*, Hilven K.*, Mallants K., Van Nieuwenhuijze A., Kelkka T., Savola P., Mustjoki S., Schlenner S.M., Liston A., Dubois B., Goris A@. A robust pipeline with high replication rate for detection of somatic variants in the adaptive immune system as a source of common genetic variation in autoimmune disease. *Human Molecular Genetics*, in press. IF 4.902
- Smets I.*, Fiddes B.*, Garcia-Perez J.E.*, He D.*, Mallants K., Liao W., Dooley J., Wang G., Humblet-Baron S., Dubois B., Compston A., Jones J., Coles A., Liston A., Ban M., Goris A.@, Sawcer S.@. Multiple sclerosis risk variants alter expression of co-stimulatory genes in B cells. *Brain*, 2018, 141:786-796. IF 10.292, 5 citations
- Lagou V., Garcia-Perez J.E., Smets I., Van Horebeek L., Vandebergh M., Chen L., Mallants K., Prezzemolo T., Hilven K., Humblet-Baron S., Moisse M., Van Damme P., Boeckxstaens G., Bowness P., Dubois B., Dooley J., Liston A.*@, Goris A.*@. Interrelationship between genetic control of human immune system variation and disease susceptibility. *Cell Reports*, 2018, 25, 798–810. IF 8.32
- Liston A. and Goris A. The origins of diversity in human immunity (invited News and Views feature). *Nature Immunology*, 19:209-210. IF 21.809, 2 citations
- Imbrechts M., De Samblancx K., Fierens K., Brisse E., Vandenhaute J., Mitera T., Libert C., Smets I., Goris A., Wouters C., Matthys P. IFN-γ stimulates CpG-induced IL-10 production in B cells via p38 and JNK signalling pathways. *European Journal of Immunology*, 2018, 48:1506-1521. IF: 4.248, 1 citation
- Hilven K.*, Vandebergh M.*, Smets I., Mallants K., Goris A.@, Dubois B.. Genetic basis for relapse rate in multiple sclerosis: association with *LRP2* genetic variation. *Multiple Sclerosis Journal*, 2018, 24:1773-1775. IF: 5.280, 1 citation

7. Team publications within project duration 2017-2018

* indicates shared first/senior authors and @ indicates corresponding author

- Van Horebeek L.*, Hilven K.*, Mallants K., Van Nieuwenhuijze A., Kelkka T., Savola P., Mustjoki S., Schlenner S.M., Liston A., Dubois B., Goris A@. A robust pipeline with high replication rate for detection of somatic variants in the adaptive immune system as a source of common genetic variation in autoimmune disease. *Human Molecular Genetics*, in press. IF 4.902

- Goris A.@ and Dubois B. Leveraging human genetics to inform intervention strategies for multiple sclerosis (Invited Editorial). Neurology 2018, in press. IF 8.32
- The International Multiple Sclerosis Genetics Consortium. The Multiple Sclerosis Genomic Map: Role of peripheral immune cells and resident microglia in susceptibility. preprint vailable on http://dx.doi.org/10.1101/143933
- The International Multiple Sclerosis Genetics Consortium. Low-Frequency and Rare-Coding Variation Contributes to Multiple Sclerosis Risk. *Cell*, 2018, 175, 1–9. IF: 30.41
- Lagou V., Garcia-Perez J.E., Smets I., Van Horebeek L., Vandebergh M., Chen L., Mallants K., Prezzemolo T., Hilven K., Humblet-Baron S., Moisse M., Van Damme P., Boeckxstaens G., Bowness P., Dubois B., Dooley J., Liston A.*@, Goris A.*@. Interrelationship between genetic control of human immune system variation and disease susceptibility. *Cell Reports*, 2018, 25, 798–810. IF 8.32
- Liston A. and Goris A. The origins of diversity in human immunity (invited News and Views feature). *Nature Immunology*, 19:209-210. IF 21.809, 2 citations
- Imbrechts M., De Samblancx K., Fierens K., Brisse E., Vandenhaute J., Mitera T., Libert C., Smets I., Goris A., Wouters C., Matthys P. IFN-γ stimulates CpG-induced IL-10 production in B cells via p38 and JNK signalling pathways. *European Journal of Immunology*, 2018, 48:1506-1521. IF: 4.248, 1 citation
- Fenoglio C., Oldoni E., Serpente M., De Riz M.A., Arcaro M., D'Anca M., Pietroboni A.M., Calvi A., Lecchi E., Goris A., Mallants K., Dubois B., Comi C., Cantello R., Scarpini E., Galimberti D. LncRNAs expression profile in peripheral blood mononuclear cells from multiple sclerosis patients. *Journal of Neuroimmunology*, 2018, 15:129-135. IF 3.033, 1 citation
- Gille B., De Schaepdryver M., Goossens J., Dedeene L., De Vocht J., Oldoni E., Goris A., Van Den Bosch L., Depreitere B., Claeys K.G., Tournoy J., Van Damme P., Poesen K. Serum neurofilament light chain levels as a marker of upper motor neuron degeneration in patients with Amyotrophic Lateral Sclerosis. *Neuropathology and Applied Neurobiology*, 2018, doi: 10.1111/nan.12511. [Epub ahead of print] IF 6.059
- Smets I.*, Fiddes B.*, Garcia-Perez J.E.*, He D.*, Mallants K., Liao W., Dooley J., Wang G., Humblet-Baron S., Dubois B., Compston A., Jones J., Coles A., Liston A., Ban M., Goris A.@, Sawcer S.@. Multiple sclerosis risk variants alter expression of co-stimulatory genes in B cells. *Brain*, 2018, 141:786-796. IF 10.292, 5 citations
- Hilven K.*, Vandebergh M.*, Smets I., Mallants K., Goris A.@, Dubois B.. Genetic basis for relapse rate in multiple sclerosis: association with *LRP2* genetic variation. *Multiple Sclerosis Journal*, 2018, 24:1773-1775. IF: 5.280, 1 citation
- Put K., Vandenhaute J., Avau A., Van Nieuwenhuijze A., Brisse E., Dierckx T., Rutgeerts O., Garcia-Perez J., Toelen J., Waer M., Leclercq G., Goris A., Van Weyenbergh J., Liston A., De Somer L., Wouters C., Matthys P.@ (2017). Inflammatory gene expression profile and defective IFN-γ and granzyme K in natural killer cells of systemic juvenile idiopathic arthritis patients. *Arthritis & Rheumatology*, 69, 213-224. IF 6.918, 21 citations
- McLaughlin R.*, Schijven D.*, van Rheenen W., van Eijk K., O'Brien M., Project MinE GWAS Consortium, Schizophrenia Working Group of the Psychiatric Genomics Consortium, Kahn R., Ophoff R., Goris A., Bradley D., Al-Chalabi A., van den Berg L., Luykx J.@, Hardiman O.@, Veldink J.# (2017). Genetic correlation between amyotrophic lateral sclerosis and schizophrenia. *Nature Communications*, 8, 14774-14774. IF 12.353, 25 citations

8. References

1. Dendrou, C. A., Fugger, L. & Friese, M. A. Immunopathology of multiple sclerosis. *Nat Rev Immunol* **15**, 545-558, doi:10.1038/nri3871 (2015).
2. Consortium;, T. I. M. S. G. Low-Frequency and Rare-Coding Variation Contributes to Multiple Sclerosis Risk. *Cell*, doi:10.1016/j.cell.2018.09.049 (2018).
3. Dooley, J. *et al.* Immunological profiles of multiple sclerosis treatments reveal shared early B cell alterations *Neurol Neuroimmunol Neuroinflamm* **3**, e240 (2016).
4. Miyazaki, Y. *et al.* Suppressed pro-inflammatory properties of circulating B cells in patients with multiple sclerosis treated with fingolimod, based on altered proportions of B-cell subpopulations. *Clin Immunol* **151**, 127-135, doi:10.1016/j.clim.2014.02.001 (2014).
5. Schubert, R. D. *et al.* IFN-beta treatment requires B cells for efficacy in neuroautoimmunity. *J Immunol* **194**, 2110-2116, doi:10.4049/jimmunol.1402029 (2015).
6. Ceronie, B. *et al.* Cladribine treatment of multiple sclerosis is associated with depletion of memory B cells. *J Neurol* **265**, 1199-1209, doi:10.1007/s00415-018-8830-y (2018).
7. Krumbholz, M., Derfuss, T., Hohlfeld, R. & Meinl, E. B cells and antibodies in multiple sclerosis pathogenesis and therapy. *Nat Rev Neurol* **8**, 613-623, doi:10.1038/nrneurol.2012.203 (2012).
8. Baker, D., Pryce, G., Amor, S., Giovannoni, G. & Schmierer, K. Learning from other autoimmunities to understand targeting of B cells to control multiple sclerosis. *Brain* **141**, 2834-2847, doi:10.1093/brain/awy239 (2018).
9. Liston, A., Carr, E. J. & Linterman, M. A. Shaping Variation in the Human Immune System. *Trends in Immunology* **37**, 637-646, doi:10.1016/j.it.2016.08.002 (2016).

10. Orru, V. *et al.* Genetic variants regulating immune cell levels in health and disease. *Cell* **155**, 242-256, doi:10.1016/j.cell.2013.08.041 (2013).
11. Carr, E. J. *et al.* The cellular composition of the human immune system is maintained in multiple stable equilibriums shaped by age and cohabitation *Nat Immunol* **417**, 461-468 (2016).
12. Brodin, P. *et al.* Variation in the human immune system is largely driven by non-heritable influences. *Cell* **160**, 37-47, doi:10.1016/j.cell.2014.12.020 (2015).
13. Roederer, M. *et al.* The genetic architecture of the human immune system: a bioresource for autoimmunity and disease pathogenesis. *Cell* **161**, 387-403, doi:10.1016/j.cell.2015.02.046 (2015).
14. Aguirre-Gamboa, R. *et al.* Differential Effects of Environmental and Genetic Factors on T and B Cell Immune Traits. *Cell Rep* **17**, 2474-2487, doi:10.1016/j.celrep.2016.10.053 (2016).
15. Hedrick, E., Cheng, Y., Jin, U. H., Kim, K. & Safe, S. Specificity protein (Sp) transcription factors Sp1, Sp3 and Sp4 are non-oncogene addiction genes in cancer cells. *Oncotarget* **7**, 22245-22256, doi:10.18632/oncotarget.7925 (2016).
16. Nunez, G., Hockenbery, D., McDonnell, T. J., Sorensen, C. M. & Korsmeyer, S. J. Bcl-2 maintains B cell memory. *Nature* **353**, 71-73, doi:10.1038/353071a0 (1991).
17. Stavraka, C. & Blagden, S. The La-Related Proteins, a Family with Connections to Cancer. *Biomolecules* **5**, 2701-2722, doi:10.3390/biom5042701 (2015).
18. Fonseca, B. D. *et al.* La-related Protein 1 (LARP1) Represses Terminal Oligopyrimidine (TOP) mRNA Translation Downstream of mTOR Complex 1 (mTORC1). *J Biol Chem* **290**, 15996-16020, doi:10.1074/jbc.M114.621730 (2015).
19. Hong, S. *et al.* LARP1 functions as a molecular switch for mTORC1-mediated translation of an essential class of mRNAs. *Elife* **6**, pii: e25237, doi:10.7554/eLife.25237 (2017).
20. Iwata, T. N. *et al.* Conditional Disruption of Raptor Reveals an Essential Role for mTORC1 in B Cell Development, Survival, and Metabolism. *J Immunol* **197**, 2250-2260, doi:10.4049/jimmunol.1600492 (2016).

Geneeskundige Stichting Koningin Elisabeth
Fondation Médicale Reine Elisabeth
Königin-Elisabeth-Stiftung für Medizin
Queen Elisabeth Medical Foundation

Progress report of the research group of

Prof. dr. Leybaert Luc, MD. PhD

Universiteit Gent (UGent)

Principal investigator

Prof. dr. Leybaert Luc, MD. PhD
Dept. Basic Medical Sciences
Faculty of Medicine and Health Sciences
Ghent University
Belgium
Tel.: +32 9 332 33 66
Fax: +32 16 33 09 39
E-mail: Luc.Leybaert@UGent.be

Exploring the role of astroglial Cx43 hemichannels as therapeutic targets in stroke

1. Introduction

Stroke is, like cancer, associated with a major mortality risk and is the second important cause of death, next to ischemic heart disease. The majority of strokes are caused by blood vessel obstruction, either by a clot (thrombus) or an embolism, resulting in decreased perfusion of certain brain areas and rapid development of ischemia, leading to cell injury and neuronal cell death. Current therapeutic possibilities include clot lysis by means of tissue plasminogen activator (tPA) administration within 3 hours or endovascular clot removal (endarterectomy) within 6 hours after the insult. As a result of these limited time windows and possible side effects of these treatments, a majority of patients fall outside the selection criteria to receive these treatments. Hence, there is an urgent need for further research towards identifying novel therapeutic targets and developing new treatments. The work performed in this project aims to investigate connexin proteins as potential targets to protect the brain against ischemic cell injury. Brain cells not only encompass neurons but also glial cells that are in fact more numerous than neurons (at least 3 times more numerous depending on the species). Research over the past 20 years has demonstrated that astrocytes (star shaped glial cells), which form a bridge between neurons and blood vessel cells, exert crucial functions in substrate delivery to the neurons (energy substrate, neurotransmitter precursors) and removal of end products of metabolism as well as ions, which are transferred away from active zones and transferred to the blood. This crucial role of astrocytes is, in part, facilitated by connexin proteins that form channels, called gap junctions, that connect cells to form a large glial network, called the glial syncytium (reviewed in Ref. 2, Publications under GSKE support). Gap junctions are formed by two half gap junction channels called 'hemichannels'; these hemichannels are also present in the plasma membrane in their free form, i.e. not as part of a gap junction. As such, hemichannels form non-selective pores that, when open, pass ions and molecules up to ~1.5 kDa, which may disturb cell function and lead to cell injury/cell death. The purpose of the present work is to investigate whether blocking hemichannels protects the neural tissue against post-ischemic cell injury. Over the past 10 years, the Leybaert group has provided a detailed characterization of hemichannel control by cytoplasmic Ca^{2+} and developed, based on these insights, a peptide toolset that allows to specifically modulate hemichannel function. One of these compounds is Gap19 that inhibits hemichannels composed of Cx43, the most abundant connexin in the brain that is largely present in astrocytes. Interestingly, Gap19 does not inhibit gap junctions and as such leaves the crucial physiological functions of these junctional channels intact. The work presented below reports on the second year research activities performed in the context of investigating connexin hemichannels as a potential target to protect the brain against ischemic injury. We include an account on the first year activities to provide context for the research steps performed in year 2, which have been directed at investigating the role of connexin hemichannels as a vascular as well as glial target to prevent blood-brain barrier dysfunction, thereby providing brain protection at the blood-brain interface.

2. Summary of results obtained over the 2017 and 2018 periods

We characterized a mutant Cx43 with a 'phospho-dead' MAP kinase domain and found it to phenotypically present with a loss of hemichannel function in brain astrocytes. In an animal model of permanent occlusion of the mid-cerebral artery, Cx43 MAP-kinase mutant animals (further called MK4 mice with 4 Ser to Ala modified residues) had significantly smaller brain infarcts and less cell death compared to WT animals. We tested other Cx43 phosphorylation sites (PKC, CK1) but those did not

protect against permanent brain ischemia. We also tested whether blocking hemichannels with Gap19, added as TAT-Gap19 to improve cell membrane permeation, could provide protection in WT animals. We found that this peptide gave a similar reduction in brain infarct size as observed in the Cx43 MAP-kinase mutants. Interestingly, this protection was obtained by a single i.p. administration of TAT-Gap19 2 hours after vessel occlusion, mimicking a therapeutic setting. The paper concerning this work has been expanded with data on functional recovery of the animals whereby MK4 mice showed improved behavioral performance; this paper is now in minor revision (Ref. 1, Publications under GSKE support). A one sentence summary, graphical abstract and abstract of this work are given below; a more detailed description of this part of the work is presented under 'III. Targeting connexin hemichannels to protect the brain against ischemic injury'.

Summary. The study demonstrates that astrocytic connexin43 hemichannels are largely controlled by 4 C-terminal tail located serine residues, and provides mechanistic insight on how phosphorylation of these residues affects recovery from stroke.

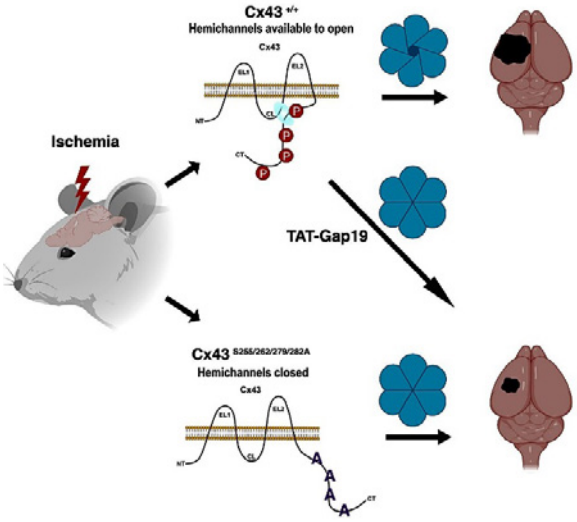

Abstract. Cx43 function is influenced by kinases that phosphorylate specific serine sites located near its C-terminus. Stroke is a powerful inducer of kinase activity, but its effect on Cx43 is unknown. We investigated the impact of wild-type (WT) and knock-in Cx43 with serine to alanine mutations at the protein kinase-C site $Cx43^{S368A}$ (PKC), the casein kinase-1 sites $Cx43^{S325A/328Y/330A}$ (CK1) and the mitogen-activated protein kinase sites $Cx43^{S255/262/279/282A}$ (MK4), on a permanent middle cerebral artery occlusion (pMCAO) stroke model. We demonstrate that MK4 transgenic animals exhibit a significant decrease in infarct volume which was associated with significant improvement in behavioral performance. An increase in astrocyte reactivity with a concomitant decrease in microglial reactivity was observed in MK4 mice. In contrast to WT, MK4 astrocytes displayed reduced Cx43 hemichannel activity. Pharmacological blockade of Cx43 hemichannels with TAT-Gap19 significantly decreased infarct volume in WT animals. This study provides novel molecular insights and charts new avenues for therapeutic intervention associated with Cx43 function.

While this work demonstrated a crucial role of astrocytic Cx43 in protecting against brain infarct volume and cellular as well as functional recovery, we wondered whether protection by TAT-Gap19 could also involve effects at the level of the blood-brain barrier (BBB). To this purpose, we performed *in vivo* animal BBB studies in a model of inflammation-induced barrier leakage instigated by intraperitoneal lipopolysaccharide (LPS) administration. Inflammation is indeed a major, but less characterized, component of stroke pathophysiology. We found that TAT-Gap19 significantly inhibited LPS-induced BBB leakage which was mediated by effects on both astrocytes and BBB endothelial cells, with the astrocytic contributuion being particularly potent. A detailed patch-clamp study demonstrated that

peripheral (vascular) inflammation was associated with calcium-dependent Cx43 hemichannel opening in BBB endothelial cells as well as in astrocytes, the blocking of which prevented BBB failure. A more extended account of this part of the work is presented under 'IV. Targeting connexin hemichannels to protect against blood-brain barrier leakage'. This work will be further continued towards completion and publication in 2019.

3. Targeting connexin hemichannels to protect the brain against ischemic injury

Hemichannels are composed of six connexin subunits, which are tetraspan proteins that contain two extracellular loops, one intracellular loop and N- and C-terminal domains located inside the cell (Fig. 1). Opening of Cx43 hemichannels necessitates an interaction of the C-terminal tail with the intracellular loop as demonstrated by previous work from our group (*1*). We started the present work from the observation that the C-terminal tail of Cx43 has two different domains that interact with the intracellular loop: the CT9 domain composed of the last 9 amino acids (*2-4*) of the C-terminal and the Src homology-3 (SH3) binding domain located ~100 amino acids upstream in N-terminal direction (*5*). This SH3 domain is part of a larger stretch of amino acids that contain 4 Ser residues from a MAP-kinase (MAPK) domain (Fig. 1).

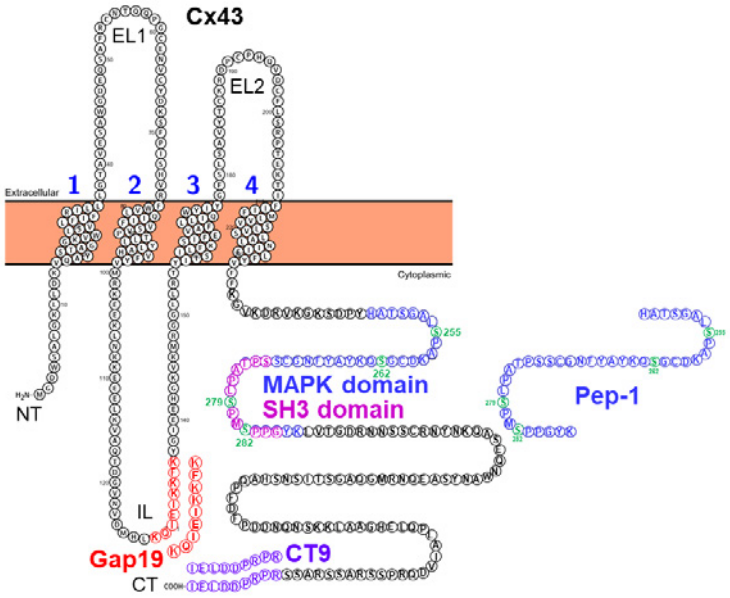

Fig. 1. Cx43 topology with indication of the CT9, SH3 and MAPK domains, and the peptides Gap19, Pep-1 and CT9. *The MAPK domain is as indicated by the Pep-1 sequence (amino acids 248-287) with the 4 Ser residues marked in green; the SH3 domain is a sub-domain within the MAPK stretch. In MK4 mice the 4 Ser residues are modified to Ala.*

To investigate whether the MAPK domain, which is larger than the SH3 domain, is also involved in hemichannel regulation, we performed experiments on Cx43 in which the 4 Ser residues in the MAPK domain (S255, S262, S279 & S282 – marked green in Fig. 1) were each modified to Ala rendering this domain 'phospho-dead'; these MAPK phosphorylation null mutants are further referred to as MK4. In collaboration with the group of Dr. P. Lampe (Translational Research Program, Fred Hutchinson Cancer Research Center, Seattle, USA) we obtained transgenic MK4 mutant mice and performed single channel patch-clamp experiments on Cx43 hemichannel function. In astrocytes isolated from WT animals, hemichannel openings were triggered by a small increase of the intracellular Ca^{2+} concentration ($[Ca^{2+}]_i$) from 50 to 200 nM at normal resting potential of -70 mV (Fig. 2A). Gap19, a nonapeptide derived from the cytoplasmic loop of Cx43 (Fig. 1), which was previously shown by our group to inhibit hemichannel activity without inhibiting gap junctions (*6*), abolished the unitary current activities (Fig. 2A). All-point histograms furthermore indicated a unitary conductance in the range of 230-245 pS, i.e. in the range

of ~220 pS reported for Cx43 hemichannels (*7, 8*) (Fig. 2B). As illustrated in Fig. 2C, charge transfer mediated by hemichannels was negligible at 50 nM $[Ca^{2+}]_i$, but was significantly enhanced at 200 nM $[Ca^{2+}]_i$ and was reduced to the basal level by Gap19 (in these experiments we could use the non-TAT version as it was applied in the whole-cell patch pipette (Fig. 2C). Remarkably, in astrocytes isolated from MK4 Cx43 phosphorylation-null mutant animals, 200 nM $[Ca^{2+}]_i$ stimulation did not trigger any hemichannel current activity indicating loss of hemichannel function (Fig. 2D). We next tested whether supplying MK4 mutant astrocytes with a cell-penetrating peptide called Pep-1 composed of His-248 to Lys-287 on the Cx43 CT encompassing the 4 Ser residues modified in MK4 mice (Fig. 1), could rescue hemichannel activity. Strikingly, preincubating astrocytes isolated from MK4 mutant animals with Pep-1 rescued hemichannel activities at 200 nM $[Ca^{2+}]_i$ (Fig. 2D). As illustrated in Fig. 2E, the unitary conductance of restored hemichannel currents in MK4 mutant astrocytes was in the range of 220-240 pS, not different from the conductance in WT astrocytes. We further quantified the effect of Pep-1 on charge transfer associated with hemichannel openings and demonstrated significantly increased charge transfer at 200 nM $[Ca^{2+}]_i$ in MK4 mutant astrocytes exposed to Pep-1 peptide as compared to those in non-treated MK4 mutants (Fig. 2F).

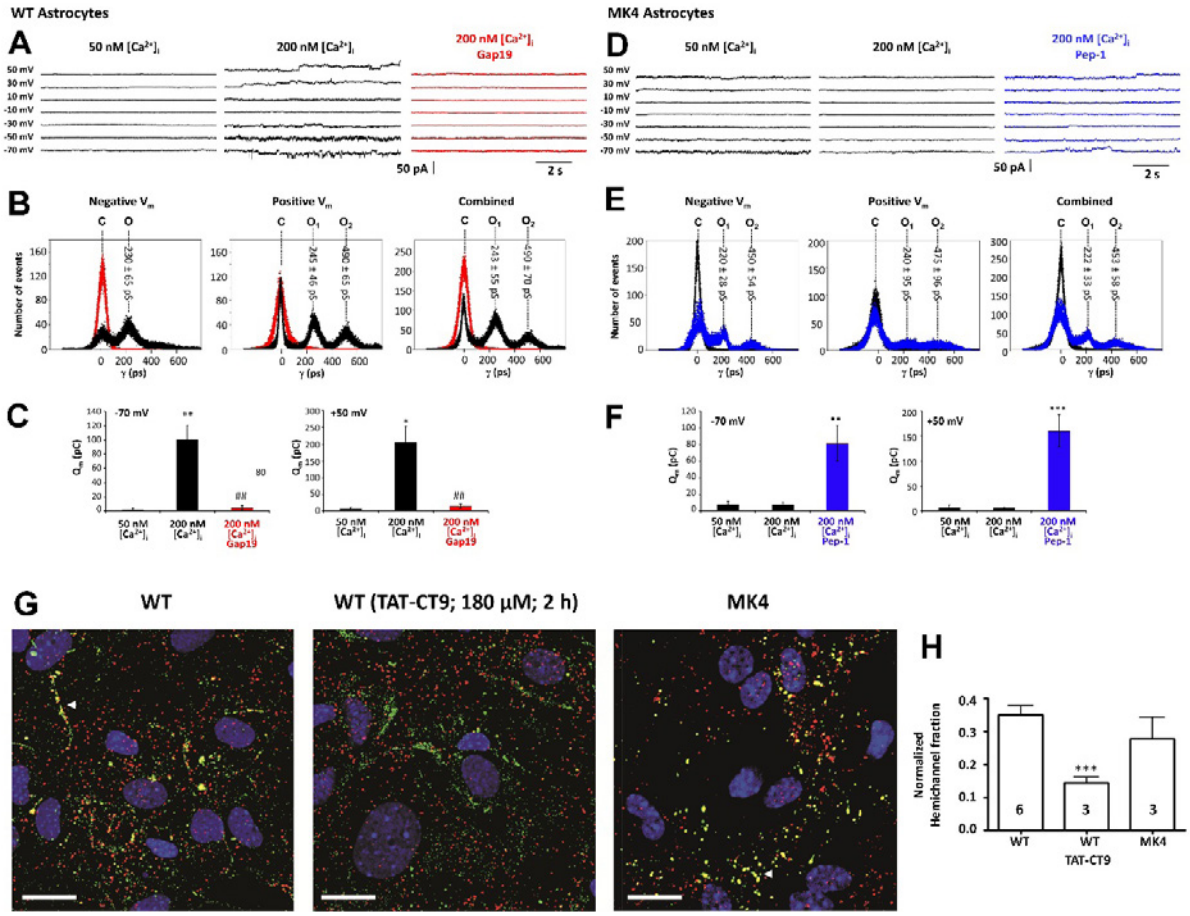

Fig. 2. Hemichannel activity is reduced in MK4 Cx43 phosphorylation null mutant astrocytes. A. *Current traces in WT astrocytes for voltage steps indicated left. Unitary current activity appeared at both negative and positive V_m when $[Ca^{2+}]_i$ was elevated from 50 nM to 200 nM. Gap19 (100 µM, added via the pipette) suppressed unitary activity (red traces).* ***B.*** *All-point histogram of current activities at negative, positive and combined V_m. Unitary conductance of one (O_1) or two open hemichannels (O_2) are indicated above each peak (mean ± s.d.). Gap19 abolished all current activity (red peak at baseline).* ***C.*** *Charge transfer (Q_m) associated with unitary current activities for recordings at -70 and +50 mV (n = 6). * P<0.05 vs 50 nM $[Ca^{2+}]_i$; ** P<0.01; ##, P<0.01 vs 200 nM $[Ca^{2+}]_i$.* ***D.*** *Current traces in MK4 mutant astrocytes. Unitary activity was absent at 200 nM $[Ca^{2+}]_i$ but pre-treatment with Pep-1 peptide (35 µM, 1 h) restored activity (blue traces).* ***E.*** *All-point histogram showing that currents restored by Pep-1 had a single channel conductance similar to WT.* ***F.*** *Q_m charge transfer data illustrating restoration of opening activities with Pep-1 (n = 6). ** P<0.01 compared to 200 nM $[Ca^{2+}]_i$; *** P<0.001.* ***G.*** *Confocal images of Duolink (red) and Cx43 (green) stainings in WT and MK4 mutant astrocytes; yellow co-localization signal corresponds to hemichannels. WT astrocytes (left) displayed clear hemichannel signal (arrowhead) that was decreased after TAT-CT9 treatment, which promotes incorporation of hemichannels into gap junctions. Hemichannel signal was also present in MK4 mutant astrocytes (right).* ***H.*** *Summary data of normalized yellow signal, demonstrating that the signal from MK4 mutant astrocytes was not different from WT. ***P < 0.001 WT vs WT (TAT-CT9). Scale bars are 20 µm. All error bars represent s.e.m.*

To exclude the possibility that the lower unitary hemichannel activity is due to a smaller pool of plasma membrane hemichannels in MK4 mutants, we performed Duolink in situ proximity ligation assays in isolated WT and MK4 mutant astrocytes. This assay reports the spatial hemichannel organization relative to gap junctions through amplification of Cx43/ZO-1 complexes that represent hemichannels (*9*). As illustrated in Fig. 2G, red Duolink fluorescence occurred throughout the cells while the yellow signal produced by red-green co-localized spots at gap junctions (arrowhead), representing hemichannels underway to gap junctions as reported for other cell types (*10*). We next tested TAT-CT9, a peptide composed of the last 9 amino acids of the Cx43 C-terminal end fused to the TAT membrane translocation sequence; this peptide promotes incorporation of hemichannels into gap junctions by competing for ZO-1 binding for which the 4 last amino acids of the C-terminal tail are crucial (*11*). WT astrocytes treated with TAT-CT9 (180 µM, 2 hr) displayed markedly less Duolink fluorescence signal, in line with its promotive effect on hemichannel assembly into gap junctions (Fig. 2G). Quantification of the yellow signal relative to the green Cx43 signal corresponding to the normalized plasma membrane hemichannel fraction, showed that the signal in MK4 mutant astrocytes was not different from the signal in WT cells (Fig. 2H). Thus, the lower hemichannel activity in MK4 mutant astrocytes is the consequence of altered gating and not the result of a decreased hemichannel pool.

The results discussed above demonstrated that MK4 Cx43 phosphorylation null mutant animals have a loss of hemichannel function in brain astrocytes. In a next step, we tested whether this is associated with a protective effect following ischemic stroke. To that purpose we collaborated with Dr. C.C. Naus (Cellular & Physiological Sciences, Faculty of Medicine, The University of British Columbia, Vancouver, Canada) and made use of various Cx43 phosphorylation null mutants generated by and Dr. P. Lampe (Translational Research Program, Fred Hutchinson Cancer Research Center, Seattle, USA). These mutants included the MK4 mutant but also a CK1 and PKC mutant; MAPK, CK1 and PKC kinases have all been shown to be active in ischemic conditions (*12-15*). To test whether disrupting CK1, PKC or MAPK phosphorylation sites of the C43 C-terminal tail impacts stroke outcome, a cohort of male and female WT and Cx43 phosphorylation null mutants for CK1, PKC and MAPK (MK4) mice were subjected to permanent occlusion of the mid-cerebral artery (pMCAO). Four days after pMCAO the CK1 and PKC Cx43 phosphorylation null mutant mice did not show significant changes in infarct volume with respect to WT controls (Fig. 3a and b). However, MK4 mutant mice exhibited a significant ($P = 0.0181$) 58.3% reduction in infarct volume compared with WT counterparts (Fig. 3a and b). In light of the compelling phenotype observed in MK4 mutant ischemic mice, a larger cohort of WT and MK4 mutant male and female animals were subjected to pMCAO. Consistent with our initial study, MK4 mutant mice exhibited a significant ($P = 0.0053$) 40.2% reduction in infarct volume compared with WT counterparts (Fig. 3c). Apoptosis triggered by an ischemic event may occur over several days and contribute to delayed neuronal death and loss of viable peri-infarct tissue (*16*). To investigate whether the difference in infarct volume found in WT and MK4 mutant ischemic mice is correlated with differences in the level of apoptosis, WT and MK4 brain sections from ischemic mice were subjected to TUNEL immunostaining. In contrast to WT mice, TUNEL staining exhibited a significant ($P = 0.0337$) 70.0% reduction in the number of apoptotic TUNEL+ cells within the infarct region of MK4 mutant brain tissue sections, 4-days after pMCAO (Fig. 3d and e).

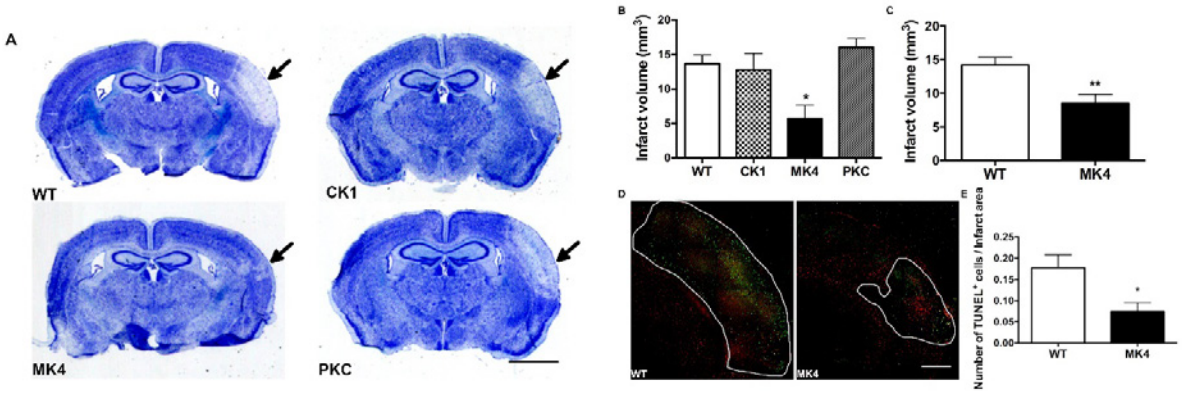

Fig. 3. Disrupting the MAPK phosphorylation sites of Cx43 C-terminus results in both a decrease in infarct volume and TUNEL staining 4-days after pMCAO. (a) *Representative photomicrographs of thionin-stained sections from WT and Cx43 null phosphorylation mutant CK1, PKC and MAPK (MK4) mutant mice, 4-days post-pMCAO. Scale bar = 2 mm.* ***(b)*** *Quantification of infarct volume from WT and Cx43 null phosphorylation mutant CK1, PKC and MAPK (MK4) thionin-stained brain sections, 4-days post-pMCAO (One-way ANOVA followed by Bonferroni post-test; *P = 0.0181; WT: n = 5 mice; CK1: n = 4; PKC: n = 4; MK4: n = 4).* ***(c)*** *Quantification of infarct volume from WT and MK4 thionin-stained brain sections, 4 days post-pMCAO (unpaired Student's t-test; **P = 0.0053; WT: n = 10 mice; MK4: n = 11 mice).* ***(d)*** *Co-immunofluorescence staining of cerebral cortex from WT (left micrograph) and MK4 (right micrograph) mice, 4 days after pMCAO, using the astrocyte marker GFAP (red) with TUNEL apoptosis marker (green). White outline on WT and MK4 micrographs delineates infarct area. Scale bar = 500 µm.* ***(e)*** *Quantification of average number of TUNEL+ cells in brain sections from WT and MK4 mice 4 days after pMCAO (unpaired Student's t-test; *P = 0.0337; WT: 4 sections, n = 5 mice; MK4: 4 sections, n = 4 mice). All error bars represent s.e.m.*

We next asked whether the decreased hemichannel activity exhibited in MK4 astrocytes is a key factor in the neuroprotective phenotype of these animals subjected to pMCAO. To test this hypothesis, we subjected WT animals to pMCAO followed by administration of either the hemichannel blocker TAT-Gap19 (*6*) or its scrambled form TAT-GAP19^{scrambled}. Fusion of Gap19 to the TAT (transactivator of transcription) sequence facilitates cellular uptake of the peptide, allowing it to cross the blood-brain barrier (*17*). Intraperitoneal (i.p.) injection of 0.75 µmol/Kg or 7.5 µmol/Kg TAT-Gap19 2hrs after pMCAO, significantly reduced infarct volume by 47.8 %, and 77.6 %, respectively 4-days after pMCAO, compared with those mice that received saline or scrambled alone (Fig. 4a and b). Mice treated with the negative control TAT-Gap19^{scrambled} did not show significant changes with respect to saline controls (Fig. 4a and b). Mice treated with 7.5 µmol/Kg TAT-Gap19 showed a significant reduction in infarct volume compared to mice treated with 0.75 µmol/Kg of TAT-Gap19 (Fig. 4b).

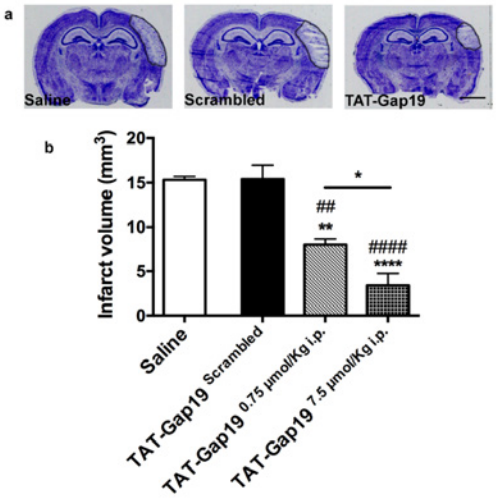

Fig. 4. TAT-Gap19 Cx43 hemichannel blocker is neuroprotective in mice subjected to pMCAO. (a) *Representative photomicrographs of thionin-stained sections, 4 days after pMCAO, in WT mice treated with either saline (left micrograph), 7.5 µmol/Kg i.p. scrambled TAT-Gap19 Scrambled (center micrograph), or 0.75 µmol/Kg i.p. hemichannel blocker TAT-Gap19 (right micrograph), 2 hrs after pMCAO. Black outline highlights infarct. Scale bar = 2 mm.* ***(b)*** *Quantification of infarct volume, 4 days after pMCAO, from WT mice treated with either saline, 7.5 µmol/Kg i.p. scrambled TAT-GAP19Scrampled, 0.75 µmol/Kg i.p or 7.5 µmol/Kg i.p.. TAT-Gap19, 2 hrs after pMCAO. (One-way ANOVA followed by Tukey's multiple comparisons test; Saline vs Scrambled: P = > 0.9999; Saline vs 0.75 µmol/Kg TAT-Gap19: **P = 0.0021; Saline vs 7.5 µmol/Kg TAT-GAP19: ****P = < 0.0001; Scrambled vs 0.75 µmol/Kg TAT-Gap19: ## P = 0.0019; Scrambled vs 7.5 µmol/Kg TAT-Gap19: #### P = < 0.0001; 0.75 µmol/Kg TAT-Gap19 vs 7.5 µmol/Kg TAT-Gap19: * P = 0.0484; Saline: n = 4 mice; 7.5 µmol/Kg TAT-Gap19scrampled: n = 4 mice; 7.5 µmol/Kg TAT-Gap19: n = 4 mice; 0.75 µmol/Kg TAT-Gap19: n = 4). All error bars represent s.e.m.*

We further characterized the functional recovery of the animals after pMCAO by the adhesive tape removal test. In WT mice, pMCAO significantly increased the time it took for mice to remove tape from the left (impaired) paw 3 days [WT = 39.78 ± 54.90 sec. vs MK4 = 7.33 ± 4.30 sec. (P = 0.0345)] after surgery (Fig. 5a). In addition, 5 and 9 days after surgery WT mice exhibited a non-significant latency in tape removal compared with MK4 animals (Fig. 5a). By 14 and 21 days post-pMCAO, WT mice became as efficient on the tape removal test as their MK4 counterparts (Fig. 5a). For the right (non-impaired) forepaw, there was no significant effect of pMCAO on tape removal latency between the two genotypes (Fig. 5b).

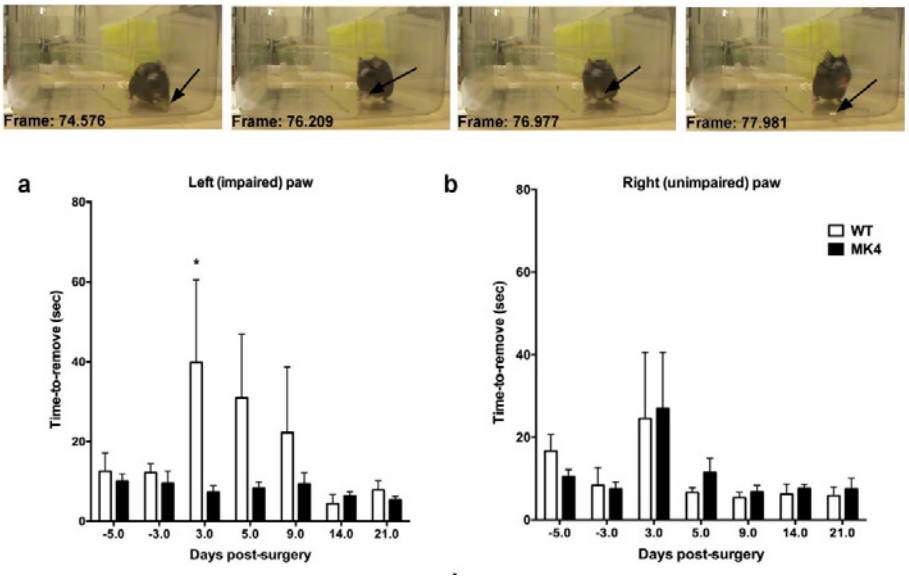

Fig. 5. MK4 mice show improved sensory function after pMCAO. (a) *Quantification of average time to remove adhesive tape from left (impaired) forepaw. Time-5 and -3 represent pre-pMCAO.* ***(b)*** *Latencies for right forepaw were unaffected by pMCAO. (Two-way ANOVA with repeated measures followed by Bonferroni's multiple comparisons test, main effect of genotype, main effect of genotype, P = 0.1200; main effect of time, P = 0.1178; subjects (matching), **P = 0.0027; interaction, P = 0.1534). The observed power for the interactions is 0.588. The effect size of interaction between time and genotype is 0.3, according to Cohen's f (medium to large effect). WT mice vs MK4 mice 3 days post-pMCAO *P = 0.0345; WT: n = 7 mice; MK4: n = 8 mice).*

4. Targeting connexin hemichannels to protect against blood-brain barrier leakage

This part is confidential and can therefore not be shown.

5. Publications under GSKE support

1. Freitas-Andrade M, Wang N, Bechberger JF, De Bock M, Lampe PD*,**Leybaert L***, Naus CC. "Targeting MAPK phosphorylation sites of the Connexin43 C-terminus provides neuroprotection in stroke", *J Exp Med*, provisionally accepted after minor revision (copy of editorial decision is given on p.20 of this document).*shared senior authorship
   Impact factor: 10.8, category: MEDICINE, RESEARCH & EXPERIMENTAL, rank: 6/133, Vigintile: 1 (top 5%).
2. Giaume C, Naus CC, Saez JC and **Leybaert L**. "Glial connexins and pannexins in healthy and diseased brain", *Physiol Rev*, invited review paper, status: submitted.
   Impact factor: 24.0, category: PHYSIOLOGY, rank: 1/83, Vigintile: 1 (top 5%).
3. Delvaeye T, Vandenabeele P, Bultynck G, **Leybaert L***, Krysko DV. "Therapeutic Targeting of Connexin Channels: New Views and Challenges." *Trends Mol Med* 24(12):1036-1053. doi: 10.1016/j.molmed.2018.10.005, 2018. *shared senior authorship
   Impact factor: 11.0, category: MEDICINE, RESEARCH & EXPERIMENTAL, rank: 5/133, Vigintile: 1 (top 5%).
4. Maatouk L, Yi C, Carrillo-de Sauvage MA, Compagnion AC, Hunot S, Ezan P, Hirsch EC, Koulakoff A, Pfrieger FW, Tronche F, **Leybaert L**, Giaume C, Vyas S. "Glucocorticoid receptor in astrocytes regulates midbrain dopamine neurodegeneration through connexin hemichannel activity." *Cell Death Differ* Jul 13, doi: 10.1038/s41418-018-0150-3 [Epub ahead of print], 2018.
   Impact factor: 8.00, category: BIOCHEMISTRY & MOLECULAR BIOLOGY, rank: 26/292, Decile: 1 (top 10%).
5. Walrave L, Pierre A, Albertini G, Aourz N, De Bundel D, Van Eeckhaut A, Vinken M, Giaume C, **Leybaert L***, Smolders I, 2018. "Inhibition of astroglial connexin43 hemichannels with TAT-Gap19 exerts anticonvulsant effects in rodents". *Glia* Apr 23, doi: 10.1002/glia.23341 [Epub ahead of print], 2018. *shared senior authorship
   Impact factor: 5.85, category: NEUROSCIENCES, rank: 33/261, Quartile: 1 (top 25%).
6. **Leybaert L**, Lampe PD, Dhein S, Kwak BR, Ferdinandy P, Beyer EC, Laird DW, Naus CC, Green CR, Schulz R. "Connexins in Cardiovascular and Neurovascular Health and Disease: Pharmacological Implications." *Pharmacol Rev* 69(4):396-478, 2017.
   Impact factor: 17.9, category: PHARMACOLOGY & PHARMACY, rank: 2/256, Vigintile: 1 (top 5%).

6. References

1. L. Leybaert, P. D. Lampe, S. Dhein, B. R. Kwak, P. Ferdinandy, E. C. Beyer, D. W. Laird, C. C. Naus, C. R. Green, R. Schulz, Connexins in Cardiovascular and Neurovascular Health and Disease: Pharmacological Implications. *Pharmacol Rev* **69**, 396-478 (2017).
2. R. Ponsaerts, E. De Vuyst, M. Retamal, C. D'Hondt, D. Vermeire, N. Wang, H. De Smedt, P. Zimmermann, B. Himpens, J. Vereecke, L. Leybaert, G. Bultynck, Intramolecular loop/tail interactions are essential for connexin 43-hemichannel activity. *FASEB J* **24**, 4378-4395 (2010).
3. M. Bol, N. Wang, M. De Bock, B. Wacquier, E. Decrock, A. Gadicherla, K. Decaluwe, B. Vanheel, H. V. van Rijen, D. V. Krysko, G. Bultynck, G. Dupont, J. Van de Voorde, L. Leybaert, At the cross-point of connexins, calcium, and ATP: blocking hemichannels inhibits vasoconstriction of rat small mesenteric arteries. *Cardiovasc Res* **113**, 195-206 (2017).
4. C. D'Hondt, J. Iyyathurai, N. Wang, R. G. Gourdie, B. Himpens, L. Leybaert, G. Bultynck, Negatively charged residues (Asp378 and Asp379) in the last ten amino acids of the C-terminal tail of Cx43 hemichannels are essential for loop/tail interactions. *Biochem Biophys Res Commun* **432**, 707-712 (2013).
5. J. Iyyathurai, N. Wang, C. D'Hondt, J. X. Jiang, L. Leybaert, G. Bultynck, The SH3-binding domain of Cx43 participates in loop/tail interactions critical for Cx43-hemichannel activity. *Cell Mol Life Sci*, (2017).
6. N. Wang, E. De Vuyst, R. Ponsaerts, K. Boengler, N. Palacios-Prado, J. Wauman, C. P. Lai, M. De Bock, E. Decrock, M. Bol, M. Vinken, V. Rogiers, J. Tavernier, W. H. Evans, C. C. Naus, F. F. Bukauskas, K. R. Sipido, G. Heusch, R. Schulz, G. Bultynck, L. Leybaert, Selective inhibition of Cx43 hemichannels by Gap19 and its impact on myocardial ischemia/reperfusion injury. *Basic Res Cardiol* **108**, 309 (2013).
7. J. E. Contreras, J. C. Saez, F. F. Bukauskas, M. V. Bennett, Gating and regulation of connexin 43 (Cx43) hemichannels. *Proc Natl Acad Sci U S A* **100**, 11388-11393 (2003).
8. N. Wang, M. De Bock, G. Antoons, A. K. Gadicherla, M. Bol, E. Decrock, W. H. Evans, K. R. Sipido, F. F. Bukauskas, L. Leybaert, Connexin mimetic peptides inhibit Cx43 hemichannel opening triggered by voltage and intracellular Ca2+ elevation. *Basic Res Cardiol* **107**, 304 (2012).
9. J. M. Rhett, J. Jourdan, R. G. Gourdie, Connexin 43 connexon to gap junction transition is regulated by zonula occludens-1. *Mol Biol Cell* **22**, 1516-1528 (2011).
10. J. A. Palatinus, J. M. Rhett, R. G. Gourdie, The connexin43 carboxyl terminus and cardiac gap junction organization. *Biochim Biophys Acta* **1818**, 1831-1843 (2012).

11. C. Jin, K. D. Martyn, W. E. Kurata, B. J. Warn-Cramer, A. F. Lau, Connexin43 PDZ2 binding domain mutants create functional gap junctions and exhibit altered phosphorylation. *Cell Commun Adhes* **11**, 67-87 (2004).
12. N. Kaneko, J. Y. Hwang, M. Gertner, F. Pontarelli, R. S. Zukin, Casein kinase 1 suppresses activation of REST in insulted hippocampal neurons and halts ischemia-induced neuronal death. *J Neurosci* **34**, 6030-6039 (2014).
13. S. V. Demyanenko, S. N. Panchenko, A. B. Uzdensky, Expression of neuronal and signaling proteins in penumbra around a photothrombotic infarction core in rat cerebral cortex. *Biochemistry (Mosc)* **80**, 790-799 (2015).
14. M. Freitas-Andrade, P. Carmeliet, D. B. Stanimirovic, M. Moreno, VEGFR-2-mediated increased proliferation and survival in response to oxygen and glucose deprivation in PlGF knockout astrocytes. *J Neurochem* **107**, 756-767 (2008).
15. Z. Jiang, Y. Zhang, X. Chen, P. Y. Lam, H. Yang, Q. Xu, A. C. Yu, Activation of Erk1/2 and Akt in astrocytes under ischemia. *Biochem Biophys Res Commun* **294**, 726-733 (2002).
16. T. Nakase, G. Sohl, M. Theis, K. Willecke, C. C. Naus, Increased apoptosis and inflammation after focal brain ischemia in mice lacking connexin43 in astrocytes. *Am J Pathol* **164**, 2067-2075 (2004).
17. V. Abudara, J. Bechberger, M. Freitas-Andrade, M. De Bock, N. Wang, G. Bultynck, C. C. Naus, L. Leybaert, C. Giaume, The connexin43 mimetic peptide Gap19 inhibits hemichannels without altering gap junctional communication in astrocytes. *Front Cell Neurosci* **8**, 306 (2014).

Geneeskundige Stichting Koningin Elisabeth
Fondation Médicale Reine Elisabeth
Königin-Elisabeth-Stiftung für Medizin
Queen Elisabeth Medical Foundation

Progress report of the research group of

Dr. Laurent Nguyen, PhD &
dr. Brigitte Malgrange

Université de Liège (ULg)

Dr. Laurent Nguyen, PhD

Laboratoire de régulation moléculaire de la neurogenèse
GIGA-Neurosciences
ULiège
4000 Liège
Belgium
Tel.: 32 4 366 59 87
Fax: 32 4 366 59 12
E-mail: lnguyen@ulg.ac.be
www.giga.ulg.ac.be

Dr. Brigitte Malgrange

Unité de Neurobiologie du développement
GIGA-Neurosciences
ULiège
4000 Liège
Belgium
Tel.: 32 4 366 59 87
Fax: 32 4 366 59 12
E-mail: bmalgrange@ulg.ac.be
www.giga.ulg.ac.be

Deciphering the role of protein ubiquitination in human cortical malformation and hearing impairment

1. State of the art and objectives

The cerebral cortex is an evolutionary advanced brain structure that contains different classes of neurons distributed within layers that are regionally organized into sensory, motor and association areas[1]. Cortical layering arises inside-out as progenitors give birth to successive waves of pyramidal projection neurons in the dorsal telencephalon[2] and, GABAergic interneurons in the ventral forebrain[3]. Projection neurons migrate radially to settle in appropriate cortical layers and they grow axonal projections towards cortical or sub-cortical targets. Interneurons migrate from the ganglionic eminences along multiple tangential paths to integrate local cortical networks. More generally, the development of the cortex implies a continuous rearrangement of a primordial structure that progresses through successive steps including, proliferation, specification, migration, and neuronal differentiation. Disrupting the completion of one or several of these events often lead to Malformations of Cortical Development (MCD). MCDs correspond to a heterogeneous group of focal or diffuse anatomical brain abnormalities with wide spectrum of clinical presentations, developmental delay or motor and intellectual disabilities. They usually occur during the first two trimesters of human pregnancy and involve cells that contribute to the formation of the cortex [4,5]. They are frequently associated with drug-resistant epilepsy, and more surprisingly, to neuro-sensory deafness and treatments are generally limited to symptom relief (reviewed in [6]). Most MCD are believed to have a genetic origin and their classification arises from diagnoses established by histopathological analyses, magnetic resonance imaging (MRI), electro-clinical studies and further identification of mutation in genes involved in cortical development.

Ubiquitination is a biochemical process that affect proteins in many ways: it can act as a signal for their degradation via the proteasome, change their cellular location, or modify their activity [7]. This process involves the covalent attachment of ubiquitin to a target protein, and is carried out by three enzymes: ubiquitin activating enzyme, E1, ubiquitin conjugating enzyme, E2, and ubiquitin ligase, E3. Each E3 enzyme targets a small number of proteins for ubiquitin modification but the exact substrates are mostly unknown and their identification continues to be a challenge. Regulation of protein turnover is essential for cellular homeostasis in all tissues, including the brain and the inner ear [8-10]; therefore the mutation of any enzyme involved in this process may affect brain and inner ear development. Along this line, our collaborator, Professor Jamel Chelly (IGBMC, Strasbourg, France), has identified novel human NEDD4-2 (a E3 ubiquitin ligase) mutations (c.2690G>A, p.Glu893Lys and c.2677G>A, p.Glu893Lys) in patients suffering from intellectual disabilities, MCD (the main feature being periventricular nodular heterotopia), epilepsy as well as hearing impairment (manuscript under revision at Nature Genetics). Identification of this novel MCD gene is important for diagnosis and genetic counselling of patients and their families, but also to better understand the molecular processes of corticogenesis and cochlear development in health and disease.

2. Outstanding questions and objectives

The aim of our proposal is to characterise the physiological functions of E3 ubiquitin ligases in the development of the cerebral cortex (WP1) and the formation of the cochlea, the auditory portion of the inner ear (WP2). For this purpose, we will focus on the pathophysiological mechanisms trigger by novel mutations in the HECT domain of *Nedd4-2* that lead to MCD and hearing impairment in patients. The Nguyen laboratory will focus on cortical interneurons whose contribution to MCD remains poorly understood and the Malgrange laboratory will study the mechanisms of deafness associated

with *Nedd4-2* mutations. The project will combine mouse genetics with molecular and cell biology to decipher the physiological functions of *Nedd4-2,* as well as its closely related gene *Nedd4-1,* and to further untangle the pathomechanisms downstream its patient-related mutations.

3. Research program

3.1. WP1. Deciphering the role of Nedd4-1/-2 in the developing cerebral cortex in health and disease

The molecular connections existing between MCD and ubiquitination defects remain largely unknown. *Nedd4-2* codes for a HECT-domain E3-ubiquitin ligase, a protein involved in substrate ubiquitination whose mutation is associated with some MCD.
Our current project uncovers both the physiological role of *Nedd4-2* and the impact of its MCD-associated mutations on the biology of cortical interneurons using the mouse as a model.

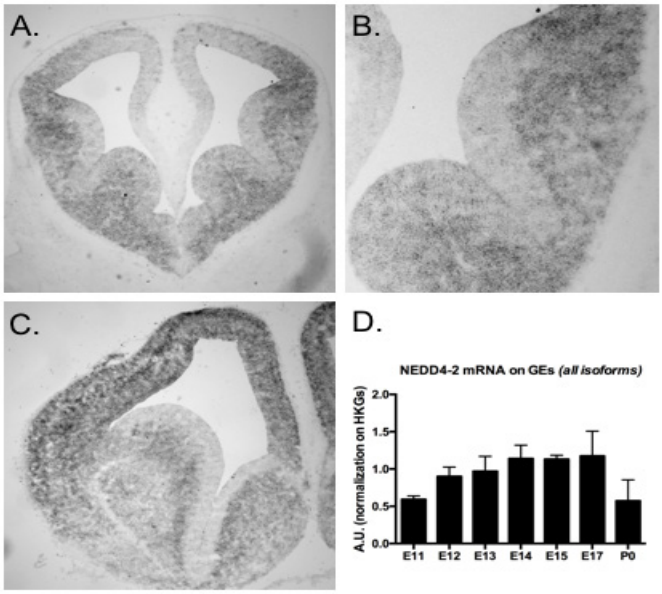

Fig.1. *Nedd4-2* expression pattern **A, B.** E12.5 MF1 mouse, whole brain coronal slice (A) and higher magnification focusing on medial (MGE) and lateral (LGE) ganglionic eminences (B), ISH. *Nedd4-2* mRNAs are expressed in the subventricular zone of both MGE and LGE, **C.** E14.5 MF1 mouse, one hemisphere coronal slice, ISH. Expression of Nedd4-2 now expands towards the cortex **D.** qRT-PCR performed on whole GE extracts. Nedd4-2 is expressed throughout embryonic stages in the brain and drops at birth.

We have first established the spatial (using ISH) and temporal (by qRT-PCR) expression patterns of Nedd4-2 messengers (Fig.1A-1D) Our findings are consistent with the expression of Nedd4-2 in post-mitotic interneurons during their tangential migration into the cortex (Fig. 1A, 1B). Our collaborators demonstrated earlier a role of Nedd4-2 in projection neuron migration (Broix et al. Nat Genet. 2016 Nov;48(11):1349-1358). According to its expression pattern in the ventral forebrain (Fig.1B), Nedd4-2 is likely also expressed by newborn migrating cortical interneurons (cINs). This will be confirmed by IHC on brain section from WT mouse embryos. While impaired migration or maturation of cINs can contribute to the physiopathology of epilepsy (several mutations carriers suffer from seizure), poor migration and differentiation of cINs in MCD remains to be assessed. In order to address this question, we generated a conditional knockout (cKO) mouse model to genetically invalidate *Nedd4-2* in newborn cINs. For this purpose, we crossed *Nedd4-2*$^{flox/flox}$ mice (collaboration with H. Kawabe, Max Planck Institute of Experimental Medicine, Göttingen, Germany) with *Dlx5,6*:CRE-GFP mice (available in our laboratory) to generate cKO embryos. Due to high sequence homology between *Nedd4-2* and *Nedd4-1*, the ancestral member of the NEDD family, and to exclude any compensatory mechanisms, we also generated and analysed cKO cINs, using *Nedd4-1*$^{flox/flox}$ and *Nedd4-1* $^{flox/flox}$ */Nedd4-2*$^{flox/flox}$.

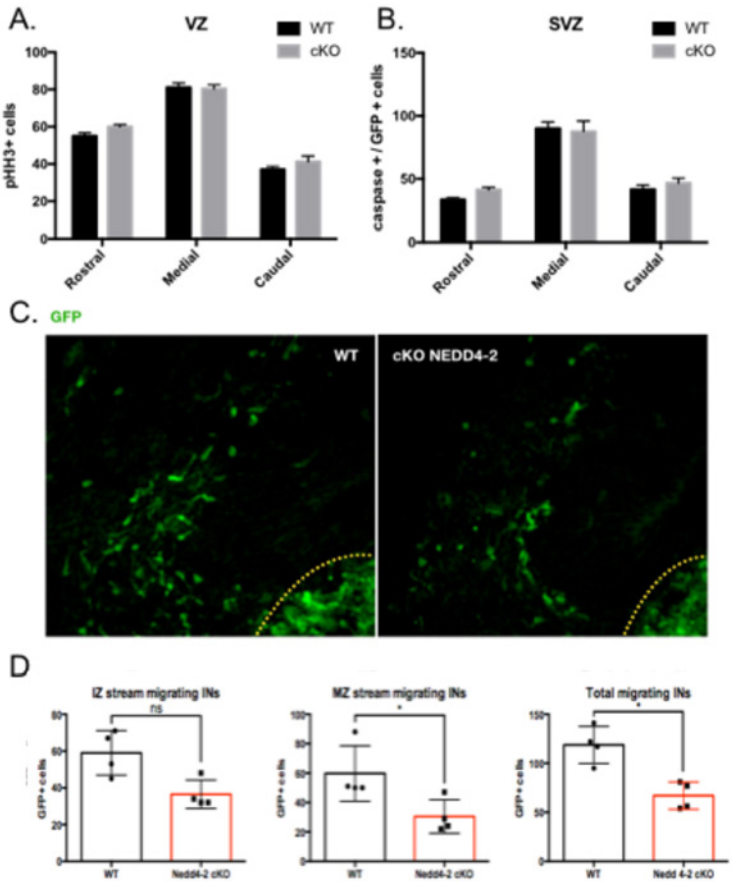

Fig. 2. Analysis of cell biological parameters in the cerebral cortex of *Nedd4-2* cKO and WT mouse embryos **A.** IHC quantification. No significant difference in number of phospho-histone H3 positive cells in the ventricular zone of E14.5 embryos GEs. **B.** IHC quantification. No significant difference in number of caspase/GFP double positive cells in the subventricular zone of E14.5 embryos GEs. **C.** Confocal microscopy analyses of the cerebral cortex of E13.5 mice. Yellow dotted lines delineate GE/cortex border. **D.** Quantification of data shown in C. Non-parametric tests were applied due to too low a number of animal in each group. Number of animals needs to be increased to perform parametrical t-test.

The analyse of these different cKO mouse lines did not revealed any developmental impairment of proliferation or survival of cINs and their progenitors (Fig. 2A, 2B). We next performed time lapse recording on cultured brain slices from embryonic day (E14.5) mice to further explore the migration of the cINs in the cortical wall. We observed a defect of migration marked at early stages ***by a decreased number of cINs exiting the ganglionic eminences*** (GEs ; Fig. 2C, 2D). The positioning of the migration front of cINs at later stages was also affected upon loss of *Nedd4-2* expression (data not shown).

In order to perform a fine analysis of the morphological remodelling of cINs during migration, we performed time lapse recordings on explants culture of medial GEs (MGEs) Migrating cINs exhibit a peculiar migratory pattern known as nucleokinesis. The cell develops an expansion known as the leading process, senses the environment and then, upon correct positioning of this leading process, the nucleus jumps forward. During those recordings, many parameters of migration were measured: average cell migration speed (Fig. 3B, 3C), frequency (Fig. 3D) and amplitude of nucleokinesis (Fig. 3E) as well as migration persistence - the ability to follow a straight line - of migrating cINs (Fig. 3.F).

Neither nucleokinesis amplitude nor migration persistence were affected by the genetical loss of *Nedd4-2* expression. ***However, our results underline a decreased frequency of nucleokinesis in Nedd4-2 cKO cINs resulting in a reduced speed of migration***. This defect may account for the migration phenotype observed in brain slices (Fig. 2C, 2D) Importantly, we couldn't find any migration defects in Nedd4-1 cKO cINs.

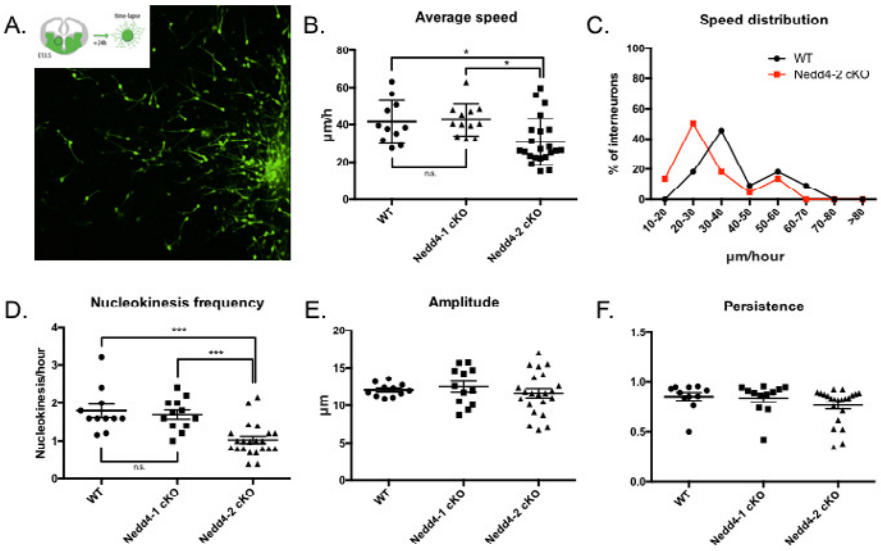

Fig. 3. *Ex vivo* imaging **A.** GE explants of E13.5 embryos are micro-dissected and cultured on cortical feeder. Five-hour recordings are held 24 to 48 hours later under controlled conditions. **B-F.** Quantification of migration features (see text). (*) P value < 0.05 (***) P value < 0.001

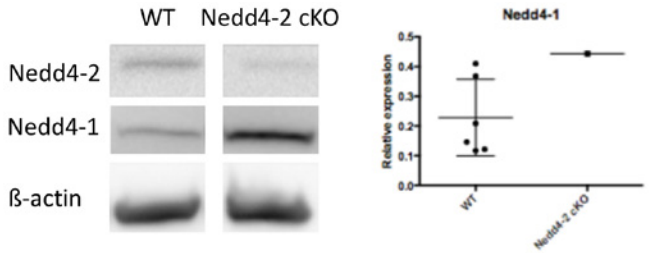

Fig. 4. *Western blotting showing the expression level of Nedd4-1, Nedd4-2 and beta-actin in cortical exttacts from WT or Nedd4-2 cKO. These are preliminary data as only one Nedd4-2 cKO animal has been analysed.*

Preliminary western blotting analyses performed on cortical extracts from E14.5 WT and Nedd4-2 cKO mouse embryos suggested the existence of a compensatory upregulation of the closely related protein Nedd4-1. In order to decipher whether the migration defects seen upon the conditional loss of Nedd4-2 may partly arise from the upregulation of Nedd4-1, we performed overexpression of Nedd4-1 in WT cINs and measured they migratory parameters. We could not see any differences when compared with WT cINs transfected with empty vectors (data not shown), suggesting that the migratory defects seen upon loss of Nedd4-2 are resulting from loss of its activity towards direct targets. We are currently consolidating this hypothesis by knocking down acutely Nedd4-1 in Nedd4-2 cKO cINs and further testing whether this would rescue the migration defects seen upon loss of Nedd4-2. We are also analysing the migration of cINs from WT and *Nedd4-2* cKO mouse embryos using genetic tools to assess microtubule remodelling and actomyosin dynamics, which both contribute to cell movement. Calcium imaging with the ratiomeric FuraRed is also being set up as calcium influxes are associated with nucleokinesis and thus migration of cINs.

Ultimately, genetic replacement experiments integrating MCD-related mutated proteins into *Nedd4-2* cKO cINs will be performed in order to decipher their pathophysiological implication. We will also assess cINs migration in the NEDD4-2 R897Q (K5810) "humanized" mouse and compare their migration parameters to the Nedd4-2 cKO cINs to measure the impact of the MCD-mutation on the migration of interneurons.

Since Nedd4-2 is an E3 ligase, we will next study the level of expression of relevant proteic substrates, by first focussing on ion channels (as impaired membrane depolarization defect may explain why cINs are not migrating properly).

For this purpose, we will combine UbiScan on FACS-isolated cells with western-blot and IHC in the developing mouse cortex in both WT and Nedd4s cKO mice. Co-immunoprecipitation between Nedd4-2 and the strongest candidates will be assessed in cell culture.

In conclusion and to further contextualize our work, identification of novel genes whose mutations lead to MCD is not only important for diagnosis and genetic counselling of patients and their families, but also to better understand the molecular processes of cerebral cortical development. Here, we could originally underline the involvement of both ubiquitination and interneurons migration defects in neurodevelopmental disorders characterized by MCD.

3.2. WP2. Deciphering the role of Nedd4-1/-2 in the developing inner ear and age-related hearing loss

Our preliminary data indicate that Nedd4-1 and Nedd4-2 mRNAs are expressed in the developing cochlea (starting at E14.5 in mice). While both are expressed at E17.5 in the organ of Corti, the stria vascularis and in the spiral ganglion (table 1), Nedd4.2 is not any more present postnatally.
We next performed preliminary experiments at the cellular level. We start in the organ of Corti and performed immunohistochemistry in E17.5 cochlea (Fig.5). We found that Nedd41/2 are more specifically expressed at cellular junctions between hair cells and supporting cells.

To further decipher the roles of Nedd4-1/2 during cochlear development, we made use of a conditional knockout strategy: Nedd4-2lox/lox mice have been crossed to a Foxg1:Cre transgenic mouse line that express the Cre recombinase in the early otocyst to obtain Nedd4-2-cKO mice. The first analysis showed that those mice are viable. We performed scanning electron microscopy and immunolabelings at different stages to see whether the organ of Corti is normal (Figure 7). We found a progressive decline of the number of hair cells starting at P45 (45 days postnatally). We will check whether this cell death is apoptotic by performing active caspase-3 immunolabellings. This late cell death is surprising since Nedd4.2 is not expressed postnatally. We will therefore study what could explain this progressive disappearance of hair cells and look at other cell types that could progressively impair hair cell survival. We will also check the integrity of cell junctions in the organ of Corti, since their misfunction could be at the origin of this progressive cell degeneration.

	E14.5	E17.5	P0	P3	P7
Cochlear duct	**+++/+++**	**++/++**	**++ / -**	**++ / -**	**++ / -**
Hair cells	NA	**++/++**	**++ / -**	**++ / -**	**++ / -**
Spiral ganglion	**+ / ++**	**+++/++**	**++ / -**	**++ / -**	**++ / -**
Stria vascularis	NA	**++/++**	**++ / -**	**++ / -**	**++ / -**

Table 1: Developmental pattern of expression of Nedd4.1 and Nedd4.2 in the developing cochlea

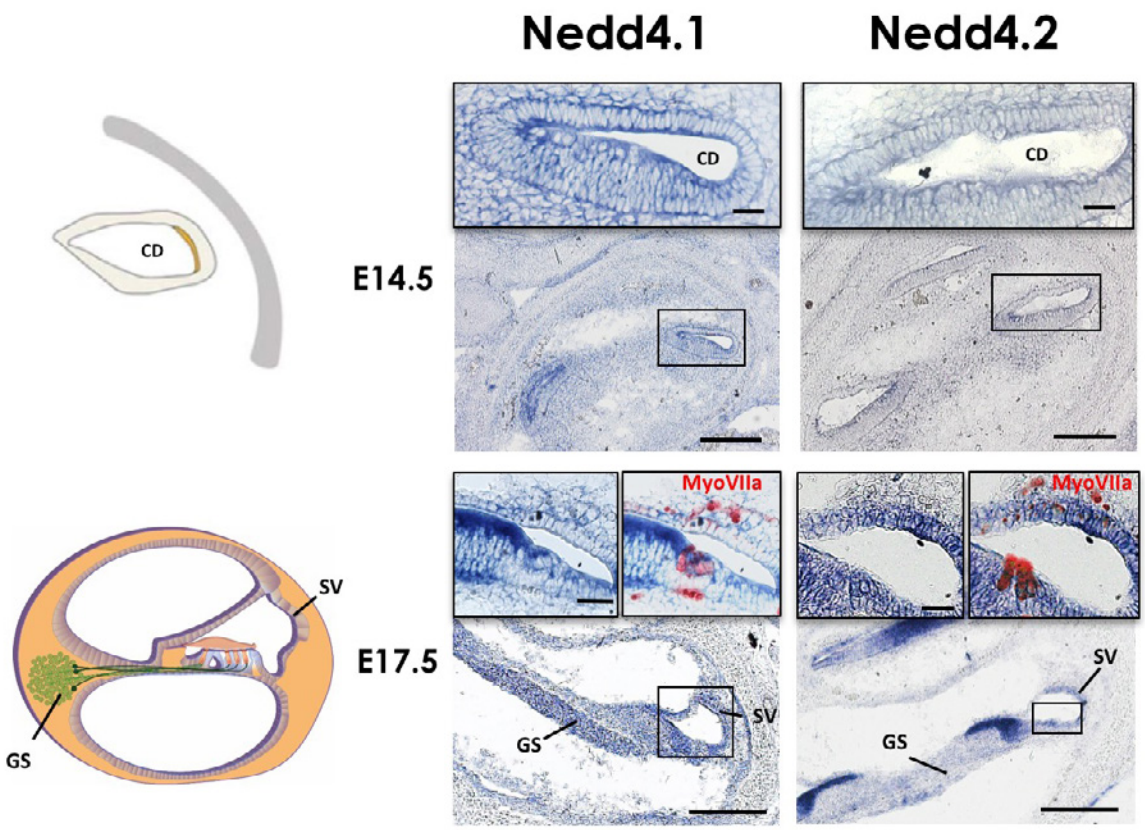

Fig. 5 Nedd4.1 and Nedd4.2 mRNA expression pattern in the developing cochlea. SV=stria vascularis, GS= spiral ganglion, CD= cochlear duct.

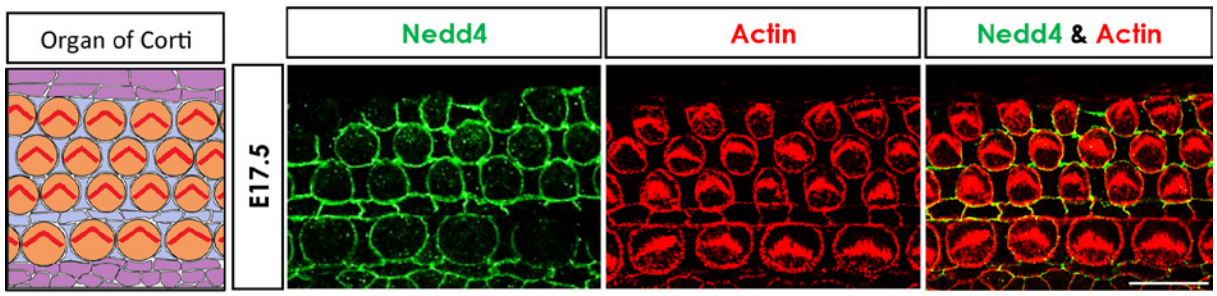

Fig. 6 Nedd4.1/2 are specifically expressed in cell junctions in the developing organ of Corti.

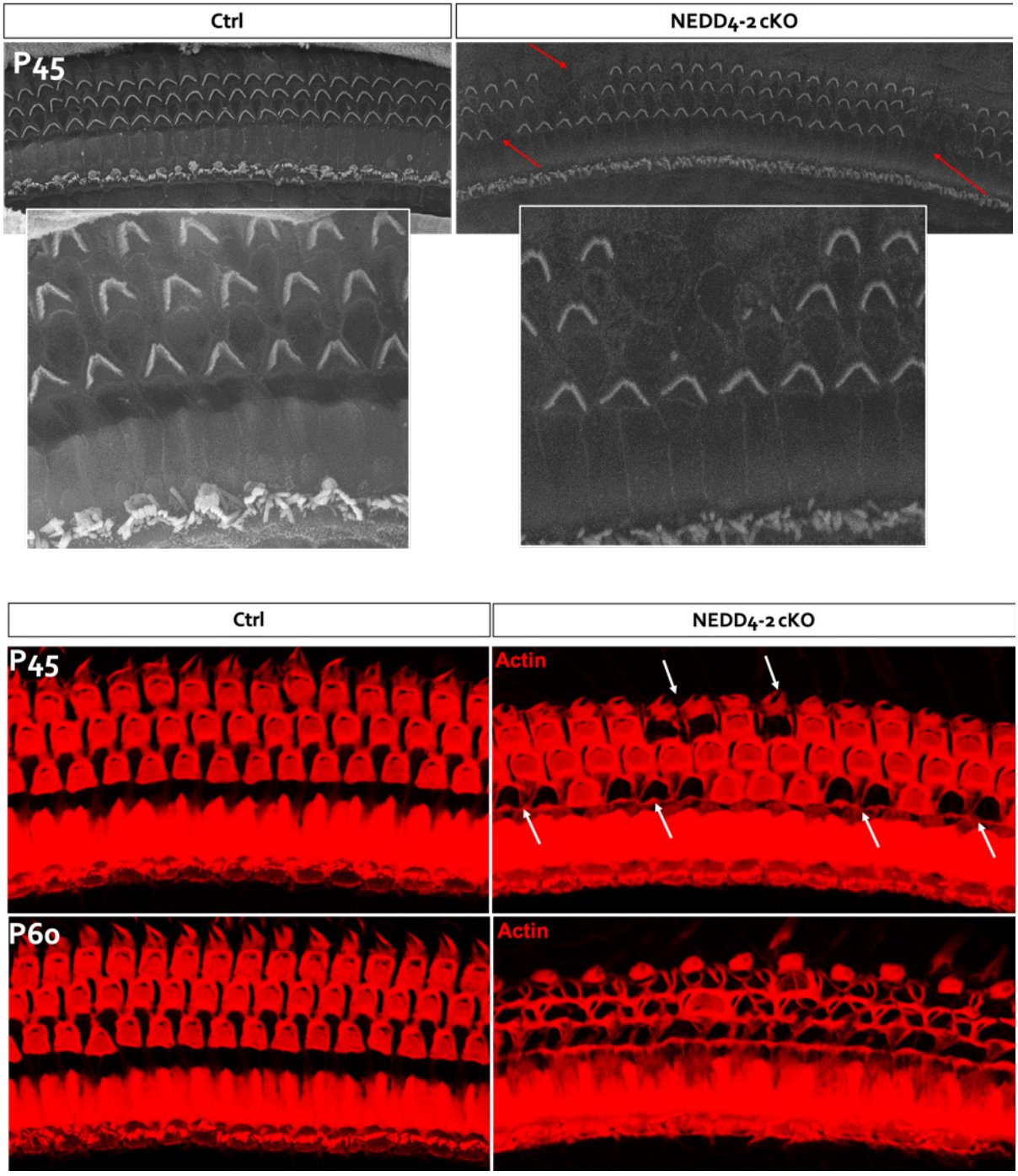

Figure 7 Nedd4.2-cKO mice present progressive degeneration of hair cells as shown by scanning electron microscopy (upper panel) and phalloidin labelling (lower panel).

4. Bibliography

1. Rash, B. G. & Grove, E. A. Area and layer patterning in the developing cerebral cortex. *Curr Opin Neurobiol* **16**, 25-34 (2006).
2. Gupta, A., Tsai, L. H. & Wynshaw-Boris, A. Life is a journey: a genetic look at neocortical development. *Nat Rev Genet* **3**, 342-355 (2002).
3. Anderson, S. A., Eisenstat, D. D., Shi, L. & Rubenstein, J. L. Interneuron migration from basal forebrain to neocortex: dependence on Dlx genes. *Science* **278**, 474-476 (1997).
4. Sarnat, H. B. & Flores-Sarnat, L. A new classification of malformations of the nervous system: an integration of morphological and molecular genetic criteria as patterns of genetic expression. *European journal of paediatric neurology : EJPN : official journal of the European Paediatric Neurology Society* **5**, 57-64 (2001).
5. Sarnat, H. B. & Flores-Sarnat, L. Neuroembryology and brain malformations: an overview. *Handbook of clinical neurology* **111**, 117-128, doi:10.1016/B978-0-444-52891-9.00012-9 (2013).
6. Spreafico, R. & Tassi, L. Cortical malformations. *Handbook of clinical neurology* **108**, 535-557, doi:10.1016/B978-0-444-52899-5.00047-2 (2012).
7. Mateo Sanchez, S., Freeman, S. D., Delacroix, L. & Malgrange, B. The role of post-translational modifications in hearing and deafness. *Cell Mol Life Sci*, doi:10.1007/s00018-016-2257-3 (2016).
8. Nelson, R. F. *et al.* Selective cochlear degeneration in mice lacking the F-box protein, Fbx2, a glycoprotein-specific ubiquitin ligase subunit. *J Neurosci* **27**, 5163-5171, doi:10.1523/JNEUROSCI.0206-07.2007 (2007).
9. Kazmierczak, M. *et al.* Progressive Hearing Loss in Mice Carrying a Mutation in Usp53. *J Neurosci* **35**, 15582-15598, doi:10.1523/JNEUROSCI.1965-15.2015 (2015).
10. Narimatsu, M. *et al.* Regulation of planar cell polarity by Smurf ubiquitin ligases. *Cell* **137**, 295-307, doi:10.1016/j.cell.2009.02.025 (2009).

4. Publications of the laboratory in 2017 and 2018 supported by the F.M.R.E.

– Morelli, g., Avila, A., Ravanidis, S., Aourz, N., Neve, R.L., Rigo, J.-M.*, **Nguyen, L**.*, and Brône, B*. : Cerebral cortical circuitry formation requires functional glycine receptors.
Cereb Cortex (2017), 27(3):1863-1877 (I.F. 2015= 6.559) *equal contribution
– Van den Ackerveken, P., Mounier, A., Huyghe, A., Sacheli, R., Vanlerberghe, P.-B., Volvert, M.-L., Delacroix, L., **Nguyen, L.**, and **Malgrange, B.**: The miR183/ItgA3 axis is a key regulator of prosensory area during early inner ear development
Cell Death Differ (2017), 24(12):2054-2065. (I.F. 2016= 8.339)
– Laguesse, S., Close, P., Van Hees, L., Chariot, A., **Malgrange, B.**, and **Nguyen, L** . : Loss of Elp3 impairs the acetylation and distribution of connexin-43 in the developing cerebral cortex.
Front Cell Neurosci (2017), (11:#122). doi: 10.3389/fncel.2017.00122. eCollection 2017.8 (I.F. 2016=4.555)
– Agirman, G. Broix, L., and **Nguyen L**. : Cerebral cortex development: an outside-in perspective.
FEBS Lett (2017) 591(24): 3978-3992 (I.F. 2016= 3.623.)
– Gladwyn-Ng, I., Cordon Barris, L., Alfano, C., Creppe, C., Couderc, T., Morelli, G., Thelen, N., America, M., Bessières, B., Ench-Razavi, F., Bonnière, M., Susuki, I., Flamand, M., Vanderhaeghen, P., Lecuit, M., and **Nguyen, L** . : Loss of Stress-induced unfolded protein response contributes to Zika virus-associated microcephaly.
Nature Neuroscience (2018), 21(1):63-71 (I.F. 2018= 19.912)
– Silva, C. G., Peyre, E., Adhikari, M. H., Tielens, S., Tanco, S., Van Damme, P., Magno, L., Krusy, N., Agirman, G., Magiera, M. M., Kessaris, N., **Malgrange, B.**, Andrieux, A., Janke, C., and **Nguyen, L**.: Cell intrinsic control of interneuron migration drives cortical morphogenesis.
Cell (2018), 172(5): 1063-78 (I.F. 2018= 31.398)
– Marlier, Q., Jibassia, f., Verteneuil, S., Linden, J., Kaldis, P., Meijer, L., **Nguyen, L.**, Vandenbosch, R., and **Malgrange, B.**: Genetic and pharmacological inhibition of Cdk1 provides neuroprotection towards ischemic neuronal death.
Cell death discovery (2018), 4(43) doi: 10.1038/s41420-018-0044-7. eCollection 2018 (I.F. 2018= n.a.)
– Morelli, G., Even, A., Gladwyn-Ng, I., Le Bail, R., Shilian, M., Godin, J.D., Peyre, E., Hassan, B., Besson, A., Rigo, J.-M., Weil, M., Brône, B., Janke, C., and **Nguyen, L.**: p27Kip1 modulates axonal transport by regulating α tubulin acetyltransferase 1 stability.
Cell Reports (2018), 23(8): 2429-2442 (I.F. 2018= 8.032)
– Caron, N. Genin, E.C., Marlier, Q., Verteneuil, S., Beukelaers, P., Morel, L., Hu, M. G., Hinds, P. W., Meijer, L., **Nguyen, L.**, Vandenbosch, R., and **Malgrange, B.**
Cell Mol Lifes Sci (2018), 75(20): 3817-3827 (I.F. 2018= 6.721)

- Uzquiano, A., Gladwyn-ng, I., **Nguyen L.**, Reiner, O., Götz, M., Matsuzaki, F., and Francis, F. : Cortical progenitor biology: key features mediating proliferation versus differentiation.
  J Neurochem (2018) 146(5): 500-525 (I.F. 2017= 4.609.)
- Lecuit, M., and **Nguyen L**. : Lessons learnt from the emergence of Zika virus.
  Nature Microbiology (2018) 591(24): 3978-3992 (I.F. 2017= 14.174.)

5. Other publications of the laboratory in 2017 and 2018

- Broix, L., Asselin, L., Silva, C. G., Ivanova, E. L., Tilly, P., Gilet, J. G., Lebrun, N., Jagline, H., Muraca, G., Saillour, Y., Drouot, N., Reilly, M. L., Francis, F., Benmerah, A., Bahi-Buisson, N., Belvindrah, R., **Nguyen, L.**, Godin, J. D., Chelly, J., and Hinckelmann, M. V.: Ciliogenesis and cell cycle alteraions to KIF2A-related malformations of cortical development
  Hum Mol Genet (2017), in press, Oct 25. doi: 10.1093/hmg/ddx384. (I.F. 2016= 5.340)
- Bento-Abreu, A., Jager, G., Swinnen, B., Rué, L., Hendrickx, S., Jones, A., Staats, K. A.,Taes, I., Eykens, C., Nonneman, A., Nuyts, R., Timmers, M., Silva, L., Chariot, A., **Nguyen,L**., Ravits, J., Lemmens, R., Cabooter, D., Ludo, VDB, Van Damme, P., Al-Chalabi, A.,Bystrom, A., and Robberecht, W. : Elongator subunit 3 (ELP3) modifies ALD trough tRNA Modification.
  Hum Mol Genet (2018), *in press* (I.F. 2018= 4.902).
- Nganou, G., Silva, C.G., Gladwyn-Ng, I., Engel, D., Coumans, B., Delgado-Escueta, A.V., Tanaka, M., **Nguyen, L**., Grisar, T., de Nijs, L., and Lakaye, B. : Importin-8 modulates division of apical progenitors, dendritogenesis and tangential migration during development of mouse cortex
  Front Cell Neurosci (2018), (9, #129): 1-18 (I.F. 2018= 4.300)
- Kum, D.B., Mishra, N., Boudewijns, R., Gladwyn-Ng, I., Alfano, C., Ma, J., Schmid, M.A., Marques, R.E., Schols, D., Patein, S., **Nguyen, L**., Neyts, J., and Dallmeier, K. : A yellow fever virus 17D based chimeric Zika virus vaccine cabndidate that protects against lethal Zika infection and congenital malformation in mice
  NPJ Vaccines (2018), 3:56 (I.F. 2018= 3.143)
- Beaufrère, A., Bessières, B., Bonnière, M., Driessen, M., Alfano, C., Couderc, T., Thiry, M., Thelen, N., Lecuit, M., Attiè-Bitach, T., Vekemans, M., Ville, Y., **Nguyen, L**., Leruez-Ville, M., and Encha-Razavi, F.,: A clinical and histopathological study of malformations observed in fetuses infected by the Zika virus.
  Brain Pathol (2019), 29(1):114-125 (I.F. 2018= 6.187)
- Defourny, J., Peuckert, C., Kullander, K. & **Malgrange, B.** EphA4-ADAM10 Interplay Patterns the Cochlear Sensory Epithelium through Local Disruption of Adherens Junctions. iScience 11, 246-257 (2018). (I.F. 2018= n.a.)
- Czajkowski, A., Mounier, A., Delacroix, L. & **Malgrange, B.** Pluripotent stem cell-derived cochlear cells: a challenge in constant progress. Cell Mol Life Sci (2018). (I.F. 2018= 6.721)

Geneeskundige Stichting Koningin Elisabeth
Fondation Médicale Reine Elisabeth
Königin-Elisabeth-Stiftung für Medizin
Queen Elisabeth Medical Foundation

Progress report of the research group of

Prof. dr. Timmerman Vincent, PhD

Universiteit Antwerpen (UA)

Principal investigator:

Prof. dr. Timmerman Vincent, PhD
Peripheral Neuropathy Research Group,
University of Antwerp – CDE,
Parking P4, Building V, Room 1.30,
Universiteitsplein 1
2610 Antwerpen
Belgium
E-mail: vincent.timmerman@uantwerpen.be

Unravelling the novel molecular pathways contributing to distal Hereditary Motor Neuropathy caused by mutant HSPB8, with the aim to identify potential therapeutic targets

1. Research report:

1.1. State of the art

Charcot-Marie-Tooth (CMT) neuropathies comprise a clinically diverse and genetically heterogeneous group of monogenic disorders affecting the peripheral nervous system. A remarkable group of genes mutated in CMT are those coding for *small heat shock proteins* (HSPBs). Although regulated by all types of stress, HSPBs are constitutively expressed and responsible for protein quality control and protein folding. The HSPBs are not only molecular chaperones but also involved in many essential cellular processes such as apoptosis, autophagy, splicing and translation, cytoskeleton dynamics and neuronal survival. In this report we will also discuss the mechanisms of disease caused by mutations in *atlastin* and *mitofusin* in the context of their role in the endoplasmic reticulum and mitochondrial associated membranes, an important knowledge in relation to the development of therapeutic approaches to treat axonal degeneration.

1.2. Aims of the GSKE project

The development of induced pluripotent stem cells (iPSC) has brought together the genetic accuracy of a patient-derived model and the possibility of having the disease-specific cell type. This model promises to influence modern medicine and drug development particularly for neurological disorders by providing an unlimited access to patient-derived neurons. We will take advantage of the iPSC model along with a knock-in/knock-out mouse model that we have recently developed for distal hereditary motor neuropathy (dHMN and/or axonal CMT), caused by mutations in the small heat shock protein HSPB8, to identify and validate translationally relevant pathway(s) leading to axonal degeneration, and with the ambition to select and test promising therapeutic targets. In this 3-year project we aim to: 1) identify altered molecular pathway(s) responsible for dHMN / axonal CMT by differential proteomics, and 2) obtain preclinical evidence to rescue these altered pathways with repurposed drugs. We also decided to expand this knowledge to other genes involved in axonal degeneration of the peripheral nervous system.

1.3. Results

To delineate the **molecular deficits and functional consequences of *HSPB8* mutations** we published our results of a knock-in model for the K141N mutation mimicking the dHMN phenotype. We observed that homozygous knock-in mice (*Hspb8*$^{K141N/K141N}$) develop a progressive axonopathy resulting in locomotor deficits. At the ultrastructural level, mice accumulate the mutant Hspb8 protein and display degenerative patterns similar to dHMN patients. Interestingly, these animals also develop a progressive myofibrillar myopathy as observed in some rare patients with HSPB8 mutations. Additionally, our mouse model allowed us to generate an *Hspb8* knock-out using the same targeting construct. Strikingly, the homozygous *Hspb8* knock-out animals (*Hspb8*$^{-/-}$) do not show any sign of axonopathy and display a much milder myopathy than the *Hspb8* knock-in animals (Bouhy et al. 2018).

These insights opened up a new therapeutic strategy which we are currently exploring. Given the absence of any overt phenotype in the knock-out mouse we hypothesized that **reducing the expression of *Hspb8* might improve the dHMN and myofibrillar myopathy phenotype** (i.e. phenocopying the *Hspb8*$^{-/-}$ mouse). Thanks to this GSKE project, Leen Vendredy, was attracted as PhD student and obtained a competitive FWO-SB fellowship (starting from 1/1/2018). Leen Vendredy already tested

compounds from a high-throughput screen that was performed in the lab of our collaborator Prof. A. Poletti (Crippa et al, 2016; Sci. Rep. 6, 22827). In this published screen, an FDA/EMA approved library was used to identify compounds that affect the expression of human HSPB8. As we are interested in downregulating the expression of HSPB8, we validated the top 10 expression inhibitors. We performed a dose-response study for the selected compounds in different cell lines for different treatment durations. In HeLa cells, meclofenamate sodium (MFS) treatment resulted in a dose-dependent decrease of HSPB8. Unfortunately, the drug was unable to reproduce and inhibit the HSPB8 expression in NSC34 or C2C12 cells (respectively motor-neuron-like cells and myoblast). This discrepancy could be explained by the fact that Hela cells are human lines, while the C2C12 and NSC34 are murine cell lines. The high-throughput screen mentioned above was performed with the human HSPB8 gene promoter, and although these drugs are working for human cell lines, these might not be effective for the mouse *Hspb8* promoter. Since our aim is to validate these drugs on our published *Hspb8* mouse model, it is a prerequisite for them to be effective on the mouse *Hspb8* promoter. We therefore plan to set up a new screen with a higher basal luciferase expression than obtained in the initial screen by Crippa et al. (Crippa et al, 2016; Sci. Rep. 6, 22827). This will increase our chances of identifying HSPB8 expression inhibitors. In addition, the new screen will be performed on mouse embryonal fibroblasts (MEF) derived from the abovementioned mouse model, ensuring that the identified compounds are effective in murine cells and can later on be administered *in vivo*.

Similar to HSPB8, the small heat shock protein HSPB1 also causes dHMN and/or axonal CMT. Mansour Haidar obtained his PhD in 2018 and found that **mutations in *HSPB1* lead to impairment of the autophagic flux**. In *HSPB1* knock-out cells, he demonstrated that HSPB1 is necessary for autophagosome formation, which was rescued upon re-expression of HSPB1. Employing a label-free LC-MS/MS analysis on various HSPB1 variants (wild-type and mutants), we identified autophagy-specific interactors. We revealed that the wild-type HSPB1 protein binds to the autophagy receptor SQSTM1 (sequestosome) and that the PB1-domain of SQSTM1 is essential for this interaction. Mutations in *HSPB1* lead to a decrease in the formation of p62 bodies, and subsequent impairment of phagophore formation, suggesting a regulatory role for HSPB1 in autophagy via interaction with SQSTM1. Remarkably, autophagy deficits could also be confirmed in patient iPSC-derived motor neurons thereby indicating that the impairment of autophagy might be one of the pathomechanisms by which mutations in *HSPB1* lead to peripheral neuropathy (Haidar et al. in press). Thanks to the GSKE project we attracted Angela Sisto as a second PhD student who will proceed and identify FDA/EMA-approved molecules that are able to reverse the autophagic deficits caused by mutant HSPB1 and HSPB8. We will validate the effect of the selected drugs in motor neurons differentiated from patient-derived iPSCs with the aim to improve the neurodegenerative phenotype. In parallel with the drug screening, we will characterize the role of HSPBs in autophagosome formation, thereby providing insights in the mechanism of action of new drugs. In summary, we aim to target autophagy, the first shared pathomechanism between these two genes, and it will contribute to our understanding of the underlying molecular deficits.

Data obtained with the support of a previous GSKE-grant demonstrated that mitochondrial transport was severely compromised in a mutant HSPB1 transgenic mouse model (in collaboration with Prof. L. Van Den Bosch, KULeuven). In this study we were able to identify a potential novel treatment for HSPB1 as restoration of mitochondrial transport led to amelioration of the phenotype. However, why abundant cytosolic chaperones like HSPB1 would cause a mitochondrial transport defect remained enigmatic. The work from PhD student Elias Adriaenssens now identified a possible answer to this question. **Unexpectedly, HSPBs were found to translocate into mitochondria**. This raised the possibility that mutations in HSPB1 are the direct cause of mitochondrial dysfunction. Indeed, mutations in the highly conserved alpha-crystallin domain of HSPB1 were found to increase mitochondrial residence as a consequence of binding stronger to molecular client proteins inside mitochondria. A mutation (P182L) in the C-terminal domain of HSPB1, which is associated with a more severe disease phenotype,

even prohibited HSPB1 from being imported into the mitochondria. These results may thus form an explanation as for why restoring mitochondrial transport was beneficial in a mutant HSPB1 mouse model. Moreover, our preliminary data suggested that HSPB8 is also imported into the mitochondria and mitochondrial transport defects may thus also form a shared disease mechanism. A hypothesis we are currently exploring further.

As mentioned in our initial GSKE project description, there is also an urgent unmet need to identify **molecular signatures that are common to multiple axonal CMT-subtypes** (including CMT2 and dHMN) that can aid in the development of novel therapeutic strategies and measuring disease outcomes in patients. Postdoc Manisha Juneja performed a differential proteomics based approach on lymphoblasts obtained from patients genetically diagnosed with different gene mutations to identify differentially regulated proteins compared to control lymphoblasts. The results were validated using RT-qPCR and/or western blot analysis on a large axonal CMT patient cohort. The proteomic profiling of patient derived lymphoblasts resulted in the identification of *profilin 2* (PFN2) and *guanidinoacetate methyltransferase* (GAMT) as commonly down-regulated proteins in different genotypes compared to healthy controls. This decrease was also observed at the transcriptional level upon screening 43 CMT2 patients and 22 controls ($p=0.005$ and $p=0.01$ respectively). Furthermore, a progressive decrease in the PFN2 expression with age was observed in patients, in contrast to the healthy age-matched controls, wherein PFN2 expression progressively increases with age. The reduced expression of PFN2 was also observed in motor neurons differentiated from patient-derived iPSCs (with missense mutations in the *HSPB1*, *HSPB8*, *MFN2* or *NFL* genes) and in sciatic nerves of the symptomatic *Mfn2* and *Hspb8* mouse models (a published *Mfn2* transgenic model, see further below, and our in-house *Hspb8* knock-in model, see above) when compared to their respective controls. However, no change in GAMT expression levels was observed in the motor neurons and CMT2 mouse-derived sciatic nerves. Our results revealed PFN2 and GAMT as molecular determinants for CMT2 neuropathy, with possible indications of the role of PFN2 in the pathogenesis and disease progression. These biomarkers could boost the development of therapeutic strategies targeting a larger group of axonal CMT patients with different CMT2 mutations (Juneja et al. 2018). Note that the University of Antwerp has filed this finding (September 2018, PTC/EP2018/077133).

Although not originally described in the current GSKE proposal, we also studied the **altered molecular pathways in hereditary sensory and autonomous neuropathy** (HSAN, a predominantly sensory-axonal disorder) through the PhD project of Michiel Krols. We studied how the HSAN-causing mutations in *atlastin,* ATL3, influence ER membrane shaping and mitochondrial associated membranes (MAM). In patient fibroblasts and in HeLa cells expressing disease-causing mutations in ATL3, the number of ER-mitochondria contact sites was increased. This increase in membrane contact sites correlated with augmented ER-mitochondria crosstalk, resulting in upregulated phosphatidylserine and phosphatidylethanolamine levels, increased autophagy induction and higher ER-mitochondria calcium transfer. In neurons expressing mutant ATL3, a lowered axonal mitochondrial density indicated a defect in mitochondrial distribution and positioning. These findings show that the disruption of ER dynamics has repercussions also for mitochondrial homeostasis and axonal trafficking, which likely has adverse effects on neuronal survival and may underlie the neurodegenerative phenotype caused by mutations in ATL3. In conclusion, this work significantly contributed to the understanding of ATL3 biology and the underlying pathology of HSAN (Krols et al. 2018).

In addition, we also studied the altered interplay between ER and mitochondria in frame of mutations in the *mitofusin* gene *MFN2* causing the axonal CMT neuropathy or CMT2A. This work was in collaboration with Prof. B.L. Schneider (France) and R. Chrast (Sweden). Using both *in vivo* and *in vitro* models of CMT2A, we observed that expression of the R94Q mutation in the mouse *Mfn2* induces a distal axonal degeneration without causing neuronal death. The presence of the mutant MFN2 protein leads to a

reduction in ER and mitochondria contacts in CMT2A patient-derived fibroblasts, in primary neurons and *in vivo* (in the *Mfn2* transgenic model). These changes are accompanied with the activation of an ER stress response, dysregulated calcium signalling, altered mitochondrial morphology and their axonal transport. Importantly, pharmacological treatments reinforced ER-mitochondria crosstalk, reduced the ER stress, restored the mitochondria morphology and prevented axonal degeneration (Bernard-Marissal et al, in press). **These results further expand the defects in MAMs as a possible pathomechanism in axonal neuropathies caused by mutations in *MFN2* and *ATL3***.

Finally, in this GSKE report Manisha Juneja also included a review on '*Challenges in modelling the Charcot-Marie-Tooth neuropathies for therapy development*', in which we shed light on the exciting advancement in CMT disease modelling, the breakthroughs, pitfalls, current challenges for scientists, and key considerations to move the field forward towards successful therapies (Juneja et al. 2018).

2. Research activities

Articles in International Journals – Acknowledging the GSKE in 2018:

1. Bouhy D, Juneja M, Katona I, Holmgren A, Asselbergh B, De Winter V, Hochepied T, Goossens S, Haigh JJ, Libert C, Ceuterick-de Groote C, Irobi J, Weis J, Timmerman V. A knock-in/knock-out mouse model of HSPB8-associated distal hereditary motor neuropathy and myopathy reveals toxic gain-of-function of mutant Hspb8. Acta Neuropathologica, 2018;135:131-148 (IF: 12.21)
2. Juneja M, Azmi A, Baets J, Roos A, Jennings MJ, Saveri P, Pisciotta C, Bernard-Marissal N, Schneider BL, Verfaillie C, Chrast R, Seeman P, Hahn AF, De Jonghe P, Maudsley S, Horvath R, Pareyson D, Timmerman V. PFN2 and GAMT as common molecular determinants of axonal Charcot-Marie-Tooth disease. Journal of Neurology Neurosurgery and Psychiatry, 2018;89(8):870-878 (I.F.: 7.14)
3. Krols M*, Asselbergh B*, De Rycke R, De Winter V, Seyer A, Muller FJ, Kurth I, Bultynck G, Timmerman V*, Janssens S*. Sensory neuropathy-causing mutations in ATL3 affect ER-mitochondria contact sites and impair axonal mitochondrial distribution. Human Molecular Genetics, Epub: 18-Oct-2018 (PMID: 30339187) (I.F.: 4.902) (* equal contributions) (I.F.: 4.90)
4. Juneja M, Burns JM, Saporta MA, Timmerman V. Challenges in modelling the Charcot-Marie-Tooth neuropathies for therapy development. Journal of Neurology, Neurosurgery and Psychiatry, 2019;90(1):58-67 (I.F.: 7.14)
5. Haidar M, Asselbergh B, Adriaenssens E, De Winter V, Timmermans J-P, Auer-Grumbach M, Juneja M, Timmerman V. Neuropathy-causing mutations in HSPB1 impair autophagy by disturbing the formation of SQSTM1/p62 bodies autophagy. Autophagy, in press (I.F.: 11.1)
6. Bernard-Marissal N, Hameren GV, Juneja M, Rochat C, Mansour OE, Médard JJ, Croisier M, Maclachlan C, Poirot O, Timmerman V, Tricaud N, Schneider BL, Chrast R. Altered interplay between endoplasmic reticulum and mitochondria contributes to Charcot–Marie–Tooth type 2A neuropathy. PNAS, in press (I.F.:9.5)

Awards and fellowships:

- **Leen Vendredy**: FWO-SB PhD fellowship started on 1st January 2018
- **Leen Vendredy:** PNS fellowship to attend the Annual Meeting of the Peripheral Nerve Society (PNS and CMTR consortium meeting), Baltimore, 21-25 July 2018
- **Elias Adriaenssens**: PNS fellowship to attend the Annual Meeting of the Peripheral Nerve Society (PNS and CMTR consortium meeting), Baltimore, 21-25 July 2018
- **Elias Adriaenssens**: FWO travel fellowship to attend the 3rd CSSI workshop on Small Heat Shock Proteins, Québec City, USA, 26-29 August 2018

PhD thesis:

- **Mansour Haidar**: *Autophagy in inherited peripheral neuropathies: focus on the small heat shock protein HSPB1*; PhD in Biochemistry and Biotechnology, Universiteit Antwerpen, 29 March 2018

Master theses:

- **Rani Boons:** *The role and import of small heat shock protein HSPB1 in mitochondria*. Master in Bioscience Engineering, Cell- and Gene technology, KULeuven, June 2018
- **Liedewei Van de Vondel:** *Functional genomics and pathogenic validation of ARHGEF15 de novo mutation in epileptic encephalopathy*. ERASMUS Master in Biochemistry & Biotechnology, University of Barcelona, June 2018

Chair and organizational activities:

- **Vincent Timmerman**: secretary of the CMTR consortium meeting at the Annual Meeting of the Peripheral Nerve Society (PNS), Baltimore, 21-25 July 2018
- **Manisha Juneja**: chair at the CMTR consortium meeting at the Annual Meeting of the Peripheral Nerve Society (PNS), Baltimore, 21-25 July 2018

Invited research seminars:

- **Vincent Timmerman:** *Can we find common pathomechanisms in CMT neuropathies?* 6 December 2018, Research seminar organized by Prof. V. Delague, Université Aix-Marseille, France

Invited lectures at international meetings:

- **Vincent Timmerman**: *HSPB1/HSPB8 in axonal neuropathy and distal myopathy*, published in: 234th ENMC International Workshop: Chaperone dysfunction in muscle disease Naarden, The Netherlands, 8-10 December 2017, by Weihl CC, Udd B, Hanna M; ENMC workshop study group. Neuromuscular Disorders 2018;28(12):1022-1030.
- **Vincent Timmerman:** *Identification of common molecular determinants of axonal Charcot-Marie-Tooth disease*. 4th joint meeting of the Belgian-Dutch neuromuscular study club and German Reference Center for Neuromuscular Diseases of the DGNN, Naarden, Netherlands, May 25-26, 2018.
- **Vincent Timmerman**: *New genes and mechanisms in inherited neuropathies*. Plenary lecture at the 15th International Congress on Neuromuscular Diseases (ICNMD 2018), Vienna, Austria, July 6-10, 2018
- **Vincent Timmerman**: *Disease mechanisms in the inherited neuropathies*. Educational lecture at the Peripheral Nerve Society (PNS 2018), Baltimore, USA, 21-25 July, 2018

Slide presentations selected at international meetings:

- **Manisha Juneja**: *Molecular phenotyping of neurons derived from CMT2 patient-iPSC lines* (oral poster). Peripheral Nerve Society (PNS 2018), Baltimore, USA, 21-25 July, 2018
- **Elias Adriaenssens**: *How does mitochondrial dysfunction contribute to the CMT2F pathogenesis caused by HSPB1 mutations.* CMTR and Peripheral Nerve Society (PNS 2018), Baltimore, USA, 21-25 July, 2018
- **Leen Vendredy:** *A preclinical study to treat neuromuscular diseases caused by mutations in the small heat shock proteins HSPB8*. 3rd CSSI workshop on Small Heat Shock Proteins, Québec City, USA, 26-29 August 2018
- **Elias Adriaenssens:** *Small heat shock proteins operate as chaperones in the mitochondrial intermembrane space*. 3rd CSSI workshop on Small Heat Shock Proteins, Québec City, USA, 26-29 August 2018

Poster presentations at international meetings:

- **Manisha Juneja:***Molecular phenotyping of neurons derived from CMT2 patient-iPSC lines.* Peripheral Nerve Society (PNS 2018), Baltimore, USA, 21-25 July, 2018
- **Elias Adriaenssens:** *How does mitochondrial dysfunction contribute to the CMT2F pathogenesis caused by HSPB1 mutations.* Peripheral Nerve Society (PNS 2018), Baltimore, USA, 21-25 July, 2018
- **Leen Vendredy:** *A preclinical study to treat neuromuscular diseases caused by mutations in the small heat shock proteins HSPB8.* Peripheral Nerve Society (PNS 2018), Baltimore, USA, 21-25 July, 2018

Slide presentations selected at national meetings:

- **Elias Adriaenssens:** *CRISPR/Cas9: Everything you need to know.* KVCV seminar Antwerp, 22 February 2017

Poster presentations at national meetings:

- **Manisha Juneja:** *Molecular phenotyping of neurons derived from CMT2 patient-iPSC lines*. Belgian Society for Stem Cell Research (BeSSCR 2018), Leuven, Belgium, 26 October, 2018

Societal activities:

– **Jonas Van lent**: *"Stamcelonderzoek: veelbelovend?"* CMT studie- en contactdag, Antwerpen, 20/10/2018
– **Vincent Timmerman**: "*Resultaten voorgesteld tijdens het CMT-congres in Baltimore*" CMT studie- en contactdag, Antwerpen, 20/10/2018

Valorisation of research findings:

– EP17195108-PTC/EP2018/077133: "*Biomarkers for Charcot-Marie-Tooth disease*" (inventors M. Juneja and V. Timmerman)

Geneeskundige Stichting Koningin Elisabeth
Fondation Médicale Reine Elisabeth
Königin-Elisabeth-Stiftung für Medizin
Queen Elisabeth Medical Foundation

Progress report of the research group of

Prof. Fadel Tissir, PhD

Université Catholique de Louvain (UCL)

Principal investigator

Prof. Fadel Tissir, PhD, Maître de Recherches FNRS
Institute of Neuroscience, Developmental Neurobiology group
Université Catholique de Louvain
Avenue E. Mounier 73, Box B1.73.16
B1200 Bruxelles
Belgium
Tel.: +32 2 764 73 84
Fax: +32 2 764 74 85
E-mail: Fadel.Tissir@uclouvain.be

Cortical development and malformations

The cerebral cortex is the seat of higher brain functions. It is essential for sensory and motor processing, as well as for human-specific mental functions such as logical reasoning and language. The formation of cerebral cortex requires the production of the right number and diversity of neurons for intricate circuit assembly. During cortical histogenesis, neural stem cells (NSC) divide symmetrically in the ventricular zone (VZ) and both daughter cells re-enter the cell cycle, amplifying the pool of NSC. At the onset of neurogenesis, apical neural progenitor cells (aNPC, also known as apical radial glia) shift from a symmetric/proliferative to an asymmetric/differentiative/neurogenic mode of division (neurogenic switch). Asymmetric divisions produce aNPC daughter cells as well as neurons, either directly or indirectly through intermediate/basal progenitors (IP/BP) which have limited self-renewal capacity and are committed to produce excitatory glutamatergic neurons. In the dorsal telencephalon, aNPC give rise sequentially to deep layer (DL: layers 5 and 6), upper layer (UL: layers 2– 4) neurons. Given the remarkable expansion of the cerebral cortex during evolution, but also the tight relationship between dysfunctions of cortical development and neurological disorders, a hot topic of neuroscience is to understand how the proliferation and differentiation of aNPC are orchestrated at the molecular and cellular levels and to identify genes and genetic pathways that control these processes.

During the last year, we have tremendously progressed on our understanding of how Diaphanous 3 (Diaph3) regulates division of NSC and of the relationship between its loss and neurodevelopmental disorders

1. Function of Diaph3 in cortical development and function

Using a functional candidate approach and gene expression profiling, we identified five formins as potential regulators of NSC division downstream of the Wnt/planar polarity signaling. Among these, Diaph3 is highly and specifically expressed by NSC in telencephalon. To better understand its function, we generated and analyzed a mouse line carrying a mutation in the *Diaph3* gene. In Diaph3 knockout (ko) mice, cortical progenitor cells undergo apoptosis as early as e10.5. Using flow cytometry analysis, we found a sevenfold increase in the proportion of aneuploid cells in the mutant telencephalon. These cells die, which depletes progressively the population of progenitors and leads to cortical hypoplasia. Aneuploidy could eventually give rise to neoplastic transformation. Remarkably, mutations in the human *DIAPH3* gene are frequently found in metastatic cancers, and down regulation of *DIAPH3* increases metastatic invasion in xenotransplanted mice [1,2]. The nuclear asymmetric division we uncover in Diaph3-deficient mice could increase chromosomal instability, promoting the emergence of new mutations and facilitating the development of tumors and/or acquisition of metastatic properties.

By investigating the molecular mechanisms of action of Diaph3, we found that Diaph3 co-immunoprecipitates with the mitotic spindle protein BubR1 and its mutation reduces by half the overall level of BubR1. Hence, the lack of Diaph3 weakens the spindle assembly checkpoint and behaves like a BubR1 hypomorphic allele. Consistently, the phenotype of *Diaph3 ko* phenocopies that of *BubR1^{h}* mice, in which mitotic slippage, formation of micronuclei, premature chromatid separation, aneuploidy, and decreased number of mitotic cells were described [3,4]. A link between BUBR1 and chromatid separation was also reported in patients with mosaic variegated aneuploidy, a rare disease associated with intrauterine growth retardation, aneuploidy, microcephaly, and hydrocephalus [5,6], further supporting the Diaph3-BubR1-nuclear division axis. These results provide evidence that Diaph3 protects NSC against mitotic error induced apoptosis, by preserving the activity of the spindle checkpoint. Loss of Diaph3 function does not trigger nuclear division errors in the strict sense. Such events occur physiologically,

especially in fast dividing cells like mammalian cortical progenitor cells. Rather, the lack of Diaph3 unties the spindle checkpoint enabling a fraction of aberrantly dividing cells, which normally should halt in metaphase, to nevertheless “slip” into anaphase, causing aneuploidy.

Diaph3 full knockout mice die as early as e12.5, thus preventing analysis of the late function of Diaph3 during cortical neurogenesis and in the adult. To circumvent this difficulty, we generated and analyzed conditional knockout mice in which, the gene was specifically inactivated in the cerebral cortex by crossing a floxed allele with mice expressing the recombinase Cre under the control of Emx1. In the adult brain, the length of medial longitudinal fissure (Figure 1A) and cerebrum weight (Figure 1B) in *Diaph3*$^{Emx1\text{-}Cre}$ conditional knockout (cKO) mice are significantly reduced. The cortical thickness is also markedly is diminished (Figure 1C).

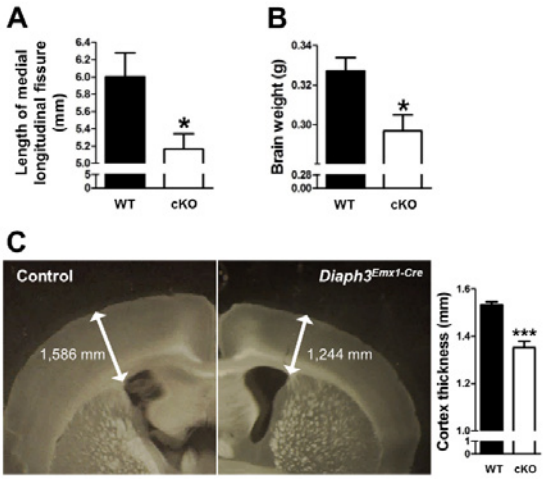

Figure 1 Impact of Diaph3 deficiency on the cerebral cortex (A) quantification of the length of the medial longitudinal fissure (A), and brain weight (B) showing a significant reduction in Diaph3$^{Emx1\text{-}Cre}$ conditional knockout (cKO) mice. (C) Coronal sections of the cerebrum showing a marked reduction of cortical thickness in Diaph3$^{Emx1\text{-}Cre}$ mutant mice. WT (wild-type): *n*=6, cKO: *n*=6, Student’s t-test, **P*<0.05, ****P*<0.001. Error bars represent: s.e.m.

We performed immunostaining with different cortical layer markers (layer II-III: Cux1; layer V: Ctip2; and layer VI: Foxp2) and found a reduction in the thickness of layer II-III and VI in *Diaph3*$^{Emx1\text{-}Cre}$ cKO (Figure 2A-D), along with a decrease in the number of cells in all cortical layers (Figure 2E).

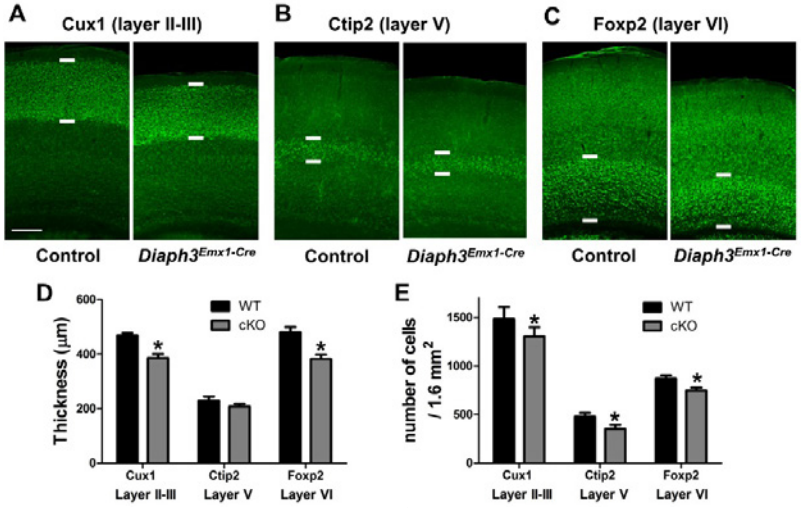

Figure 2 Different cell populations are affected in adult *Diaph3*$^{Emx1\text{-}Cre}$ mutant (A-C) Cortex-specific inactivation of Diaph3 disrupts cortical development. Coronal sections stained with Cux1 (A), Ctip2 (B) and Foxp2 (C) antibodies (green). (D) Thickness of cerebral cortex is quantified. Layer II-III and VI are thickened in *Diaph3*$^{Emx1\text{-}Cre}$ cKO. (E) Quantification of Cux1-, Ctip2- and Foxp2-positive cells. Cells were counted in 1.27 mm x 1.27 mm cortical areas from four mutants and four control littermates. Counts are expressed as number of cells per 1.6 mm^2. An average of 12%, 26% and 14% decrease in the cell populations in layer II-III (Cux1-positive), layer V (Ctip2-positive) and layer VI (Foxp2-positive) was seen in the mutant cortex. WT (wild-type) (*n*=4), cKO (*n*=4). Student’s t-test, **P*<0.05. Error bars represent s.e.m. Scale bar, 200 µm.

2. Cortical hypoplasia in *Diaph3*$^{Emx1\text{-}Cre}$ mutant

To better understand how the loss of Diaph3 impairs cortical development, we used markers of neurons (Tbr1), intermediate progenitors (Tbr2), and aNPC (Pax6) at E13.5 in immunostaining experiments; and found that the three cell populations are reduced by 37%, 17% and 11% respectively in the cKO mice (Figure 3).

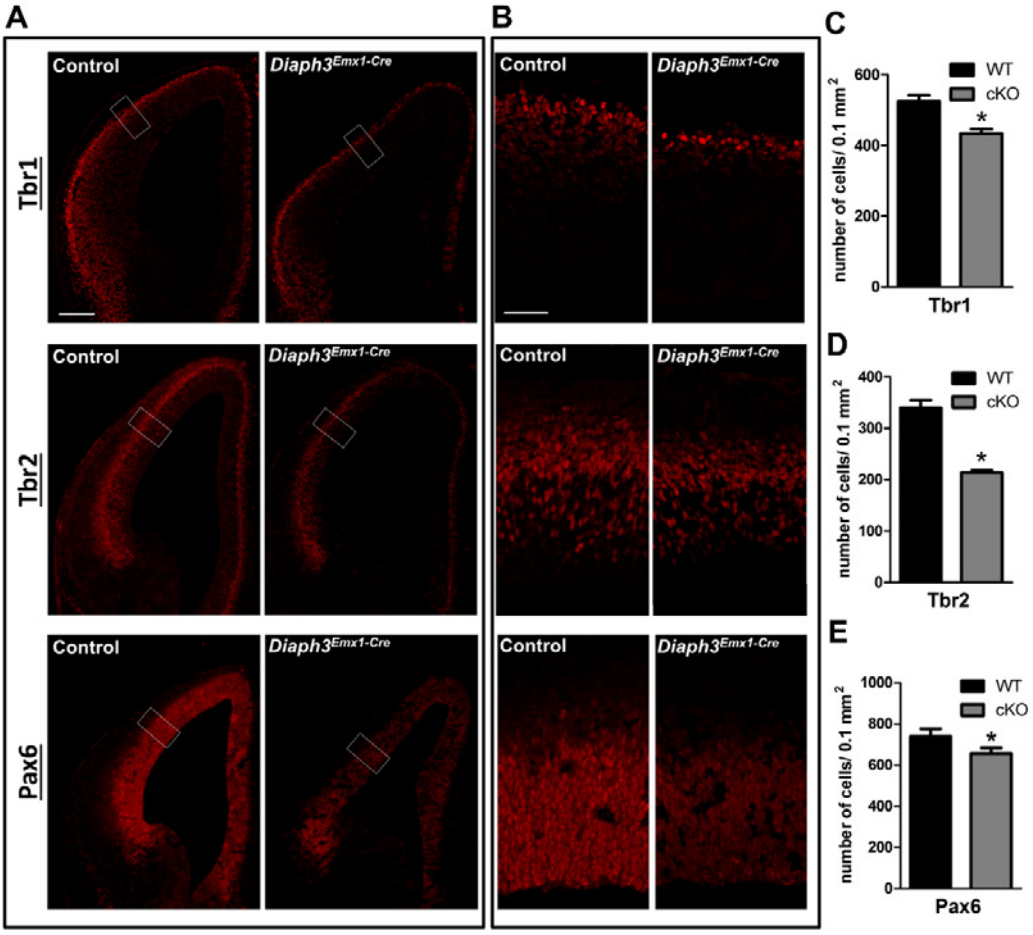

Figure 3 Cortex-specific inactivation of Diaph3 disrupts cortical development. (A) Forebrain coronal sections at e13.5 stained with Tbr1, Tbr2 and Pax6 antibodies (red). (B) Enlargements of the white boxes in (A) emphasising reduced number of the three main cell populations (neuron, Tbr1-positive; intermediate progenitor, Tbr2-positive; radial glial progenitor, Pax6-positive). Quantification are shown in (C-E). Cells were counted in 0.317 mm x 0.317 mm cortical areas from three mutants and three controls, and counts were expressed as cells per 0.1 mm^2. An average of 37%, 17% and 11% decrease in the cell populations in neuron (Tbr1-positive), intermediate progenitor (Tbr2-positive) and radial glial progenitor (Pax6-positive) was seen in the mutant tissue. WT (wild-type) (n=3), cKO (conditional knockout) (n=3). Student's t-test, *P<0.05. Error bars represent s.e.m. Scale bar, 100 µm in A, 50 µm in B.

During cortical development, the plane of cell division relative to the ventricular surface indicates whether the cell is undergoing proliferation or differentiation. Proliferative/symmetric divisions that increase the number of neuronal progenitors are characterized by a mitotic spindle parallel to the ventricular surface (Fig 4A, left). In asymmetric division, the mitotic spindle is oblique or perpendicular to the ventricular surface, giving rise to one apical progenitor and or one neuron (direct neurogenesis), or one apical progenitor and one basal progenitor. The modality of cell division is measured as shown in Figure 4A. Control and Diaph3$^{Emx1\text{-}Cre}$ sections were immuno-stained with γ-tubulin (red, centrosome) and DAPI (blue, chromosomes) to foresee the orientation of the spindle. We assessed the angles defined by the mitotic spindle and the ventricular surface at anaphase (Figure 4B), and found that in mutant tissue, aNPC undergo more neurogenic/asymmetric division at the expense of proliferation (neurogenic division: 26 % in controls versus 54 % in mutants; proliferative division: 74 % in controls versus 46% in mutants) (Figure 4C-D).

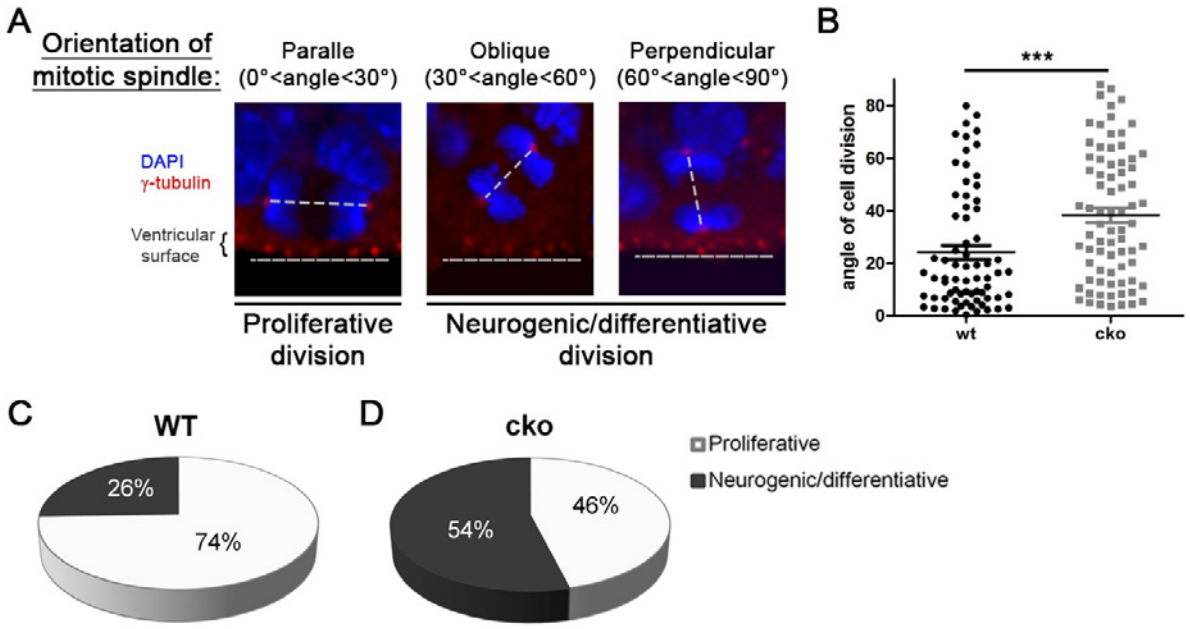

Figure 4 Cell division is disrupted in *Diaph3*$^{Emx1\text{-}Cre}$ mutant mice. (A) The orientation of the mitotic spindle with respect to the ventricular surface is categorized into 3 types: parallel (left), oblique (middle), or perpendicular (right). When the mitotic spindle is parallel to the ventricular surface (0°<angle≤30°), the cell division is proliferative. When it is oblique or perpendicular (30°<angle≤90°) to the ventricular surface, the division is neurogenic. E12.5 Cortical sections were stained for γ-tubulin (red) and DAPI (blue) to label centrosomes and chromosomes respectively. (B) Mitotic spindle angle distribution in dividing telencephalic cells. (C-D) At E12.5, *Diaph3*$^{Emx1\text{-}Cre}$ mutant mice show reduction of the proliferative and increase in the number of neurogenic/differentiative cell division. WT: *n*=70 from 3 embryos, cKO: *n*=76 from 3 embryos. Student's t-test, ***P<0.001. Error bars represent s.e.m

3. Loss of Diaph3 disrupts mitosis via interaction with Mitotic Spindle-Associated Protein P126 (MAP126)

Mitotic spindle is crucial for cell division, and position determines whether cells divide symmetrically or asymmetrically. Astral microtubules connect the centrosome to the membrane. Mitotic Spindle-Associated Protein P126 (MAP126), also called Astrin or Sperm Associated Antigen 5 (Spag5), interacts with SKAP complex at the plus-end of the astral microtubules that balance the spindle positioning force to the astral microtubule, and helps to orient the mitotic spindle. Astrin/SKAP complex also stabilizes microtubule-kinetochore attachments during metaphase and anaphase. Spag5 deficiency leads to multi-spindle pole and chromosome mis-segregation. Hence, we examined Astrin/Spag5 protein levels in the telencephalic lysate from *Diaph3*-deficient mice by Western blotting (tissue from null *Diaph3* knockout is preferred here to avoid contamination of protein from Emx1-cre negative cells in the conditional knockout mice) (Figure 5A). 40% reduction of Astrin/Spag5 protein was observed in Diaph3 ko tissue (Figure 5B). Co-immunoprecipitation by Diaph3 antibody shows that Astrin/Spag5 interacts physically with Diaph3 (Figure 5C). Previous study showed that Diaph3 localized to the concentric ring during telophase, but the subcellular localization during metaphase is unknown. To further investigate the subcellular localization of Diaph3 during mitosis, we used U2OS cell line. We found that Diaph3 localized to the centrosome during metaphase (Figure 5D). Knockdown of Diaph3 by shRNA caused mis-localization of Spag5 (Figure 5E). Diaph3 knockdown yielded errors in centrosome replication (3 centrosomes in Figure 5F & 5G; only 1 centrosome in Figure 5H). Loss of Diaph3 in centrosome (that is the microtubule organizing center, MTOC), disrupted the organization of the spindle and astral microtubules (Figure 5H), leading to aberrant cell division patterns (82% of Diaph3-knockdown cells versus 4% control, Figure 5I-J), and compromised viability in Diaph3 knockdown cells.

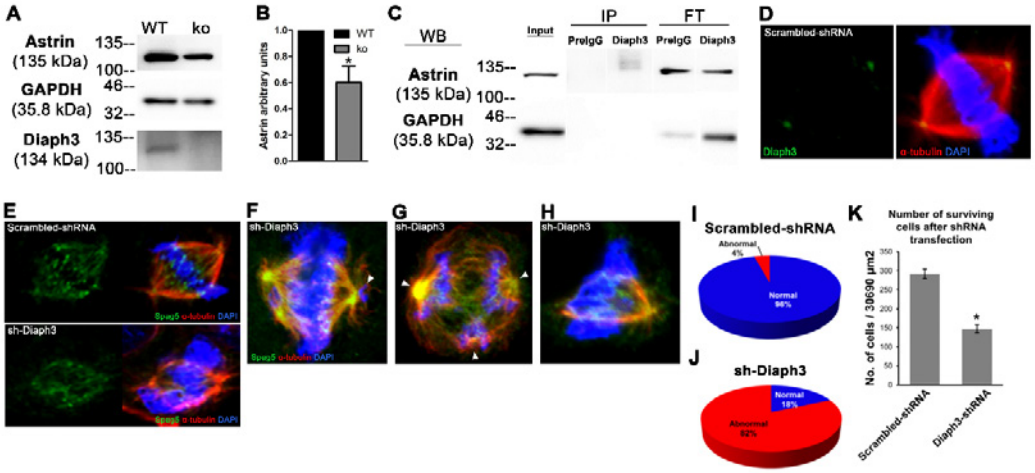

Figure 5 Down-regulation of Astrin/Spag5 and abnormal cell division in *Diaph3* mutant. (A) Reduction of Astrin/Spag5 protein levels in *Diaph3* ko telencephalon lysate detected by western blotting and quantified relatively to GAPDH. The same samples were blotted for Diaph3 to confirm the absence of the protein. (B) The level of Astrin/Spag5 decreased by 40% in the ko (n=3 embryos for each genotype). WT (wild-type), ko (knockout). Student's t-test, **P*<0.05 Error bars represent s.e.m. (C) IP with anti-Diaph3 antibodies from WT telecephalon lysates detects Astrin/Spag5 by western blotting (WB) . WB of Astrin/Spag5 in input was used as positive control for IP. (D) Immunostaining of a representative mitotic cell in scrambled-shRNA at metaphase (anti-Diaph3, green; anti-αtubulin, red; DAPI, blue). (E) Immunostaining of a representative mitotic cell showing the mis-localization of Spag5 in sh-Diaph3 cell (lower panel) compared to scrambled-shRNA (upper panel) (anti-Spag5, green; anti-αtubulin, red; DAPI, blue). (F-H) Abnormal cell division after Diaph3 knockdown. (F) Arrowhead shows lagging chromosomes. (G) Three centrosomes were seen occasionally (arrowheads) (H) depicts asymmetric metaphase plate and discontinued spindle microtubules. (I and J) Diaph3 knockdown causes nuclear division errors in 82% of cells (4% in control cells). Statistical analysis of 118 and 115 cells from 5 distinct experiments in scrambled-shRNA and shDiaph3 respectively. (K) Cell viability was reduced by 50% Diaph3 knockdown. (n=5 independent experiments from scrambled-shRNA and sh-Diaph3 knockdown cells).

4. Impact of Diaph3 deficiency on the function of cerebral cortex

In collaboration with the behavioral platform of UCLouvain (Prof. Philippe Gailly and Dr. Olivier Schakman), we investigated the behavior of the Diaph3$^{Emx1\text{-}Cre}$ cKO. Open-field test and elevated plus maze show that these mice have lower spontaneous motor activity than controls (Figure 6A-B), but no difference in time spent in exposed area indicating no difference in anxiety or attention. The 3 chamber test reveals that they spend more time in empty chamber than with a stranger mouse (stranger 1) revealing compromised sociability (Figure 6C). When a new stranger mouse (stranger 2) is presented, cKO mice spend more time with the more familiar mouse (stranger 1), indicating impairment in social novelty. These results indicate a defective social behavior in the cKO, and are in line with a clinical study that reported on a double hit in DIAPH3 locus in a patient with autism spectrum disorder [7].

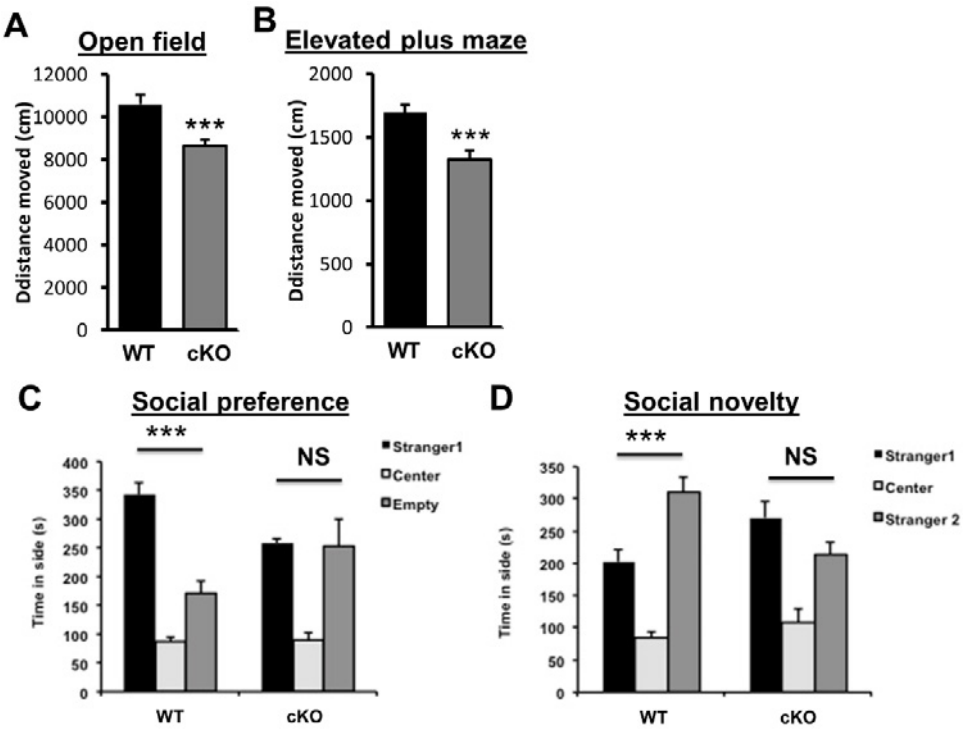

Figure 6 Abnormal behavior in Diaph3 mutant mice (**A**) Locomotor activity of males *Diaph3*$^{Emx1\text{-}Cre}$ mutant and control mice in open field test. Student's *t* test, ***P<0.001. (**B**) Distance travelled by the male mice in open areas of elevated plus maze. Student's *t* test, ***P<0.001. (**C**) Social behavior in the "3 chambers" test for males. One-way ANOVA, ***P<0.001 for both genotypes (stranger *versus* empty chamber). (**D**) Social novelty behavior in the "3 chambers" test for males. One-way ANOVA, ***P<0.001 for both genotypes (stranger 1 *versus* stranger 2 chamber). WT: n=10, cKO: n=10. Error bars represent s.e.m.

The above results have been included in a manuscript that will be submitted for publication.

5. Role of Diaph3 deficiency in glioblastoma

The involvement of Diaph3 in cancer development has been already investigated *in vitro*. Diaph3 silencing alters microtubules dynamics and favours amoeboid phenotype in cancer cells [2]. This enhances cell motility, invasion and metastatic progression. However, a role of Diaph3 in development of aneuploidy in cancer cells has never been described. In clinical studies, Diaph3 loss is more frequently found in metastatic diseases and low Diaph3 expression is associated with a shorter survival in prostate cancer [8]. We found that inactivation of Diaph3 causes aneuploidy in mouse. We hypothesize that this may lead to the neoplastic transformation. To test the potential relationship between the loss of Diaph3, aneuploidy and tumorigenesis, we co-inactivated Diaph3 and p53 in neural stem cells (NSC) of the cerebral cortex by crossing Diaph3/p53 double floxed mice with Emx1-Cre mice (to prevent the massive apoptosis given the role of p53 in aneuploidy-induced cell death). Our "proof of concept" experiments fully support this hypothesis as the Diaph3/p53 double mutants (hereafter referred to as Diaph3/p53$^{Em1\text{-}Cre}$) do develop cortical tumours between the age of 6–10 months (Fig. 7A), whereas p53$^{Em1\text{-}Cre}$ single mutants do not. Haematoxylin-eosin staining (Fig. 7B,C), and CD44, GFAP, and vimentin immunostainings strongly suggest that the tumours are GBM (Fig. 7D-F). GBM is the most frequent malignant primary tumour of the adult brain and one of the most aggressive with a median survival of about one year in humans [9] (few weeks in mice). The bad prognosis of GBM is due to its very high proliferation rate and to its invasiveness capability. Surgery remains the mainstay of treatment, but the extremely infiltrative nature of the tumour prevents its definitive removal. Radiotherapy and chemotherapy treatments also have a limited efficacy. Hence, it is essential to understand the genesis and progression of GBM, to identify early markers of its development, and improve diagnosis and/or treatment. We believe that the Diaph3/p53$^{Em1\text{-}Cre}$

model provides a valuable resource towards this objective. The virtually unlimited number of mice will help studies of the tumorigenic process and identification of cellular and molecular changes as the tumour progresses. We have produced pairs of Diaph3/p53$^{Em1\text{-}Cre}$ mutants (in which Diaph3 and p53 in embryonic or adult NSC) and littermate controls of different ages. The older pairs are 6 months and the younger are one month old. In few months we will screen them by Magnetic Resonance Imaging (MRI) using a 7 T scanner (Biospec 70/20 Avance III equipped with BGA12S gradient system) at the (pre) clinical magnetic resonance platform of UCLouvain. This set-up enables detection of tumours as small as 0.2 mm^3 (0.2 µl). Biopsies will be collected at different stages of the tumour growth (from 3 to 10 months). A part of the biopsy will be processed for histology and immunohistochemistry. Another part will be used for RNA extraction and sequencing in order to assess the molecular signature of the tumour as it appears and progresses and hopefully identify early biomarkers of GBM.

In addition to studies in mice, we have started a collaboration with Prof. Nicolas Tajeddine (oncology researcher), Prof. Christian Raftopoulos (neurosurgeon), and Dr Julie Lelotte (neuropathologist) with the aim to make use of the University hospital (Saint-Luc) biobank that comprises more 200 astrocytoma samples, among which 130 are GBM. These samples have been frozen hence enabling DNA sequencing as well as mRNA and protein analysis. Given that aneuploidy is associated with a poor prognosis in several cancers and poor response to chemotherapy, that 30-80% of high-grade gliomas contain aneuploid cells [10], and that the loss of Diaph3 causes aneuploidy we will assess the level of DIAPH3 in glioma samples and correlate this with survival, time to relapse, and radiological response to TMZ. GBM is believed to derive from transformed NSC [11], likely through asymmetric division [11,12]. Moreover, about 5% of GBM arise from low-grade astrocytomas in young patients, and the frequency of asymmetric mitosis is usually increased in high-grade tumours. To test the relationship between deregulation of Diaph3, cell division, and gliomagensesis in human, we will compare the grade of the astrocytoma on the one hand, to the level of DIAPH3 and cardinal oncogenes/tumour suppressor genes on the other hand. Interestingly, isocitrate dehydrogenase 1 (IDH1) and, to a lesser extent, IDH2 are mutated in more than 80% of low-grade astrocytomas and secondary glioblastomas. IDH1 mutation is an early event in gliomagenesis, possibly inducing subsequent oncogenic hits [13]. The mutation found in astrocytomas is a gain-of-function that confers a neomorphic activity to IDH1 [14]. IDH1 catalyses the conversion of alpha-ketoglutarate to 2-hydroxyglutarate, which inhibits the DNA-demethylating enzyme TET2, leading to a hypermethylation of the DNA. Because the expression of DIAPH3 could be controlled by methylation of its promoter, we will analyse the correlation between IDH1 mutation/expression and that of DIAPH3 in human astrocytoma samples.

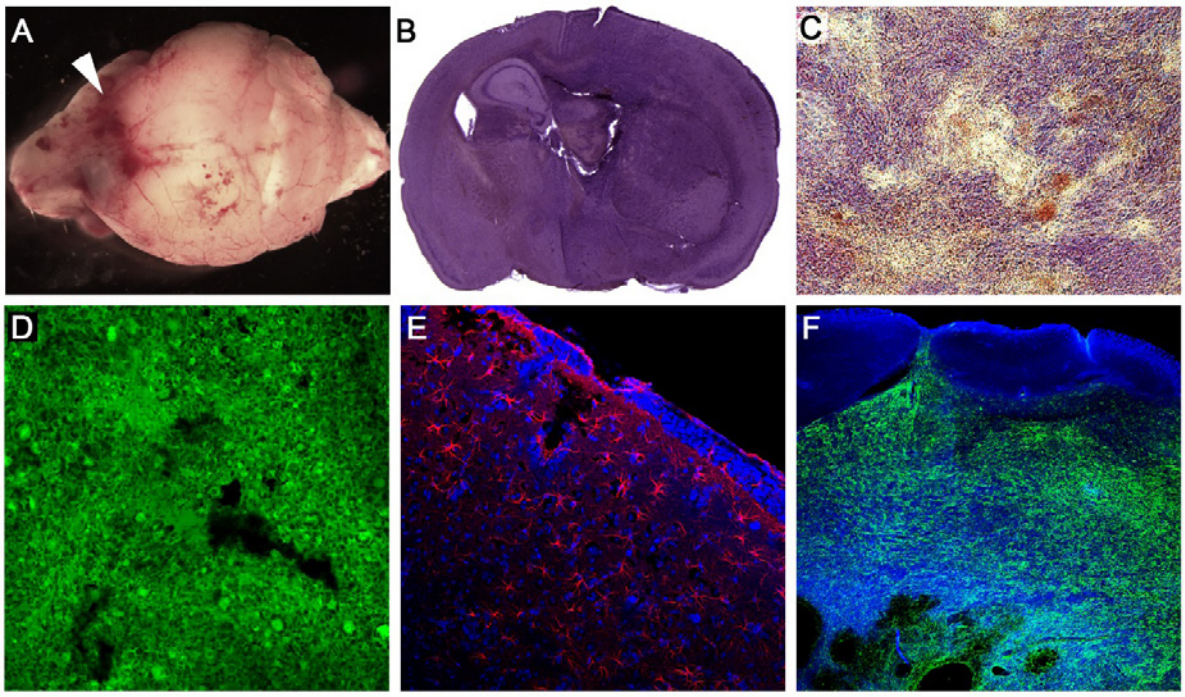

Figure 7: Diaph3/p53Em1-Cre: a mouse model to study glioblastoma. A: Dissected/unfixed brain of a Diaph3/p53Em1-Cre mouse exhibiting a metastatic brain tumour (arrowhead). B: Haematoxylin-eosin staining of a coronal section at the level the forebrain depicting the progression of the tumour in the right hemisphere. Note the absence of key structures as the hippocampus and internal capsule in this hemisphere. C: Haematoxylin-eosin staining of a tumour section. Typical features of glioblastoma like haemorrhages, and tumour cells surrounding necrotic zones are observed. D-F: Brain sections stained with CD44 (D, green), GFAP (E, red), and Vimentin (F, green) antibodies. Immunoreactivity is seen in the tumour tissue. Note the absence of reactive astrogliosis and Vimentin immunoreactivity in the "healthy" cortical tissue illustrated by the DAPI (blue) counterstain only.

6. References

1. Hager, M. H. *et al.* DIAPH3 governs the cellular transition to the amoeboid tumour phenotype. *EMBO Mol Med* **4**, 743-760, doi:10.1002/emmm.201200242 (2012).
2. Morley, S. *et al.* Regulation of microtubule dynamics by DIAPH3 influences amoeboid tumor cell mechanics and sensitivity to taxanes. *Scientific reports* **5**, 12136, doi:10.1038/srep12136 (2015).
3. Dai, W. *et al.* Slippage of Mitotic Arrest and Enhanced Tumor Development in Mice with BubR1 Haploinsufficiency. *Cancer Research* **64**, 440-445, doi:10.1158/0008-5472.can-03-3119 (2004).
4. Baker, D. J. *et al.* BubR1 insufficiency causes early onset of aging-associated phenotypes and infertility in mice. *Nat Genet* **36**, 744-749, doi:10.1038/ng1382 (2004).
5. Matsuura, S. *et al.* Monoallelic BUB1B mutations and defective mitotic-spindle checkpoint in seven families with premature chromatid separation (PCS) syndrome. *American Journal of Medical Genetics Part A* **140A**, 358-367, doi:10.1002/ajmg.a.31069 (2006).
6. Miyamoto, T. *et al.* Insufficiency of BUBR1, a mitotic spindle checkpoint regulator, causes impaired ciliogenesis in vertebrates. *Hum Mol Genet* **20**, 2058-2070, doi:10.1093/hmg/ddr090 (2011).
7. Vorstman, J. A. *et al.* A double hit implicates DIAPH3 as an autism risk gene. *Mol Psychiatry* **16**, 442-451, doi:10.1038/mp.2010.26 (2011).
8. Taylor, B. S. *et al.* Integrative genomic profiling of human prostate cancer. *Cancer Cell* **18**, 11-22, doi:10.1016/j.ccr.2010.05.026 (2010).
9. Butowski, N. A., Sneed, P. K. & Chang, S. M. Diagnosis and treatment of recurrent high-grade astrocytoma. *J Clin Oncol* **24**, 1273-1280, doi:10.1200/JCO.2005.04.7522 (2006).
10. Shioyama, T., Muragaki, Y., Maruyama, T., Komori, T. & Iseki, H. Intraoperative flow cytometry analysis of glioma tissue for rapid determination of tumor presence and its histopathological grade: clinical article. *J Neurosurg* **118**, 1232-1238, doi:10.3171/2013.1.JNS12681 (2013).
11. Lewis, K. M. & Petritsch, C. Asymmetric Cell Division: Implications for Glioma Development and Treatment. *Transl Neurosci* **4**, 484-503, doi:10.2478/s13380-013-0148-8 (2013).
12. Berger, F., Gay, E., Pelletier, L., Tropel, P. & Wion, D. Development of gliomas: potential role of asymmetrical cell division of neural stem cells. *Lancet Oncol* **5**, 511-514, doi:10.1016/S1470-2045(04)01531-1 (2004).
13. Watanabe, T., Nobusawa, S., Kleihues, P. & Ohgaki, H. IDH1 mutations are early events in the development of astrocytomas and oligodendrogliomas. *Am J Pathol* **174**, 1149-1153, doi:10.2353/ajpath.2009.080958 (2009).
14. Liu, A., Hou, C., Chen, H., Zong, X. & Zong, P. Genetics and Epigenetics of Glioblastoma: Applications and Overall Incidence of IDH1 Mutation. *Front Oncol* **6**, 16, doi:10.3389/fonc.2016.00016 (2016).

Geneeskundige Stichting Koningin Elisabeth
Fondation Médicale Reine Elisabeth
Königin-Elisabeth-Stiftung für Medizin
Queen Elisabeth Medical Foundation

Progress report of the research group of

Prof. dr. Vandenberghe Wim, MD. PhD

Katholieke Universiteit Leuven (KU Leuven)

Principal investigator

Prof. dr. Vandenberghe Wim, MD. PhD
University Hospitals Leuven, Department of Neurology
KU Leuven, Department of Neurosciences
Herestraat 49
3000 Leuven
Belgium
Tel.: +32 16 34 42 80
Email: wim.vandenberghe@uzleuven.be

LRRK2, Rab10 and mitochondrial quality control in Parkinsons's disease

1. Background

Approximately 5 % of cases of Parkinson's disease (PD) have a mendelian cause. *LRRK2* mutations are by far the most common monogenic cause of PD, accounting for ~10 % of autosomal dominant familial cases. In addition, genome-wide association studies (GWAS) identified polymorphisms in the *LRRK2* locus as a risk factor for sporadic PD [1]. *LRRK2* encodes an enzyme with a kinase domain and a GTPase domain. Rab10 and several related members of the Rab family have been identified as physiological substrates of the LRRK2 kinase [2]. The Rab family comprises ~70 small GTPases that cycle between an inactive GDP-bound and an active GTP-bound state as well as between the cytosol and membranes [3]. Rabs regulate vesicle formation, trafficking and fusion [3]. In animal models PD-causing *LRRK2* mutations increase phosphorylation of Rab10, which may disturb its membrane-cytosol equilibrium [2]. How this leads to neurodegeneration, is unknown.

Accumulating evidence implicates impairment of mitophagy as a pathogenic mechanism in PD [4]. Mitophagy is a form of selective autophagy in which damaged mitochondria are specifically labeled with ubiquitin and taken up by autophagosomes for degradation in lysosomes [4]. The E3 ubiquitin ligase parkin and the mitochondrial kinase PINK1, both encoded by genes linked to autosomal recessive PD, are critically involved in mitophagy [4]. PINK1 accumulates on damaged mitochondria and phosphorylates both parkin and ubiquitin, hereby activating parkin [4]. Parkin-mediated ubiquitination of outer mitochondrial membrane (OMM) proteins in combination with PINK1-mediated ubiquitin phosphorylation triggers recruitment of autophagy receptors, such as optineurin (OPTN), that tether ubiquitinated mitochondria to LC3 on nascent autophagosomes [5,6]. PD-linked loss-of-function mutations in the parkin or PINK1 genes disrupt mitophagy, leading to deficient mitochondrial quality control, accumulation of dysfunctional mitochondria, oxidative stress and apoptosis [4,7].

As described in my previous Activity report (2017), my lab recently discovered that mitophagy is not only disrupted in fibroblasts from parkin- and PINK1-deficient PD patients, but also in fibroblasts from PD patients with the 2 most common clinical *LRRK2* mutations (G2019S and R1441C). By contrast, non-selective, ubiquitin-independent autophagy induced by amino acid starvation was preserved in the *LRRK2* mutant cells. In wild-type cells the LRRK2 substrate Rab10 accumulated on depolarized mitochondria in a PINK1/parkin-dependent fashion, where it colocalized with the autophagy receptor optineurin and facilitated mitophagy. In *LRRK2* mutant cells accumulation of Rab10 on depolarized mitochondria, optineurin recruitment, mitophagy and mitochondrial function were all impaired. These defects were rescued by pharmacological inhibitors of the LRRK2 kinase and by *LRRK2* knockdown.

2. Aim of the project

The aim of this project is to elucidate the mechanisms by which PD-linked *LRRK2* mutations disturb mitophagy.

3. New findings in 2018

In 2018 we made important progress to further unravel the role of Rab10 in mitophagy and the mechanisms by which *LRRK2* mutations disrupt this, as described below.

3.1. Further validation of the mitophagy defect of LRRK2 mutant fibroblasts

In our previous experiments, we demonstrated the mitophagy defect of *LRRK2* mutant fibroblasts using the classical mitophagy inducer valinomycin, a K^+ ionophore. To further validate the mitophagy defect of the *LRRK2* mutant fibroblasts, we also induced mitophagy with the protonophore CCCP and with a combination of the ATP synthase inhibitor oligomycin and the complex III inhibitor antimycin A [6]. Both treatments induced mitophagy in wild-type fibroblasts but much less so in the G2019S and R1441C mutant cells (not shown). Thus, we observed a similar mitophagy defect in the *LRRK2* mutant cells with valinomycin, CCCP and oligomycin/antimycin A.

3.2. LRRK2 mutations enhance Rab10 phosphorylation in human cells

We were able to demonstrate, for the first time, that *LRRK2* mutations enhance Rab10 phosphorylation in human cells. Previously, it was shown in animal models that wild-type LRRK2 phosphorylates Rab10 on residue T73 and that the G2019S and R1441C mutations further enhance Rab10 phosphorylation [2]. Using a novel monoclonal antibody against Rab10 phosphorylated at T73 [8] we detected endogenous T73-phosphorylated Rab10 in control human fibroblasts (Fig. 1A). The phospho-Rab10 signal was dissipated after treatment with the LRRK2 kinase inhibitors PF-06447475 and MLi-2, confirming the specificity of the antibody (Fig. 1A,B). Importantly, the ratio of endogenous T73-phosphorylated Rab10 over endogenous total Rab10 was significantly higher in the G2019S and R1441C mutant patient fibroblasts than in controls, consistent with increased kinase activity of the mutant protein (Fig. 1A,B).

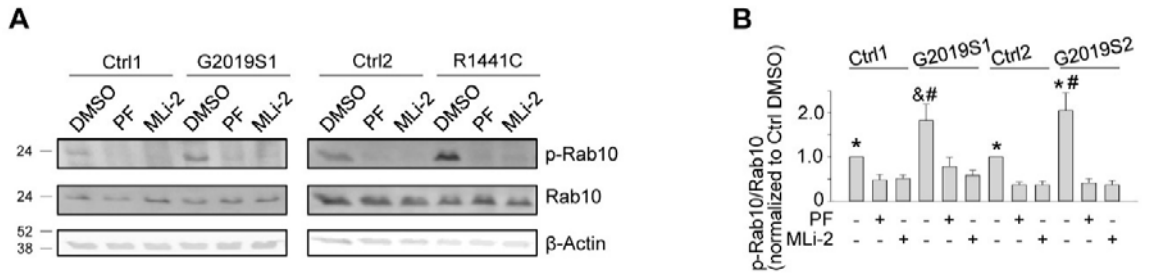

Fig. 1. Rab10 phosphorylation at T73 is enhanced in fibroblasts from PD patients with *LRRK2* mutations. Untransfected fibroblasts were treated with DMSO or the LRRK2 kinase inhibitors PF-06447475 (0.5 μM) or MLi-2 (150 nM) for 24 h. (A) Western for endogenous Rab10 phosphorylated at T73 (p-Rab10), total Rab10 and β-actin. (B) Quantification of p-Rab10/total Rab10 (n = 5-7). *P < 0.005 and &P < 0.05 compared to all other conditions in the same subject. #P < 0.05 compared to DMSO in the corresponding control subject.

3.3. Accumulation of Rab10 on depolarized mitochondria is dependent on its 2 C-terminal cysteine residues

Membrane association of Rab proteins is ensured by posttranslational modification of C-terminal cysteine residues with lipophilic geranylgeranyl groups that act as hydrophobic membrane anchors [3]. To assess the role of C-terminal geranylgeranylation in Rab10 recruitment to mitochondria, we deleted the 2 C-terminal cysteine residues of Rab10 (C199 and C200). This ΔCC Rab10 construct accumulated substantially less on depolarized mitochondria than full-length Rab10 (Fig. 2) despite similar expression levels (not shown), suggesting that C-terminal prenylation is important for Rab10 recruitment to mitochondria. Interestingly, overexpression of ΔCC Rab10 did not rescue mitochondrial recruitment of OPTN in the *LRRK2* mutant fibroblasts, in contrast to wild-type Rab10 overexpression (not shown). Thus, rescue of mitochondrial OPTN recruitment in *LRRK2* mutant cells required Rab10 that was capable of being tethered to the membrane via its C-terminal lipid anchor.

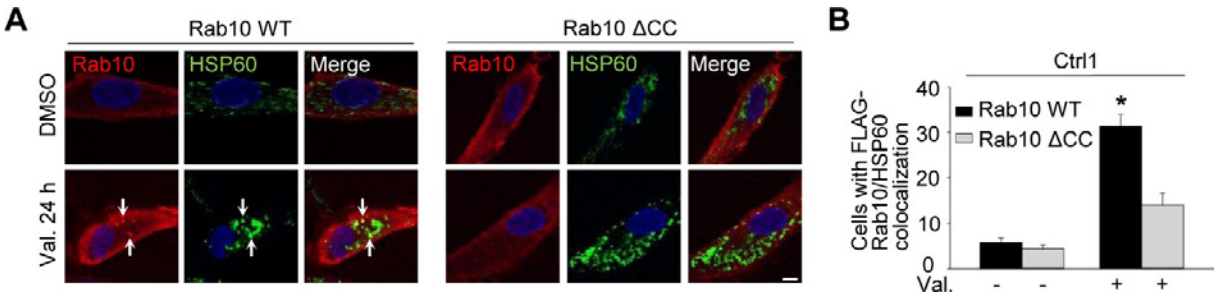

Fig. 2. Accumulation of Rab10 on depolarized mitochondria depends on C-terminal cysteine residues. Control (Ctrl1) fibroblasts were transfected with FLAG-tagged wild-type (WT) or ΔCC Rab10 WT. After 24 h cells were treated with DMSO or the mitochondrial depolarizing agent valinomycin (Val., 1 μM) for 24 h and immunostained for FLAG and the mitochondrial matrix marker HSP60. Nuclei were stained with TOTO-3. *Arrows* in (A) indicate examples of Rab10 puncta that colocalize with mitochondria. (B) Quantification of the percentage of cells with colocalization of FLAG-Rab10 and HSP60 (n = 4). *P < 0.001 compared with all other conditions. Scale bars, 10 μm.

3.4. Rab10 interacts with OPTN

The colocalization of Rab10 and OPTN on depolarized mitochondria and the facilitating effect of Rab10 on mitochondrial recruitment of OPTN suggested that the two proteins might physically interact. We expressed FLAG-tagged Rab10 in control fibroblasts and found that it co-immunoprecipitated with endogenous OPTN (Fig. 3A).

The interaction between Rab10 and OPTN already occurred in basal conditions and only marginally increased after mitochondrial depolarization (not shown), suggesting that a pre-existing Rab10/OPTN complex is recruited to depolarized mitochondria.

3.5. RAB10 interaction with OPTN is impaired in patients with LRRK2 mutations

To assess the effect of LRRK2-dependent Rab10 phosphorylation on the Rab10-OPTN interaction, we performed parallel COIP experiments in wild-type, G2019S mutant and R1441C mutant fibroblasts (Fig. 3B,C). Significantly less OPTN co-immunoprecipitated with Rab10 in the G2019S and R1441C mutant cells than in control cells (Fig. 3B,C). In G2019S and R1441C fibroblasts, the amount of OPTN co-immunoprecipitated with FLAG-Rab10, normalized to the amount of OPTN present in the input, was 35.8 ± 10.4 % (n = 3; P = 0.004) and 32.6 ± 4.9 % (n = 3; P < 0.001), respectively, of the values in control cells. The interaction increased after treatment with the LRRK2 kinase inhibitor MLi-2 (Fig. 3B), consistent with the conclusion that T73 phosphorylation of Rab10 impairs the interaction with OPTN.

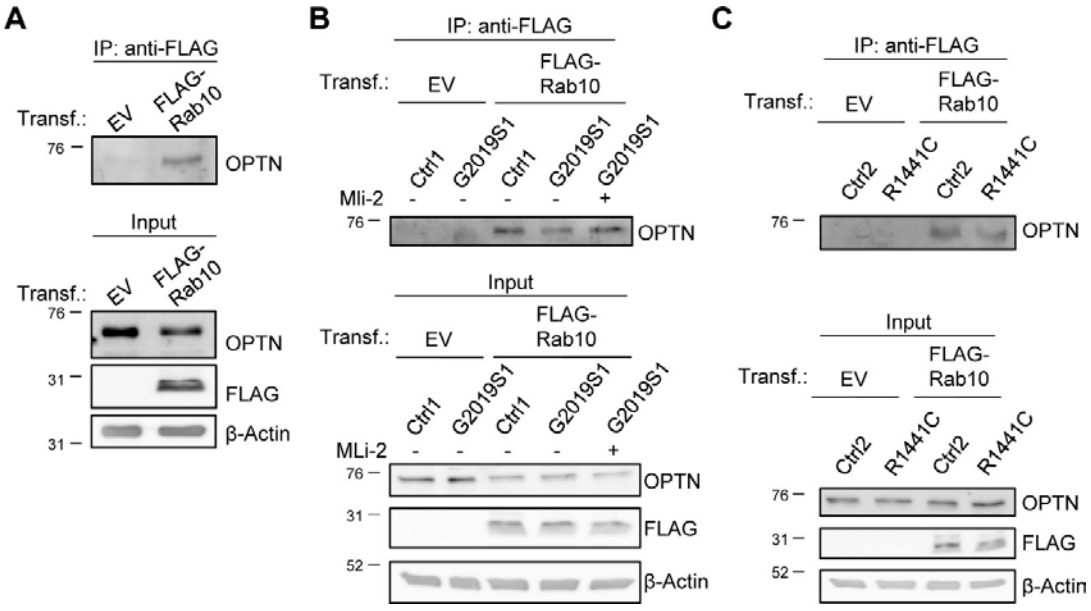

Fig. 3. Interaction of Rab10 with OPTN is impaired by *LRRK2* mutations. (A) Control fibroblasts were transfected (Transf.) with empty vector (EV) or FLAG-tagged Rab10, as indicated. After coimmunoprecipitation (COIP) with anti-FLAG beads, the immunoprecipitate (IP) and input samples were analyzed by SDS-PAGE and western using the indicated antibodies. (B, C) Control (Ctrl1, Ctrl 2), G2019S fibroblasts and R1441C fibroblasts were transfected with EV or FLAG-tagged Rab10. In (B) cells were treated or not with the LRRK2 kinase inhibitor MLi-2 (150 nM) for 24 h. After COIP with anti-FLAG beads, the IP and input samples were analyzed by SDS-PAGE and western

To further test whether T73 phosphorylation of RAB10 impedes its interaction with OPTN, its translocation to depolarized mitochondria and mitophagy, we generated a phosphomimetic T73E mutant version of RAB10. Expression levels of transfected wild-type and T73E FLAG-tagged RAB10 were similar in control and *LRRK2* mutant fibroblasts (Fig. 4A). COIP experiments in control fibroblasts showed that T73E RAB10 indeed interacted less well with OPTN than wild-type RAB10 (Fig. 4B). The amount of OPTN that was co-immunoprecipitated with T73E RAB10, divided by the amount of OPTN in the input, was 38.5 ± 6.7 % (n = 7; P < 0.001) of the value after COIP of OPTN with wild-type RAB10.

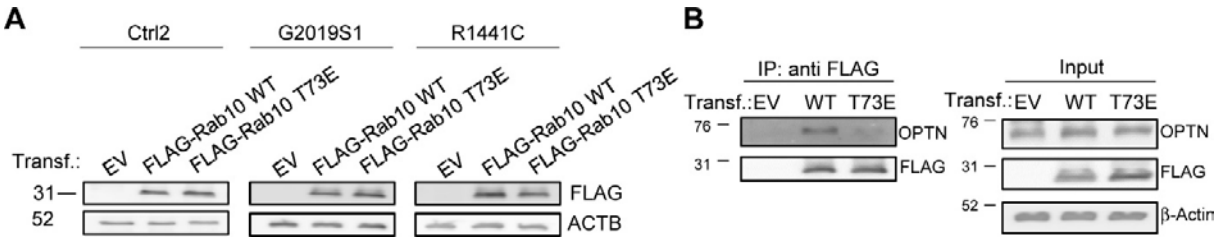

Fig. 4. Phosphomimetic T73E Rab10 binds less with OPTN. (A) Western blot for FLAG and β-Actin in control (Ctrl2) and *LRRK2* (G2019S1 and R1441C) mutant fibroblasts transfected with empty vector (EV), FLAG-tagged wild-type (WT) Rab10 or FLAG-tagged Rab10 with a phosphomimetic (T73E) mutation. (B) Control (Ctrl1) fibroblasts were transfected with EV, FLAG-tagged WT or T73E Rab10, as indicated. After COIP with anti-FLAG beads, the IP and input samples were analyzed by SDS-PAGE and western.

Moreover, the T73E mutation impaired Rab10 translocation to depolarized mitochondria (Fig. 5A,B). Finally, overexpression of T73E RAB10 failed to rescue valinomycin-induced mitophagy in G2019S and R1441C mutant cells, in contrast to overexpression of wild-type RAB10 (Fig. 5C-F).

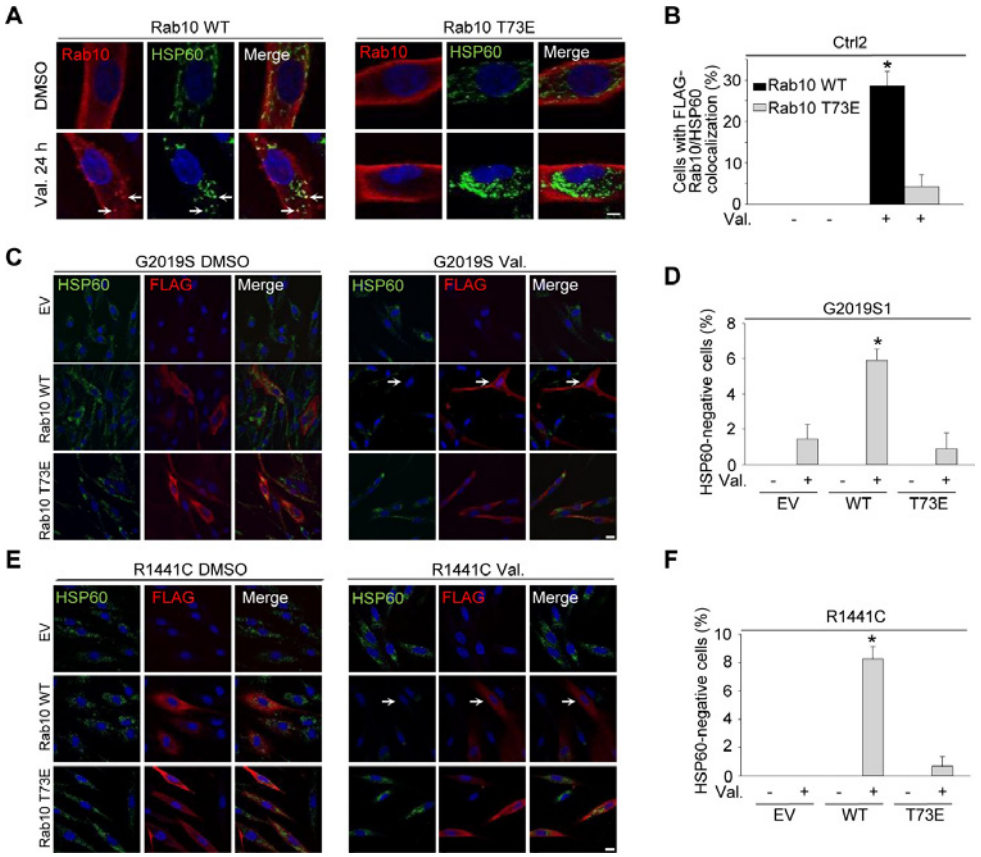

Fig. 5. Phosphomimetic T73E Rab10 accumulates less on depolarized mitochondria, and fails to rescue the mitophagy deficit of *LRRK2* mutant cells. (A,B) Control (Ctrl2) fibroblasts were transfected with FLAG-tagged wild-type (WT) or T73E Rab10 and treated with DMSO or valinomycin (Val., 1 μM) for 24 h. Fibroblasts were immunostained for FLAG and the mitochondrial matrix protein HSP60. Nuclei were stained with TOTO-3 (blue). *Arrows* in (A) indicate puncta with FLAG-Rab10/HSP60 colocalization. (B) Quantification of the percentage of FLAG-positive cells with FLAG/HSP60 colocalization (n = 3). * P < 0.005 compared with all other conditions. (C-F) G2019S1 and R1441C fibroblasts were transfected with empty vector (EV), FLAG-tagged WT or T73E Rab10 and treated with DMSO or Val. (1 μM) for 48 h, followed by immunostaining for FLAG and HSP60. *Arrows* in (C) and (E) indicate cells without detectable HSP60. (D,F) Quantification of the percentage FLAG-positive cells with no detectable HSP60 (n = 3-8). * P < 0.005 compared with all other conditions.

3.6. Conclusion

Based on these data we can depict a model in which a subpopulation of OPTN forms a complex with RAB10 in basal conditions in wild-type cells (Fig. 6). This complex translocates to mitochondria after mitochondrial depolarization. Optimal accumulation of OPTN on mitochondria requires both binding to mitochondrial ubiquitin chains and interaction with RAB10 that is capable of insertion into the membrane via its C-terminal lipid anchor. In *LRRK2* mutant cells, enhanced T73 phosphorylation of RAB10 impairs the interaction with OPTN. Some recruitment of OPTN to mitochondria is still possible (e.g. via binding of OPTN to ubiquitin), but accumulation of OPTN on mitochondria is reduced because the interaction with membrane-inserted RAB10 is lacking (Fig. 6).

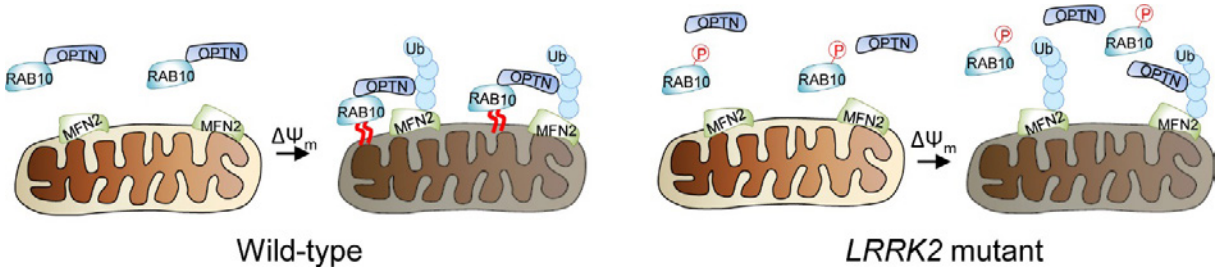

Fig. 6. Model of the role of Rab10 in mitophagy. Ub, ubiquitin. P, phosphate. $\Delta\Psi_m$, mitochondrial depolarization. Red curved lines indicate C-terminal geranylgeranyl groups.

These results suggest that the pathogenic effects of PD-causing *LRRK2*, *PARK2* and *PINK1* mutations converge on a common pathway.

A manuscript describing these findings was recently submitted for publication [9].

4. Further plans

4.1. Identification of binding partners of Rab10 in the mitophagy pathway

To identify potential novel binding partners of Rab10 that may be relevant for its association with depolarized mitochondria and mitophagy we are using a proteomics approach in collaboration with Prof. Rita Derua (Laboratory of Protein Phosphorylation and Proteomics, KU Leuven). We transiently expressed FLAG-tagged Rab10 in control fibroblasts and treated them either with valinomycin or with DMSO. FLAG-Rab10 and its binding partners were immunoprecipitated with anti-FLAG beads, followed by elution of bound proteins with free FLAG peptides. Mass spectrometric identification of the eluted proteins is currently ongoing. The abundance of identified interactors will be normalized to the abundance of eluted Rab10 in each condition. We are particularly interested in proteins that show enhanced interaction with Rab10 after mitochondrial depolarization. Newly identified interactions will be verified by coimmunoprecipitation. We will use our well-established mitophagy assays and cell biological approaches to explore the roles of the newly identified, validated Rab10 binding partners in mitophagy.

4.2. Validation of key findings from the fibroblast studies in human dopaminergic neurons

We will determine whether human dopaminergic (DA) neurons with PD-causing *LRRK2* mutations also have a mitophagy defect. In collaboration with the group of Prof. C. Verfaillie (Stem Cell Institute, KU Leuven), we successfully reprogrammed fibroblasts from two PD patients with the G2019S LRRK2 mutation and one PD patient with the R1441C LRRK2 mutation to iPSCs via Sendai virus overexpression of pluripotency-related transcription factors. These iPSCs have undergone state-of-the-art quality controls: SNP analysis to confirm genomic identity with the initial fibroblasts, analysis of expression of self-renewal genes and trilineage differentiation potential (Scorecard), detection of pluripotency markers with qPCR and immunostaining, and array comparative genomic hybridization to exclude chromosomal defects. Moreover, we successfully used CRISPR/Cas9 paired nickases to correct the point mutations

in *LRRK2* and create three isogenic control iPSC lines. The selection cassettes were excised using piggyback transposase to ensure that the isogenic control lines differ from the respective patient iPSC lines exclusively at the *LRRK2* locus. The isogenic lines underwent the same rigorous quality control as the parental lines.

We also optimized methods to differentiate iPSCs to DA neurons. In our hands the protocol of Kriks et al. [10] yields cultures in which more than 50 % of cells are DA neurons based on staining for the marker tyrosine hydroxylase. The cells also express other midbrain DA neuron markers such as LMX1A or FOXA2. Functionality of iPSC-derived DA neurons has already been confirmed via electrophysiological recording.

We will differentiate the G2019S and R1441C mutant iPSCs as well the isogenic control iPSCs to DA neurons. We will compare mitophagy between the control and *LRRK2* mutant neurons using mito-Keima imaging [7,11]. We already successfully transduced iPSCs with mito-Keima using a lentiviral vector. After differentiation of the transduced iPSC lines to DA neurons, we will quantify mitophagic flux both in basal conditions and after mitochondrial depolarization, and compare this between the *LRRK2* mutant DA neurons and the controls in a blinded fashion. If mitophagy is defective in the *LRRK2* mutant neurons, we will determine whether this is due to the same mechanisms as in fibroblasts (cfr. supra). For example, we will transduce FLAG-Rab10 into the neurons and assess Rab10 translocation after mitochondrial depolarization in wild-type and *LRRK2* mutant neurons.

5. References

1. Corti O et al. (2011) What genetics tells us about the causes and mechanisms of Parkinson's disease. *Physiol Rev* 91:1161-1218.
2. Steger M et al. (2016) Phosphoproteomics reveals that Parkinson's disease kinase LRRK2 regulates a subset of Rab GTPases. *eLife* 5:e12813.
3. Zhen Y, Stenmark H (2015) Cellular functions of Rab GTPases at a glance. *J Cell Sci* 128:3171-3176.
4. Pickrell AM et al. (2015) The roles of PINK1, Parkin and mitochondrial fidelity in Parkinson's disease. *Neuron* 85:257-73.
5. Wong YC, Holzbaur EL (2014) Optineurin is an autophagy receptor for damaged mitochondria in parkin-mediated mitophagy that is disrupted by an ALS-linked mutation. *Proc Natl Acad Sci USA* 111:E4439-4448.
6. Lazarou M et al. (2015) The ubiquitin kinase PINK1 recruits autophagy receptors to induce mitophagy. *Nature* 524:309-314.
7. Cornelissen T et al. (2018) Deficiency of parkin and PINK1 impairs age-dependent mitophagy in *Drosophila*. *eLife* 7:e35878.
8. Lis P et al. (2018) Development of phosphor-specific Rab protein antibodies to monitor in vivo activity of the LRRK2 Parkinson's disease kinase. *Biochem J* 475:1-22.
9. Wauters F*, Cornelissen T.* et al. *LRRK2* mutations impair depolarization-induced mitophagy through inhibition of mitochondrial translocation of Rab10. *Under review.* *Equal contribution.
10. Kriks S et al. (2011) Dopamine neurons derived from human ES cells efficiently engraft in animal models of Parkinson's disease. *Nature* 480:547-551.
11. Katayama H et al. (2011) A sensitive and quantitative technique for detecting autophagic events based on lysosomal delivery. *Chem Biol* 18:1042-52.

6. Publications in 2017-2018 by W. Vandenberghe on topics related to this proposal (Parkinson's disease)

1. Cornelissen T, Verstreken P, **Vandenberghe W** (2018) Imaging mitophagy in the fruit fly. *Autophagy* 14:1656-1657. Impact factor: 11,1. Times cited: 0.
2. Tinkhauser G, Torrecillos F, Duclos Y, Tan H, Pogosyan A, Fischer P, Carron R, Welter ML, Karachi C, **Vandenberghe W**, Nuttin B, Witjas T, Régis J, Azulay JP, Eusebio A, Brown P (2018) Beta burst coupling across the motor circuit in Parkinson's disease. *Neurobiol Dis* 117:217-225. Impact factor: 5,2. Times cited: 1.
3. Cornelissen T, Vilain S, Vints K, Gounko N, Verstreken P, **Vandenberghe W** (2018) Deficiency of parkin and PINK1 impairs age-dependent mitophagy in *Drosophila*. *Elife* pii: e35878. doi: 10.7554/eLife.35878. Impact factor: 7,6. Times cited: 1.

4. Nackaerts E, Michely J, Heremans E, Swinnen SP, Smits-Engelsman BCM, **Vandenberghe W**, Grefkes C, Nieuwboer A (2018) Training for Micrographia Alters Neural Connectivity in Parkinson's Disease. *Front Neurosci* 12:3. Impact factor: 3,9. Times cited: 0.
5. Nackaerts E, Michely J, Heremans E, Swinnen S, Smits-Engelsman B, **Vandenberghe W**, Grefkes C, Nieuwboer A (2018) Being on Target: Visual Information during Writing Affects Effective Connectivity in Parkinson's Disease. *Neuroscience* 371:484-494. Impact factor: 3,4. Times cited: 2.
6. Nackaerts E, Nieuwboer A, Broeder S, Swinnen S, **Vandenberghe W**, Heremans E (2018) Altered effective connectivity contributes to micrographia in patients with Parkinson's disease and freezing of gait. *J Neurol* 265:336-347. Impact factor: 3,8. Times cited: 0.
7. Nackaerts E, Broeder S, Pereira MP, Swinnen SP, **Vandenberghe W**, Nieuwboer A, Heremans E (2017) Handwriting training in Parkinson's disease: A trade-off between size, speed and fluency. *PLoS One* 12:e0190223. Impact factor: 2,8. Times cited: 0.
8. Desmet AS, Cirillo C, Tack J, **Vandenberghe W***, Vanden Berghe P* (2017) Live calcium and mitochondrial imaging in the enteric nervous system of Parkinson patients and controls. *Elife* pii: e26850. * Equal contribution. Impact factor: 7,6. Times cited: 4.
9. Strouwen C, Molenaar EA, Münks L, Keus SH, Zijlmans JC, **Vandenberghe W**, Bloem BR, Nieuwboer A (2017) Training dual tasks together or apart in Parkinson's disease: results from the DUALITY trial. *Mov Disord* 32:1201-1210. Impact factor: 8,3. Times cited: 9.
10. Koole M, Van Laere K, Ahmad R, Ceccarini J, Bormans G, **Vandenberghe W** (2017) Brain PET imaging of phosphodiesterase 10A in progressive supranuclear palsy and Parkinson's disease. *Mov Disord* 32:943-945. Impact factor: 8,3. Times cited: 0.
11. Nackaerts E, Heremans E, Smits-Engelsman BC, Broeder S, **Vandenberghe W**, Bergmans B, Nieuwboer A (2017) Validity and reliability of a new tool to evaluate handwriting difficulties in Parkinson's disease. *PLoS One* 12:e0173157. Impact factor: 2,8. Times cited: 3.

7. Use of the GSKE grant in 2018

Personnel cost:

22290 € Salary of postdoc Tom Cornelissen for 3 months (Oct-Dec 2018)

Consumables:

7710 € Reagents for cell culture, molecular biology (e.g. generation of isogenic control iPSC lines), antibodies…

Geneeskundige Stichting Koningin Elisabeth
Fondation Médicale Reine Elisabeth
Königin-Elisabeth-Stiftung für Medizin
Queen Elisabeth Medical Foundation

Progress report of the research group of

Prof. dr. Vangheluwe Peter, PhD

Katholieke Universiteit Leuven (KU Leuven)

Principal investigator

Prof. dr. Vangheluwe Peter, PhD
Laboratory of Cellular Transport Systems (LCTS)
Department Cellular & Molecular Medicine
Faculty of Medicine, KU Leuven
Campus Gasthuisberg, ON1 box 802
Herestraat 49
B-3000 Leuven
Belgium
Tel.: +32 16 33 07 20
Fax: +32 16 34 59 9.
E-mail: Peter.Vangheluwe@kuleuven.be
gbiomed.kuleuven.be/english/research/50000618

Neuroprotection by lysosomal transport mechanisms in Parkinson's disease

1. Aims of the Project

Parkinson's disease (PD) is the second most common neurodegenerative disorder. The neurons in PD patients accumulate protein aggregates and impaired mitochondria, which contributes to cell death. In healthy neurons, endo-/lysosomal pathways provide protection by the efficient removal of damaged proteins and mitochondria, while in PD the endo-/lysosomal system is disturbed. Genetic evidence points to two novel lysosomal transport systems that are impaired in PD, which are the subject of this project: ATP13A2/PARK9 and ATP10B, a novel, candidate PD gene. Both ATP10B and ATP13A2 belong to the P-type ATPase family of active transporters.

The overall aim of the study is to unravel and compare the transport function and cellular implications of ATP13A2 and ATP10B in endo-/lysosomes, establish their role in PD onset and assess their value as therapeutic targets.

2. Progress report of ATP10B

2.1. Results

- Dr. C. Van Broeckhoven (University of Antwerp), an international leader in genetics of neurodegenerative disorders, identified recessive mutations in the *ATP10B* gene as a likely cause for early onset PD (EOPD). Besides a first set of disease mutations, recent additional screening revealed an extra series of disease associated mutations in ATP10B. These results are important to determine the allele frequency in the PD population and assess its risk.
- We successfully optimized biochemical and cellular methods to measure the activity of ATP10B WT and disease mutants. With these assays, we established ATP10B WT as a lipid flippase in the late endo-/lysosomal compartment and obtained convincing evidence for the loss of function nature of the disease mutations.
- We phenotypically analyzed cell lines to study ATP10B gain and loss of function and demonstrated that ATP10B provides cellular protection against environmental PD risk factors. We found connections between ATP10B and other, established PD pathways such as alpha-synuclein.
- We confirmed the protective phenotype of ATP10B in isolated mouse cortical neurons with ATP10B knockdown, which can be rescued by ATP10B expression.
- Our study shows that ATP10B modulators may be of therapeutic interest. With our established biochemical and cellular assays, we're preparing for a high throughput screening to identify ATP10B modulators, which occurs in collaboration with the Center for Drug Design and Discovery (CD3). Assay optimization is taking place.
- We filed a patent with Dr. C. Van Broeckhoven where we claim ATP10B as a novel PD gene. (www.google.com/patents/WO2016166373A1?cl=en)
- In 2018, we submitted a manuscript that reports ATP10B as a novel candidate PD gene. This important, high impact finding is currently in revision (completion is estimated in March 2019):
  Shaun Martin#, Aline Verstraeten#, Chris Van den Haute, Bavo Heeman, Igor Beletchi, Stefanie Smolders, Sarah van Veen, David Crosiers, Géraldine Gelders, Norin Hamouda, Sebastiaan Engelborghs, Jean-Jacques Martin, Jan Eggermont, Peter P De Deyn, Patrick Cras, Veerle Baekelandt, **Peter Vangheluwe***, Christine Van Broeckhoven* Familial early-onset Parkinson's disease caused by ATP10B mutations.
  # shared first authorship; *** shared last authorship and corresponding authorship.**

2.2. Ongoing work and perspectives

A new series of disease associated mutations was discovered by genetic screening in PD and other related neurodegenerative disorders. We will determine the functional impact of the disease mutations to firmly establish the causative nature of the mutations. This will become a very important follow-up study of the project, providing new disease links, but will require a substantial investment in time and money.

We're exploring the valorization potential of ATP10B in neurodegeneration in collaboration with CD3 and industrial partners.

3. Progress report of ATP13A2

3.1. Results

- Towards the mechanism of ATP13A2 activation, we identified the important regions in ATP13A2 that are involved in the auto-inhibition mechanism. We also found the position of post-translational modifications that control this process. We're currently working towards a publication of these findings.
- With our established biochemical assays, we screened for possible candidate substrates of ATP13A2 using purified human ATP13A2 protein. Candidate substrates were further analyzed in transport assays, which provided conclusive evidence on the identity and transport direction of the substrate of ATP13A2.
- We established cell models of ATP13A2 overexpression, knockdown and also CRISPR/Cas9 mediated knockout. We further rescued the ATP13A2 KO by re-expressing ATP13A2 WT or disease mutants. We used these models to characterize the role of the transported substrate in the lysosomal phenotype, which is coupled to cell death. This provided us new insights in the disease pathway that ATP13A2 is involved in.
- At the end of 2018, we submitted a manuscript that reports the substrate identity of ATP13A2 and its role in lysosome dependent cell death. This novel, high impact finding has been submitted as a research paper, and we're currently waiting for the reviewer's comments:
  Deficient lysosomal substrate transport is at the heart of Kufor-Rakeb syndrome and familial Parkinson's disease
  Sarah van Veen, Shaun Martin, Chris Van den Haute, Veronick Benoy, Joseph Lyons, Roeland Vanhoutte, Jan Pascal Kahler, Jean-Paul Decuypere, Johannes V. Swinnen, Wim Annaert, Patrizia Agostinis, Bart Ghesquière, Steven Verhelst, Veerle Baekelandt, Jan Eggermont, **Peter Vangheluwe* (*last and corresponding authorship).**
- We obtained strong data demonstrating that ATP13A2 protects against mitochondrial stress by controlling the levels of reactive oxygen species. We're currently linking these findings with the transported substrate of ATP13A2 and a manuscript on the mitochondrial phenotype is currently in preparation (Martin S, et al.).

3.2. Ongoing work and perspectives

- In the next step of the ATP13A2 project, we want to invest in more advanced cell models, such as isolated mouse neurons or human re-differentiated dopaminergic neurons. This will require a substantial investment in time and money. We will start from patient derived fibroblasts carrying ATP13A2 loss of function mutations to generate IPSCs and re-differentiated dopaminergic neurons.

4. Publications and Activities (2017-2018)

4.1. 2017

4.1.1. Activities

On November 23rd 2017, Princess Astrid visited the Laboratory of Cellular Transport Systems of Prof. Dr. Peter Vangheluwe and the Laboratory of Ion Channel Research of Prof. Dr. Thomas Voets in the Department of Cellular and Molecular Medicine, KU Leuven. This event has been covered by the press to inform the broad public about our research activities:
http://www.robtv.be/nieuws/leuven/prinses-astrid-bezoekt-laboratoria-ku-leuven;
http://www.nieuwsblad.be/cnt/dmf20171123_03203478;
https://www.hln.be/regio/leuven/prinses-astrid-bezoekt-gasthuisberg~aeaaf126/;
https://nieuws.kuleuven.be/nl/2017/prinses-astrid-bezoekt-leuvense-labos;
https://www.facebook.com/ROBtv.be/videos/10154952286531825/;
https://www.monarchie.be/nl/agenda/vib-center-for-brain-disease-research;
http://www.fmre-gske.be/pages/nl/bezoekKULeuven3.html

4.1.2. Patents

- Screening Methods and Pharmaceutically active compounds for neurodegenerative diseases; inventors: Peter Vangheluwe, Veerle Baekelandt, Patrizia Agostinis, Chris Van den Haute, Sarah van Veen, Shaun Martin, Jan Eggermont. Filing date: July 3rd 2017; ZL916077
- PCT/EP2016/058558: A novel gene in neurodegenerative disease; inventors: Christine Van Broeckhoven, Jessie Theuns, Aline Verstraeten, Bavo Heeman, Peter Vangheluwe, Filing date: April 18th 2016

4.1.3. Publications in 2017 (* directly related to the project)

- Estrada-Cuzcano A., Martin S., Chamova T., Synofzik M., Timmann D., Holemans T., Andreeva A., Reichbauer J., De Rycke R., Chang D., van Veen S., Samuel J., Schöls L., Pöppel T., Sorensen D., Asselbergh B., Klein C., Zuchner S., Jordanova A., **Vangheluwe P.#**, Tournev I.#, Schüle R.# (2017). Loss-of-function mutations in the ATP13A2/PARK9 gene cause complicated hereditary spastic paraplegia (SPG78). Brain, 140 (2), 287-305 (most recent IF: 10.29). **#, shared last authorship**
- Demirsoy S., Martin S., Motamedi s., van Veen S., Holemans T., Van den Haute C., Jordanova A., Baekelandt V., **Vangheluwe P.#**, Agostinis P.# (2017). ATP13A2/PARK9 regulates endo-/lysosomal cargo sorting and proteostasis through a novel PI(3,5)P2-mediated scaffolding function. Human Molecular Genetics, 26 (9), 1656-1669 (most recent IF: 5.34). **#, shared corresponding author**
- Martin S., Dudek-Peric A., Garg A., Roose H., Demirsoy S., Van Eygen S., Mertens F., **Vangheluwe P.,** Vankelecom H., Agostinis P. (2017). An autophagy-driven pathway of ATP secretion supports the aggressive phenotype of BRAF(V600E) inhibitor-resistant metastatic melanoma cells. Autophagy, 13 (9), 1512-1527 (most recent IF: 8.59).
- Tharkeshwar A., Trekker J., Vermeire W., Pauwels J., Sannerud R., Priestman D., Te Vruchte D., Vints K., Baatsen P., Decuypere J., Lu H., Martin S., **Vangheluwe P.**, Swinnen J., Lagae L., Impens F., Platt F., Gevaert K., Annaert W. (2017). A novel approach to analyze lysosomal dysfunctions through subcellular proteomics and lipidomics: the case of NPC1 deficiency. Scientific Reports, 7, 41408 (most recent IF: 4.26).
- Martin S, Dudek-Peric AM, Garg AD, Roose H, Demirsoy S, Mertens F, **Vangheluwe P,** Vankelecom H & Agostinis P. An autophagy-dependent ATP secretion potentiates migration and invasion of BRAF-inhibitor resistant melanoma cells. Autophagy 13 (9), 1512-1527 (most recent IF: 8.59).
- Chen J., De Raeymaecker J., Hovgaard J., Smaardijk S., Vandecaetsbeek I., Wuytack F., Møller J., Eggermont J., De Maeyer M., Christensen S., **Vangheluwe P.** (2017). Structure/activity Relationship of Thapsigargin Inhibition on the Purified Golgi/secretory Pathway Ca2+/Mn2+ Transport ATPase (SPCA1a). Journal of Biological Chemistry, 292 (17), 6938-6951(most recent IF: 4.13).
- Smaardijk S, Chen J, Wuytack F, **Vangheluwe P.** SPCA2 couples Ca2+ influx via Orai1 to Ca2+ uptake into the Golgi/secretory pathway. Tissue Cell. 2017 49(2 Pt A):141-149.
- Bittremieux M., Gerasimenko J., Schuermans M., Luyten T., Stapleton E., Alzayady K., De Smedt H., Yule D., Mikoshiba K., **Vangheluwe P.**, Gerasimenko O., Parys J., Bultynck G. (2017). DPB162-AE, an inhibitor of store-operated Ca2+ entry, can deplete the endoplasmic reticulum Ca2+ store. Cell Calcium, 62, 60-70 (most recent IF: 3.71).
- Danny Mollerup Sørensen*, Tine Holemans*, Sarah van Veen, Shaun Martin, Tugce Arslan, Ida Winther Haagendahl, Henrik Waldal Holen, Norin Hamouda, Jan Eggermont, Michael Palmgren, **Peter Vangheluwe**. Parkinson disease related ATP13A2 evolved early in animal evolution. Plos One. In revision.

4.2. 2018

4.2.2. Activities

Ernest Solvay prize, Queen Elisabeth Foundation (25,000€) - Prof. Dr. Peter Vangheluwe (KU Leuven) - Neuroprotection by lysosomal transport mechanisms in Parkinson's disease

- Award ceremony at the Palace, 26/04/2018
- https://gbiomed.kuleuven.be/english/research/50000618/spotlight/ernest-solvay-prijs-voor-prof-peter-vangheluwe-voor-zijn-onderzoek-neuroprotection-by-lysosomal-transport-mechanisms-in-parkinsons-disease-1
- Video interview and coverage of the research topic (by Reinout Goddyn)
- https://vimeo.com/266308386

4.2.2. Publications in 2018 (* directly related to the project)

- Bittremieux M, La Rovere RM, Schuermans M, Luyten T, Mikoshiba K, **Vangheluwe P**, Parys JB, Bultynck G. Extracellular and ER-stored Ca2+ contribute to BIRD-2-induced cell death in diffuse large B-cell lymphoma cells. Cell Death Discov. 2018 Nov 2;4:101. (no IF available yet for this new journal)
- Pessina F, Gamberucci A, Chen J, Liu B, **Vangheluwe P**, Gorelli B, Lorenzini S, Spiga O, Trezza A, Sgaragli G, Saponara S. Negative chronotropism, positive inotropism and lusitropism of 3,5-di-t-butyl-4-hydroxyanisole (DTBHA) on rat heart preparations occur through reduction of RyR2 Ca2+ leak. Biochem Pharmacol. 2018 Sep;155:434-443. (most recent IF: 4.235)
- Smaardijk S, Chen J, Kerselaers S, Voets T, Eggermont J, **Vangheluwe P**. Store-independent coupling between the Secretory Pathway Ca2+ transport ATPase SPCA1 and Orai1 in Golgi stress and Hailey-Hailey disease. Biochim Biophys Acta Mol Cell Res. 2018 Jun;1865(6):855-862. (most recent IF: 4.651)
- * Sørensen DM, Holemans T, van Veen S, Martin S, Arslan T, Haagendahl IW, Holen HW, Hamouda NN, Eggermont J, Palmgren M, **Vangheluwe P**. Parkinson disease related ATP13A2 evolved early in animal evolution. PLoS One. 2018 Mar 5;13(3):e0193228. (most recent IF: 3.057)
- Mikkelsen SA, **Vangheluwe P**, Andersen JP. A Darier disease mutation relieves kinetic constraints imposed by the tail of sarco(endo)plasmic reticulum Ca2+-ATPase 2b. J Biol Chem. 2018 Mar 16;293(11):3880-3889. (most recent IF: 4.010)
- Sitsel A, De Raeymaecker J, Drachmann ND, Derua R, Smaardijk S, Andersen JL, Vandecaetsbeek I, Chen J, De Maeyer M, Waelkens E, Olesen C, **Vangheluwe P***, Nissen P*. Structures of the heart specific SERCA2a Ca2+-ATPase. EMBO J in press **(*shared last and shared corresponding author)** (most recent IF: 10.557)

4.2.3. Publications in revision or in preparation (all related to the project)

- Shaun Martin#, Aline Verstraeten#, Chris Van den Haute, Bavo Heeman, Igor Beletchi, Stefanie Smolders, Sarah van Veen, David Crosiers, Géraldine Gelders, Norin Hamouda, Sebastiaan Engelborghs, Jean-Jacques Martin, Jan Eggermont, Peter P De Deyn, Patrick Cras, Veerle Baekelandt, **Peter Vangheluwe***, Christine Van Broeckhoven* Familial early-onset Parkinson's disease caused by ATP10B mutations. # shared first authorship; *** shared last authorship and corresponding authorship.**
- Sarah van Veen, Shaun Martin, Chris Van den Haute, Veronick Benoy, Joseph Lyons, Roeland Vanhoutte, Jan Pascal Kahler, Jean-Paul Decuypere, Johannes V. Swinnen, Wim Annaert, Patrizia Agostinis, Bart Ghesquière, Steven Verhelst, Veerle Baekelandt, Jan Eggermont, **Peter Vangheluwe*** Deficient lysosomal substrate transport is at the heart of Kufor-Rakeb syndrome and familial Parkinson's disease; ***last and corresponding authorship**
- Fieke Wauters, Tom Cornelissen, Shaun Martin, Brianada Koentjoro, Carolyn Sue , **Peter Vangheluwe**, Wim Vandenberghe. LRRK2 mutations impair mitophagy through inhibition of mitochondrial accumulation of Rab10. In revision.
- Shaun Martin, Jeffry Zielich, Chris Van den Haute, Sarah van Veen, Patrizia Agostinis, Veerle Baekelandt, Jan Eggermont, Erik Lambie, **Peter Vangheluwe**. ATP13A2 activity mediates the mitochondrial unfolded protein response. In preparation.

Geneeskundige Stichting Koningin Elisabeth
Fondation Médicale Reine Elisabeth
Königin-Elisabeth-Stiftung für Medizin
Queen Elisabeth Medical Foundation

Progress report of the research group of

Prof. Vanhollebeke Benoit, PhD

Université Libre de Bruxelles (ULB)

Principal investigator

Prof. Vanhollebeke Benoit, PhD
Head of the Laboratory of Neurovascular Signaling
Department of Molecular Biology
Neuroscience Institute Faculty of Sciences
University of Brussels (ULB)
Tel.: +32 2 650 97 61
Fax: +32 2 650 97 50
E-mail: Benoit.Vanhollebeke@ulb.ac.be
nvasc.ulb.be/vanhollebekelab/

Organ-wide analysis of brain neurovascular communication in real-time and at single-cell resolution

1. State of the Art

Blood vessels are more than passive conduits for blood flow and that tissue-specific vascular beds not only match the metabolic demands of the perfused organs, but also act as important signaling centers releasing angiocrine factors that contribute to organ development, maintenance and repair. Accordingly, proper brain function relies on elaborate communications between the neural and vascular system and this organ serves as a paradigm for extensive crosstalk between the vascular system and its local microenvironment. Central nervous system (CNS) neurovascular development has been best studied in the developing mouse CNS and a number of genetic regulators of neurovascular development have been uncovered, with a subset of them further organized into networks. Despite this progress, an integrated picture of how, when and to what extent neural and vascular development are coordinated is lacking. Building this model will critically rely on the combined capacity to (i) scrutinize the cellular modalities of the intrinsically highly dynamic processes of vascular and neural development in real-time and to (ii) identify experimental settings where the signaling and circulatory functions of the intracerebral blood vessels can be, at least partially, uncoupled. Every aspect of neurovascular development and function, from blood vessels morphogenesis and BBB formation to neural cell metabolism, is indeed exquisitely sensitive to reduced tissue oxygen tension. The hypoxia response that invariably accompanies defective vascular development is a confounding factor severely blunting the scope of approachable investigations in the field.

Our previous work identified and validated the optically-clear zebrafish embryonic brain as uniquely endowed with these distinctive attributes, through the startling observation that zebrafish brains remain normoxic throughout organogenesis even in the total absence of intracerebral blood vessels and that, after prolonged periods of impaired vascular development, blood vessels invade and branch within the neural system in stereotypical patterns, implying long-prevailing physiological conditions.

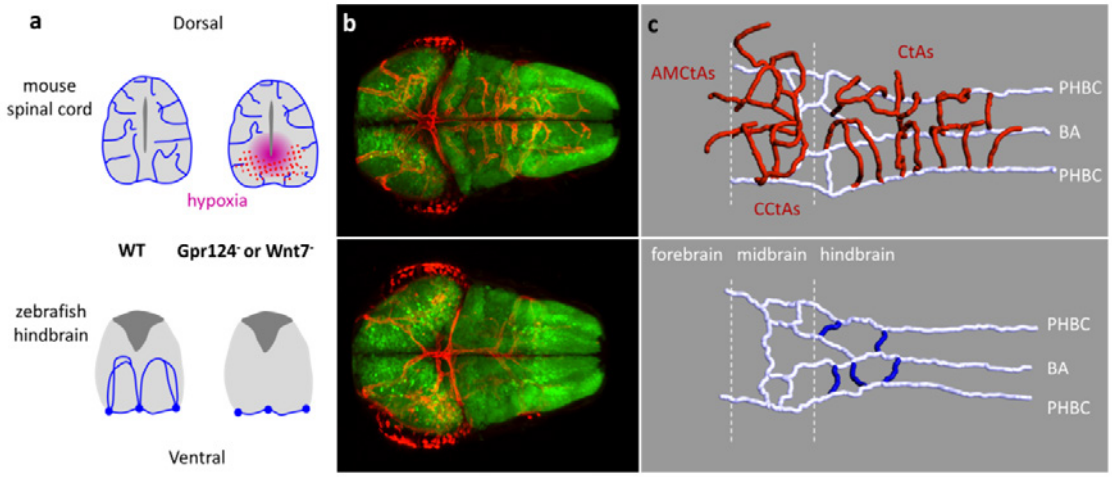

A normoxic and transparent setting to explore CNS neurovascular interactions. (**a**) Cross-section through the mouse and zebrafish central nervous system with or without impaired vascular development. (**b**) z-projection of a dorsal confocal scan through the zebrafish brain, with post-mitotic neurons labeled in green and endothelial cells in red. (**c**) Wire-diagram representation of WT and mutant zebrafish brain vasculature in dorso-lateral views. Red vessels represent the intra-cerebral BBB network.

Through the combined increase in spatio-temporal resolution, best suited to comprehend the intrinsically dynamic processes of neurovascular development and function, and the absence of confounding hypoxic signaling cascades, some fundamental questions seem now within reach: Through which cellular and molecular mechanisms is CNS vascular invasion and maturation controlled by neural signals? Reciprocally, how does the developing vascular system impact on brain patterning and function?

The physical and genetic constraints imposed to the study of the dynamic cellular mechanisms governing sprouting angiogenesis have restricted their investigation to a limited number of *in vivo* settings, most notably the postnatal mouse retina and the zebrafish ISVs. In recent years, a coherent model integrating controlled behaviors of VEGF-selected tip cells and notch-induced stalk cells within nascent sprouts has been derived from those prototypical settings. Hierarchical organization of differentially-fated endothelial cells (ECs) during sprouting angiogenesis and organ-specific adaptations are viewed as consecutive, and hence distinct, aspects of vascular development. However, through live imaging of mosaic animals, an integrated control was recently shown to operate under the control of CNS-derived signals. Neural progenitor-derived Wnt7 ligands, well-known inducers of brain EC maturation, govern CNS EC invasion through selective modulation of tip cell function within the parental perineural vessels.

2. Objectives

A major aim of our project is to address how the neural and vascular systems communicate to assemble functional neurovascular units. In particular, we study how perineural endothelial cells (ECs) selectively respond to neural-derived Wnt7 ligands during the process of brain angiogenesis.

From the initial discovery of Frizzled as Wnt receptors two decades ago to the recent crystallographic insights into their interaction mechanism, it has remained unknown how cells discriminate between multiple Wnt ligands within complex biological systems. The Wnt/Frizzled interaction chemistry is indeed incompatible with mono-specific recognition and, accordingly, when tested in pair-wise combinations, multiple Wnt ligands compete for binding to various Frizzled receptors. We are exploring a novel molecular mechanism that enables cells to bind and respond to Wnt7 ligands with strict specificity.

Our previous findings indeed identified Adgra2/Gpr124, an orphan member of the adhesion class of G protein-coupled receptors as an essential co-factor of Wnt7 signaling in CNS ECs. Adhesion G protein-coupled receptors (aGPCRs) constitute the second largest group of GPCRs in humans. Most aGPCRs are orphan receptors with no identified ligands that function through remarkably diverse mechanisms. They differ from other GPCRs by long N-terminal extensions preceding a membrane-proximal GPCR autoproteolysis-inducing (GAIN) domain containing the highly conserved GPCR proteolytic site (GPS). These N-terminal sequences typically comprise multiple protein-protein interaction domains involved in cell-cell and cell-matrix contacts. This structural hallmark significantly broadens the signaling potential and complexity of this class of GPCRs that, context-dependently, behave as adhesion molecules or signal transducing GPCRs. Gpr124, a member of this branch of GPCRs has gained considerable interest since the discovery of its essential role in brain vascular development (Kuhnert et al., 2010). Upon genetic inactivation, vascularization and blood-brain barrier maturation are impaired in all or parts of the zebrafish and mouse central nervous system, respectively (Anderson et al., 2011; Cullen et al., 2011; Kuhnert et al., 2010; Vanhollebeke et al., 2015). This receptor promotes angiogenic sprouting through endothelial cell (EC)-autonomous Wnt/β-catenin signaling stimulation upon contact with neural progenitor-derived Wnt7 ligands (Posokhova et al., 2015; Vanhollebeke et al., 2015; Zhou and Nathans, 2014).

Genetic studies in zebrafish have shown that in order to recognize these ligands, and hence to be competent for brain invasion, ECs must additionally express Reck, a GPI-anchored glycoprotein (Ulrich et al., 2016; Vanhollebeke et al., 2015). Consistently, EC-specific invalidation of RECK in the mouse leads to CNS-specific vascular defects, thereby demonstrating the evolutionary conserved role of RECK in cerebrovascular development (de Almeida et al., 2015). Gpr124 and Reck have been proposed to interact at the plasma membrane to assemble a potent and Wnt7-specific Wnt/β-catenin co-activator complex (Vanhollebeke et al., 2015). The complex also operates in neural crest-derived cells to promote dorsal root ganglia (DRG) neurogenesis in zebrafish embryos (Vanhollebeke et al., 2015). Defective DRG neurogenesis is accompanied by metamorphic pigmentation alterations in the adult Gpr124 mutant skin (Vanhollebeke et al., 2015).

While the genetic interaction between *gpr124* (also known as *adgra2*) and *reck* is well supported by studies in the zebrafish model as well as cell culture experiments, their activation and signaling mechanisms are poorly characterized, in part as a result of a lack of *in vivo* models where structure-function relationships can be probed.

3. Results

3.1. Identification of an *in vivo* model of *gpr124/adgra2*-dependent neurovascular dysfunction (Bostaille et al. *Development*)

Malmquist *et al.* (2013) phenotypically characterized the *ouchless* mutant that was recovered from an F3 forward genetic screen for defective dorsal root ganglion (DRG) neurogenesis in zebrafish. While the initial dorsoventral migration of neural crest-derived cell clusters towards presumptive DRG locales appears unaffected in *ouchless* mutants, the neurogenic program leading to the generation of *neurog1:*EGFP+ cells within the ganglion is defective, resulting in a severe reduction of DRG numbers in 72 hours post fertilization (hpf) *ouchless* mutants. *ouchless* mutants are viable but exhibit reduced growth rates and interrupted melanophore stripes in the adult skin. The *ouchless* mutation was mapped by bulk segregation analysis to a 342 kb genomic region of chromosome 8, harboring the *sorbs3* gene. No causative mutation could be identified within the coding sequence of *sorbs3*, but a mutation was suspected to reside within cis-regulatory elements, accounting for the reduced *sorbs3* transcript levels observed in *ouchless* mutants. Antisense *sorbs3* morpholino knockdown experiments, as well as BAC and mRNA rescue experiments, further supported the model that *sorbs3* regulates DRG neurogenesis and that *sorbs3* dysfunction drives the *ouchless* phenotypes (Malmquist et al., 2013).

The *ouchless* phenotypes are remarkably analogous to the DRG defects reported in *gpr124* knock-out mutants (Vanhollebeke et al., 2015). Of note *gpr124* has been renamed to *adgra2*. Along with Reck, Gpr124/Adgra2 has been shown to control DRG formation by activating Wnt signaling in neural crest-derived sox10:mRFP+ ganglion cells (Vanhollebeke et al., 2015). Given the phenotypic similarities, we therefore set out to test whether *adgra2* and *ouchless* (presumably *sorbs3*) co-operate during the process of DRG neurogenesis and brain vascularization.

We first demonstrated that *adgra2/gpr124* and *ouchless* genetically interact by functional gene dosage experiments (**Figure 1**).

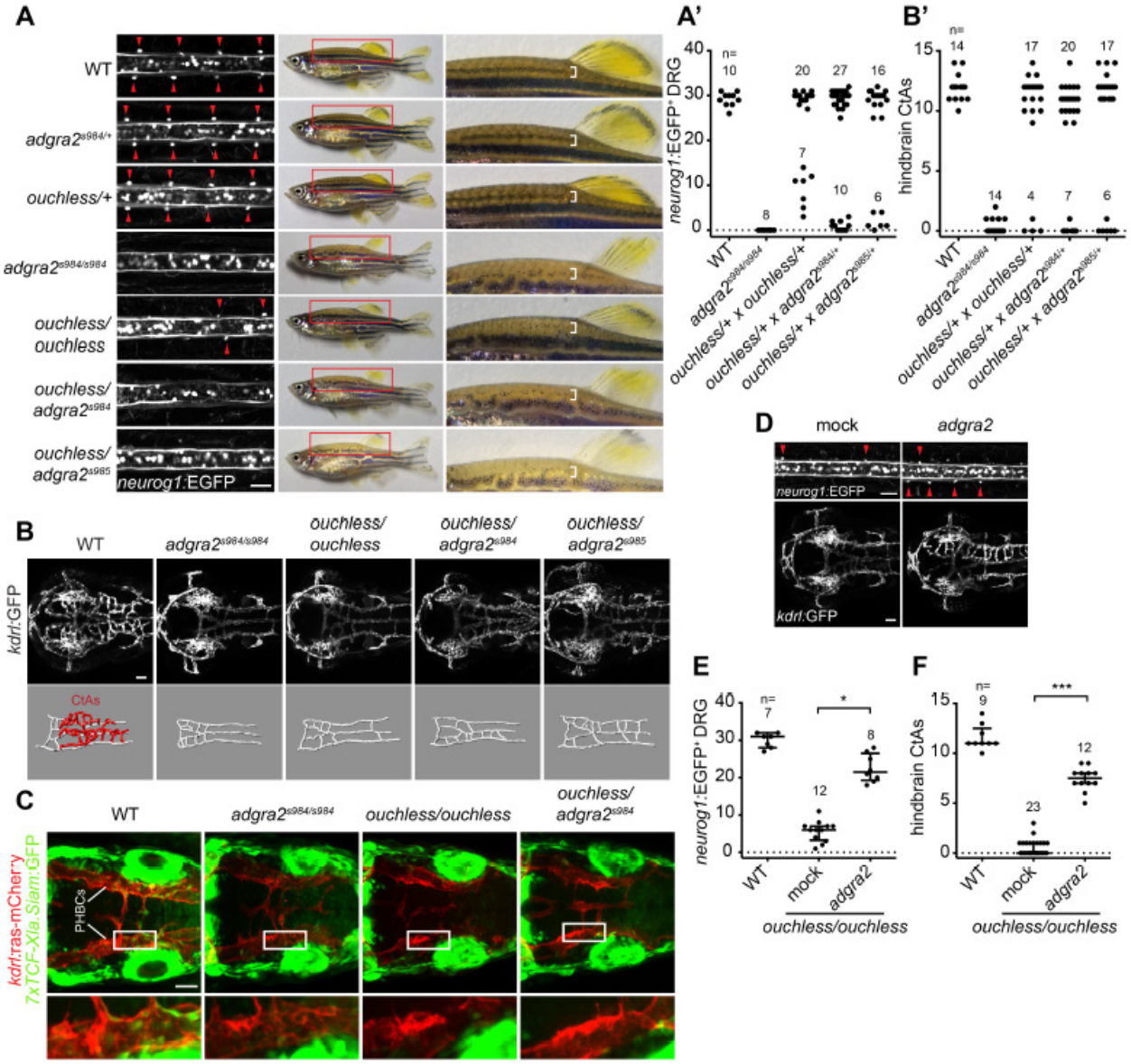

Figure 1 *gpr124/adgra2* and *ouchless* mutations fail to complement. (**A** and **A'**) Fish heterozygous for *ouchless* were crossed with the previously described *adgra2* heterozygotes, *adgra2*$^{s984/+}$ and *adgra2*$^{s985/+}$, and the offspring were assessed at 72 hpf for defects in DRG neurogenesis. From these crosses, ~25% of the offspring (annotated as *ouchless/adgra2*^{s984} and *ouchless/adgra2*^{s985}) showed an almost complete lack of *neurog1*:EGFP^{+} DRG. When raised to adulthood, these fish could be distinguished from their siblings by discontinuous dorsal melanophore stripes on their skin (brackets). (**B** and **B'**) Cerebral vasculatures of 60 hpf embryos derived from *ouchless* heterozygotes incrosses and outcrosses to *adgra2* heterozygotes. 25% of the offspring of each of the crosses displays highly penetrant brain vascular defects, characterized by a complete absence of central arteries (CtAs), similar to *adgra2* mutants. (C) Defective endothelial Wnt/β-catenin signaling in the perineural primordial hindbrain channel (PHBC) ECs. (D-F) When *ouchless* mutants are injected at the one-cell stage with mRNA encoding wild-type (WT) Adgra2, significant restoration of *neurog1:*EGFP^{+} DRG and cerebral blood vessels is observed.

The lack of complementation between *ouchless* and *adgra2*, together with the discovery of vascular phenotypes in *ouchless* mutants that mimic those of *adgra2* mutants, indicates that *ouchless* constitutes a new allele of *adgra2*. The re-evaluation of the genomic region known to harbour the *ouchless* mutation revealed that the *adgra2* gene resides within the critical interval, spanning the ca-48 and ca-37 genomic markers. In *ouchless* mutants, *adgra2* displays an essential splice site mutation inactivating Adgra2 through the in-frame deletion of a single LRR in the ectodomain of this adhesion G-protein coupled receptor (**Figure 2**).

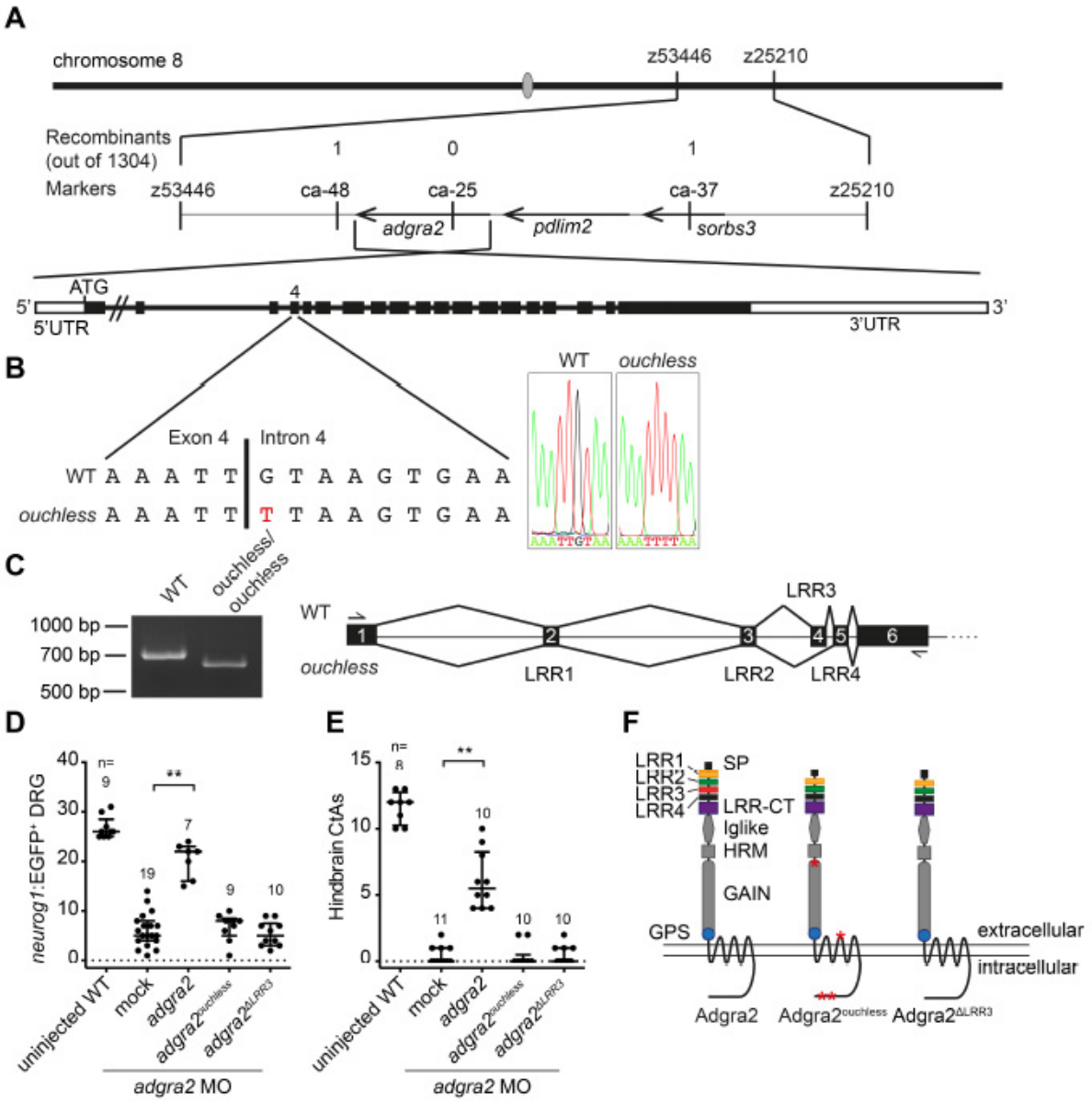

Figure 2 *adgra2* is mutated in *ouchless* mutants. (**A**) Representation of the *ouchless* locus genetic map on chromosome 8. The number of recombinants among 1304 meioses as determined by Malmquist et al. (2013) is indicated above the markers utilized for mapping. (**B**) Sanger sequencing of the exon 4-intron 4 boundary of *adgra2* in WT and *ouchless* mutant embryos. The G→T change in the *ouchless* 5′ splice donor sequence appears in red. (**C**) RT-PCR splicing analysis of *adgra2* in 48 hpf WT and *ouchless* mutant embryos. The amplification primers hybridize to exon 1 and exon 6, as illustrated in the panel on the right. (**D, E**) The capacity of the full-length *adgra2* coding sequence from *ouchless* mutants to rescue DRG and CtA defects in *adgra2* morphants was evaluated by mRNA injection at the one-cell stage. While mRNA encoding the WT receptor (annotated as *adgra2*) partially suppressed both phenotypes, the *ouchless* variant (annotated as *adgra2*^{ouchless}) did not affect either. (**F**) Comparison of a reference WT *adgra2* allele with the *adgra2* coding sequence recovered from *ouchless* mutant embryos. Four non-synonymous single nucleotide polymorphisms (SNPs; M429V, S895P, A1282V and A1302G) as well as an in-frame 72 bp deletion corresponding to exon 4 are found in *ouchless*. While all four *adgra2* SNPs identified in *ouchless* mutants had been previously identified in functionally validated *adgra2* alleles derived from mixed AB/TL genetic backgrounds, alternative splicing resulting in exon 4 skipping is absent from any known zebrafish, mouse or human *ADGRA2* isoform. When probed in zebrafish, alternative splicing of the exon 1-exon 6 sequences is undetectable by RT-PCR (C). Exon 4 corresponds precisely to the third leucine-rich repeat (LRR) unit of the LRR/CT domain of Adgra2, which comprises an array of four 24-residue-long LRR units followed by a LRR cysteine-rich C-terminal motif (LRR-CT).

Altogether, this work reveals that *ouchless* and *adgra2* mutants are allelic and that the *ouchless* phenotypes result from an essential splice site mutation inactivating Adgra2 through the in-frame deletion of a single LRR in the ectodomain of this adhesion G-protein coupled receptor (GPCR). The zebrafish *ouchless* mutant thereby constitutes the first *in vivo* model of *adgra2* N-terminal domain-specific variation.

3.2. Molecular insights into Adgra2/Gpr124 and Reck intracellular trafficking (Bostaille *et al.* Biology Open)

Taking advantage of the above-described mutation in *adgra2*, we undertook to better define the cellular and molecular modalities of the Gpr124/Reck synergistic interaction. In particular, the stoichiometry of the Gpr124/Reck complex and the molecular determinants of its trafficking, assembly and signal transduction still needed to be investigated. The N-terminal domains of Gpr124 are likely contributors to several, if not all, of these processes. Indeed, cell culture and *in vivo* experiments have revealed that Gpr124 function critically relies on its extracellular domain architecture. N-terminal truncations or substitution of the ectodomain of Gpr124 with the equivalent domain derived from the closely related Gpr125, abrogate receptor signaling (Posokhova et al., 2015; Vanhollebeke et al., 2015). Moreover, the Gpr124 potential interaction interface with Reck, a cell surface exposed GPI-anchored glycoprotein, is restricted to the extracellular parts of the receptor.

As is typically found in aGPCRs, the extracellular N-terminus of Gpr124 comprises multiple protein-protein interaction domains whose contributions to receptor function remain largely elusive. Specifically, the Gpr124 ectodomain is sequentially composed of an N-terminal LRR/CT domain, an Ig-like domain and a hormone receptor motif (HRM) preceding the membrane-proximal GPS-containing GAIN domain. The Gpr124 LRR/CT domain contains four leucine-rich repeat (LRR) units which are 20-29 residue-long structural units that assemble in a superhelical manner with tandemly arranged repeats to form curved solenoid structures acting as protein interaction frameworks. As found in Gpr124, extracellular LRR motifs are often flanked by cysteine-rich C-terminal domains (LRR-CTs) that are integral parts of the LRR domain and shield the hydrophobic core of the last LRR motif. Building a proper understanding of Gpr124 function will benefit from delineating the contribution of each N-terminal domain to receptor function.

The *adgra2* variant found in *ouchless* mutants differs from *adgra2* reference sequences by four non-synonymous SNPs as well as a 72 bp deletion corresponding to exon 4 (**Figure 3A**). While the SNPs represent naturally occurring variations, the exon 4 skipping event is caused by an ENU-induced essential splice-site mutation at the exon 4–intron 4 boundary and was shown to result in Adgra2^{ouchless} inactivation (Bostaille et al., 2017). Exon 4 encodes the third LRR motif (LRR3) of the LRR/CT domain. In order to determine how the absence of LRR3 mechanistically impairs Adgra2 function, we generated C-terminal EGFP-tagged versions of wild-type (WT) Adgra2 as well as *ouchless* (Adgra2^{ouchless}) and ΔLRR3 (Adgra2$^{\Delta LRR3}$) variants. This latter variant reproduces the exon 4 deletion found in *ouchless* in a WT allele of *adgra2*, and hence lacks the *ouchless*-associated SNPs (Bostaille et al., 2017). We first evaluated the functionality of the fusion proteins in brain angiogenic assays in zebrafish by mRNA injections at the one-cell stage. While ectopic restoration of either EGFP-tagged or untagged versions of WT Adgra2 could restore angiogenic sprouting in *adgra2*$^{s984/s984}$ hindbrains (red arrowheads in **Figure 3C**), the equivalent Adgra2^{ouchless} and Adgra2$^{\Delta LRR3}$ variants were inactive (**Figure 3B,C**). These observations extend and confirm previous findings indicating that C-terminal fusions are compatible with receptor function *in vivo* and that, in the absence of LRR3, Adgra2 is non-functional (Vanhollebeke et al., 2015, Bostaille et al., 2017).

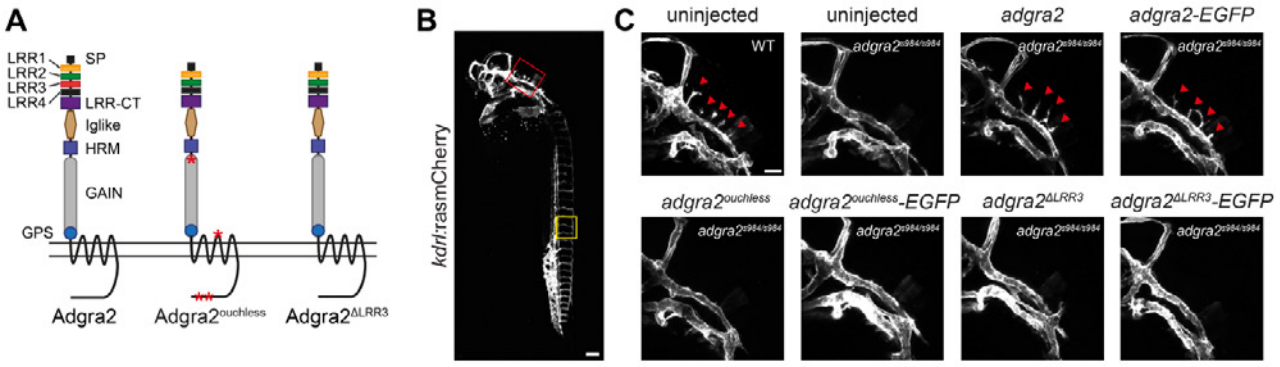

Figure 3. Adgra2^{ouchless} mislocalizes to the endoplasmic reticulum. (**A**) Schematic representation of Adgra2, Adgra2^{ouchless} and Adgra2$^{\Delta LRR3}$ topology and domain organization. Adgra2^{ouchless} and Adgra2$^{\Delta LRR3}$ lack the third LRR motif (red rectangle). The positions of the residue variations resulting from naturally occurring SNPs in *adgra2^{ouchless}* are designated by red asterisks. (**B**) Maximal intensity projection of a confocal z-stack of a WT *Tg(kdrl:ras-mCherry)* embryo at 36 hpf in lateral view. The red and yellow boxes define, respectively, the magnified areas of the hindbrain vasculature shown in C and the intersegmental vessels shown in E. Scale bar: 100 µm. (**C**) Maximal intensity projection of a confocal z-stack of WT and *adgra2$^{s984/984}$ Tg(kdrl:ras-mCherry)* embryos at 36 hpf in lateral view after injection of 100 pg of *adgra2*, *adgra2-EGFP*, *adgra2^{ouchless}*, *adgra2^{ouchless}-EGFP*, *adgra2$^{\Delta LRR3}$* or *adgra2$^{\Delta LRR3}$-EGFP* mRNA at the one-cell stage. The red arrowheads point to the CtAs invading the hindbrain rhombomeres. Scale bar: 50 µm.

We then analyzed the stability and subcellular distribution of the EGFP-tagged variants in different cell types. When examined in the large and cobblestone-shaped enveloping layer cells of the 5 h post fertilization (hpf) zebrafish blastula, WT Adgra2-EGFP labeled the plasma membrane where it colocalized with a membrane-tethered lyn-RFP marker. By contrast, the mutant fusion proteins accumulated in an intracellular reticulate compartment reminiscent of the ER. Similarly, when analyzed in ECs of mosaic transgenic zebrafish, the WT fusion decorated the EC plasma membranes, including the numerous filopodial extensions of the tip cells, while the mutant variants showed strong intracellular and perinuclear signals that did not colocalize with the ras-mCherry EC membrane marker. Finally, in order to streamline quantitative colocalization studies, we imaged the cellular distribution of the EGFP fusion proteins in cultured HEK293T cells. Whereas the WT fusion protein accumulated at the plasma membrane marked by GPI-RFP as anticipated, the mutant versions failed to reach this compartment but instead accumulated intracellularly. The accumulating compartment was identified as the ER with the help of the mCherry-fused ER protein translocation apparatus component SEC61β. This was further quantitatively evaluated by Pearson's colocalization coefficient (PCC) analysis. Moreover, a perfect correlation was observed between the capacity of the LRR chimera variants to reach the plasma membrane and their ability to support vascular sprouting in the zebrafish hindbrain or to induce the formation of DRG neurons.

When overexpressed in cultured cells, Adgra2 and Reck colocalize at the plasma membrane and proximity ligation assays further suggest that the proteins may directly interact within this compartment to assemble a receptor complex (Vanhollebeke et al., 2015). It remains to be determined whether the partners recognize and assist each other during their progression within the secretory pathway or instead meet at the plasma membrane after independent trafficking events. We took advantage of the ER retention of the LRR/CT variants to address this question. As revealed by indirect immunofluorescence assays in non-permeabilized HEK293T cells, HA-Reck reached the plasma membrane independently of the nature and trafficking status of the co-expressed Adgra2 receptor (**Figure 4A**). In addition, when expressed individually in HEK293T cells, Reck and Adgra2 localized to the plasma membrane (Vanhollebeke et al., 2015). These results suggest that Reck does not require Adgra2 in order to reach the plasma membrane and vice versa. However, as HEK293T cells express low levels of endogenous *ADGRA2* and *RECK* (Vanhollebeke et al., 2015; Zhou and Nathans, 2014), this endogenous protein pool might be sufficient to accompany ectopic Reck and/or Adgra2 during secretion. We therefore engineered *ADGRA2$^{-/-}$* and *RECK$^{-/-}$* HEK293T cells through CRISPR/Cas9 approaches and re-evaluated Adgra2 and Reck trafficking in these genetic backgrounds (**Figure 4B**). As in WT cells, both proteins accumulated at the plasma membrane when expressed individually, indicating that each partner can reach its final destination independently (**Figure 4C,D**).

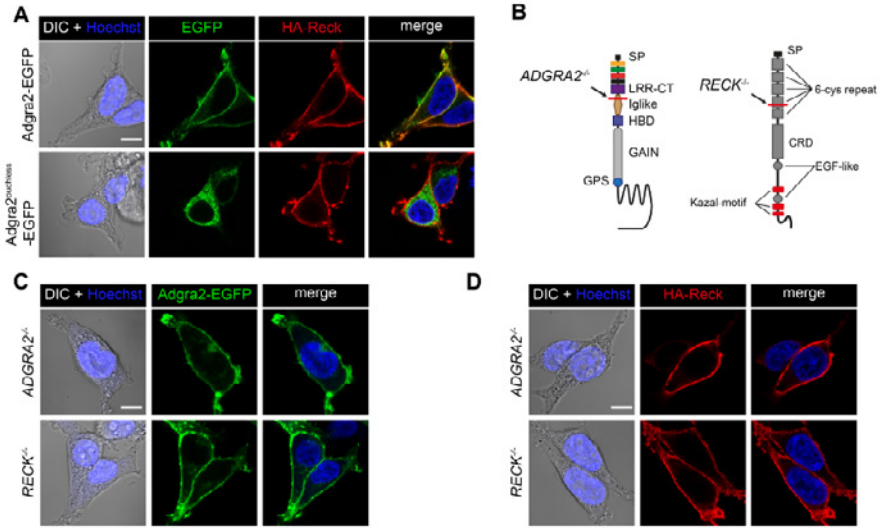

Figure 4 Independent trafficking of Reck and Adgra2 to the plasma membrane. (**A**) Single-plane confocal images of non-permeabilized HEK293T cells 48 h after transfection with *HA-reck* and *adgra2-EGFP* variants, as indicated. (**B**) Schematic representation of the genetic lesions of *ADGRA2*$^{-/-}$ and *RECK*$^{-/-}$ cells. The position of the frame-shift mutation is indicated by the red line. (**C,D**) Single-plane confocal images of non-permeabilized *ADGRA2*$^{-/-}$ and *RECK*$^{-/-}$ HEK293T cells 48 h after transfection with *adgra2-EGFP* (**C**) and *HA-reck* (**D**) constructs. In all panels, EGFP is detected by direct fluorescence and the HA-Reck fusion by anti-HA indirect immunofluorescence. Cells were additionally transfected with a *Wnt7a* (mouse gene) expression construct. Nuclei were counterstained with Hoechst. Scale bars: 10 µm.

When assessed 48 h post transfection in saponin-permeabilized HEK293T cells, a minor fraction of HA-Reck can be immunodetected in the ER and as such co-distributes with Adgra2^{ouchless} (**Figure 5A**, arrows) and presumably with a fraction of WT Adgra2 transiting through this compartment. To test whether Adgra2 is able to interact with Reck under these conditions, we performed proximity ligation assays as described previously (Vanhollebeke et al., 2015). As shown in **Figure 5B**, no interaction could be detected between HA-Reck and FLAG-Adgra2^{ouchless}, in contrast to the plasma membrane-localized signal readily detected in HA-Reck and FLAG-Adgra2 co-expressing cells. These results suggest that either the ER is not permissive for the formation of the complex or that the LRR deletion in Adgra2 impairs its interaction with Reck.

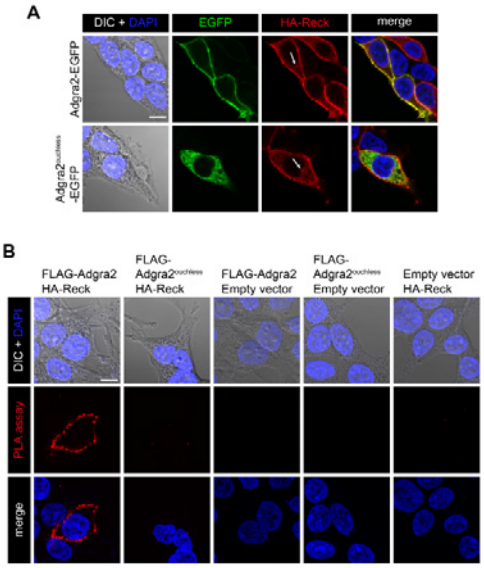

Figure 5 Cellular distribution of Adgra2 and Reck interaction. (A) Single-plane confocal images of saponin-permeabilized HEK293T cells 48 h after transfection with *HA-reck* and *adgra2-EGFP* variants, as indicated. Nuclei were counterstained with DAPI. EGFP is detected by direct fluorescence and the HA-Reck fusion by anti-HA indirect immunofluorescence. Arrows point to the ER. (B) Proximity ligation assays in HEK293T cells 48 h after transfection with *FLAG-adgra2*, *FLAG-adgra2*^{ouchless} and *HA-reck* constructs, as indicated. Nuclei were counterstained with DAPI. In all panels, cells were additionally transfected with a *Wnt7a* (mouse gene) expression construct. Scale bar: 10 µm.

This study characterized the functionally null mutation of *adgra2* recently identified in zebrafish *ouchless* mutants. The genetic lesion results in *adgra2* alternative splicing and we show that this receptor variant localizes to the ER instead of the plasma membrane. This unprecedented occurrence of an aberrantly routed Adgra2 prompted us to evaluate whether the intracellular trafficking of Reck and Adgra2 are interdependent. When co-expressed with the ER-retained Adgra2 variant, Reck still reached the plasma membrane. Extending this analysis in CRISPR/Cas9 engineered cells, Reck was shown to accumulate at the plasma membrane in both WT and *ADGRA2*$^{-/-}$ HEK293T cells and, similarly, Adgra2 trafficking to the plasma membrane was unaffected by the presence or absence of RECK. These data indicate that the partners, when expressed individually, are able to traffic independently. When co-expressed in HEK293T cells, their close proximity can be detected by PLA assays at the plasma membrane but not within the endomembrane compartments of the secretory pathway through which they transit. These combined observations indicate that the partners first meet at the plasma membrane and that their synergy is likely restricted to the events occurring subsequently at the cell surface, in agreement with the current model (Vanhollebeke et al., 2015). It is conceivable that the interaction between Adgra2 and Reck is only made possible within plasma membrane microdomains of specific proteolipidic composition or that a yet to be defined component induces complex formation within this compartment. The selective association of Reck and Adgra2 at the plasma membrane could also result from the higher concentrations reached within this final membrane compartment favoring the potentially transient encounters of the partners.

While this study describes the role of the LRR/CT domain in promoting Adgra2 progression through the ER, it does not exclude additional roles for this domain in the Adgra2/Reck signaling pathway. The LRR/CT domain might, for instance, be additionally implicated in the interactions with Reck, Wnt7 or Fzd/Lrp5/6 occurring at the plasma membrane.

3.3. Defining the molecular mechanism for Wnt ligand-specific signaling controlling brain vascularization in vertebrates (Eubelen, Bostaille et al. Science)

As outlined above, Wnt signaling is an ancient signaling pathway that has accompanied the emergence of metazoans and is key to many developmental, physiological, and disease processes. Similar to other signaling pathways, gene families for both Wnt ligand and its corresponding Frizzled receptor have undergone extensive expansion during metazoan evolution. Vertebrate genomes harbor 19 closely related Wnt genes as well as 10 Frizzled genes. Gene duplication is typically considered a major driving force in the evolution of new biological functions through neo- or subfunctionalization of emerging paralogs. How this functional diversification of Wnt ligands is structurally and molecularly organized, however, remains poorly understood. The Wnt/Frizzled molecular interaction is mediated by residues conserved across both families. This promiscuous interaction is incompatible with monospecific recognition and, accordingly, when tested in pair-wise combinations, multiple Wnt ligands compete for binding to various Frizzled receptors.

These observations raise the questions of how Wnt ligands achieve functional diversification and how cells interpret the intermingled expression patterns of simultaneous and sometimes conflicting Wnt signals. In some biological settings, cells may integrate all signaling inputs non discriminately and trigger appropriate responses by considering their total net balance. However, other biological processes exhibit strict Wnt ligand selectivity, despite complex Wnt/Frizzled expression landscapes. A prototypical example is provided by the exclusive control of mammalian forebrain and ventral spinal cord angiogenesis by Wnt7a and Wnt7b.
Within this neurovascular unit, in order to respond to neural progenitor–derived Wnt7 by activating Wnt/b-catenin signaling, cerebral endothelial cells must express a membrane protein complex consisting of the adhesion G protein–coupled receptor (GPCR) Gpr124 (Adgra2) and the glycosylphosphatidylinositol-anchored glycoprotein Reck. This Gpr124/Reck complex was recently reported to promote Wnt7-specific responses.

Using a combination of biophysical approaches and ligand-binding assays in genetically engineered cells, we demonstrated that ligand selectivity is conferred by Reck, which mediates Wnt7-specific binding in a Frizzled-independent manner. Reck orchestrates Wnt ligand discrimination by engaging the structurally disordered and highly divergent linker domain of Wnt7. The presence of Gpr124 is required to deliver Reck-bound Wnt7 to Frizzled by assembling higher-order Reck/Gpr124/Frizzled/Lrp5/6 complexes. This Gpr124 tethering function does not rely on its GPCR structure but instead on its combined capacity to interact with Reck extracellularly and recruit the Dishevelled scaffolding protein intracellularly. By bridging Gpr124 and Frizzled, Dishevelled recruitsWnt7, via its association with Reck, into dynamic Wnt/Frizzled signalosomes, resulting in increased local concentrations of ligand available for Frizzled signaling.

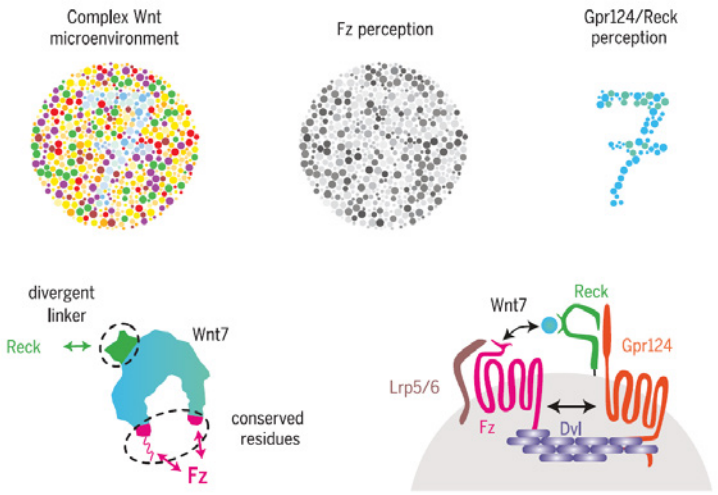

Figure 6 Task sharing for orchestrated Wnt7-specific cellular responses. (Top) Gpr124 and Reck cooperatively alter the cell's perception of its Wnt microenvironment by selectively potentiating Wnt7 signals (cyan-tinted dots). (Bottom) Reck decodes Wnt ligands by establishing monospecific contacts with the highly divergent Wnt7 linker domain. Gpr124 links Reck-bound Wnt7 to Dishevelled. Dishevelled polymers by interacting simultaneously with Gpr124 and Fz assemble Wnt7-enriched signalosomes that trigger signaling through Fz receptors and Lrp5/6 co-receptors.

Our data reveal that cells are equipped with "Wnt-decoding modules" that distinguish between Wnt ligands that are otherwise very similar. They also reveal a critical role for the linker domain in Wnt ligand evolution and functional diversification. These mechanistic insights into the Wnt decoding capacities of vertebrate cells predict that additional Wnt decoding modules exist, enabling fine-tuning of cellular behaviors in response to other Wnt or Frizzled family members. These modules expand the diversity of proximal events in Wnt signaling, opening new therapeutic opportunities for conditions in which Wnt stimulation or inhibition are desirable at the membrane level. In particular, the mechanisms uncovered here provide an opportunity for the targeted treatment of human central nervous system neurovascular disorders.

3.4. Probing the function of endothelial Wnt/β-catenin in brain vessel anastomosis and maturation (Hübner et al. Nat. Commun. 2018)

The above mentioned Wnt/β-catenin signaling mechanism is essential for brain vascular invasion. Upon disruption, vertebrate brains exhibit profound CNS-specific vascular defects. This signaling pathway is considered as a master regulator of CNS vascular biology and further functions are suspected at later steps of the establishment of the cerebrovasculature. In search for these functions, we contributed to a study that investigated the subsequent requirements of Wnt/β-catenin signaling during CNS blood vessel morphogenesis and maturation. Canonical Wnt signaling is crucial for vascularization of the central nervous system and blood-brain barrier (BBB) formation. BBB formation and modulation are not only important for development, but also relevant for vascular and neurodegenerative diseases. However, there is little understanding of how Wnt signaling contributes to brain angiogenesis and BBB

formation. Here we show, using high resolution in vivo imaging and temporal and spatial manipulation of Wnt signaling, different requirements for Wnt signaling during brain angiogenesis and BBB formation. In the absence of Wnt signaling, premature Sphingosine-1-phosphate receptor (S1pr) signaling reduces VE-cadherin and Esama at cell-cell junctions (Figure 7). We suggest that Wnt signaling suppresses S1pr signaling during angiogenesis to enable the dynamic junction formation during anastomosis, whereas later S1pr signaling regulates BBB maturation and VE-cadherin stabilization. Our data provides a link between brain angiogenesis and BBB formation and identifies Wnt signaling as coordinator of the timing and as regulator of anastomosis.

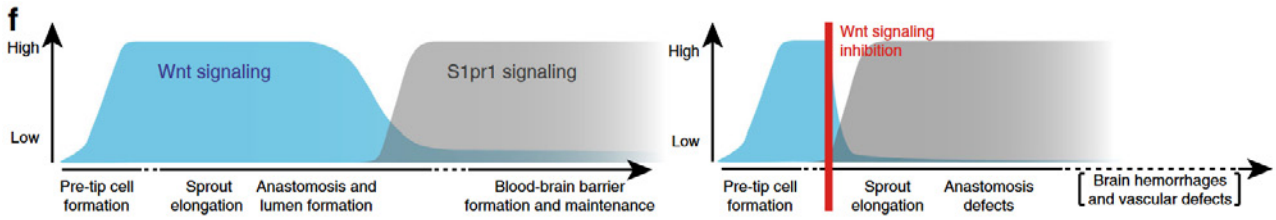

Figure 7. Illustration of Wnt and S1pr1 signaling during brain vascularization in wild type and Wnt-depleted embryos.

4. Outlook

Based on the previous findings, our project will continue to study brain angiogenesis and blood-brain barrier formation at the single-cell and real-time resolution in order to unravel the mechanisms through which neural signaling molecules couple brain vascular invasion and barriergenesis**.** We will more particularly determine whether the brain-specific angiogenic program redefines our understanding of the basic molecular and cellular regulatory logic of sprouting angiogenesis.

5. Publications

- Bonnin E[§], Cabochette P[§], Filosa A, Jühlen R, Komatsuzaki S, Hezwani M, Dickmanns A, Martinelli V, Vermeersch M, Supply L, Martins N, Pirenne L, Ravenscroft G, Lombard M, Port S, Spillner C, Janssens S, Roets E, Van Dorpe J, Lammens M, Kehlenbach RH, Ficner R, Laing NG, Hoffmann K, Vanhollebeke B[#], Fahrenkrog B[#]. Biallelic mutations in nucleoporin NUP88 cause lethal fetal akinesia deformation sequence. ***PLoS Genet.*** 2018 Dec 13;14(12):e1007845. doi: 10.1371/journal.pgen.1007845. [§] co-first authors, [#] co-corresponding authors.
- Hübner K, Cabochette P, Diéguez-Hurtado R, Wiesner C, Wakayama Y, Grassme KS, Hubert M, Guenther S, Belting HG, Affolter M, Adams RH, Vanhollebeke B, Herzog W. Wnt/β-catenin signaling regulates VE-cadherin-mediated anastomosis of brain capillaries by counteracting S1pr1 signaling. ***Nat Commun.*** 2018 Nov 19;9(1):4860. doi: 10.1038/s41467-018-07302-x.
- Eubelen M[§], Bostaille N[§], Cabochette P, Gauquier A, Tebabi P, Dumitru AC, Koehler M, Gut P, Alsteens D, Stainier DYR, Garcia-Pino A, Vanhollebeke B. A molecular mechanism for Wnt ligand-specific signaling. ***Science.*** 2018 Aug 17;361(6403). pii: eaat1178. doi: 10.1126/science.aat1178. [§] co-first authors
- Guerra A, Germano RF, Stone O, Arnaout R, Guenther S, Ahuja S, Uribe V, Vanhollebeke B, Stainier DY, Reischauer S. Distinct myocardial lineages break atrial symmetry during cardiogenesis in zebrafish. ***eLife***. 2018 May 15;7. pii: e32833. doi: 10.7554/eLife.32833.
- Bostaille N, Gauquier A, Stainier DY, Raible DW, Vanhollebeke B. Defective adgra2 (gpr124) splicing and function in zebrafish ouchless mutants. ***Development.*** 2017 Jan 1;144(1):8-11.
- Bostaille N, Gauquier A, Twyffels L, Vanhollebeke B. Molecular insights into Adgra2/Gpr124 and Reck intracellular trafficking. ***Biol Open.*** 2016 Dec15;5(12):1874-1881.
- Fontaine F, Lecordier L, Vanwalleghem G, Uzureau P, Van Reet N, Fontaine M, Tebabi P, Vanhollebeke B, Büscher P, Pérez-Morga D, Pays E. APOLs with low pH dependence can kill all African trypanosomes. ***Nat Microbiol.*** 2017 Nov;2(11):1500-1506.

– Horáková E, Changmai P, Vancová M, Sobotka R, Van Den Abbeele J, Vanhollebeke B, Lukeš J. The Trypanosoma brucei TbHrg protein is a heme transporter involved in the regulation of stage-specific morphological transitions. ***J Biol Chem.*** 2017 Apr 28;292(17):6998-7010.
– De Muylder G, Vanhollebeke B, Caljon G, Wolfe AR, McKerrow J, Dujardin JC. Naloxonazine, an Amastigote-Specific Compound, Affects Leishmania Parasites through Modulation of Host-Encoded Functions. ***PLoS Negl Trop Dis.*** 2016 Dec 30;10(12):e0005234.

6. Additional References

– Anderson K. D., Pan L., Yang X., Hughes V. C., Walls J. R., Dominguez M. G., Simmons M. V., Burfeind P., Xue Y., Wei Y. et al. (2011). Angiogenic sprouting into neural tissue requires Gpr124, an orphan G protein-coupled receptor. ***Proc. Natl. Acad. Sci. USA*** 108, 2807-2812. 10.1073/pnas.1019761108
– Bostaille N., Gauquier A., Stainier D. Y. R., Raible D. W. and Vanhollebeke B. (2017). Defective *adgra2 (gpr124)* splicing and function in zebrafish *ouchless* mutants. ***Development***, doi:10.1242/dev.146803. 10.1242/dev.146803
– Bostaille N, Gauquier A, Twyffels L, Vanhollebeke B. Molecular insights into Adgra2/Gpr124 and Reck intracellular trafficking. ***Biol Open.*** 2016 Dec15;5(12):1874-1881.
– Cullen M., Elzarrad M. K., Seaman S., Zudaire E., Stevens J., Yang M. Y., Li X., Chaudhary A., Xu L., Hilton M. B. et al. (2011). GPR124, an orphan G protein-coupled receptor, is required for CNS-specific vascularization and establishment of the blood-brain barrier. ***Proc. Natl. Acad. Sci. USA*** 108, 5759-5764. 10.1073/pnas.1017192108
– de Almeida G. M., Yamamoto M., Morioka Y., Ogawa S., Matsuzaki T. and Noda M. (2015). Critical roles for murine Reck in the regulation of vascular patterning and stabilization. ***Sci. Rep.*** 5, 17860 10.1038/srep17860
– Kuhnert F., Mancuso M. R., Shamloo A., Wang H.-T., Choksi V., Florek M., Su H., Fruttiger M., Young W. L., Heilshorn S. C. et al. (2010). Essential regulation of CNS angiogenesis by the orphan G protein-coupled receptor GPR124. ***Science*** 330, 985-989. 10.1126/science.1196554
– Malmquist, S. J., Abramsson, A., McGraw, H. F., Linbo, T. H. and Raible, D. W. (2013). Modulation of dorsal root ganglion development by ErbB signaling and the scaffold protein Sorbs3. ***Development*** 140, 3986-3996. doi:10.1242/dev.084640
– Posokhova E., Shukla A., Seaman S., Volate S., Hilton M. B., Wu B., Morris H., Swing D. A., Zhou M., Zudaire E. et al. (2015). GPR124 functions as a WNT7-specific coactivator of canonical β-catenin signaling. ***Cell Rep.*** 10, 123-130. 10.1016/j.celrep.2014.12.020
– Ulrich F., Carretero-Ortega J., Menendez J., Narvaez C., Sun B., Lancaster E., Pershad V., Trzaska S., Veliz E., Kamei M. et al. (2016). Reck enables cerebrovascular development by promoting canonical Wnt signaling. ***Development*** 143, 147-159. 10.1242/dev.123059
– Vanhollebeke B., Stone O. A., Bostaille N., Cho C., Zhou Y., Maquet E., Gauquier A., Cabochette P., Fukuhara S., Mochizuki N. et al. (2015). Tip cell-specific requirement for an atypical Gpr124- and Reck-dependent Wnt/β-catenin pathway during brain angiogenesis. ***eLife*** 4, e06489 10.7554/eLife.06489
– Zhou Y. and Nathans J. (2014). Gpr124 controls CNS angiogenesis and blood-brain barrier integrity by promoting ligand-specific canonical Wnt signaling. ***Dev. Cell*** 31, 248-256. 10.1016/j.devcel.2014.08.018

Geneeskundige Stichting Koningin Elisabeth
Fondation Médicale Reine Elisabeth
Königin-Elisabeth-Stiftung für Medizin
Queen Elisabeth Medical Foundation

Progress report of the research group of

Prof. dr. Geert van Loo, PhD

Universiteit Gent (UGent)

Principal investigator

Prof. dr. Geert van Loo, PhD

Co-investigators

Prof. Dr. Mohamed Lamkanfi

Inflammation Research Center
VIB – Gent University
Technologiepark 927
9052 Gent-Zwijnaarde
Belgium
Tel.: +32 9 331 37 61
Fax: +32 9 221 76 73
E-mail: geert.vanloo@irc.vib-ugent.be

1. A20 critically controls microglia activation and inhibits inflammasome-dependent neuroinflammation

Microglia, the mononuclear phagocytes of the central nervous system (CNS), are important for the maintenance of CNS homeostasis, but also critically contribute to CNS pathology. Here, we demonstrate that the nuclear factor kappa B (NF-κB) regulatory protein A20 is crucial in regulating microglia activation during CNS homeostasis and pathology. In mice, deletion of A20 in microglia increases microglial cell number and affects microglial regulation of neuronal synaptic function. Administration of a sublethal dose of lipopolysaccharide induces massive microglia activation, neuroinflammation and lethality in mice with microglia-confined A20 deficiency. Microglia A20 deficiency also exacerbates multiple sclerosis (MS)-like disease, due to hyperactivation of the Nlrp3 inflammasome leading to enhanced interleukin-1β secretion and CNS inflammation. Finally, we confirm a Nlrp3 inflammasome signature and IL-1β expression in brain and cerebrospinal fluid from MS patients. Collectively, these data reveal a critical role for A20 in the control of microglia activation and neuroinflammation.

1.1. Phenotype of mice with A20 deficiency in microglia

Transcriptome analysis of purified brain cell types of mouse cortex identifies the A20 encoding gene Tnfaip3/A20 as highly expressed in microglia, in contrast to its expression in neurons, astrocytes, endothelial cells, pericytes, and oligodendrocytes in various maturation stages (Zhang et al., 2014). To investigate the importance of A20 for microglia development and function, we first examined the expression of A20 in different microglial developmental stages, including yolk sac precursors (EMPs, A1, A2), embryonic microglia and adult microglia (Fig. 1a). Although A20 is only marginally expressed in early development, an increase in expression is seen in the later stages of embryonic development, and A20 expression is further enhanced in adult microglia. To assess its function in vivo, we crossed mice carrying a floxed A20 allele ($A20^{FL}$) (Vereecke et al., 2010) to Cx3Cr1CreErt2 transgenic mice allowing Cre-mediated gene deletion following tamoxifen (TAM) treatment. Targeting of microglia using this system is based on microglia longevity and capacity of self-renewal without any appreciable input from circulating blood cells (Goldmann et al., 2013). $A20^{Cx3Cr1CreErt2}$ mice were injected with TAM inducing A20 deletion in all Cx3Cr1 expressing cells. However, due to their short half-life, Cx3Cr1 Ert2Cre+ expressing blood-derived monocytes are gradually replaced by their monocyte precursors harboring non-rearranged A20 alleles. A20 deletion in microglia was confirmed at the protein level by Western blotting of fluorescence-activated cell sorted (FACS) microglia ex vivo (Fig. 1b) and of primary microglia cultured *in vitro* (Fig. 1c).

Mice with TAM-induced A20 deficiency in microglia (named $A20^{Cx3Cr1\text{-}KO}$) do not display overt spontaneous abnormalities, and histological analysis of brain sections of $A20^{Cx3Cr1\text{-}KO}$ mice do not reveal any gross morphological defects, astrogliosis or demyelination. However, immunohistochemical examination with the microglia marker Iba-1+ revealed a significant increase in the number of microglia both in brain ($p = 0.0286$) and spinal cord sections of $A20^{Cx3Cr1\text{-}KO}$ mice compared to control littermates (Fig. 1d-f). Quantitative morphometric three-dimensional analysis of Iba-1+ microglia in the adult cortex showed that A20-deficient microglia have an altered morphology, characterized by significantly longer processes and increased number of segments, branching and terminal points relative to microglia from control mice (Fig. 1g-h). Together, these data suggest that lack of A20 induces proliferation of adult microglia with altered morphology.

Next, to determine whether A20 deficiency in microglia affects microglia activation or its immune function under homeostatic conditions, we expression profiled sorted $CD45^{int}CD11b^{hi}$ microglia from brains of $A20^{Cx3Cr1\text{-}KO}$ and control littermate mice by quantitative deep sequencing of RNA transcripts. We

observed significant differences in the mRNA profiles of microglial genes in A20$^{Cx3Cr1\text{-}KO}$ relative to control mice. In total, 216 genes were significantly upregulated and 39 genes were downregulated ($p < 0.01$ and fourfold change) in A20$^{Cx3Cr1\text{-}KO}$ microglia compared to controls. Many genes typically expressed under physiological conditions (P2ry12, Cx3cr1, Sall1, Gpr34, Fcrls, Rhob, Olfml3) are selectively downregulated in A20$^{Cx3Cr1\text{-}KO}$ microglia (Fig. 1i). Among all upregulated transcripts in A20$^{Cx3Cr1\text{-}KO}$ microglia, we identified genes linked to cell activation (Cd45, F4/80, Cd86, Cd40, Cd11c), microglia polarization (Cxcl10, C4a/C4b, Tnfsf10, Cxcl9, Ccl2, Ccl5, Tlr1, Il1b), MHC class I (H2k1, H2d1, B2m, H2q7, H2m3, H2q8), type I interferon signaling (Irf-1, Irf-7, Irf-9, Stat1, Stat2, Ifi35, Ifit1, Ifit3, IfitM3), and inflammatory signaling (Nfkb1, Nfkb2, Relb,Il1b, Il12b, Ccl2, Ccl5, Ccl12, Cxcl9, Cxcl10, Cxcl11, Cxcl13) (Fig. 1j). Next, we analysed the expression of 'disease-associated microglia' (DAM) markers that have recently been identified (Keren-Shaul et al., 2017), and demonstrate the significant upregulation of many of these DAM genes (Axl, Cst7, Ctsl, Cd9, Csf1, Itgax, Clec7a, Lilrb4, Timp2, Ctsd, Ctsb) in A20$^{Cx3Cr1\text{-}KO}$ microglia. Network analysis on differentially expressed genes identified 'Antimicrobial response, inflammatory response, cell signaling' as the most differential between both populations, and IPA canonical pathway analysis identified pathways associated with interferon signaling, pattern recognition receptor signaling, complement system and inflammatory signaling as being enriched in A20$^{Cx3Cr1\text{-}KO}$ microglia. Overall, the gene expression analysis suggests that upon A20 deletion microglia decrease their homeostatic 'surveilling' state expression profile, and acquire an inflammatory, disease-associated signature. In conclusion, morphometric 3D analysis and genome signature comparison between microglia from A20$^{Cx3Cr1\text{-}KO}$ and control animals suggests a crucial role for A20 in the control of microglia activation under steady-state conditions, and demonstrates that in the absence of A20 microglia adopt a dysfunctional phenotype.

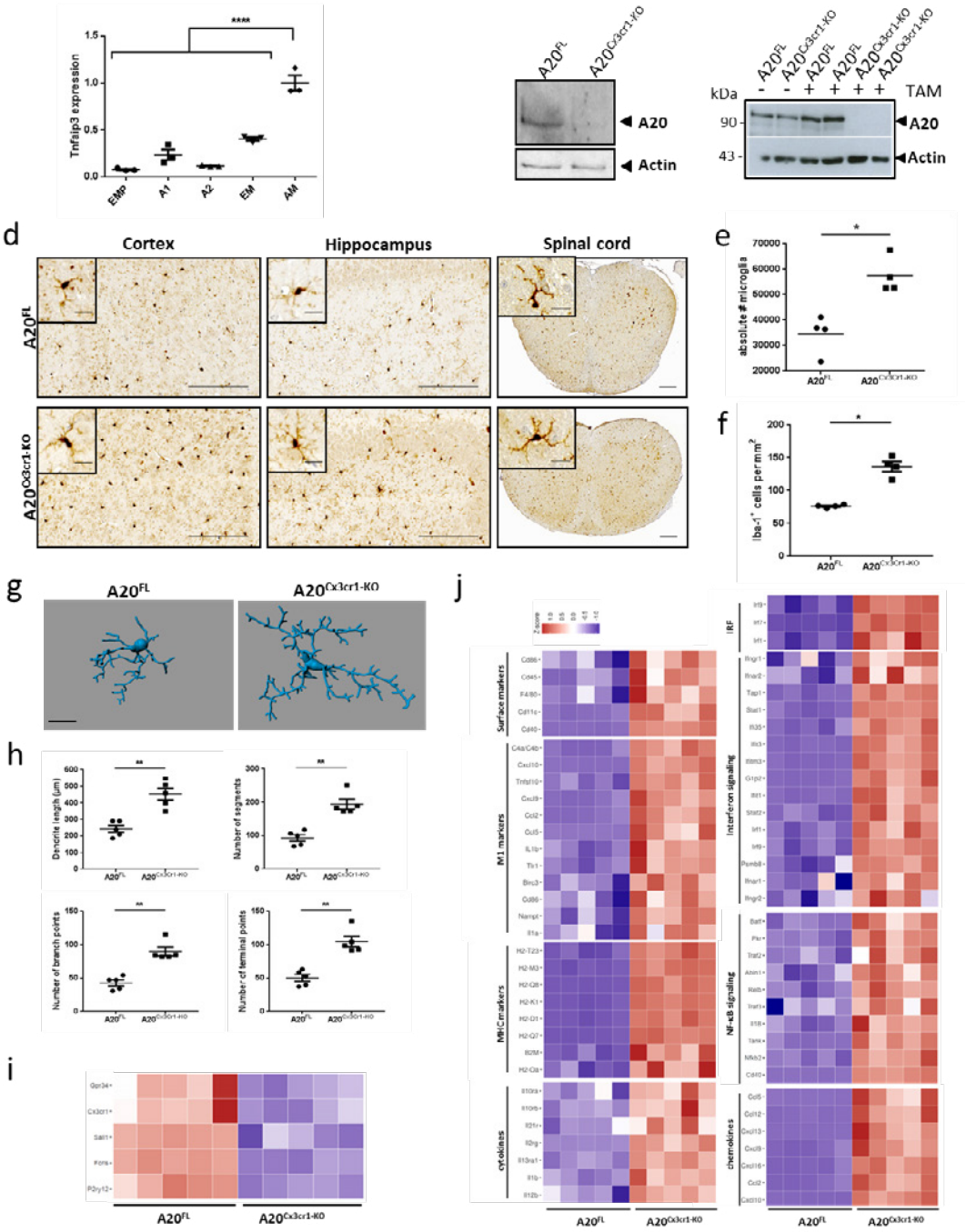

Figure 1. CNS phenotypel of A20$^{Cx3Cr1\text{-}KO}$ mice. (a) A20 expression during microglial cell development. Cells were sorted according to Kierdorf et al, 2013. EMP; Erythromyeloid precursors (yolk sac), A1; immature CD45^{+} c-kit^{lo} Cx3Cr1- cells (yolk sac), A2; mature CD45^{+} c-kit^{-} Cx3Cr1+ cells (yolk sac), EM; embryonic microglia (E14), AM; adult microglia. Each symbol represents one mouse, n=3 per group. Data presented as mean ± SEM. Significant differences determined by a one-way ANOVA with Tukey correction for multiple comparison (**** $p < 0.0001$). (b) Immunoblot for A20 expression on ex vivo FACS-sorted microglia from control (A20^{FL}) and A20$^{Cx3Cr1\text{-}KO}$ mice 4 (left) or 35 weeks (right) after TAM injection. Actin is shown as loading control. (c) Immunoblot for A20 expression on lysates from primary microglia from control (A20^{FL}) and A20$^{Cx3Cr1\text{-}KO}$ mice after stimulation with 4-OH-TAM. Actin is shown as loading control. Data are representative of two independent experiments. (d) Immunohistochemistry for Iba-1+ in the cerebral cortex, hippocampus and spinal cord of control (A20^{FL}) and A20$^{Cx3Cr1\text{-}KO}$ mice. Scale bars: 100 µm (cortex and hippocampus) and 200 µm (spinal cord), insert: 10 µm and 20 µm, respectively. Representative images are displayed. (e) Flow cytometric quantification of the number of CD11b^{+} CD45^{int} microglia in brain of control (A20^{FL}) and A20$^{Cx3Cr1\text{-}KO}$ mice 4 weeks post TAM injection. Each symbol represents one mouse. Data are representative of two independent experiments and presented as mean ± SEM. Significant differences determined by Mann-Whitney U statistical test (* $p < 0.05$). . (f) Number of Iba-1+ ramified parenchymal microglia. Each symbol represents one mouse, with four mice per group. Data presented as mean ± SEM. Significant differences determined by a Mann-Whitney U statistical test (* $p < 0.05$) (g-h) 3D reconstruction (scale bars: 10 µm) (g) and Imaris-based quantification of cell morphology (h) of cortical Iba-1+ microglia. Each symbol represents one mouse; three cells analyzed per mouse; n=5 per condition. Data presented as mean ± SEM. Significant differences determined by a Mann-Whitney U statistical test (** $p < 0.01$). (i-j) RNA sequencing on FACS-sorted microglia from TAM-injected control (A20^{FL}) and A20$^{Cx3Cr1\text{-}KO}$ mice . Each column represents microglia from one individual mouse, n=5 per group. Color code presents linear scale. (i-j) Pathway analysis of RNA-Seq datasets demonstrates downregulation of homeostatic genes (i) and upregulation of genes involved in microglia activation, polarization, MHC class I, interferon and inflammatory signaling (j) in A20$^{Cx3Cr1\text{-}KO}$ microglia.

1.2. A20 deficiency in microglia affects synaptic function

Previous studies indicated that alterations in microglial number or activation can result in functional and structural deficits in cortical circuits (Parkhurst et al., 2013). To evaluate the functional consequences of increased microglial number and/or activation status for neuronal function, we prepared acute slices from P30-35 control and $A20^{Cx3Cr1\text{-}KO}$ mice, and analyzed spontaneous glutamatergic synaptic transmission in layer V pyramidal neurons in S1 cortex. No changes in action potential spiking profiles or intrinsic membrane properties were found between pyramidal neurons from control and $A20^{Cx3Cr1\text{-}KO}$ mice (Fig. 2a), indicating that cell-autonomous parameters are likely unaffected in $A20^{Cx3Cr1\text{-}KO}$ mice. However, we observed a marked increase in spontaneous excitatory postsynaptic current (sEPSC) frequency in $A20^{Cx3Cr1\text{-}KO}$ S1 layer V pyramidal neurons compared to those from control mice (Fig. 2b-e). The robust increase in sEPCS frequency in $A20^{Cx3Cr1\text{-}KO}$ mice with increased microglial number and (hyper)activation is consistent with previous studies showing an increased frequency of spontaneous synaptic transmission following microglia activation18 and a decreased frequency following microglia depletion (Parkhurst et al., 2013). A small, but significant decrease in sEPSC amplitude was also observed (Fig. 2b, f-g), indicating that microglia activation could negatively influence the density of postsynaptic glutamate receptors on dendrites.

Next, to evaluate whether the observed aberrant excitatory synaptic function affects learning and memory, $A20^{Cx3Cr1\text{-}KO}$ and control littermate mice were examined in the hidden platform protocol of the Morris water maze (MWM), a very reliable and robust protocol to investigate hippocampus-dependent spatial learning and memory (Hooghe et al., 2001). Over 10 training days, 6 month old female control and $A20^{Cx3Cr1\text{-}KO}$ mice showed similar learning curves to locate the hidden platform using distal visual cues. Interspersed probe trials on day 6 and 11 showed no difference in spatial reference memory and a robust preference for the correct target quadrant (data not shown). Cognitive flexibility, a measure for executive function, was assessed in a consecutive 5 day reversal training where the platform position was relocated to the opposite quadrant. $A20^{Cx3Cr1\text{-}KO}$ and control mice showed similar learning curves (repeated measures 2-way ANOVA for factor day: $F(4,76)=16.8$; $p<0.0001$) (Fig. 2h). Interestingly, during the reversal probe trial only control mice showed a significant preference for the target quadrant over the other three quadrants (repeated measures 2-way ANOVA for factor quadrant preference: $F(3, 57)=11,4$; $p<0.0001$) (Fig. 2i) and were at any given time point significantly closer to the location of the reversal platform than to the location of the acquisition platform (expressed as total distance to target) (2-way ANOVA for factor platform location: $F(1,38)=14,36$; $p=0.0005$) (Fig. 2j). Together these findings indicate that after 5 days of reversal learning, $A20^{Cx3Cr1\text{-}KO}$ mice do not have a robust spatial representation of the platform's correct location and were not capable of forming a robust reference memory. Together, these results show that the aberrantly activated microglia in $A20^{Cx3Cr1\text{-}KO}$ mice affect excitatory synaptic function with consequences for proper cognitive function.

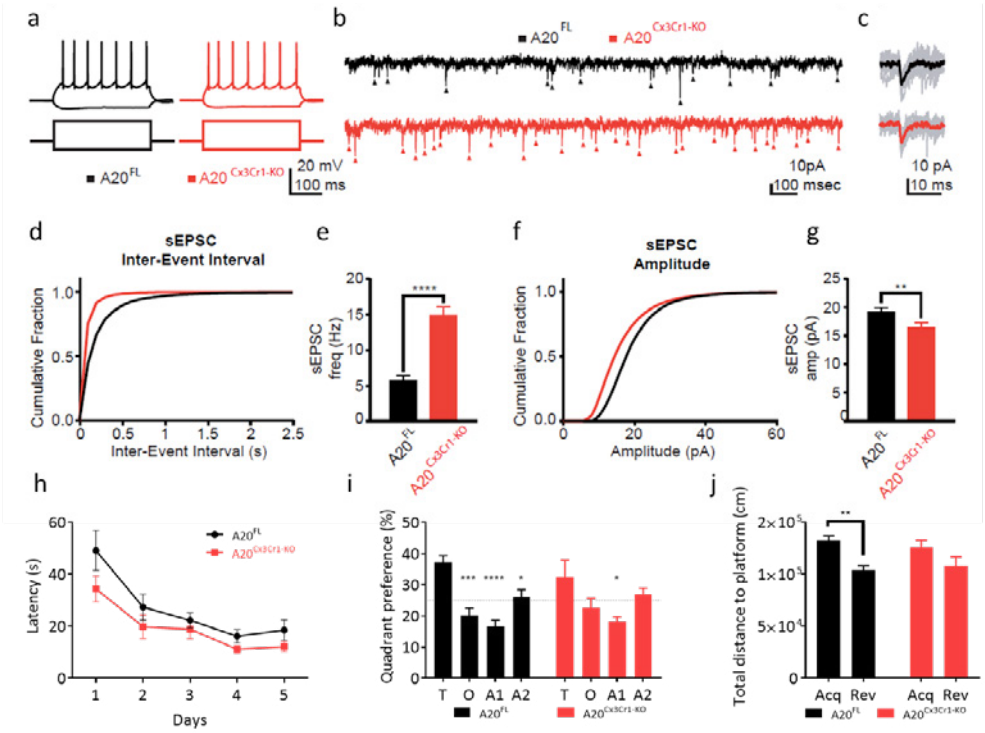

Figure 2. Effect of microglia hyperactivation on basal network activity in somatosensory pyramidal neurons. (a) Example action potential (AP) firing profiles, showing the typical regular spiking behavior of layer V S1 pyramidal neurons both in control and in A20$^{Cx3Cr1\text{-}KO}$ neurons. Responses to hyperpolarizing (-150 pA) and suprathreshold (400 pA) current injections are shown. (b) Example sEPSC traces, 2s stretches. (c) Examples of individual sEPSC events. Individual events shown in grey, averaged event shown as overlay (control, black; A20$^{Cx3Cr1\text{-}KO}$, red). (d) Cumulative probability distributions of inter-event sEPSC intervals (IEIs) for control (black) or A20$^{Cx3Cr1\text{-}KO}$ (red) cells. (e) sEPSC frequency (Control (black) 5.76 ± 0.58 Hz, n/m=21/3; A20$^{Cx3Cr1\text{-}KO}$ (red) 14.8 ± 1.29 Hz, n/m=20/3; **** $p < 0.0001$). Data represents means ± SEM. Number of cells (n), number of animals (m). Statistical differences were determined by a two-tailed Wilcoxon matched-paired t-test. (f) Cumulative probability distributions for sEPSC amplitudes in control (black) or A20$^{Cx3Cr1\text{-}KO}$ (red) cells. (g) sEPSC amplitudes. (Control 19.3 ± 0.69 pA, n/m=21/3; A20$^{Cx3Cr1\text{-}KO}$ 16.5 ± 0.87 pA, n/m=20/3; ** $p=0.0013$). Data represents means ± SEM. Number cells (n), number of animals (m). Statistical differences were determined by a two-tailed unpaired Mann-Whitney t-test. (h) Cognitive flexibility in Morris water maze reversal learning was similar in control (A20FL, n=12) and A20$^{Cx3Cr1\text{-}KO}$ mice (n=9). (i) In the reversal probe trial, controls displayed significant target quadrant preference, while A20$^{Cx3Cr1\text{-}KO}$ mice did not (T: target quadrant, O: opposite quadrant, A1: adjacent 1 quadrant, A2: adjacent 2 quadrant). Chance level at 25 % is indicated. (j) During the reversal probe trial, control animals searched closer to the correct reversal location for the platform than to the old location (distance to platform), while A20$^{Cx3Cr1\text{-}KO}$ mice searched at equidistance to both locations. All data (h-j) are represented as means ± SEM and statistical differences were determined by repeated-measures two-way ANOVA (h-i) and two-way ANOVA (j) using Bonferroni correction for post hoc analysis (h-j) (* $p<0.05$, ** $p<0.01$, *** $p<0.001$, **** $p<0.0001$).

1.3. A20 in microglia protects against LPS-induced inflammation

Microglia are the CNS-resident immune cells acting as the first responders to microbial infections of the brain (Waisman et al., 2015). To investigate the importance of A20 for microglia function in a model of neuroinflammation, A20$^{Cx3Cr1\text{-}KO}$ and control littermate mice were injected with a single sublethal dose of the TLR4 agonist lipopolysaccharide (LPS), known to induce neuroinflammation through microglia activation and expression of pro-inflammatory cytokines (Qin et al., 2007). Surprisingly, in contrast to control mice, which only exhibit a modest drop in body temperature in the first hours after systemic LPS injection, A20$^{Cx3Cr1\text{-}KO}$ mice displayed severe hypothermia (Fig. 3a) and increased mortality (Fig. 3b). Histological analysis of the CNS 10 hours after systemic LPS administration, a time point at which all A20$^{Cx3Cr1\text{-}KO}$ mice are still alive, demonstrated increased microgliosis in A20$^{Cx3Cr1\text{-}KO}$ brain and spinal cord compared to control tissue (Fig. 3c). Since A20 knockout mice with A20 deficient microglia already spontaneously display a pro-inflammatory phenotype characterized by microglia hyperproliferation (Fig. 1), no further effect on microglia proliferation is seen after LPS (Fig. 3d). Microglia morphology analysis 10 hours post LPS suggests a reactive phenotype in A20$^{Cx3Cr1\text{-}KO}$ mice compared to wild type littermates, as evidenced by a significantly higher number of processes, branching points, terminal point and segments. (Fig 3e-f). In agreement, significantly elevated levels of inflammatory cytokines were detected in CNS tissue and cerebrospinal fluid (CSF) of A20$^{Cx3Cr1\text{-}KO}$ relative to littermate A20^{FL} mice after systemic LPS challenge (Fig. 3g). Finally, microglia from LPS-injected A20$^{Cx3Cr1\text{-}KO}$ and A20^{FL} control

mice were isolated and global gene expression was determined by RNA sequencing. Investigation of the gene ontology enrichment network on differentially expressed genes revealed that inflammatory pathways are highly affected in LPS-stimulated microglia compared to unstimulated microglia, as expected (data not shown). However, 2774 genes were differentially expressed between $A20^{Cx3Cr1\text{-}KO}$ and control microglia isolated 10 h after systemic LPS injection (cut-off: $p < 0.01$ and at fold change ≥4; 1609 upregulated, 1165 downregulated in $A20^{Cx3Cr1\text{-}KO}$ compared to control), and LPS-stimulated $A20^{Cx3Cr1\text{-}KO}$ microglia expressed much higher levels of inflammatory cytokine and chemokine pathways compared to LPS-stimulated control microglia, demonstrating their hyperactivation (Fig. 3h). Together, these results demonstrate that A20 expression in microglia controls inflammatory CNS responses and is essential to prevent a detrimental response to LPS-induced neuroinflammation.

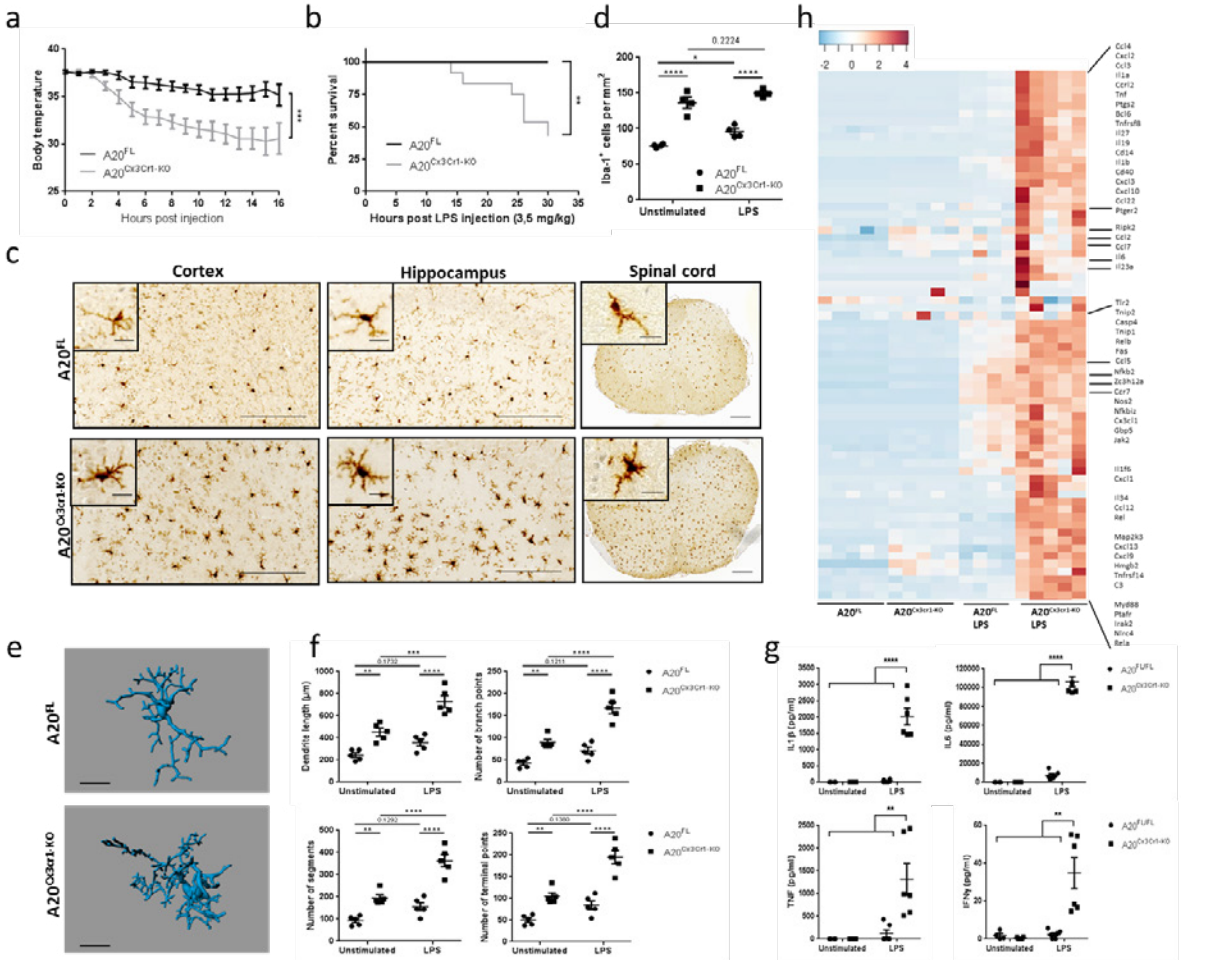

Fig

Figure 3. $A20^{Cx3Cr1\text{-}KO}$ mice are hypersensitive to LPS. (a) Rectal body temperature responses and (b) survival were analyzed in function of time in control ($A20^{FL}$; n=13) and $A20^{Cx3Cr1\text{-}KO}$ (n=14) mice after intraperitoneal injection of 3.5 mg/kg LPS. The combined results of three independent experiments are shown. Body temperature data are means ± SEM. Statistical differences were determined by a REML analysis for rectal body temperatures and a Mantel-Cox test for the survival curve (** $p < 0.01$, *** $p < 0.001$). (c) Immunohistochemistry images showing Iba-1+ expression in the cerebral cortex, hippocampus and spinal cord of control ($A20^{FL}$) and $A20^{Cx3Cr1\text{-}KO}$ mice 10 hours post LPS challenge. Scale bars represent 100 µm (cortex and hippocampus) and 200 µm (spinal cord), insert: 10µm and 20 µm, respectively. Representative images are displayed. Data are representative of two independent experiments. (d) Number of Iba-1+ ramified parenchymal microglia in brain. Each symbol represents data from one mouse, n=4 per group. Data are presented as mean ± SEM. Significant differences were determined by a two-way ANOVA with Tukey correction for multiple comparison. (* $p < 0.05$, **** $p < 0.0001$) (e-f) Three-dimensional reconstruction (scale bars represent 10 µm, e) and Imaris-based semi-automatic quantification of cell morphology (f) of cortical Iba-1+ microglia. Each symbol represents the average of three measured cells per mouse; n = 5 per group. Data are presented as mean ± SEM. Significant differences were determined by two-way ANOVA with Tukey correction for multiple comparison (** $p < 0.01$, *** $p < 0.001$, **** $p < 0.0001$). (g) Bioplex analysis of cytokine levels in CSF 10 hours post LPS. Each symbol represents one mouse. Data are representative of three independent experiments. Significant differences were determined by a one-way ANOVA with Tukey correction for multiple comparison (** $p < 0.01$, **** $p < 0.0001$). (h) RNA prepared from FACS-sorted microglia from control ($A20^{FL}$) and $A20^{Cx3Cr1}$ mice either or not injected with LPS for 10 h was submitted for RNA sequencing. Heat map of expression values for inflammatory genes that are upregulated in LPS stimulated $A20^{Cx3Cr1}$ microglia compared to LPS stimulated control microglia. Each column represents microglia data from one individual mouse, with four or five mice per group. Color code presents linear scale.

1.4. Nlrp3 inflammasome hyperactivation in A20-deficient microglia

An inflammatory cytokine that was significantly upregulated in microglia from LPS stimulated A20$^{Cx3Cr1\text{-}KO}$ mice and can be detected in the CSF of A20$^{Cx3Cr1\text{-}KO}$ mice was IL-1β (Fig. 3g-h). LPS induced a strong upregulation of pro-IL-1β in both control and A20$^{Cx3Cr1\text{-}KO}$ microglia compared to non-injected mice, however, this upregulation is significantly stronger in microglia from LPS-injected A20$^{Cx3Cr1\text{-}KO}$ mice compared to LPS-injected control mice (Fig. 4a). IL-1β is the prototype cytokine secreted by cells upon activation of inflammasomes, multi-protein complexes that enable the activation of caspase-1 leading to the processing and secretion of biologically active IL-1β. Also IL-18 is produced through the activation of inflammasomes (Lamkanfi and Dixit, 2014), however, no difference in IL-18 expression could be observed between FACS-sorted microglia from LPS-injected A20$^{Cx3Cr1\text{-}KO}$ and control mice (data not shown). Microglia are capable of engaging different inflammasome types in response to infectious agents and host-derived danger signals that are associated with neurological diseases (Walsch et al., 2014). To study the contribution of inflammasome signaling to inflammatory responses of A20$^{Cx3Cr1\text{-}KO}$ microglia, we assessed caspase-1 processing in primary cultured microglia isolated from A20$^{Cx3Cr1\text{-}KO}$ and control littermate mice. Secreted levels of IL-1β and IL-18 were significantly increased in LPS-primed A20$^{Cx3Cr1\text{-}KO}$ microglia that were treated with soluble (ATP and nigericin) or crystalline (silica) stimuli of the Nlrp3 inflammasome compared to control microglia (Fig. 4b). In accordance, caspase-1 autoprocessing was substantially increased in A20$^{Cx3Cr1\text{-}KO}$ relative to control microglia (Fig. 4c). Besides their roles in maturation and secretion of IL-1β and IL-18, a major effector mechanism of inflammasomes is the induction of pyroptosis, a pro-inflammatory and lytic mode of cell death occurring mainly in myeloid cells including microglia (Walsch et al., 2014). Pyroptosis induces cell swelling and rupture of the plasma membrane, causing massive leakage of cytosolic contents provoking inflammatory reactions. Similarly to the effect on caspase-1 autoprocessing and IL-1β/IL-18 secretion, the induction of cell death was also enhanced in A20$^{Cx3Cr1\text{-}KO}$ microglia (Fig. 4d). Activation of the Nlrp3 inflammasome, one of the most pleiotropic inflammasomes, requires a priming signal that results in the upregulation of Nlrp3 expression along with the inflammasome substrate proIL-1β via the pro-inflammatory transcription factor NF-κB (Bauernfiend et al., 2009). A20 negatively regulates Nlrp3 inflammasome signaling by suppressing NF-κB-dependent production of Nlrp3 and proIL-1β in macrophages (Vande Walle et al., 2014). Indeed, a pharmacological inhibitor of IKK2, TPCA-1, significantly reduced ATP-induced caspase-1 autoprocessing and IL-1β secretion in LPS-primed A20$^{Cx3Cr1\text{-}KO}$ microglia (Fig. 4e-f). Together, these results demonstrate that A20 negatively controls Nlrp3 inflammasome priming and activation in microglia.

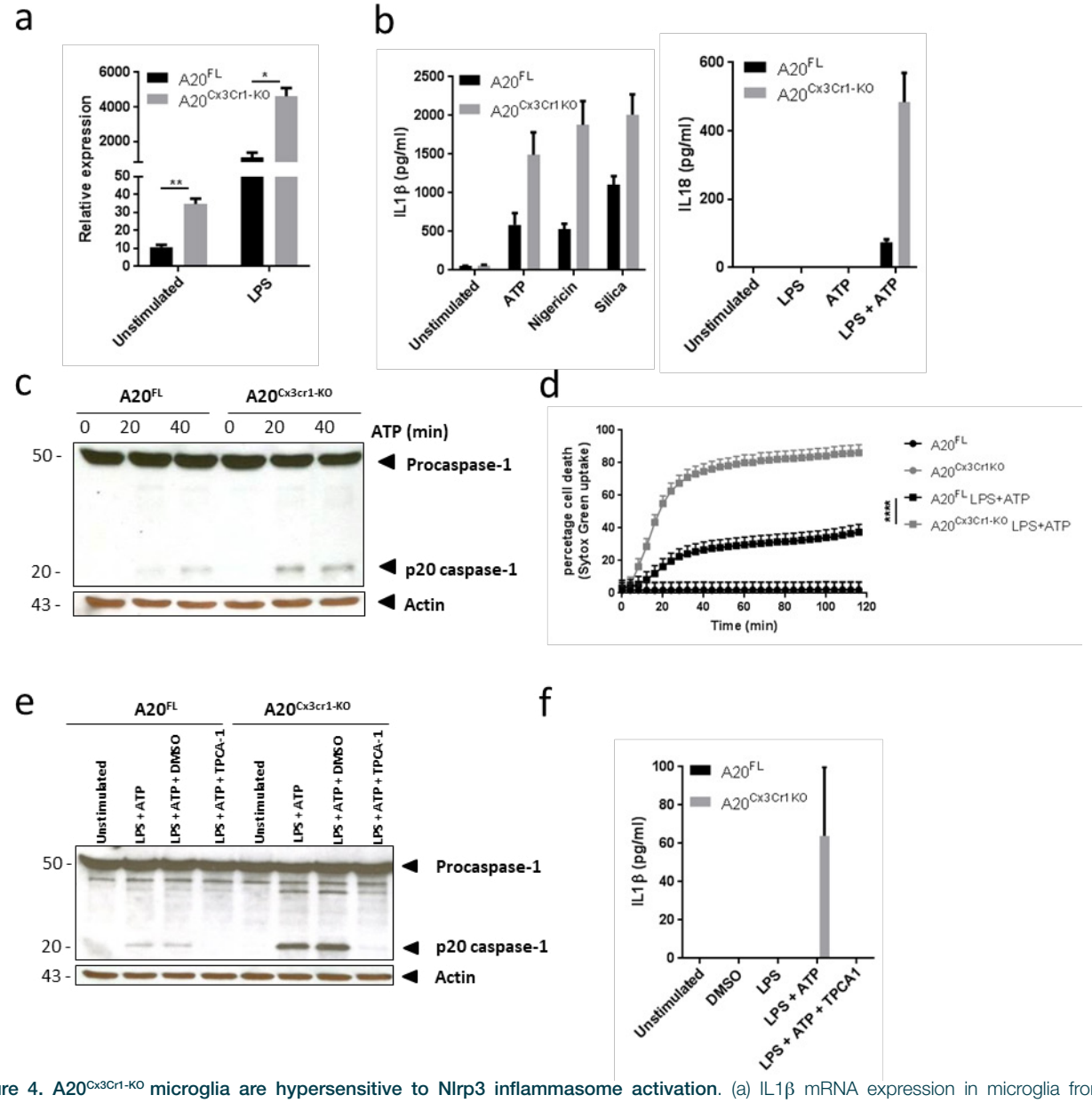

Figure 4. A20$^{Cx3Cr1-KO}$ microglia are hypersensitive to Nlrp3 inflammasome activation. (a) IL1β mRNA expression in microglia from A20$^{Cx3Cr1-KO}$ mice compared to control mice either or not injected with LPS. Each symbol represents an individual mouse. Data are presented as mean ± SEM. Significant differences were determined by a Mann-Whitney t-test (* $p < 0.05$, ** $p < 0.01$). (b) IL1β and IL18 protein levels in the supernatant of primary cultured microglia stimulated with LPS alone or together with ATP, Silica or Nigericin. Data represent the mean ± SD of three technical replicates of pooled microglial cells from control (A20^{FL}) and A20$^{Cx3Cr1-KO}$ mice. Data are representative of three independent experiments. (c) Immunoblot for procaspase-1 and cleaved caspase-1 (p20) in primary cultured microglia from control (A20^{FL}) and A20$^{Cx3Cr1-KO}$ mice stimulated with LPS and/or ATP. Actin is shown as loading control. Data are representative of two independent experiments. (d) Pyroptosis induction in primary microglia from control (A20^{FL}) and A20$^{Cx3Cr1-KO}$ mice stimulated with LPS and ATP, as measured by Sytox Green uptake. Data are presented as mean ± SEM and are representative of two independent experiments. Significant differences were determined by a REML analysis (**** $p < 0.0001$). (e) Immunoblot showing procaspase-1 and cleaved caspase-1 in primary cultured microglia from control (A20^{FL}) and A20$^{Cx3Cr1-KO}$ mice either or not pretreated *in vitro* with TPCA-1 and stimulated with LPS and/or ATP. Actin is shown as loading control. Data are representative of two independent experiments. (f) IL1β protein in supernatant of primary cultured microglia from control (A20^{FL}) and A20$^{Cx3Cr1-KO}$ mice either or not pretreated *in vitro* with TPCA-1 and stimulated with LPS and/or ATP. Data represent the mean ± SD of three technical replicates of pooled microglial cells, and are representative of two independent experiments.

1.5. Mice with A20-deficient microglia are hypersensitive to EAE

Based on our results, we investigated the microglia-specific function of A20 in a model of autoimmune CNS inflammation, namely experimental autoimmune encephalomyelitis (EAE). A20$^{Cx3Cr1-KO}$ and control mice were immunized with a myelin oligodendrocyte glycoprotein (MOG) peptide (MOG35-55) and disease progression was monitored by assessing clinical disease symptoms and body weight (Fig. 5a-b). Both A20$^{Cx3Cr1-KO}$ and control mice developed EAE, however, A20$^{Cx3Cr1-KO}$ mice developed earlier disease onset and exhibited a more severe disease course as compared to control mice (Fig. 5a-b),

demonstrating a crucial role for microglia A20 activity in EAE pathogenesis. In contrast, A20 deletion in other CNS cell types (all CNS progenitor cells, neurons, astrocytes or oligodendrocytes) did not result in differences in EAE clinical pathology (data not shown). Clinical pathology in $A20^{Cx3Cr1\text{-}KO}$ was confirmed by histology and flow cytometry on spinal cord sections at start of the clinical manifestations, showing extensive demyelination, axonal damage, inflammation and immune cell infiltration in $A20^{Cx3Cr1\text{-}KO}$ mice, while nearly no immune cell infiltration, demyelination or axonal loss could be detected in the spinal cord of control mice at this early time-point (Fig. 5c-d). As A20 deficiency enhances the activation of the Nlrp3 inflammasome in isolated primary microglia (Fig. 4), we speculated that the hyperactivation of the Nlrp3 inflammasome is responsible for the aggravated EAE phenotype in $A20^{Cx3Cr1\text{-}KO}$ mice. Indeed, gene expression analysis of spinal cord tissue showed enhanced expression of pro-IL-1b, ASC, Nlrp3 and caspase-1 in $A20^{Cx3Cr1\text{-}KO}$ mice compared to control mice, suggesting a contribution of inflammasome activities in the observed phenotype (Fig. 5e). To test this hypothesis, Nlrp3–/– mice were crossed with $A20^{Cx3Cr1\text{-}KO}$ mice and EAE disease development was monitored. In contrast to $A20^{Cx3Cr1\text{-}KO}$ mice, which develop a more severe pathology, $A20^{Cx3Cr1\text{-}KO}$-Nlrp3–/– mice show a significantly reduced clinical pathology, comparable to control $A20^{FL}$ littermate mice (Fig. 5f). These results are in line with previous studies demonstrating a critical role for Nlrp3 in the development of EAE by mediating peripheral immune responses (Gris et al., 2010; Shaw et al., 2010). However, $Nlrp3^{-/-}$ mice lack the Nlrp3 protein ubiquitously, and the specific contribution of inflammasome signaling inside the CNS to EAE pathogenesis is unknown. To study the specific function of inflammasomes within microglia during EAE, caspase-1 conditional knockout mice having a floxed allele (Caspase-1^{FL}) were generated (Van Gorp et al., 2016) and crossed with $A20^{Cx3Cr1\text{-}KO}$ mice to produce mice lacking both A20 and caspase-1 in microglia (caspase-1-$A20^{Cx3Cr1\text{-}KO}$). In contrast to single $A20^{Cx3Cr1\text{-}KO}$ mice, caspase-1/$A20^{Cx3Cr1\text{-}KO}$ mice developed less severe disease upon immunization with MOG35-55 peptide (Fig. 5g). Together, these results demonstrate the role of A20 in the control of Nlrp3 inflammasome activation locally in microglia, and indicate the importance of this microglial A20/Nlrp3 inflammasome axis in EAE pathogenesis.

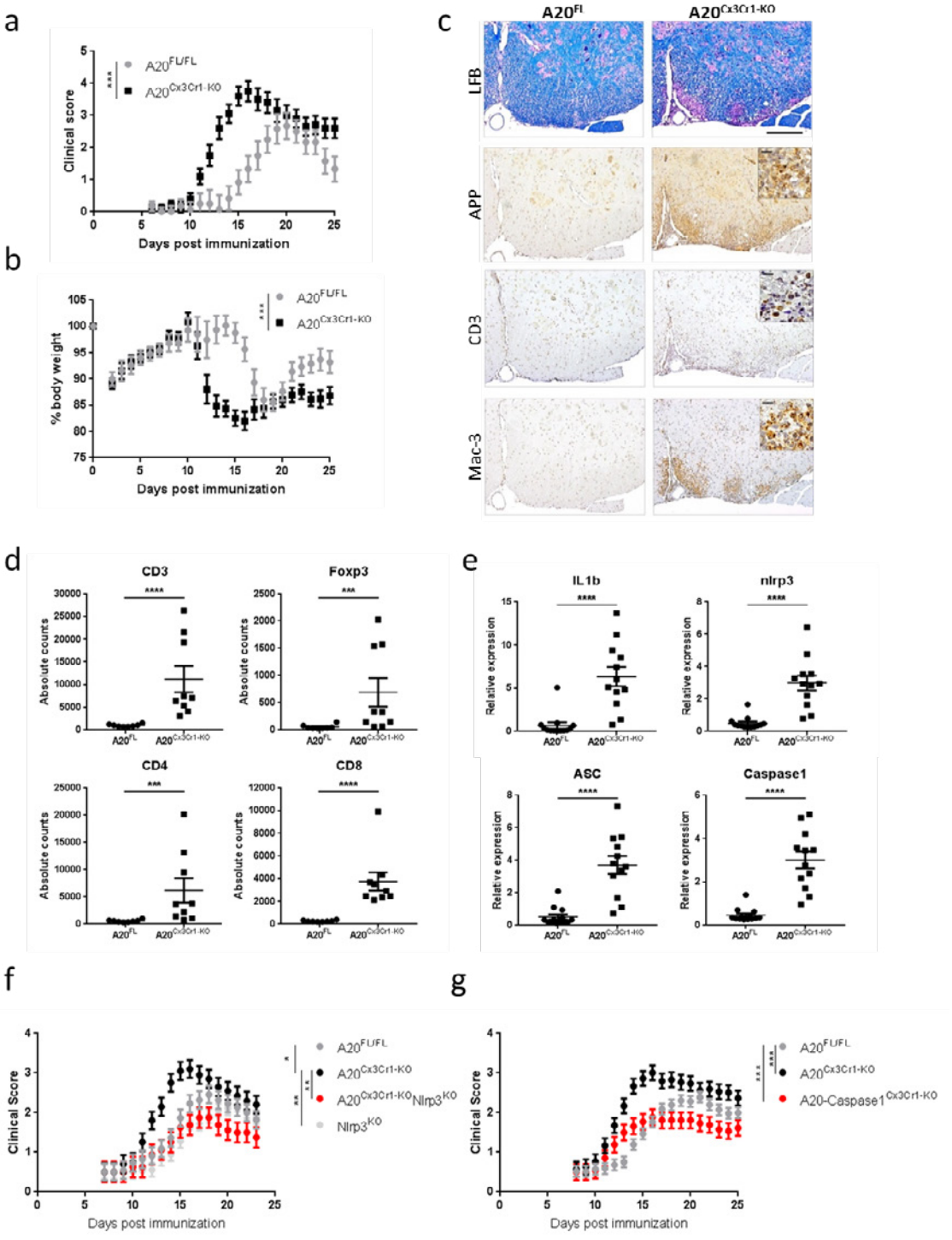

Figure 5. Microglia A20 deficiency aggravates autoimmune CNS inflammation due to Nlrp3 inflammasome hyperactivation. (a-b) EAE was induced by active immunization of control $A20^{FL}$ (n=6) and $A20^{Cx3Cr1\text{-}KO}$ mice (n=10) with MOG peptide, and clinical disease development (a) and body weight (b) was followed over time. Each data point represents the mean ± SEM as estimated by the REML analysis. Changes in clinical score and relative body weight differ significantly (*** $p < 0.001$; F-test) between genotypes across the time span. Data are representative of three independent experiments. (c) Representative images of spinal cord of control ($A20^{FL}$) and $A20^{Cx3Cr1\text{-}KO}$ mice 13 days post-immunization using LFB, APP, CD3 and MAC-3 antibodies. Scale bars represent 200 µm (overview) and 20 µm (zoom). Representative images from at least four mice per group are displayed. (d) Assessment of immune cell (CD3, CD4 and CD8 T cell, Treg) infiltration in the CNS of control ($A20^{FL}$) and $A20^{Cx3Cr1\text{-}KO}$ mice by flow cytometry just before disease onset. Each symbol represents one mouse. Data are expressed as mean ± SEM and significant differences are determined by a Mann-Whitney U statistical test (*** $p < 0.001$, **** $p < 0.0001$). (e) Expression of inflammasome-associated factors in the spinal cord of TAM-injected control ($A20^{FL}$) and $A20^{Cx3Cr1\text{-}KO}$ mice 12 days post immunization. Each symbol represents one mouse. Data are expressed as the ratio of the mRNA expression normalized to endogenous housekeeping genes and expressed as mean ± SEM. Significant differences are determined by a Mann-Whitney U statistical test (**** $p < 0.0001$). (f-g) Active immunization of control ($A20^{FL}$, n=11), $A20^{Cx3Cr1\text{-}KO}$ (n=10), $Nlrp3^{KO}$ (n=18) and $A20^{Cx3Cr1\text{-}KO}$-$Nlrp3^{KO}$ (n=8) mice (f) and of control ($A20^{FL}$, n=28), $A20^{Cx3Cr1\text{-}KO}$ (n=15) and A20/$Caspase1^{Cx3Cr1\text{-}KO}$ (n=13) mice (g), and clinical disease development over time. Each data point represents the mean ± SEM as estimated by the REML analysis. Changes in clinical score and relative body weight differ significantly between genotypes across the time span(* $p < 0.05$, ** $p < 0.01$, *** $p < 0.001$; F test). Graph represents combined data from three independent experiments.

Finally, to investigate the relevance of our findings to human CNS pathology, post-mortem brain tissue and CSF of multiple sclerosis (MS) patients were analyzed for expression of A20 and for the presence of an inflammasome 'signature'. Expression of A20/TNFAIP3, as well as the expression levels of IL-1β and NLRP3 were significantly increased in MS plaques compared to NAWM (Normal appearing white matter), and a trend, albeit not significant, in enhanced IL-18 and caspase-1 in MS plaques could be observed (Fig. 6a-b). Higher IL-18 and IL-1β protein levels were also detected in CSF of MS patients compared to controls, suggestive of inflammasome activation in microglia, although also other immune cells may have contributed to this (Fig. 6c). Our data analyzing the expression levels of inflammasome mediators in brain plaques isolated from normal and MS patients show that brain tissue affected by MS clearly exhibits enhanced activation of the NLRP3 inflammasome, as shown in previous studies.

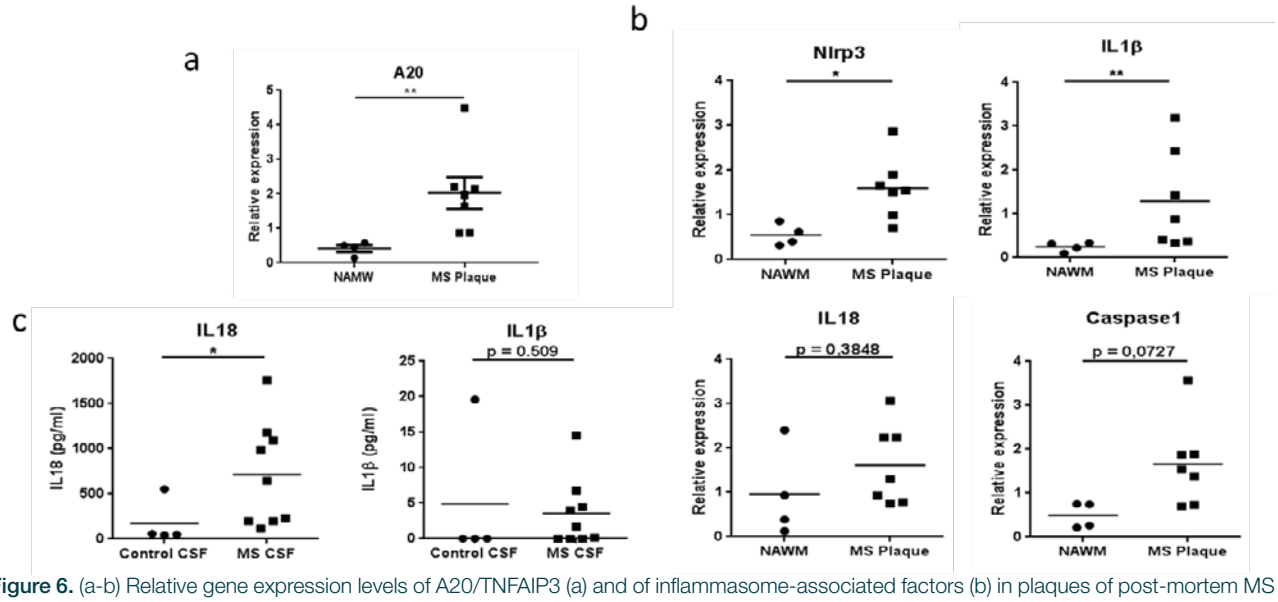

Figure 6. (a-b) Relative gene expression levels of A20/TNFAIP3 (a) and of inflammasome-associated factors (b) in plaques of post-mortem MS patients (Plaque) or post-mortem control tissue (NAWM). Each symbol represents one patient. Data are expressed as the ratio of the mRNA expression normalized to endogenous housekeeping genes (Sdha and Tbp) and expressed as mean ± SEM. Significant differences are determined by Mann-Whitney U statistical test (* $p < 0.05$, ** $p < 0.01$). (c) IL1β and IL18 cytokine levels in the CSF of post-mortem MS patients or control samples. Each symbol represents one CSF sample. Significant differences are determined by Mann-Whitney U statistical test (* $p < 0.05$).

In summary, we found that A20 critically controls microglia activation both in steady-state as in conditions of neuroinflammation. In experimental models of neuroinflammation, the expression of A20 by microglia is crucial in keeping NLRP3 inflammasome activation at bay. These results may contribute to a better understanding and treatment of inflammatory and neurodegenerative diseases. Strategies targeting microglia to suppress their activation eventually through expression of A20 might prove useful for the treatment of these diseases.

2. References

- Bauernfeind FG, Horvath G, Stutz A, et al. Cutting edge: NF-kappaB activating pattern recognition and cytokine receptors license NLRP3 inflammasome activation by regulating NLRP3 expression. J Immunol. 183(2), 787-791 (2009).
- Goldmann T, Wieghofer P, Müller PF, et al. A new type of microglia gene targeting shows TAK1 to be pivotal in CNS autoimmune inflammation. Nat Neurosci. 16(11), 1618-1626 (2013).
- Gris D, Ye Z, Iocca HA, et al. NLRP3 plays a critical role in the development of experimental autoimmune encephalomyelitis by mediating Th1 and Th17 responses. J Immunol. 185(2), 974-981 (2010).
- Hooge RD, Deyn PP De. Applications of the Morris water maze in the study of learning and memory. Brain Res Rev. 36(1), 60-90 (2001).
- Keren-shaul H, Spinrad A, Weiner A, et al. A Unique Microglia Type Associated with Restricting Development of Alzheimer ' s Disease. Cell. 169(7), 1276-1290 (2017).
- Kierdorf K, Erny D, Goldmann T, et al. Microglia emerge from erythromyeloid precursors via Pu.1- and Irf8-dependent pathways. Nat Neurosci. 16(3), 273-280 (2013).
- Lamkanfi M, Dixit VM. Mechanisms and functions of inflammasomes. Cell. 157(5), 1013-1022 (2014).
- Parkhurst CN, Yang G, Ninan I, et al. Microglia Promote Learning-Dependent Synapse Formation through Brain-Derived Neurotrophic Factor. Cell. 155(7), 1596-1609 (2013).
- Shaw PJ, Lukens JR, Burns S, Chi H, McGargill MA, Kanneganti T-D. Cutting edge: critical role for PYCARD/ASC in the development of experimental autoimmune encephalomyelitis. J Immunol. 184(9), 4610-4614 (2010).
- Vande Walle L, Van Opdenbosch N, Jacques P, et al. Negative regulation of the NLRP3 inflammasome by A20 protects against arthritis. Nature. 512(7512), 69-73 (2014).
- Van Gorp H, Saavedra PH V, Vasconcelos NM De, Opdenbosch N Van. Familial Mediterranean fever mutations lift the obligatory requirement for microtubules in Pyrin inflammasome activation. Proc Natl Acad Sci U S A. 113(50), 5-10 (2016).
- Vereecke L, Sze M, Guire CM, et al. Enterocyte-specific A20 deficiency sensitizes to tumor necrosis factor-induced toxicity and experimental colitis. J Exp Med. 207(7), 1513-1523 (2010).
- Waisman A, Ginhoux F, Greter M, Bruttger J. Homeostasis of Microglia in the Adult Brain: Review of Novel Microglia Depletion Systems. Trends Immunol. 36(10), 625-636 (2015).
- Walsh JG, Muruve DA, Power C. Inflammasomes in the CNS. Nat Rev Neurosci. 15(2), 84-97 (2014).
- Qin L, Wu X, Block ML, et al. Systemic LPS causes chronic neuroinflammation and progressive neurodegeneration. Glia. 55(5), 453-462 (2007).
- Zhang Y, Chen K, Sloan SA, et al. An RNA-Sequencing Transcriptome and Splicing Database of Glia, Neurons, and Vascular Cells of the Cerebral Cortex. J Neurosci. 34(36), 11929-11947 (2014).

3. Publications van Loo group 2018 (acknowledging GSKE support)

- Voet, S., Prinz, M. and **van Loo, G.** Microglia in central nervous system inflammation and multiple sclerosis pathology. Trends in Molecular Medicine, in press. (IF : 11.0)
- Voet, S., Mc Guire, C., Hagemeyer, N., Martens, A., Schroeder, A., Wieghofer, P., Daems, C., Staszewski, O., Vande Walle, L., Costa Jordao, M.J., Sze, M., Vikkula, H., Demeestere, D., Van Imschoot, G., Scott, C.L., Hoste, E., Gonçalves, A., Guilliams, M., Lippens, S., Libert, C., Vandenbroucke, R., Kim, K.W., Jung, S., Callaerts-Vegh, Z., Callaerts, P., de Wit, J., Lamkanfi, M., Prinz, M. and **van Loo, G**. (2018) A20 critically controls microglia activation and inhibits inflammasome-dependent neuroinflammation. Nature Communications, 9 (1), 2036. (IF : 13.1)
- Slowicka, K. and **van Loo, G.** (2018) Optineurin functions for Optimal immunity. Frontiers Immunology, 9, 769. (IF : 6.42)
- Catrysse, L. and **van Loo, G.** (2018) Adipose tissue macrophages and their polarization in health and obesity. Cellular Immunology, 330, 114-119. (IF : 3.17)

Geneeskundige Stichting Koningin Elisabeth
Fondation Médicale Reine Elisabeth
Königin-Elisabeth-Stiftung für Medizin
Queen Elisabeth Medical Foundation

Progress report of the research group of

Prof. dr. Verfaillie Catherine

Katholieke Universiteit Leuven (KU Leuven)

Principal investigator

Prof. dr. Verfaillie Catherine
Interdepartementaal Stamcel Instituut
Katholieke Universiteit Leuven
UZ Gasthuisberg
Herestraat 49
3000 Leuven
Belgium
Tel.: +32 16 33 02 95
Fax: +32 16 33 02 94
E-mail: catherine.verfaillie@med.kuleuven.be

Unraveling the Role of TREM2 Mutations in Alzheimer's Disease using Human Pluripotent Stem Cells

As described in previously submitted report in 2017, we have successfully:

1. Created *TREM2 R47H HE, TREM2*$^{+/-}$ and *TREM2*$^{-/-}$ hPSC lines using CRISPR/Cas9 mediated genome engineering technology.
2. Differentiated *TREM2 R47H HE, TREM2*$^{+/-}$ and *TREM2*$^{-/-}$ hPSC lines to monocytes and microglia-like cells using the Yanagimachi protocol.
3. Showed that the *TREM2*$^{+/-}$ and *TREM2*$^{-/-}$ hPSC-derived monocytes and tMG reveal a severe reduction of phagocytic capacity compared to *wt,* in contrast to minimal effects observed for *R47H HE* hPSC-derived monocytes and tMG.
4. Demonstrated, to our knowledge, the first evidence for defective amyloid phagocytosis caused by heterozygous or homozygous loss of *TREM2* in hPSC-derived monocytes and tMG.

The above results represent several key milestones achieved for the ***AIM 1: Generate TREM2 mutant hPSC lines and assess their phagocytic ability.***

In this report, we present new experiment data obtained that further fulfilling the *AIM 1* and provide an update on the progress made for *AIM2* and *AIM 3*:

1. AIM 1: Generate TREM2 mutant hPSC lines and assess their phagocytic ability.

Comparison of RNA sequencing data between hPSC-derived tMGs, hPSC monocytes and PB monocytes.

Previously, we reported that the typical microglial transcripts were not higher expressed in the generated hPSC-derived tMGs (except for TREM2, APOE, and CSF1R) as compared to hPSC monocytes, while the marker of definitive bone marrow–derived macrophages (i.e. CD45) was lower in tMGs (including hPSC monocytes) than PB monocytes. Nevertheless, the tMGs expressed significantly lower levels of the monocyte gene CCR2 and the monocyte-specific transcription factor KLF4 than hPSC monocytes and PB monocytes. Thus, this limited transcriptional analysis suggested that hPSC-derived tMGs resemble microglia. Surprisingly, monocytes derived via the Yanagimachi protocol from hPSCs were more similar to tMGs than PB monocytes.

To further corroborate these findings, we performed genome-wide RNA sequencing (RNAseq) studies, where we compared hPSC-derived tMGs and hPSC-derived monocytes generated in this study with the RNAseq data from Abud *et al.*, 2017. Principal component analysis of both data sets demonstrated that tMGs (*indicated as tMG; light blue circles*) and hPSC monocytes (*indicated as MC; dark-red circles*) generated from our study clustered together with *in vitro* cultured human fetal microglia (*indicated as fMG; light-purple circles*) and adult human microglia (*indicated as aMG; yellow circles*), and with hPSC-induced microglia-like cells (*indicated as iMGLs; light-green circles*), but not with CD141 PB monocytes (***Fig. 1***).

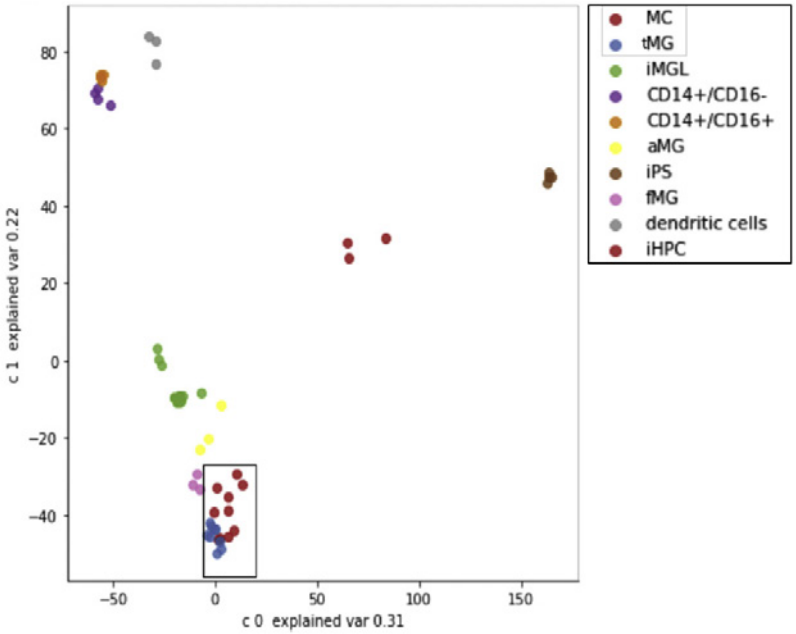

Figure 1: *The principal component analysis plot of RNAseq data (hPSC-monocytes [MC] and tMG, marked) merged with the data set from the Abud et al., 2017, including their samples from iMGLs (hPSC-derived microglia-like cells), CD141 peripheral blood monocytes, aMG (cultured human primary adult microglia), iPS (human-induced pluripotent stem cells), fMG (cultured human primary fetal microglia), dendritic cells, and iHPC (stem cell-derived hematopoietic progenitors).*

The above results were further confirmed by performing gene expression analysis, including *CSF1R*, *APOE*, *CD45*, *C1QA* and *KLF4*. The results showed similarity in the gene expression patterns observed for the normalized log1p CPM (counts per million) for a set of genes of the two RNAseq studies involving the pooled transcriptome data from our study (hPSC-tMG and hPSC-monocytes (for 0', 30', 24 h, 48 h on cryosections) and the study from Abud et al., 2017 (***Fig. 2***). Thus, hPSC monocytes derived using the Yanagimachi protocol differ from PB monocytes, which we hypothesize that this was caused by *in vitro* culture.

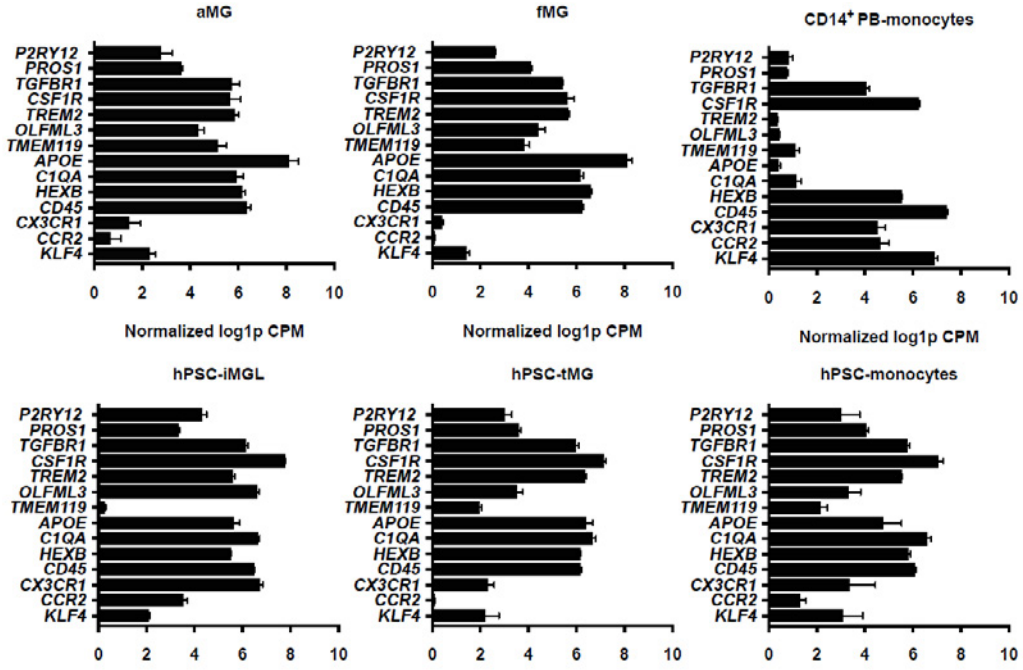

Figure 2: *Normalized log1p CPM values of pooled transcriptome data from our study (hPSC-tMG and hPSC-monocytes for 0', 30', 24 h, 48 h on cryosections) and the study from Abud et al., 2017 (adult human primary microglia in culture (aMG), fetal human microglia in culture (fMG), hPSC-derived microglia-like cells Abud protocol (hPSC-iMGL), CD14+ primary PB-monocytes) for a set of microglial and monocyte-related genes.*

Indeed, *in vitro* culture of PB monocytes (*indicated as PB mc 48h in vitro*) for 48 h in the culture medium used to create monocytes from hPSCs (*indicated as PB mc*) increased expression of a set of microglial genes as compared to the *wt* microglia (*indicated as WT mc*) (***Fig. 3***). In particular, the expression of *PROS1*, *TGFBR1*, *CSF1R*, *C1Q*, *TREM2*, *TREM119* and *APOE* were significantly upregulated. Thus, we do not only provide evidence that the tMGs described in the present study resemble microglia-like cells generated in other published studies, and cultured human primary microglia, but we also demonstrate that hPSC monocytes more closely resemble tMGs cells than primary PB monocytes, likely caused by the *in vitro* culture of hPSC monocytes.

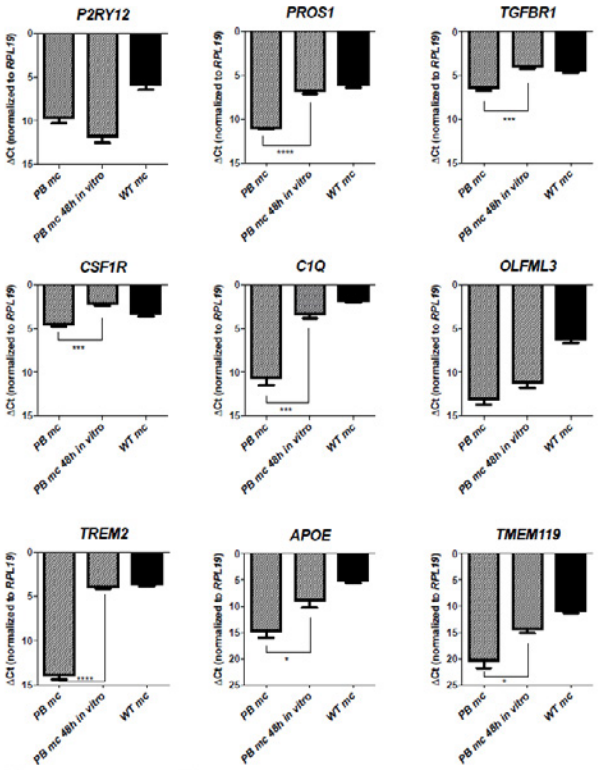

Figure 3: *qRT-PCR of PB-monocytes vs. PB-monocytes cultured 48 hours in vitro vs. hPSC-monocytes (WT mc), based on a set of microglial genes (ΔCt normalised to RPL19).*

For gaining insights into the mechanism whereby *TREM2*$^{-/-}$ tMGs display decreased phagocytic clearance in brain slices, we performed migration assay in a microfluidic system to assess if there is a different in migration pattern between *TREM2*$^{-/-}$ tMGs and WT tMGs towards Aβ42. However, no significant difference in the migration behaviour between the two cell types was observed (n = 3) (data not shown).

2. AIM 2: Compare the effect of normal donor, TREM2R47H and TREM2-/- tMGs derived from hPSC on neuronal survival in vitro.

Neuroinflammation is known to worsen neurodegeneration due to excessive secretion of pro-inflammatory cytokines. To study this phenomenon, we are currently performing *in vitro* monolayer co-cultures of hPSC-derived tMGs and hPSC-derived neuronal progenitor cells to assess the loss of neuronal cells as readout for the level of neurodegeneration by LPS treated or non-treated tMGs. Subsequently, we will also assess the effect of mutations in, or loss of *TREM2* on neuronal cell death, neurodegeneration and neuroinflammation by co-culturing *TREM2*^{R247H} and *TREM2*$^{-/-}$ tMGs with WT and mutant *TAU* (Garcia et al, 2018) hPSC-derived neuronal progenitors. These studies should be completed in 2019.

3. AIM 3: Assess the effect of the normal donor, TREM2R47H and TREM2-/- tMGs on neuronal survival in vivo in an APP, PS1+/- NOD-SCID and NOD-SCID mouse model.

In collaboration with the De Strooper lab (KU Leuven), we have transplanted hPSC-derived wild-type tMGs in Rag2$^{-/-}$CSF1$^{h/h}$ mice (as an improved humanized mouse model) in order to determine if the tMGs can replace the microglia in the brain *in vivo*. tMGs were GFP labeled, allowing their re-isolation from the murine brain. We performed single cell RNAseq on the re-isolated tMGs in comparison with freshly isolated human microglia. The initial data suggest that tMGs acquire as hypothesized a more microglia like phenotype once transplanted in the mouse brain. These studies are being further analyzed.
We now plan to also graft *TREM2*^{R247H} and *TREM2*$^{-/-}$ tMGs in WT Rag2$^{-/-}$CSF1$^{h/h}$ as well as APP/PS1$^{+/-}$ Rag2$^{-/-}$CSF1$^{h/h}$ mice to address the effect of the mutant microglia in a WT and genetically mutant AD environment, to cause in neuroinflammation and neurodegeneration in AD. This study is planned in 2019.

4. AIM 4: Global gene expression analysis.

This study has been in part completed and is in part pending, but will be initiated if aberrant function of *TREM2*^{R247H} tMGs is detected in the *in vivo* studies above.
We performed transcriptome studies comparing WT and *TREM2*$^{-/-}$ tMG. This analysis revealed that loss of *TREM2* is associated with a decreased expression of genes involved in extracellular matrix structure (integrin signaling) and transmembrane transporter activity (see ***Table 1***), which suggests that loss of *TREM2* may not only impair tMG mediated phagocytosis, but may in general affect the extent to which microglia can react/adapt to a changing microenvironment. *TREM2*$^{-/-}$ tMG also expressed numerous genes involved in receptor-ligand activity, receptor-regulator activity, calcium ion binding and cytokine activity more highly than WT tMG, suggesting that *TREM2* mutant tMG might be pro-inflammatory. Future studies will be of interest to further uncover deranged integrin and cytokine/chemokine signaling in *TREM2*$^{-/-}$ tMG. As discussed in Aim 1, we did not find abnormal function of T*REM2*^{R247H} tMGs *in vitro*. Therefore, single cell RNAseq will be performed to identify differentially regulated transcripts in tMGs from WT, TREM2^{R247H} and TREM2$^{-/-}$ PSCs following grafting *in vivo*.

TOP DOWNREGULATED FUNCTIONS in *TREM2*$^{-/-}$ tMG vs. WT tMG (overtime)	
Function	**Genes**
ECM structural constituent	COL1A1 COL1A2 COL2A1 Integrins (ITGA2,..) ..
Transmembrane transporter activity	COX6A2 ..
TOP UPREGULATED FUNCTIONS in *TREM2*$^{-/-}$ tMG vs. WT tMG (overtime)	
Function	**Genes**
Receptor-ligand activity: Chemokine activity Cytokine activity	Chemokine receptor-ligand interaction (CXCL9, CXCL12,..) Cytokine receptor-ligand interaction (IL1A, IL6,..)

Table 1: *transcriptome studies on WT and TREM2*$^{-/-}$ *tMGs*

5. Conclusion and future work

Within the first 2 years of this project, we have provided data on the generation of TREM2 mutants from hPSC, and showed that these mutants posess phagocytic ability and expressed transcriptome profiles that resemble the WT monocytes/microglias. We have therefore achieved the Aim 1. These findings have led to a scientific publication in an IF >10 journal of the field (*Claes C et al. Alzheimer's and Dementia; Impact factor 12.74*), 1 invited review (*Claes C et al. Cell Imunol*) and the defence of 1 PhD student (Christel Claes; defended her PhD on 24 September 2018) as well as current training of a second PhD student (Johanna Van Den Daele) and the recruitemt of Dr. Yoke-Chin Chai, postdoctoral fellow, who contributes 50% of his time to Aim 2 and 3 of this proposal. Since the studies pertaining to Aim 2 and Aim 3 are currently ongoing concurrently (*see above*), we expect to complete these studies within the duration of this project.

6. Publications from the work

- Claes C, Van Den Daele J, Boon R, Schouteden S, Colombo A, Monasor LS, Fiers M, Ordovas L, Nami FA, Bohrmann B, Tahirovic S, De Strooper B, Verfaillie CM. Human stem cell-derived monocytes and microglia-like cells reveal impaired amyloid plaque clearance upon heterozygous or homozygous loss of TREM2. Alzhemier's & Dementia. 2018. In Press. http://doi.org/10.1016/j.jalz.2018.09.006
- Claes C, Van den Daele J, Verfaillie CM. Generating tissue-resident macrophages from pluripotent stem cells: Lessons learned from microglia. Cell Immunol. 2018 Aug;330:60-67. doi: 10.1016/j.cellimm.2018.01.019

7. References for the summary of work:

- Abud EM, Ramirez RN, Martinez ES, Healy LM, Nguyen CHH, Newman SA, et al. iPSC-Derived human microglia-like cells to study neurological diseases. Neuron 2017;94:278–9.
- Claes C, Van Den Daele J, Boon R, Schouteden S, Colombo A, Monasor LS, Fiers M, Ordovas L, Nami FA, Bohrmann B, Tahirovic S, De Strooper B, Verfaillie CM. Human stem cell-derived monocytes and microglia-like cells reveal impaired amyloid plaque clearance upon heterozygous or homozygous loss of TREM2. Alzheimer's & Dement. 2018. Nov. 7. http://doi.org/10.1016/j.jalz.2018.09.006
- García-León JA, Cabrera-Socorro A, Eggermont K, Swijsen A, Terryn J, Fazal R, Nami F, Ordovás L, Quiles A, Lluis F, Serneels L, Wierda K, Sierksma A, Kreir M, Pestana F, Van Damme P, De Strooper B, Thorrez L, Ebneth A, Verfaillie CM. Generation of a human induced pluripotent stem cell-based model for tauopathies combining three microtubule-associated protein tau mutations which displays several phenotypes linked to neurodegeneration. Alzheimers & Dement. 2018 Jul 20. pii: S1552-5260(18)30161-4.
- Yanagimachi MD, Niwa A, Tanaka T, Honda-Ozaki F, Nishimoto S, Murata Y, Yasumi T, Ito J, Tomida S, Oshima K, Asaka I, Goto H, Heike T, Nakahata T & Saito MK. Robust and Highly-Efficient Differentiation of Functional Monocytic Cells from Human Pluripotent Stem Cells under Serum- and Feeder Cell-Free Conditions. PLoS ONE (2013) 8: e59243

Geneeskundige Stichting Koningin Elisabeth
Fondation Médicale Reine Elisabeth
Königin-Elisabeth-Stiftung für Medizin
Queen Elisabeth Medical Foundation

Progress report of the research group of

Prof. Voets Thomas

Katholieke Universiteit Leuven (KU Leuven)

Principal investigator

Prof. Thomas Voets
Laboratory of Ion Channel Research
VIB-KU Leuven Center for Brain & Disease Research
KU Leuven, Department of Cellular and Molecular Medicine
Herestraat 49 bus 802
3000 Leuven
Belgium
Tel.: +32 16 33 02 17
E-mail: Thomas.voets@kuleuven.vib.be

Table of contents

Unraveling the role of TRPM3 in neuropathic and inflammatory pain

1. Background

It is estimated that about 1 million Belgians suffer from moderate-to-severe chronic pain. Chronic back pain, migraine, diabetic neuropathy, osteoarthritis, cancer pain and chemotherapy-induced neuropathic pain are just a few examples of common conditions associated with persistent pain, which in many cases is very difficult to treat (Grayson, 2016; Reid et al., 2011). Indeed, about 50 % of the chronic pain sufferers report inadequate pain control. Over-the-counter analgesics such as paracetamol or nonsteroidal anti-inflammatory drugs often show limited efficacy in the treatment of severe chronic pain. Alternatives such as the gabapentionoids, which act by blocking $\alpha 2\delta$ subunit-containing voltage-dependent calcium channels, or the tricyclic antidepressants such as amitriptyline have good analgesic activity in only a minority of treated patients, and can have significant effects on the central nervous activity. Opioids such as morphine, hydrocodone or fentanyl are increasingly used as potent analgesic drugs to treat moderate to severe pain, but these cause tolerance and addiction and can have severe adverse effects including the risk of overdose (Reid et al., 2011). Of note, a dramatic increase in the use of prescription and non-prescription opioids has been observed in the last two decades, referred to as the “opioid epidemic”, resulting in an alarming rise in the number of fatalities from prescription opioids and heroin (Wilson-Poe & Moron, 2017). Therefore, there is a large unmet need for newer and safer treatments for pain, which requires identification of potential druggable targets in the pain pathway (Grayson, 2016).

Recently, our research group has identified TRPM3, a member of the transient receptor potential family of cation channels, as a key player in the pain pathway and a potential novel target for pain treatment. We found that TRPM3 is highly expressed in sensory neurons, in particular in the small-diameter pain-signaling (nociceptor) neurons, and demonstrated that direct activation of TRPM3 in sensory nerve endings in the skin causes acute pain and neurogenic inflammation. In addition, we found that genetic ablation (using knockout mice) or pharmacological inhibition (using specific antagonists) of TRPM3 function leads to significant analgesia in various animal models of persistent pain, without obvious side-effects(Vriens et al., 2011). In particular, we found that pharmacological inhibition of TRPM3 causes a strong reduction of the hypersensitivity (hyperalgesia and allodynia) of inflamed/injured tissue to thermal and mechanical stimuli(Vriens et al., 2011).

2. Objective, hypothesis and specific aims

The overall *objective* of this project is to uncover the molecular and cellular mechanisms whereby TRPM3 contributes to the onset and persistence of pain and hypersensitivity, as a fundamental basis for the further development of TRPM3 antagonists as a novel class of analgesic drugs for human use.

We *hypothesized* that inflammation and peripheral nerve injury leads to a functional upregulation of TRPM3 in nociceptor neurons, either at the transcriptional or at the posttranscriptional level. Increased TRPM3 functionality then increases the excitability of these neurons and renders them more responsive to thermal and mechanical stimuli, which leads to hypersensitivity and persistent pain. Accordingly, we hypothesized that inhibiting TRPM3 activity would reduce neuronal excitability and alleviate hypersensitivity in various painful conditions.

These hypotheses were addressed using rodent models of inflammatory and neuropathic pain, and we aimed at (1) evaluating the role of TRPM3 in the detection of acute painful stimuli; assessing possible alterations in TRPM3 expression and functionality in nociceptor neurons in the context of inflammation and nerve injury; and (3) analyzing the in vivo effects of TRPM3 inhibition/ablation on hypersensitivity and ongoing pain in animal models of inflammatory and neuropathic pain.

3. Results

In the course of the first two years of the project funded by GSKE, we made important progress in elucidating the role of TRPM3 as a pain sensor and obtained exciting novel insights into its involvement in the development of pathological pain, further highlighting its role as a potential target for novel pain therapies.

3.1. Identification of the role of TRPM3 in acute heat sensing

At the onset of the project, it was well established that TRPM3 acts as a heat sensor involved in the detection of noxious heat. However, pharmacological inhibition or genetic elimination of TRPM3 in mice provokes only a minor reduction of heat responses in sensory neurons and a moderate increase in response latencies to painful heat stimuli *in vivo*, indicative of the co-existence of multiple heat sensors in these neurons (Straub et al., 2013; Vriens, Nilius, & Voets, 2014; Vriens et al., 2011). To understand how TRPM3 contributes to thermal hypersensitivity in pathological conditions such as inflammation or nerve injury, it was essential to first identify the full set of heat sensors in sensory neurons and their relative role in heat-induced pain. We initially focused on TRPV1, also known as the capsaicin/vanilloid receptor, an extensively studied heat-activated channel in sensory neurons. To this aim, we first produced and analyzed double knockout (DKO) mice lacking expression of both TRPM3 and TRPV1 ($DKO^{M3/V1}$ mice). Whereas the number of heat-sensitive sensory neurons was further reduced, we still observed robust heat responses in ~40% of $DKO^{M3/V1}$ neurons (**Figure 1a,g**).

An important breakthrough in the course of this project was our discovery that the remaining heat responses in $DKO^{M3/V1}$ neurons are mediated by TRPA1, a channel that in mammals has been implicated in the detection of noxious chemicals such as acrolein, mustard oil and H_2O_2 (Bautista et al., 2006), but was not associated with heat sensing. Pharmacological inhibition of TRPA1 eliminated the residual heat responses in $DKO^{M3/V1}$ neurons (**Figure 1b-d,g**), and triple knockout (TKO) mice lacking all three TRP channels also lacked neuronal responses to noxious heat (**Figure 1e,g**). Mice lacking expression of both TRPM3 and TRPA1 ($DKO^{M3/A1}$ mice) or TRPV1 and TRPA1 ($DKO^{V1/A1}$ mice) showed robust heat responses in ~35-40% of the tested neurons.

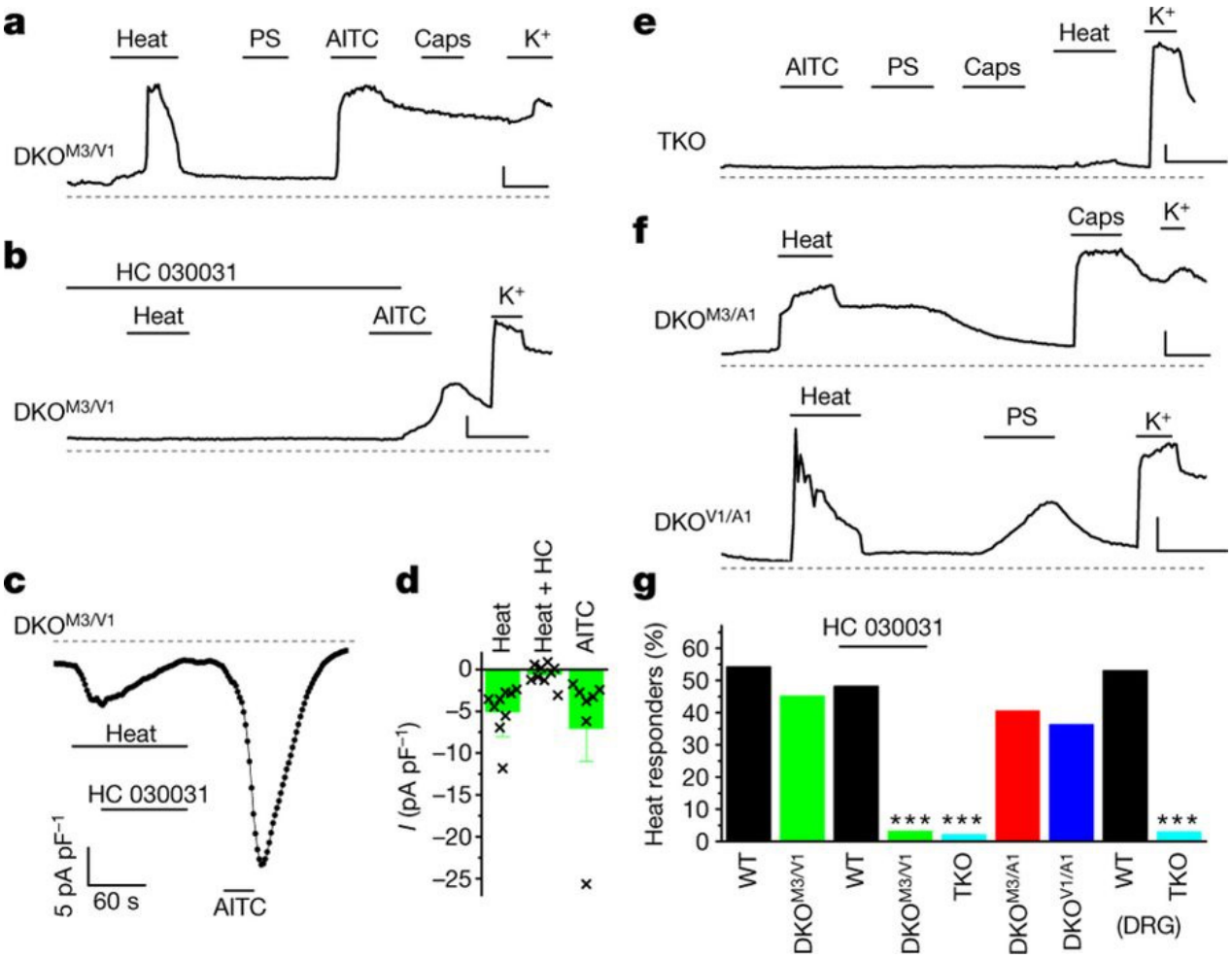

Figure 1. a, **b**, Responses to heat (45 °C) and AITC (50 µM) in sensory neurons from DKO$^{M3/V1}$ mice in the absence and presence of the TRPA1 antagonist HC030031 (100 µM). WT, wild-type; PS, pregnenolone sulfate; Caps, capsaicin. **c**, Example of a HC030031-sensitive heat-activated inward current in an AITC-sensitive DKO$^{M3/V1}$ neuron. **d**, Mean (± s.e.m.) current densities for experiments as in **c**($n = 9$ cells). **e**, **f**, Heat and ligand responses in sensory neurons from TKO and indicated DKO mice. Scale bars in **a**, **b**, **e**, **f**, 60 s/100 nM. **g**, Percentages of heat-responding sensory neurons in mice of the indicated genotypes, in the absence or presence of HC030031. ***$P < 0.00001$; Fisher's exact test with Holm–Bonferroni correction.
From Vandewauw *et al.*, Nature (2018).

Strikingly, the TKO mice (DKO$^{M3/V1}$, DKO$^{M3/A1}$ or DKO$^{V1/A1}$ mice) showed a dramatic and specific deficiency in the avoidance of noxious heat. Indeed, in tail flick or hot plate experiments, TKO mice would not withdraw from the noxiously heat stimulus and obtain burn injuries unless the experiment was terminated by the experimenter (**Figure 2a-c**). In contrast, the TKO mice showed normal pain responses to cold or mechanical stimuli and normal thermal preference (**Figure 2d-k**). Taken together, these data indicate that TRPM3 is one of three redundant noxious heat sensors - as long as one of these three channels is functional, acute heat sensing is conserved.

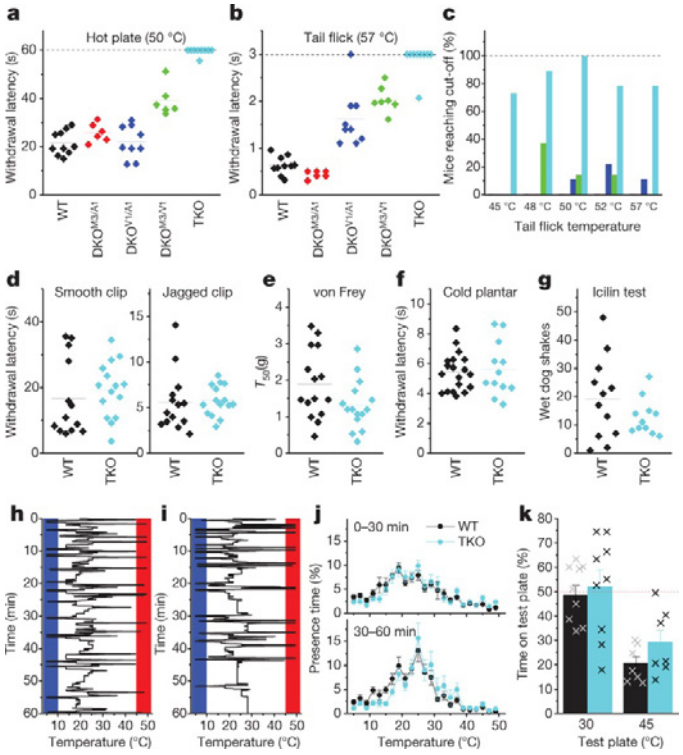

Figure 2. a, **b**, Withdrawal latencies of male mice in the hot-plate (**a**) and tail-flick (**b**) assays. Dotted lines indicate cut-off times. Horizontal lines in **a**, **b**, **d**–**g**indicate mean. **c**, Percentage of tested animals (WT: $N=16$; $DKO^{M3/A1}$: $N=12$; $DKO^{V1/A1}$: $N=15$; $DKO^{M3/V1}$: $N=12$; TKO: $N=16$) that did not withdraw their tail before the cut-off. **d**, Withdrawal latencies of wild-type ($N=13$–14) and TKO ($N=15$) mice to smooth plastic and jagged metal clips. $P=0.50$ and 0.86, respectively; two-sided Student's *t*-test. **e**, Sensitivity of wild-type ($N=15$) and TKO ($N=15$) mice to calibrated von Frey hairs ($P=0.09$; two-sided Student's *t*-test). T_{50}, 50% paw withdrawal threshold. **f**, Withdrawal latencies of wild-type ($N=19$) and TKO ($N=12$) mice in the cold plantar test ($P=0.76$; two-sided Student's *t*-test). **g**, Number of icilin-induced wet dog shakes in wild-type ($N=12$) and TKO ($N=11$) mice ($P=0.20$; two-sided Student's *t*-test). **h**, **i**, Representative experiments depicting the positions of a wild-type (**h**) and a TKO (**i**) mouse on a thermal gradient. Border zones of the gradient are red (>45 °C) and blue (<10 °C). **j**, Mean presence time ± s.e.m. in the different temperature zones during the first and second 30-min periods ($N=10$ mice for each genotype). **k**, Two-temperature choice test with control plate set at 30 °C and test plate set at 30 °C or 45 °C. Mean percentage ± s.e.m. of the total time spent on the test plate ($N=9$ mice for each genotype; $P=0.77$ at 30 °C, $P=0.16$ at 45 °C; two-sided Student's *t*-test). Both genotypes showed statistically significant avoidance at 45 °C ($P=0.001$; one-sample *t*-test versus 50%).
From Vandewauw *et al.*, Nature (2018).

These findings not only represent a fundamental breakthrough in the fieled of pain transduction, but are also of high importance for the future development of TRPM3 antagonists for chronic pain. In particular, it has been questioned whether TRPM3 inhibition could lead to hyposensitivity to noxious heat, leading to a high risk of burn injury. However, our data indicate that as long as TRPM3 antagonists do not inhibit TRPV1 and TRPA1, acute heat sensing remains largely preserved. A manuscript describing these findings and acknowledging the support of the Queen Elisabeth Medical Foundation was published in *Nature* (Vandewauw et al., 2018).

3.2. Functional upregulation of TRPM3 in sensory neurons during inflammation

Based on published and unpublished data showing that pharmacological inhibition or genetic ablation of TRPM3 eliminates thermal hypersensitivity in the context of inflammation and peripheral nerve injury (Vriens et al., 2011; Vriens & Voets, 2018), we hypothesized that these disease states leads to an upregulation of TRPM3 expression in nociceptor neurons, leading to increased neuronal excitability.

To test this hypothesis, we have recently succeeded in developing a novel approach that allows us to analyze changes in TRPM3 expression and functionality specifically in those nociceptive neurons that innervate injured tissue. To achieve this, we made use a mouse model that expresses a genetically encoded calcium indicator in nociceptor neurons, by crossing the TRPV1-cre reporter mouse line, which expressed cre-recombinase in heat-sensitive C and Aδ fibers, with a mouse line expressing

GCaMP6 in a cre-dependent manner. We injected the retrograde label WGA-AlexaFluor647 in the hind paws of these mice, which after 5 days resulted in the fluorescent staining of a subset of sensory neuron cell bodies in the lumbal L3-L6 dorsal root ganglia (**Figure 3a-c**). Then, one hind paw was injected with complete Freud's adjuvans (CFA) leading to a strong inflammatory response and while the other paw was used as vehicle control. On the next day, using confocal imaging, we imaged GCaMP6 fluorescence in intact dorsal root ganglia, and measured changes induced by application of specific agonists for TRPM3 (pregnenolone sulfate), TRPV1(capsaicin) and TRPA1 (Mustard Oil) (**Figure 3d**).

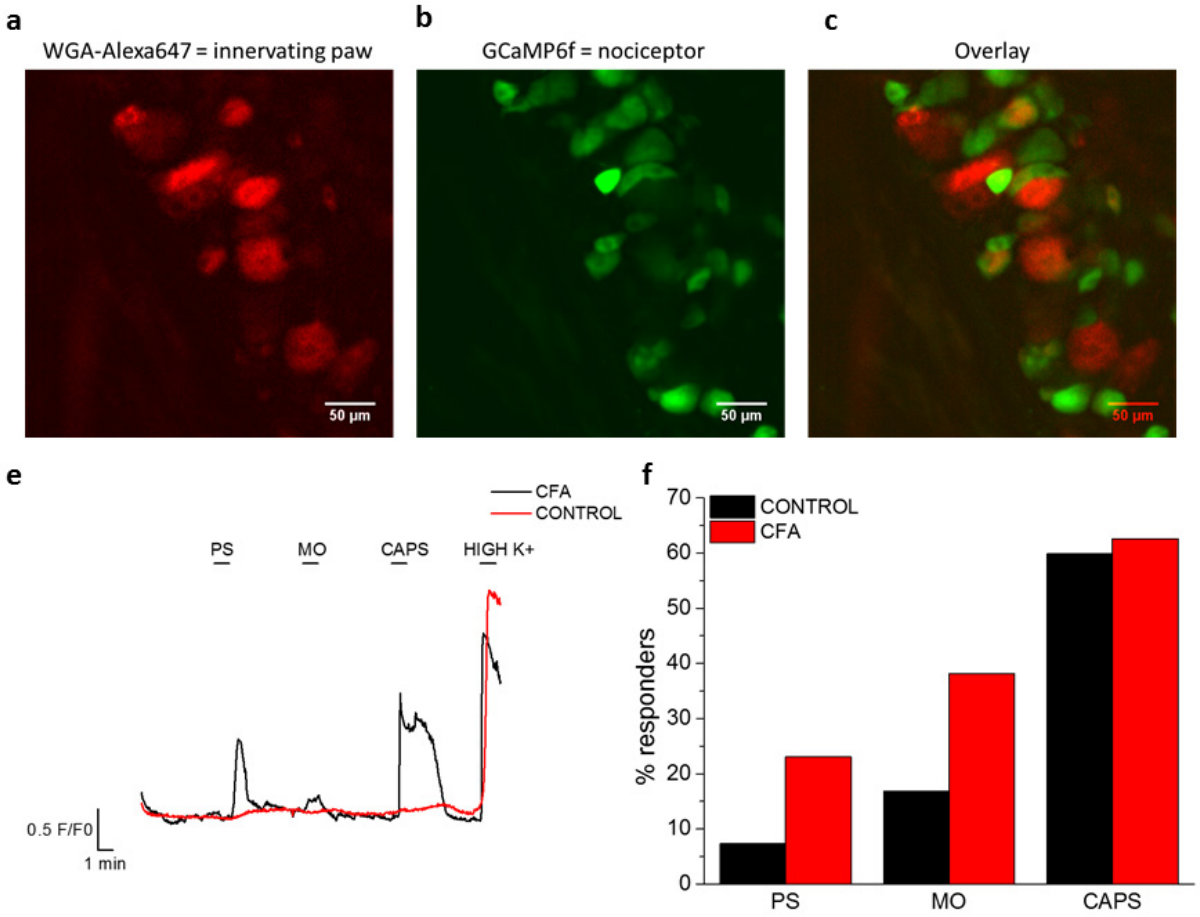

Figure 3. a-c, Confocal images of WGA-AlexaFluor647 and GCaMP6 in an L5 dorsal root ganglion retrogradely labeled by injection of WGA-AlexaFluor647 into the ipsilateral paw. **d**, representative traces showing calcium-dependent changes in GCaMP6 fluorescence in response to agonists of TRPM3(pregnenolone sulfate), TRPV1(capsaicin) and TRPA1 (mustard oil). **e**, Summary of the percentage of TRPM3, TRPA1 and TRPV1 positive neurons determined as shown in panel (**d**).
Mulier, Moilanen & Voets - unpublished results.

By comparing the responses in AlexaFluor647-positive neurons in the ganglia ipsilateral and contralateral to the CFA-injected paw, we were able to specifically measure alterations in functional TRP channel expression caused by inflammation. This approach revealed a 3-fold increase in TRPM3-responses in neurons innervating the inflamed paw (**Figure 3e**). This is of high importance, as it provides the first demonstration of a functional upregulation of TRPM3 in neurons that innervate inflamed tissue. This upregulation may contribute to thermal and mechanical hypersensitivity of inflamed tissue, and provides and explanation for the lack of inflammatory hypersensitivity in TRPM3 knockout mice. Moreover, reducing this upregulated TRPM3 activity in sensory neurons using specific antagonists may explain the efficacy of experimental TRPM3 antagonists in animal models of inflammatory hypersensitivity. The key finding that TRPM3 functionality is upregulated in nociceptor neurons innervating inflamed tissue raised important follow-up questions.

A first question is whether the upregulated TRPM3 function is due to increased transcription or to post-transcriptional regulation. To address this question, we are following two different routes to assess changes at the mRNA level in dorsal root ganglion neurons innervating the injured paw. In the first year of the project, we established the RNAscope-technology (Wang et al., 2012) to detect the expression at the mRNA level of TRPM3 and other sensory TRP channels in dorsal root ganglia tissue (**Figure 4a**), and we are currently combining this approach with the WGA-AlexaFluor647-based retrograde labeling to compare expression in cell bodies of sensory neurons innervating the inflamed versus contralateral control paw. A second, even more challenging approach that we are currently developing is to compare the single cell transcriptomes of sensory neurons. To achieve this, we isolate retrogradely labeled ganglia, disperse the cells, and submit them to FACS sorting based on combined AlexaFluor647 and GCaMP6 fluorescence (**Figure 4b**). With the use of the BD Influx™ high-speed cell sorter, available via the VIB-KU Leuven Flow Cytometry Facility, individual cells will then be sorted and subjected to single-cell RNA-seq using the SMARTseq technology, available via the Genomics core (KU Leuven/UZ Leuven). We expect that in the last year of the project, using this approach, we will obtained invaluable new data with regard to inflammation-induced changes in expression in sensory neurons, and the contribution of TRPM3.

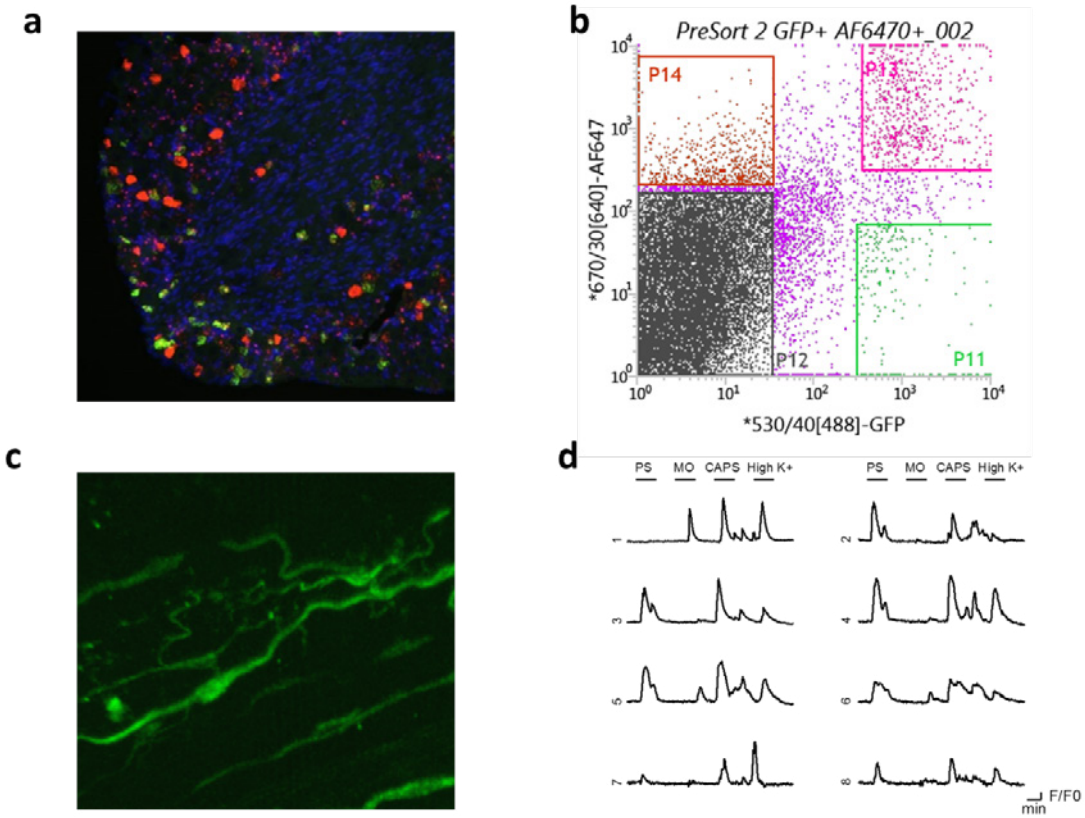

Figure 4. a, Multiplex fluorescent *in situ* hybridization using RNAscope probes against TRPM3 (magenta), TRPM8 (red) and TRPV1 (green) in a mouse dorsal root ganglion. Nuclei are stained using DAPI (blue). **b**, FACS sorting of retrogradely labeled DRG neurons, showing a specific population of Alexa647 and GCaMP6-positive neurons. **c**, GCaMP6 fluorescence in sensory neurons innervating the mouse hind paw skin. **d**, Representative traces of individual free nerve endings in the skin in response to agonists of TRPM3 (pregnenolone sulfate), TRPV1(capsaicin) and TRPA1 (mustard oil).
Mulier, Moilanen & Voets - unpublished results.

A second question is whether the functional upregulation of TRPM3 at the level of the cell bodies in the dorsal root ganglia is also reflected in an increased TRPM3 activity in the sensory nerve endings. To address this question, we have established a novel assay whereby we image free nerve endings in the paw skin of mice expressing GCaMP6 in TRPV1-positive neurons (see above for a description of these mice). In this assay, the skin and innervated nerve is carefully dissected and imaged from the external side using spinning-disk confocal microscopy (**Figure 4c**). Application of agonists for TRPM3, TRPA1 or TRPV1 revealed specific calcium responses in fine nerve endings in the skin, and we are currently

using this novel approach to analyze whether CFA-induced inflammation affects TRPM3 functionality in nociceptor nerve endings.

3.3. Analgesic effects of TRPM3 inhibition in disease-relevant pain models

The ultimate goal of this line of research is to provide a firm scientific basis for the development of novel analgesic treatments using TRPM3 as a pharmacological target. To reach this goal, relevant animal models as well as accurate assays to assess both hypersensitivity and ongoing pain are essential.

In addition to the CFA model described in the project, which is a model of acute inflammation but has no direct relevance for human disease, we have also introduced a mouse model of chronic bladder pain. In this model, mice received intraperitoneal injections of cyclophosphamide (40 mg/kg) every 2 days for 7 days, resulting in a chronically inflamed bladder (**Figure 5a**) associated with pain and hypersensitivity. Importantly, we found that systemic application of the selective TRPM3 antagonist isosakuranetin (10 mg/kg) completely reversed mechanical hyperalgesia in the chronic pain model, as assessed using von Frey hairs to stimulate the suprapubic area (**Figure 5b**). In addition, we found that inhibition of TRPM3 reduced signs of ongoing pain using the Dynamic Weight Bearing (DWB) assay (Tetreault, Dansereau, Dore-Savard, Beaudet, & Sarret, 2011), as evidenced by increased locomotion as well as by a reduction of the weight on the front paws in the treated animals. These results further strengthen the potential of TRPM3 antagonism to treat pain and hypersensitivity associated with visceral pathology.

Finally, we have also recently established the monoiodoacetate (MIA) model of osteoarthritis. In this model, injection of MIA in the knee joint of mice or rats leads to the development of experimental osteoarthritis, characterized by hypersensitivity in the von Frey assay, as well as by a shift of the body weight towards the non-injured hindpaw. We are currently evaluating the effect of TRPM3 antagonism in on pain behavior in this MIA model.

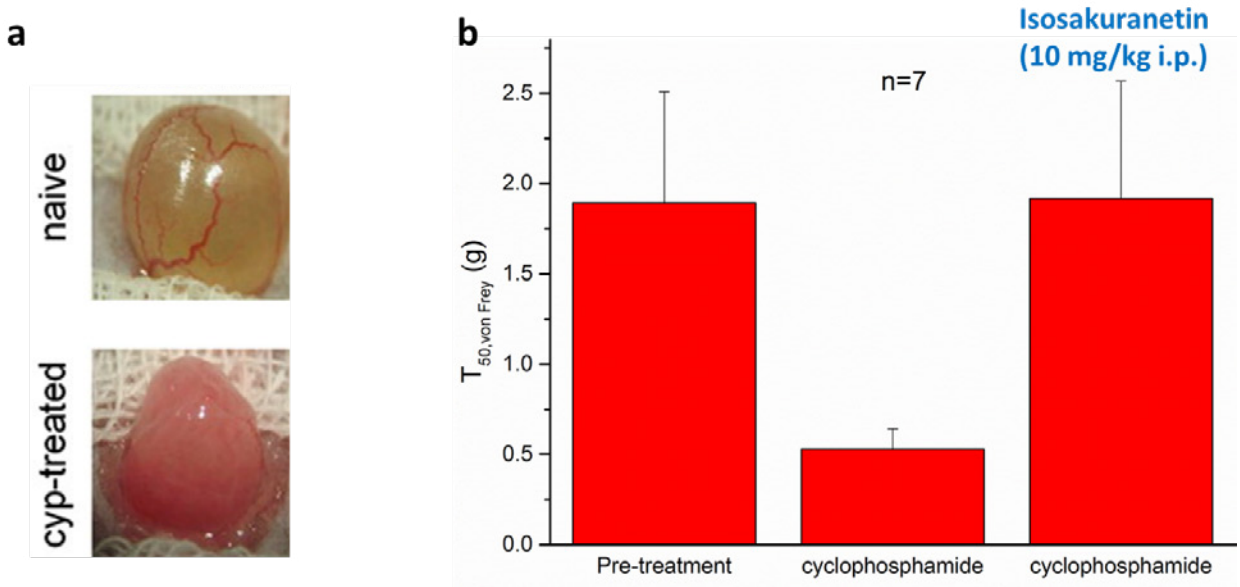

Figure 5. a, Images of bladders of mice treated with vehicle (saline) or cyclophosphamide. **b**, Reduction of the mechanical threshold following cyclophosphamide treatment, and reversal by the TRPM3 antagonis Isosakuranetin.
Moilanen, Mulier & Voets - unpublished results.

4. Outlook and budget

With the financial support of the GSKE, our lab has been able to delineate the role of TRPM3 in acute heat sensing, to establish that TRPM3 is functionally upregulated in inflammatory conditions, and to demonstrate that TRPM3 antagonism shows analgesic efficacy in disease-relevant animal assays of ongoing pain and hypersensitivity. The 2018 budget received from the Queen Elisabeth Medical Foundation was used to cover part of the costs related to the housing and breeding of the different mouse lines used for experiments as described in **Figure 3-5**, as well as to cover part of the salary of Dr. Lauri Moilanen, a postdoctoral researcher specialized in animal pain models who made important contributions to the described experimental progress.

Following up on the important progress made in the first two years of the project, several novel experimental approaches have been initiated that go beyond what was originally described in the research plan. These include the 1) FACS-based single-cell transcriptome analyses of retrogradely labeled sensory neurons, 2) *ex vivo* imaging of sensory nerve endings in the skin using spinning-disk confocal microscopy, 3) as well as *in vivo* experiments using the disease-relevant mouse models for bladder pain and osteoarthritis.

We estimated the following additional working costs:

Use of BD Influx™ high-speed cell sorter:	10 sorting sessions × 125 €/hour:	1250 €
SmartSeq2:	RNAseq of 4000 cells × 13 €/cell:	5200 €
Use of spinning disk confocal microscope:	60 imaging sessions of 4 hours × 25 €/hour:	6000 €
Use of imaging computer and Imaris software:	30 sessions of 4 hours × 15 €/hour	1800 €

Purchase, breeding and housing of additional animals (mice and rats) for the bladder pain and osteoarthritis models. Based on current animalium invoices, the additional costs associated with these two pain models is estimated at 1500 Euro/month × 12 months: 16000 €

Total estimated additional working costs: 30250 €

Note that these calculations do not take the additional personal costs into account. We appreciate performing these additional experiments with the continued support of GSKE.

5. Publications acknowledging support from GSKE

- Vandewauw, I., De Clercq, K., Mulier, M., Held, K., Pinto, S., Van Ranst, N., . . . Voets, T. (2018). A TRP channel trio mediates acute noxious heat sensing. *Nature, 555*(7698), 662-666. doi:10.1038/nature26137.
- Vangeel, L. & Voets, T. (2019). Transient Receptor Potential (TRP) Channels and Calcium Signaling. *Cold Spring Harbour Perspectives on Calcium Signaling,* **in press**.

6. References

- Bautista, D. M., Jordt, S. E., Nikai, T., Tsuruda, P. R., Read, A. J., Poblete, J., . . . Julius, D. (2006). TRPA1 mediates the inflammatory actions of environmental irritants and proalgesic agents. *Cell, 124*(6), 1269-1282. doi:10.1016/j.cell.2006.02.023
- Grayson, M. (2016). Pain. *Nature, 535*(7611), S1. doi:10.1038/535S1a
- Reid, K. J., Harker, J., Bala, M. M., Truyers, C., Kellen, E., Bekkering, G. E., & Kleijnen, J. (2011). Epidemiology of chronic non-cancer pain in Europe: narrative review of prevalence, pain treatments and pain impact. *Curr Med Res Opin, 27*(2), 449-462. doi:10.1185/03007995.2010.545813
- Straub, I., Krugel, U., Mohr, F., Teichert, J., Rizun, O., Konrad, M., . . . Schaefer, M. (2013). Flavanones that selectively inhibit TRPM3 attenuate thermal nociception in vivo. *Mol Pharmacol, 84*(5), 736-750. doi:10.1124/mol.113.086843
- Tetreault, P., Dansereau, M. A., Dore-Savard, L., Beaudet, N., & Sarret, P. (2011). Weight bearing evaluation in inflammatory, neuropathic and cancer chronic pain in freely moving rats. *Physiol Behav, 104*(3), 495-502. doi:10.1016/j.physbeh.2011.05.015
- Vandewauw, I., De Clercq, K., Mulier, M., Held, K., Pinto, S., Van Ranst, N., . . . Voets, T. (2018). A TRP channel trio mediates acute noxious heat sensing. *Nature, 555*(7698), 662-666. doi:10.1038/nature26137
- Vriens, J., Nilius, B., & Voets, T. (2014). Peripheral thermosensation in mammals. *Nat Rev Neurosci, 15*(9), 573-589. doi:10.1038/nrn3784
- Vriens, J., Owsianik, G., Hofmann, T., Philipp, S. E., Stab, J., Chen, X., . . . Voets, T. (2011). TRPM3 is a nociceptor channel involved in the detection of noxious heat. *Neuron, 70*(3), 482-494. doi:10.1016/j.neuron.2011.02.051
- Vriens, J., & Voets, T. (2018). Sensing the heat with TRPM3. *Pflugers Arch*. doi:10.1007/s00424-017-2100-1
- Wang, F., Flanagan, J., Su, N., Wang, L. C., Bui, S., Nielson, A., . . . Luo, Y. (2012). RNAscope: a novel in situ RNA analysis platform for formalin-fixed, paraffin-embedded tissues. *J Mol Diagn, 14*(1), 22-29. doi:10.1016/j.jmoldx.2011.08.002
- Wilson-Poe, A. R., & Moron, J. A. (2017). The dynamic interaction between pain and opioid misuse. *Br J Pharmacol*. doi:10.1111/bph.13873

Geneeskundige Stichting Koningin Elisabeth
Fondation Médicale Reine Elisabeth
Königin-Elisabeth-Stiftung für Medizin
Queen Elisabeth Medical Foundation

Progress report of the research group of

Prof. dr. Vonck Kristl

Universiteit Gent (UGent)

Principal investigator

Prof. dr. Vonck Kristl
Reference Center for Refractory Epilepsy
Laboratory for Clincial and Experimental Neurophysiology
Institute for Neuroscience
Department of Neurology
Ghent University Hospital
De Pintelaan 185
9000 Gent
Belgium
Tel.: +32 50 61 06 51
E-mail: Kristl.Vonck@UGent.be
www.uzgent.be
H-index: 28

The role of locus coeruleus noradrenergic neurons in the mechanism of vagus nerve stimulation and the effect of selective activation of these neurons in epilepsy.

1. Achieved results 2018

Workpackage 1: Chemogenetic modulation of the locus coeruleus: effect on *normal* hippocampal activity

Task 1.1 Validation of DREADD-based modulation of the locus coeruleus (LC)

Induction of DREADD expression in LC neurons in rats

To selectively induce expression of DREADDs in LC neurons, male adult Sprague-Dawley rats (n=37) were injected with an adeno-associated viral vector (AAV) serotype 2/7 carrying a plasmid with aPRSx8-hM3Dq-mCherry construct (5.99E+12 GC/ml, provided by the group of Veerle Baekelandt and Chris Van Den Haute) . (Hwang et al. 2001)

Animals were anesthetized with a mixture of medical oxygen and isoflurane (5% for induction, 2% for maintenance). The rat was placed in a stereotaxic frame and the skull was exposed. Bregma was lowered 2mm relative to lambda (~15° head angle) to target the LC. Using a Hamilton syringe (1µl) and Quintessential Stereotaxic Injection system (flow rate 2nl/min), bilateral injections (10nl/site) of an adeno-associated viral vector (AAV) serotype 2/7 were done in the locus coeruleus (3.9 AP, +/- 1.15 ML relative to lambda; -5.7 DV below dura). In the experimental group the AAV carried a construct encoding for hM3Dq-mCherry under control of the LC specific promotor PRSx8 (n=9; 5.99 E+12 GC/ml). In the control group the AAV carried a construct encoding for eGFP under control of the PRSx8 promotor (n=8, 6.72 E+12 GC/ml). After injection the syringe was left in place for an additional 5 min and was then withdrawn slowly to avoid backflow. In addition we injected twenty animals unilaterally in the right LC using the same injection procedure (DREADD n=11, control n=9). Following surgery, animals recovered three weeks in their home cage to allow optimal viral vector expression. Three animals of the bilateral control group died during surgery.

In vivo extracellular recording in genetically modified LC neurons in anesthetized rats

To validate the functionality of hM3Dq receptors expressed in LC neurons and to determine whether low doses of clozapine can be used as selective ligand to activate genetically modified LC neurons, rats were systemically injected with clozapine (0.01 and 0.1 mg/kg). We chose to use clozapine instead of clozapine-N-oxide (CNO) because of its higher specificity and affinity. Additionally a recent study by the group of Gomez et al. has shown that DREADD activation upon systemic injection of CNO is mainly due to converted clozapine since CNO does not pass the blood brain barrier (Gomez et al. 2017)

Extracellular unit recording was performed in thirty-four animals (325-430 g) three weeks after viral vector injection to allow for optimal expression levels of the hM3Dq receptor. Rats were anesthetized with a mixture of medical oxygen and isoflurane (5% for induction, 1.5% for maintenance, n=19) or were induced with isoflurane followed by an intraperitoneal injection of urethane (1.5 g/kg, n=15). Rats were placed in the stereotaxic frame as described above. LC units were recorded using a tungsten microelectrode (impedance ≥ 1.5 MΩ) referenced against two scalp electrodes placed in the frontal plates of the skull. Electrophysiological recordings from one channel coupled to the tungsten electrode were amplified (x10 000) and filtered below 300Hz and above 3kHz and digitized at 31 kHz using a 1401 micro and Spike2 software (CED, Cambridge Electronic Design) for online visualization and offline analysis of the action potentials. LC neurons were identified online based on their phasic burst firing

followed by inhibition after a foot pinch. After confirming its LC identity the firing rate of the neuron was recorded during a stable baseline period of 300s followed by subsequent subcutaneous injections of clozapine starting with the lowest dose 0.01 and 0.1 mg/kg. Firing frequency was recorded for 900s after each injection of which the first 300s epoch was excluded from data analysis. Before stopping the recording, clonidine (0.04 mg/kg, s.c.), an α2 agonist which inhibits LC discharges, was injected to confirm the LC identity of recorded neurons (fig.1). Two animals died during unit recording surgery.

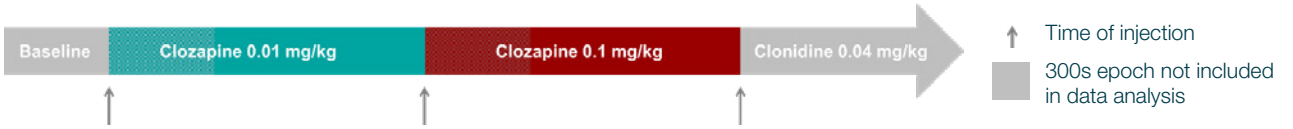

Figure 1: Schematic overview LC unit recording in anesthetized rats.

At the end of unit recording sessions, animals were deeply anesthetized with an overdose of sodium pentobarbital (200 mg/kg, i.p.) and transcardially perfused with phosphate-buffered saline (PBS) followed by paraformaldehyde (4%, pH 7.4). The brains were post fixed in paraformaldehyde (4%, pH 7.4) for 24h and subsequently cryoprotected in a sucrose solution of 10-20-30% at 4°C, snap-frozen in isopentane and stored in liquid nitrogen at -196°C. After 1 hour on -20°C, coronal cryosections of 40 µm were made using a cryostat (Leica). Immunofluorescence staining was performed with primary antibodies anti-TH (tyrosine hydroxylase, against TH$^+$ noradrenergic cells), anti-RFP (red fluorescent protein, against mCherry) or anti-GFP (green fluorescent protein). The viral vector expression levels were determined using a fluorescence microscope (Carl Zeiss, Axiovert 200M and Nikon Eclipse TE2000-E). Pictures of DAPI, TH and GFP or mCherry were taken with the AxioVision Microscope Software (6D acquisition) connected to the Carl Zeiss fluorescence microscope on the 4x, 10x and 20x magnification. Animals are categorized in the DREADD group when there is a presence of TH$^+$/mCherry$^+$ cells. Animals injected with the control vector AAV2/7-PRSx8-eGFP or animals with absence of TH$^+$/mCherry$^+$ cells are included as control in data analysis. High variability of hM3Dq-mCherry expression was observed in all animals. One animal injected with DREADD viral vector, showed no TH$^+$/mCherry$^+$ cells and was categorized in the control group for data analysis.

A

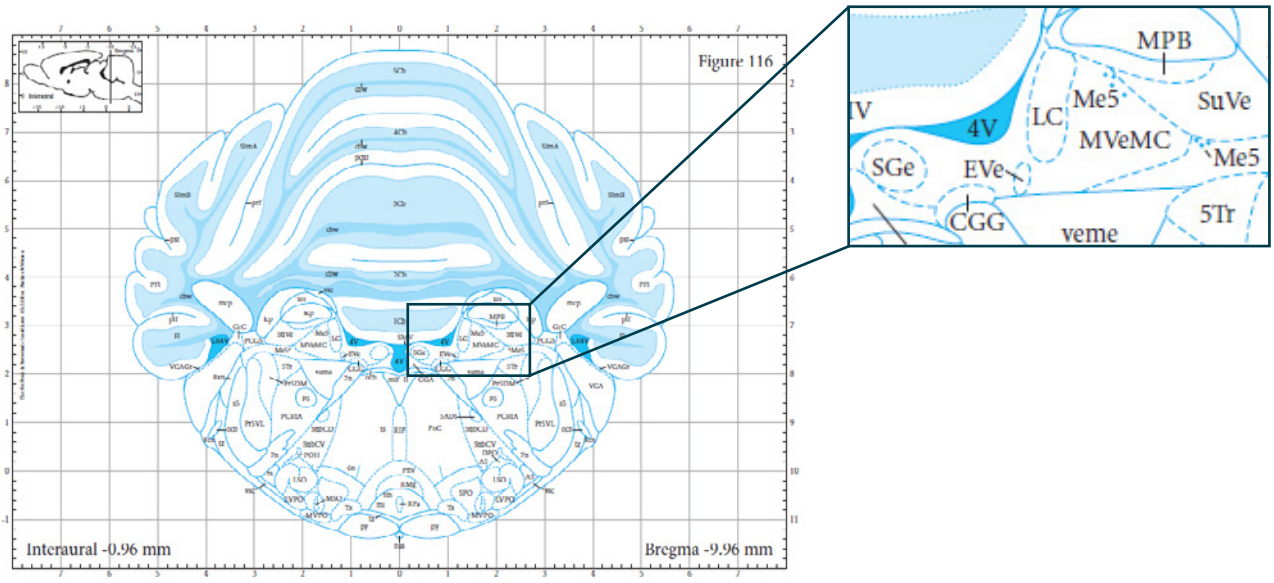

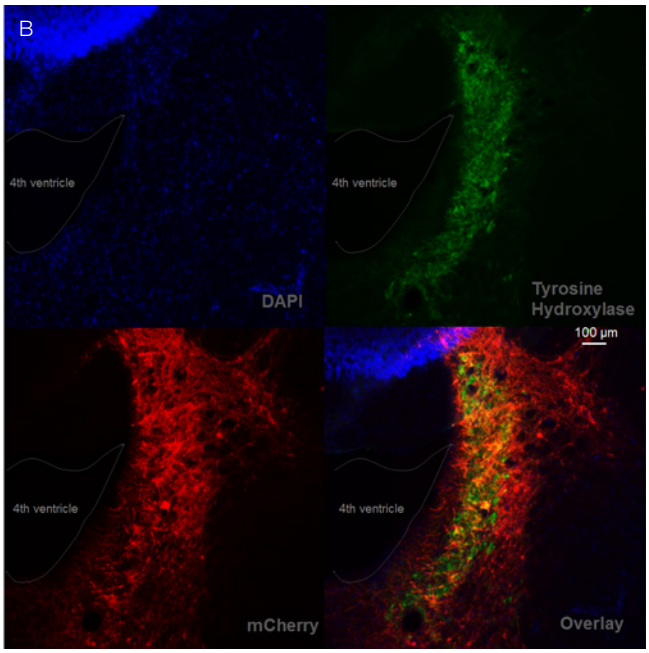

Fig 2: A. Schematic representation of anatomical position of Locus Coeruleus in the brain stem. Figure adjusted from Rat brain atlas, Paxinos and Watson, 2007

B. Transduction level of hM3Dq in LC demonstrated by immunofluorescence staining
for tyrosine hydroxylase (marker for LC-NA neuron) and Red-Fluorescent Protein (RFP) to visualize mCherry-tag coupled to hM3Dq receptor. (Scale bar 100µm) High levels of transduction were observed in this animal injected with DREADD viral vector.

Successful LC unit recording could be performed in 13/34 animals injected with viral vector. In 6/14 animals injected with control viral vector (n=3 unilateral, n=3 bilateral), six neurons could be recorded under anesthesia (n=3 isoflurane, n=3 urethane). In 7/20 animals injected with DREADD viral vector (n=3 bilateral, n=4 unilateral), a total of 8 neurons were measured (n=4 isoflurane, n=4 urethane). All recorded neurons had the typical phasic burst response to a foot pinch and were classified as LC.
Linear mixed model analysis stated that there was no significant interaction between group (DREADD or control) and the effect of the dose of clozapine on firing frequency. No significant increase in mean firing rate relative to baseline was observed after systemic administration of the lowest dose of clozapine (0.01 mg/kg) in all recorded neurons both in DREADD and control group. The highest dose of clozapine (0.1mg/kg) increased the firing rate with 67% in control animals and 42% in DREADD animals compared to baseline firing frequency (fig.3).
In one hM3Dq-animal, a small decrease in firing frequency was observed in response to clozapine administration.

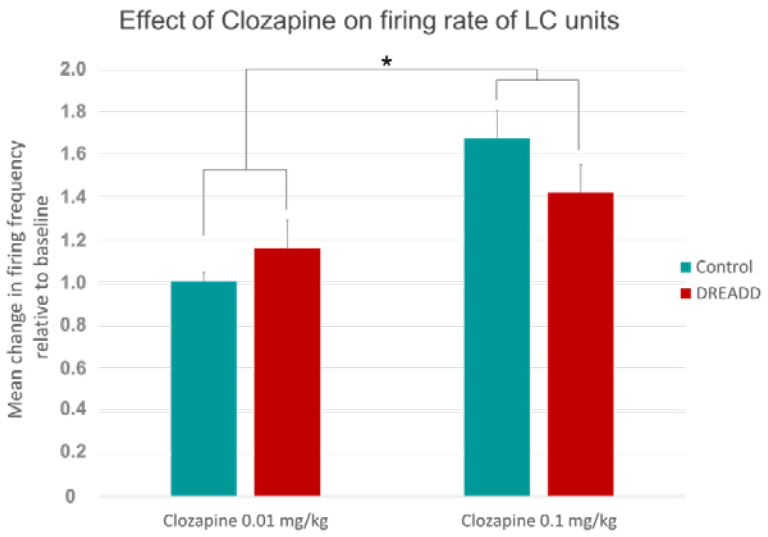

Figure 3: Effect of Clozapine administration on firing rate of LC units. *Successful LC-unit recording was performed in 13/37 injected rats (isoflurane n=6; urethane n=7). A total of 14 units were measured (control n=6, DREADD n=7), all responding to foot pinch with phasic burst inhibition and decreased firing rate in response to clonidine (0.04 mg/kg) injection. Data represented as mean change in firing frequency relative to baseline (SEM error bars) compared between DREADD and control units for the different doses of clozapine (0.01 and 0.1 mg/kg). Linear mixed model analysis showed a significant effect of the highest dose (*p< 0.05) but no difference between control or DREADD (p>0.05).*

Two main findings can be concluded. First, the increased firing rate after administering the highest dose of clozapine in both control and DREADD animals indicates the presence of a DREADD-independent effect. It has been known that clozapine has affinity for a variety of endogenous receptors such as dopamine, serotonin, noradrenaline, acetylcholine and histamine receptors. (Coward 1992) A previous study in healthy animals showed an increased discharge rate of LC and ventral tegmental area neurons after intravenous administration of clozapine (0.075, 1.25-10 mg/kg) due to involvement of glutamatergic mechanisms. (Schwieler et al. 2008; Nilsson et al. 2005) Pretreatment with an antagonist at the glycine site of the NMDA receptor inhibited the clozapine-induced activation of LC neurons but cannot solely explain the increased firing rates after administration of the highest dose of clozapine as administration of a selective partial agonist did not increase the LC activity. This study suggests a combination of NMDA receptor activity and increased glutamatergic release by afferents to LC. (Nilsson et al. 2005) Second, no effect was observed after administration of the lowest dose of clozapine in this study. This result is contradictory to previous preliminary studies where 1mg/kg CNO increased firing rate (up to 300% relative to baseline). In the present study we used 0.01mg/kg as Gomez et al. stated that it exerts the same effects as CNO 1mg/kg (Gomez et al. 2017). A possible explanation for the absence of increased LC activity is the variability in hM3Dq-expression. In most animals low expression levels were observed, which is in contrast to high specificity and expression levels of >95% observed in previous studies using PRSx8 promotor (Vazey and Aston-Jones 2014)we investigated the causal relationship between LC-NE activity and general anesthetic state under isoflurane. Selective activation of LC-NE neurons produced cortical electroencephalography (EEG. The lack of high expression levels increases the risk of recording a non-transduced LC neuron, explaining the absence of changes in firing frequency.
We can conclude that the highest dose of clozapine cannot be used for chemogenetic activation of genetically modified LC neurons because of effects seen in control animals. It is not clear from the present study whether the absence of effects on LC activity after administration of 0.01 mg/kg is due to high variability in expression levels and recording of non-transduced LC neurons or because of the dose itself.

1.1. Task 1.2 Validation of PSAM-based modulation of the locus coeruleus (LC)

Because of the variable hM3Dq expression levels and DREADD-independent effect of clozapine, another promising chemogenetic approach was investigated. Expression of genetically engineered ionotropic receptors, more specific pharmacologically selective actuator molecule (PSAM), was induced in LC by injection of a canine-associated viral vector (CAV) under control of a specific promotor PRSx8. PSAM is the ligand-binding domain of the α7nicotinic acetylcholine-receptor, which is genetically engineered to prevent binding of its endogenous ligand acetylcholine but to be selectively gated by synthetic ligands called Pharmacologically Selective Effector Molecules (PSEM). (Magnus et al. 2011; Snowball and Schorge 2015)

Induction of PSAM expression in LC neurons in rats

To induce expression of PSAM in a maximum number of LC neurons, the chemogenetic CAV vector is injected in LC or in hippocampus using the retrograde transport characteristics of CAV viral vector along the LC axons projecting to hippocampus.

In a first phase animals were anesthetized with a mixture of medical oxygen and isoflurane (5% for induction, 2% for maintenance). The rat was placed in a stereotaxic frame and the skull was exposed. Bregma was lowered 2mm relative to lambda (~15° head angle) to target the LC. CAV2-eGFP-PRSx8-PSAM ($9x10^{12}$ TU/ml) was unilaterally injected in hippocampus (5.5 AP; 5 ML; -7.5; -6; -4,5 DV). Per injection site 0.3 µl of vector, 3 times diluted in sterile PBS (Phosphate buffered saline powder dissolved in MilliQ), was delivered using a Hamilton syringe and QSI injection system (flow rate 150nl/min).

After two weeks, rats were euthanized and transcardially perfused to determine expression levels using immunofluorescence staining with primary antibodies anti-TH and anti-GFP. Only a few transduced cells were observed (fig.4).

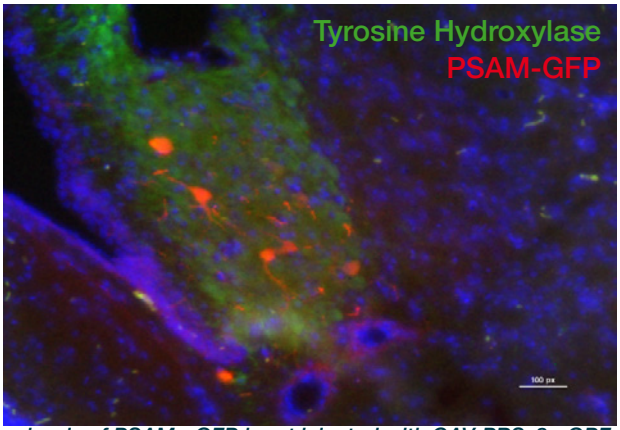

Figure 4: Visualization of expression levels of PSAM-eGFP in rat injected with CAV-PRSx8-eGPF-PSAM using immunofluorescence staining*. A. Primary antibodies anti-tyrosine hydroxylase (green) and anti-green fluorescent protein (GFP, red) were used for visualization of LC-NA neurons and GFP coupled to PSAM respectively. Scale bar 100 px.*

Because of low expression levels, the experiment was repeated using non-diluted viral vector. The viral vector (0.1 µl/injection site) was administered as described above, three animals were injected at three sites along the anterior-posterior axis in the hippocampus (-3 AP; -2 ML; -3, -4 DV ; -4.5 AP; -4.8 ML; -4.5, -6, -7.5 DV ; -6 AP; -5.5 ML; -4.5, -6, -7.5 DV) and in another rats were injected in LC (-3.9 AP; -1.15 ML; -5.8, -5.5, -5.3 DV).

After three weeks allowing optimal expression, animals were euthanized and immunofluorescence staining was performed. PSAM-expression was checked both on LC-NA cell bodies and noradrenergic projections in hippocampus. No clear expression was observed (fig.5,6).

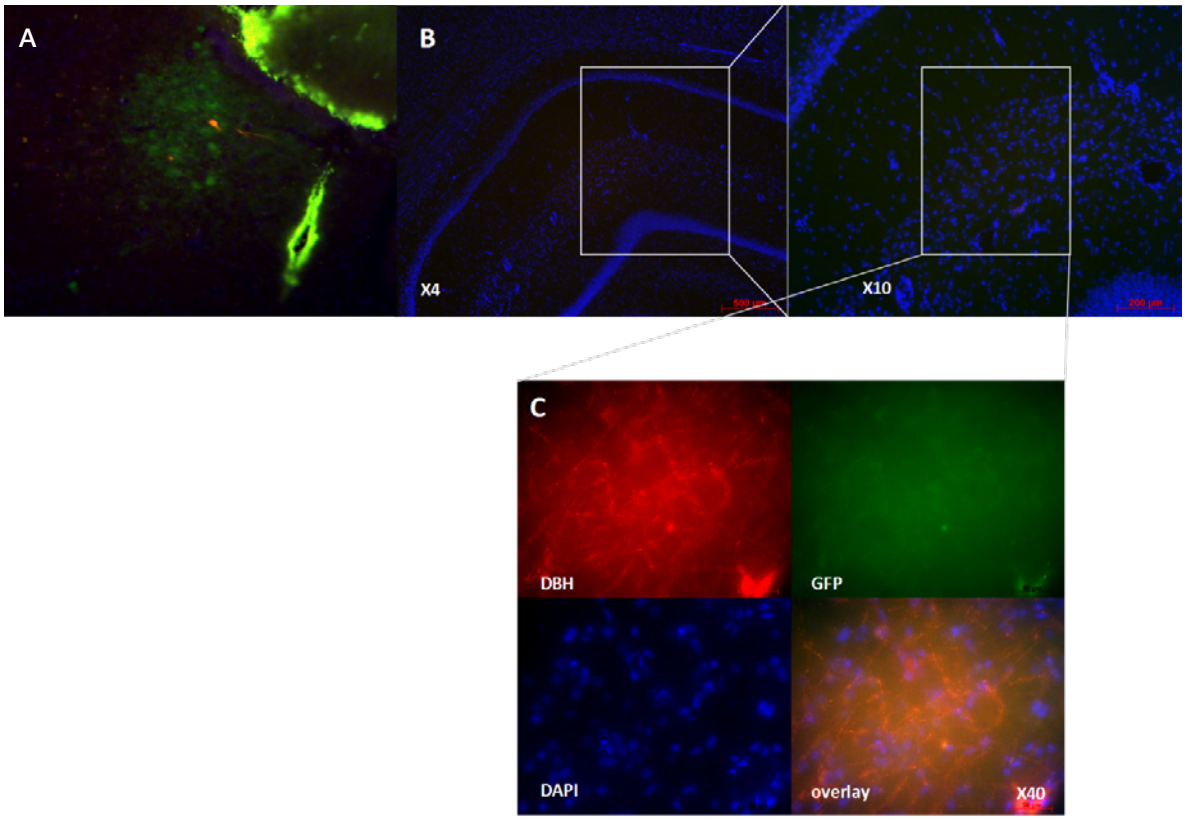

Figure 5: PSAM-GFP expression in LC and hippocampus of rats injected with CAV-PRSx8-eGFP-PSAM in hippocampus. *A. Positive cell in red (GFP), LC neurons (green). B. Overview x4 and x10 of hippocampus. C. Noradrenergic neurons visualized using anti-dopamine β-hydroxylase (DBH) and PSAM-GFP using anti-GFP primary antibodies. x40 (scale bar 500µm).*

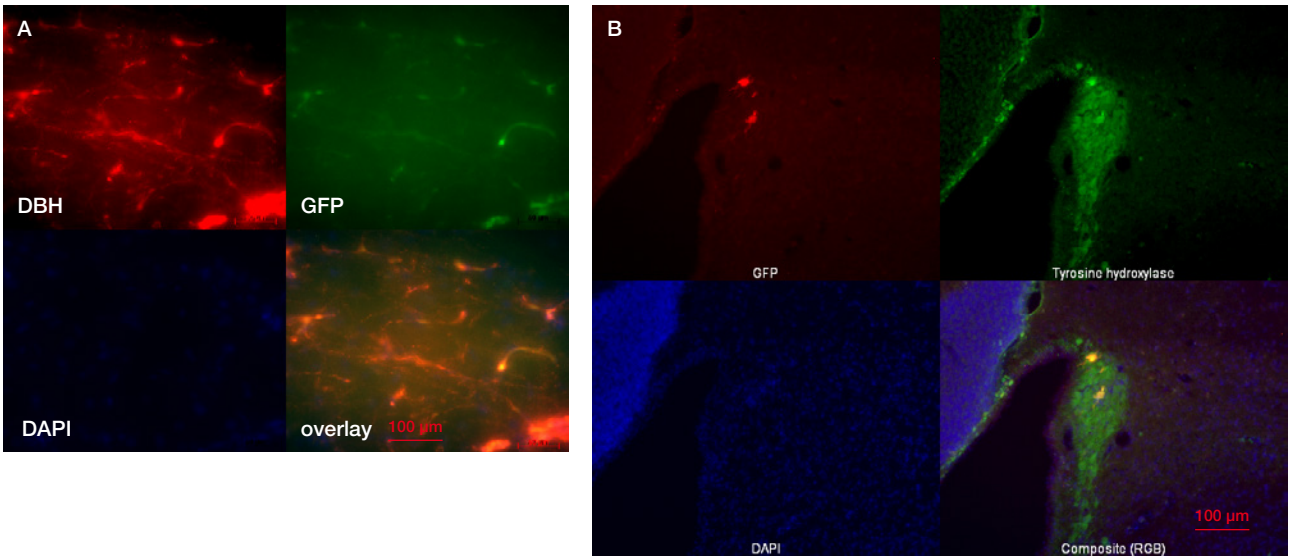

Figure 6: PSAM-GFP expression in hippocampus and LC in rat injected with CAV-PRSx8-eGFP-PSAM in LC (undiluted). *A. Noradrenergic axonal projections in hippocampus visualized using primary anti-bodies anti-dopamine β hydroxylase (DBH, red) and anti-GFP (green) for GFP tag. B. LC-NA neurons expressing PSAM-GFP. Antibodies against tyrosine hydroxylase (green) and GFP (red) to visualize PSAM-GFP. Scale bar 100 µm.*

Workpackage 2: Optogenetic modulation of the locus coeruleus: effect on *normal* hippocampal activity

Task 2.1 Validation of optogenetic modulation of the locus coeruleus (LC)

Induction of ChR2 expression in LC neurons in rats

Due to negative results using the chemogenetic approach, optogenetics was introduced to modulate LC. In case of optogenetic modulation, LC neurons are induced to express light-sensitive ion channels

allowing subsequent activation [e.g. with channelrhodopsin (ChR2)] of the cells with high temporal specificity using light. Phasic bursts of activity can be induced in ChR2 expressing LC neurons with short blue light pulses. (Carter et al. 2010) The optogenetic viral vector was injected in locus coeruleus to induce high expression levels needed due to low pore conductance of channelrhodopsin. (Li et al. 2016) To induce expression of ChR2 in LC, CAV-PRSx8-Chr2-mcherry ($1.3x10^{12}$TU/ml) was unilaterally injected in LC (n=3 rats) at three sites along the dorso-ventral axis (AP +3.9; ML -1.15; DV -5.3, -5.5, -5.7; n=3). Per site 0.3 µl at 150nl/min, 5 times diluted in sterile PBS. Injection procedure similar as above mentioned expression. After two weeks, rats were euthanized and transcardially perfused to determine expression levels of ChR2 in locus coeruleus and axonal projections in hippocampus using immunofluorescence staining. All rats injected with CAV2-PRSx8-Chr2-mCherry showed high expression levels in LC neurons and axons located in hippocampus (fig.7).

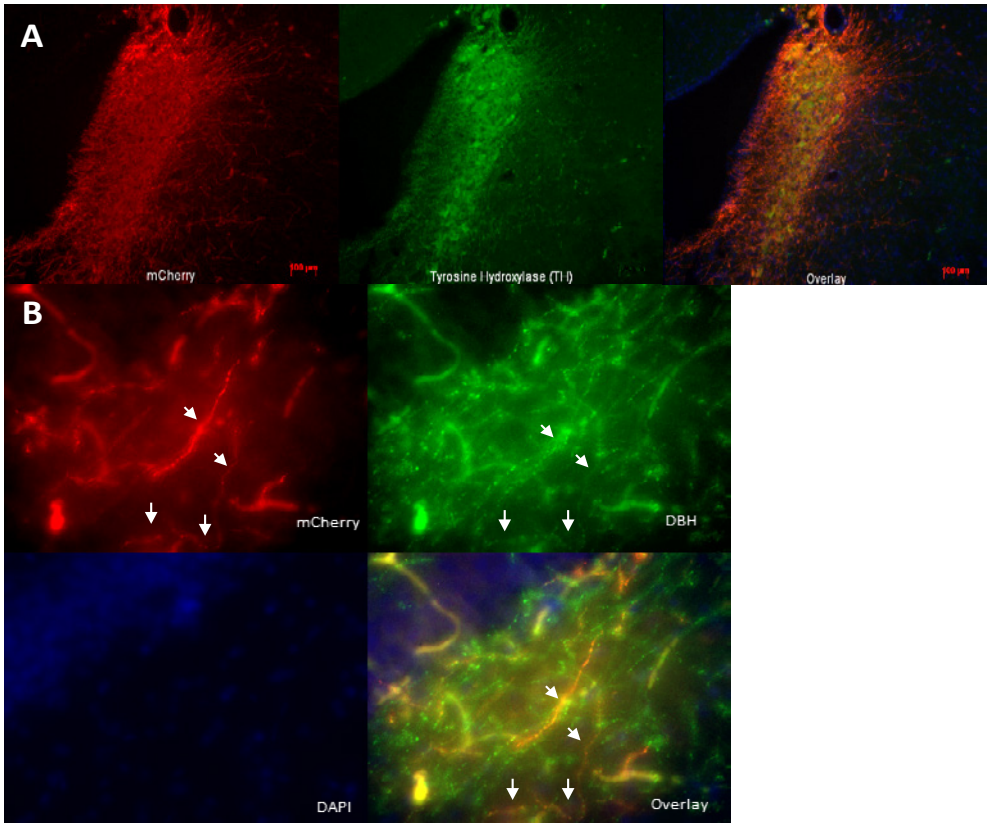

Figure 7: Visualization of expression levels of ChR2-mCherry in rat injected with CAV-PRSx8-ChR2-mCherry using immunofluorescence staining*. A. Primary antibodies anti-tyrosine hydroxylase (green) and anti-red fluorescent protein (RFP, red) were used for visualization of LC-NA neurons and mCherry coupled to ChR2 respectively.*
B. Anti-dopamine β hydroxylase (DBH, green) and anti-RFP (red) were used for visualizing LC axonal projections in hippocampus.

Validation optic fiber implantation

To determine correct positioning of the optic fiber and to check whether implantation has an effect on ChR2-expression, three animals were injected with viral vector as described above. Additionally, a self-manufactured optic fiber (8mm length, Ø220µm) was implanted in LC (3.9AP, 1.15 ML, -5.5 DV). After two weeks, rats were euthanized to check fiber position and expression using immunofluorescence staining. Fiber positioning was only visible in one animal showing damage in LC (fig.8). From these results we can conclude that the dorsoventral coordinate needs to be changed to prevent damage in dorsal LC, as this location projects to the hippocampus which we want to modulate.

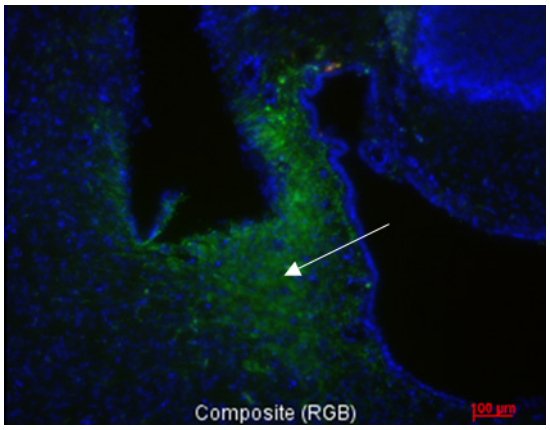

Figure 8: Optic fiber position *showing damage to dorsal LC using immunofluorescence staining with primary anti-body against anti-DBH (LC-NA cells). White arrow indicating exact location of optic fiber in LC. Scale bar 100µm.*

No clear expression of the opsin was visible in all three animals, indicating the need of further validation of the injection procedure. Six additional animals were bilaterally injected in LC using the same coordinates and injection procedure as before, but extra care was taken with viral vector storage between injections (storage on ice in the fridge). One animal died during surgery. Immunofluorescence staining was performed on coronal sections of four animals and clear expression of ChR2-mCherry was observed in one or both injected LC.

2. Future experiments

Optogenetic activation of LC and its effect on hippocampal excitability in healthy and epileptic rats

High expression levels of ChR2 are obtained using a validated injection procedure. The next step is to determine the ideal position of the optic fiber to activate dorsal LC and modulate hippocampal electrophysiology. Animals will be bilaterally injected with the CAV viral vector in LC. After three weeks, allowing optimal expression, optic fibers will be implanted in both LCs. After one day, excluding possible mechanical activation of LC neurons by implantation procedure, unilateral optogenetic activation of LC followed by acute transcardial perfusion to detect the presence of cfos, a neuronal activity marker, to map the range of light induced activitiy. (Stone, Zhang, and Carr 1995; Carter et al. 2010)piriform, parietal, frontal cortex, and the olfactory tubercle. Prior lesion of the LC with 6-hydroxydopamine (6-OHDA In a next experiment, the effect of optogenetic activation of LC on hippocampal excitability can be determined by the recording of perforant path (PP) evoked potentials in the dentate gyrus (DG) under anesthesia in healthy and epileptic animals. CAV-PRSx8-ChR2-mCherry will be injected in LC as described above. Three weeks later, allowing optimal expression, a bipolar stimulation and recording electrode will be implanted in the perforant path and dentate gyrus respectively. Additionally, an optical fiber will be lowered to activate LC and determine the effect of different stimulation paradigms on paired-pulse evoked potentials in hippocampus under anesthesia. Previous studies under anesthesia using iontophoretic or glutamatergic/orexinergic activation to modulate the LC-NA pathway show an β-mediated and protein synthesis dependent long-lasting potentiation effects of the population spike. (Lacaille and Harley 1985; Walling et al. 2004; Harley and Milway 1986)a decrease in population spike onset latency (94% of control A recent study by the group of Harley and Walling showed also delayed long-term potentiation of population spike in response to optogenetic LC activation paired with perforant path-dentate gyrus evoked potentials under urethane anesthesia. (Quinlan et al. 2019)

3. References

- Carter, Matthew E, Ofer Yizhar, Sachiko Chikahisa, Hieu Nguyen, Antoine Adamantidis, Seiji Nishino, Karl Deisseroth, and Luis de Lecea. 2010. “Tuning Arousal with Optogenetic Modulation of Locus Coeruleus Neurons.” *Nature Neuroscience*. doi:10.1038/nn.2682.
- Coward, D M. 1992. “General Pharmacology of Clozapine.” *British Journal of Psychiatry*. doi:10.1007/978-3-642-60551-2.
- Gomez, Juan L, Jordi Bonaventura, Wojciech Lesniak, William B Mathews, Polina Sysa-Shah, Lionel A Rodriguez, Randall J Ellis, et al. 2017. “Chemogenetics Revealed: DREADD Occupancy and Activation via Converted Clozapine.” *Science* 357: 503–7. doi:10.1126/science.aan2475.
- Harley, C. W., and J. S. Milway. 1986. “Glutamate Ejection in the Locus Coeruleus Enhances the Perforant Path-Evoked Population Spike in the Dentate Gyrus.” *Experimental Brain Research* 63 (1): 143–50. doi:10.1007/BF00235656.
- Hwang, Dong-Youn, William A Carlezon, Ole Isacson, and Kwang-Soo Kim. 2001. “A High-Efficiency Synthetic Promoter That Drives Transgene Expression Selectively in Noradrenergic Neurons.” *HUMAN GENE THERAPY* 12. Mary Ann Liebert, Inc: 1731–40.
- Lacaille, Jean-Claude, and Carolyn W. Harley. 1985. “The Action of Norepinephrine in the Dentate Gyrus: Beta-Mediated Facilitation of Evoked Potentials in Vitro.” *Brain Research* 358 (1): 210–20. doi:10.1016/0006-8993(85)90965-5.
- Li, Yong, Louise Hickey, Ray Perrins, Emilie Werlen, Amisha A Patel, Stefan Hirschberg, Matt W Jones, Sara Salinas, Eric J Kremer, and Anthony E Pickering. 2016. “Retrograde Optogenetic Characterization of the Pontospinal Module of the Locus Coeruleus with a Canine Adenoviral Vector.” *Brain Research*. doi:10.1016/j.brainres.2016.02.023.
- Magnus, Christopher J, Peter H Lee, Deniz Atasoy, Helen H Su, Loren L Looger, and Scott M Sternson. 2011. “Chemical and Genetic Engineering of Selective Ion Channel – Ligand Interactions.” *Science* 333 (2011): 1292–96. doi:10.1126/science.1206606.
- Nilsson, Linda K, Lilly Schwieler, Göran Engberg, Klas R Linderholm, and Sophie Erhardt. 2005. “Activation of Noradrenergic Locus Coeruleus Neurons by Clozapine and Haloperidol: Involvement of Glutamatergic Mechanisms.” *International Journal of Neuropsychopharmacology* 8 (3): 329–39. doi:10.1017/S1461145705005080.
- Quinlan, Meghan A. L., Vanessa M. Strong, Darlene M. Skinner, Gerard M. Martin, Carolyn W. Harley, and Susan G. Walling. 2019. “Locus Coeruleus Optogenetic Light Activation Induces Long-Term Potentiation of Perforant Path Population Spike Amplitude in Rat Dentate Gyrus.” *Frontiers in Systems Neuroscience* 12 (January): 1–14. doi:10.3389/fnsys.2018.00067.
- Schwieler, Lilly, Klas R Linderholm, Linda K Nilsson-Todd, Sophie Erhardt, and Göran Engberg. 2008. “Clozapine Interacts with the Glycine Site of the NMDA Receptor: Electrophysiological Studies of Dopamine Neurons in the Rat Ventral Tegmental Area.” doi:10.1016/j.lfs.2008.05.014.
- Snowball, Albert, and Stephanie Schorge. 2015. “Changing Channels in Pain and Epilepsy: Exploiting Ion Channel Gene Therapy for Disorders of Neuronal Hyperexcitability.” *FEBS Letters* 589: 1620–34. doi:10.1016/j.febslet.2015.05.004.
- Stone, Eric A, Yi Zhang, and Kenneth D Carr. 1995. “Massive Activation of C-Fos in Forebrain after Mechanical Stimulation of the Locus Coeruleus.” *Brain Research Bulletin* 36 (1): 77–80. doi:10.1016/0361-9230(94)00167-Y.
- Vazey, Elena M, and Gary Aston-Jones. 2014. “Designer Receptor Manipulations Reveal a Role of the Locus Coeruleus Noradrenergic System in Isoflurane General Anesthesia.” *Proceedings of the National Academy of Sciences* 111 (10). National Academy of Sciences: 3859–64. doi:10.1073/pnas.1310025111.
- Walling, Susan G, David J Nutt, Margaret D Lalies, and Carolyn W Harley. 2004. “Behavioral/Systems/Cognitive Orexin-A Infusion in the Locus Ceruleus Triggers Norepinephrine (NE) Release and NE-Induced Long-Term Potentiation in the Dentate Gyrus.” doi:10.1523/JNEUROSCI.1587-04.2004.

4. Publications

- Latoya Stevens, Robrecht Raedt, Wouter Van Lysebettens, Paul Boon, Kristl Vonck. Induction of DREADD expression in LC rats and its effects on neuronal firing. Abstract presented at Sectie Wetenschappelijk Onderzoek, Amsterdam, The Netherlands; Jan2018
- Latoya Stevens, Robrecht Raedt, Wouter Van Lysebettens, Paul Boon, Kristl Vonck. Induction of DREADD expression in LC rats and its effects on neuronal firing. Abstract presented at European Congress on Epileptology ECE, Vienna, Austria; Aug2018
- Latoya Stevens, Kristl Vonck, Wouter Van Lysbettens, Veerle Baekelandt, Chris Van Den Haute, Paul Boon, Robrecht Raedt. Presumed subclinical doses of clozapine not useful as selective ligand for chemogenetic activation of locus coeruleus neurons in rat. (manuscript in preparation)

5. Financial report 2018

cfr separate report

Geneeskundige Stichting Koningin Elisabeth – G.S.K.E.

Fondation Médicale Reine Elisabeth – F.M.R.E.

Queen Elisabeth Medical Foundation – Q.E.M.F.

Mailing address:

The scientifique director:
Prof. dr. Jean-Marie Maloteaux
3, avenue J.J. Crocq laan
1020 Bruxelles - Brussel
Belgium
Tel.: +32 2 478 35 56
E-mail: jean-marie.maloteaux@uclouvain.be

and

Secretary:
Mr. Erik Dhondt
3, avenue J.J. Crocq laan
1020 Bruxelles - Brussel
Belgium
Tel.: +32 2 478 35 56
E-mail: fmre.gske@skynet.be
E-mail: erik.dhondt@skynet.be, e.l.dhondt@skynet.be
www.fmre-gske.be
www.fmre-gske.eu
www.fmre-gske.com